FUNDAMENTAL SOLUTIONS FOR MULTI-LAYERED TRANSVERSELY ISOTROPIC ELASTIC MEDIA AND BOUNDARY ELEMENT APPLICATIONS

BY

YAOPING WANG

A dissertation
submitted to the University of Manitoba
in partial fulfillment of the requirements
for the Degree of

DOCTOR OF PHILOSOPHY

Department of Civil Engineering, University of Manitoba
Winnipeg, Manitoba, Canada.

ISBN 0-315-81763-1

Name Yaoping Wang

Dissertation Abstracts International is arranged by broad, general subject categories. Please select the one subject which most nearly describes the content of your dissertation. Enter the corresponding four-digit code in the spaces provided.

Applied Mechanics
SUBJECT TERM

0346
SUBJECT CODE

U·M·I

Subject Categories

THE HUMANITIES AND SOCIAL SCIENCES

COMMUNICATIONS AND THE ARTS
Architecture 0729
Art History 0377
Cinema 0900
Dance 0378
Fine Arts 0357
Information Science 0723
Journalism 0391
Library Science 0399
Mass Communications 0708
Music 0413
Speech Communication 0459
Theater 0465

EDUCATION
General 0515
Administration 0514
Adult and Continuing 0516
Agricultural 0517
Art 0273
Bilingual and Multicultural 0282
Business 0688
Community College 0275
Curriculum and Instruction 0727
Early Childhood 0518
Elementary 0524
Finance 0277
Guidance and Counseling 0519
Health 0680
Higher 0745
History of 0520
Home Economics 0278
Industrial 0521
Language and Literature 0279
Mathematics 0280
Music 0522
Philosophy of 0998
Physical 0523
Psychology 0525
Reading 0535
Religious 0527
Sciences 0714
Secondary 0533
Social Sciences 0534
Sociology of 0340
Special 0529
Teacher Training 0530
Technology 0710
Tests and Measurements 0288
Vocational 0747

LANGUAGE, LITERATURE AND LINGUISTICS
Language
- General 0679
- Ancient 0289
- Linguistics 0290
- Modern 0291

Literature
- General 0401
- Classical 0294
- Comparative 0295
- Medieval 0297
- Modern 0298
- African 0316
- American 0591
- Asian 0305
- Canadian (English) 0352
- Canadian (French) 0355
- English 0593
- Germanic 0311
- Latin American 0312
- Middle Eastern 0315
- Romance 0313
- Slavic and East European 0314

PHILOSOPHY, RELIGION AND THEOLOGY
Philosophy 0422
Religion
- General 0318
- Biblical Studies 0321
- Clergy 0319
- History of 0320
- Philosophy of 0322

Theology 0469

SOCIAL SCIENCES
American Studies 0323
Anthropology
- Archaeology 0324
- Cultural 0326
- Physical 0327

Business Administration
- General 0310
- Accounting 0272
- Banking 0770
- Management 0454
- Marketing 0338

Canadian Studies 0385
Economics
- General 0501
- Agricultural 0503
- Commerce-Business 0505
- Finance 0508
- History 0509
- Labor 0510
- Theory 0511

Folklore 0358
Geography 0366
Gerontology 0351
History
- General 0578
- Ancient 0579
- Medieval 0581
- Modern 0582
- Black 0328
- African 0331
- Asia, Australia and Oceania 0332
- Canadian 0334
- European 0335
- Latin American 0336
- Middle Eastern 0333
- United States 0337

History of Science 0585
Law 0398
Political Science
- General 0615
- International Law and Relations 0616
- Public Administration 0617

Recreation 0814
Social Work 0452
Sociology
- General 0626
- Criminology and Penology 0627
- Demography 0938
- Ethnic and Racial Studies 0631
- Individual and Family Studies 0628
- Industrial and Labor Relations 0629
- Public and Social Welfare 0630
- Social Structure and Development 0700
- Theory and Methods 0344

Transportation 0709
Urban and Regional Planning 0999
Women's Studies 0453

THE SCIENCES AND ENGINEERING

BIOLOGICAL SCIENCES
Agriculture
- General 0473
- Agronomy 0285
- Animal Culture and Nutrition 0475
- Animal Pathology 0476
- Food Science and Technology 0359
- Forestry and Wildlife 0478
- Plant Culture 0479
- Plant Pathology 0480
- Plant Physiology 0817
- Range Management 0777
- Wood Technology 0746

Biology
- General 0306
- Anatomy 0287
- Biostatistics 0308
- Botany 0309
- Cell 0379
- Ecology 0329
- Entomology 0353
- Genetics 0369
- Limnology 0793
- Microbiology 0410
- Molecular 0307
- Neuroscience 0317
- Oceanography 0416
- Physiology 0433
- Radiation 0821
- Veterinary Science 0778
- Zoology 0472

Biophysics
- General 0786
- Medical 0760

EARTH SCIENCES
Biogeochemistry 0425
Geochemistry 0996
Geodesy 0370
Geology 0372
Geophysics 0373
Hydrology 0388
Mineralogy 0411
Paleobotany 0345
Paleoecology 0426
Paleontology 0418
Paleozoology 0985
Palynology 0427
Physical Geography 0368
Physical Oceanography 0415

HEALTH AND ENVIRONMENTAL SCIENCES
Environmental Sciences 0768
Health Sciences
- General 0566
- Audiology 0300
- Chemotherapy 0992
- Dentistry 0567
- Education 0350
- Hospital Management 0769
- Human Development 0758
- Immunology 0982
- Medicine and Surgery 0564
- Mental Health 0347
- Nursing 0569
- Nutrition 0570
- Obstetrics and Gynecology 0380
- Occupational Health and Therapy 0354
- Ophthalmology 0381
- Pathology 0571
- Pharmacology 0419
- Pharmacy 0572
- Physical Therapy 0382
- Public Health 0573
- Radiology 0574
- Recreation 0575
- Speech Pathology 0460
- Toxicology 0383

Home Economics 0386

PHYSICAL SCIENCES
Pure Sciences
Chemistry
- General 0485
- Agricultural 0749
- Analytical 0486
- Biochemistry 0487
- Inorganic 0488
- Nuclear 0738
- Organic 0490
- Pharmaceutical 0491
- Physical 0494
- Polymer 0495
- Radiation 0754

Mathematics 0405
Physics
- General 0605
- Acoustics 0986
- Astronomy and Astrophysics 0606
- Atmospheric Science 0608
- Atomic 0748
- Electronics and Electricity 0607
- Elementary Particles and High Energy 0798
- Fluid and Plasma 0759
- Molecular 0609
- Nuclear 0610
- Optics 0752
- Radiation 0756
- Solid State 0611

Statistics 0463

Applied Sciences
Applied Mechanics 0346
Computer Science 0984

Engineering
- General 0537
- Aerospace 0538
- Agricultural 0539
- Automotive 0540
- Biomedical 0541
- Chemical 0542
- Civil 0543
- Electronics and Electrical 0544
- Heat and Thermodynamics 0348
- Hydraulic 0545
- Industrial 0546
- Marine 0547
- Materials Science 0794
- Mechanical 0548
- Metallurgy 0743
- Mining 0551
- Nuclear 0552
- Packaging 0549
- Petroleum 0765
- Sanitary and Municipal 0554
- System Science 0790

Geotechnology 0428
Operations Research 0796
Plastics Technology 0795
Textile Technology 0994

PSYCHOLOGY
General 0621
Behavioral 0384
Clinical 0622
Developmental 0620
Experimental 0623
Industrial 0624
Personality 0625
Physiological 0989
Psychobiology 0349
Psychometrics 0632
Social 0451

Nom _____

Dissertation Abstracts International est organisé en catégories de sujets. Veuillez s.v.p. choisir le sujet qui décrit le mieux votre thèse et inscrivez le code numérique approprié dans l'espace réservé ci-dessous.

U·M·I

CODE DE SUJET

SUJET

Catégories par sujets

HUMANITÉS ET SCIENCES SOCIALES

COMMUNICATIONS ET LES ARTS

Architecture 0729
Beaux-arts 0357
Bibliothéconomie 0399
Cinéma 0900
Communication verbale 0459
Communications 0708
Danse 0378
Histoire de l'art 0377
Journalisme 0391
Musique 0413
Sciences de l'information 0723
Théâtre 0465

ÉDUCATION

Généralités 515
Administration 0514
Art 0273
Collèges communautaires 0275
Commerce 0688
Économie domestique 0278
Éducation permanente 0516
Éducation préscolaire 0518
Éducation sanitaire 0680
Enseignement agricole 0517
Enseignement bilingue et multiculturel 0282
Enseignement industriel 0521
Enseignement primaire. 0524
Enseignement professionnel 0747
Enseignement religieux 0527
Enseignement secondaire 0533
Enseignement spécial 0529
Enseignement supérieur 0745
Évaluation 0288
Finances 0277
Formation des enseignants 0530
Histoire de l'éducation 0520
Langues et littérature 0279
Lecture 0535
Mathématiques 0280
Musique 0522
Orientation et consultation 0519
Philosophie de l'éducation 0998
Physique 0523
Programmes d'études et enseignement 0727
Psychologie 0525
Sciences 0714
Sciences sociales 0534
Sociologie de l'éducation 0340
Technologie 0710

LANGUE, LITTÉRATURE ET LINGUISTIQUE

Langues
- Généralités 0679
- Anciennes 0289
- Linguistique 0290
- Modernes 0291

Littérature
- Généralités 0401
- Anciennes 0294
- Comparée 0295
- Médiévale 0297
- Moderne 0298
- Africaine 0316
- Américaine 0591
- Anglaise 0593
- Asiatique 0305
- Canadienne (Anglaise) 0352
- Canadienne (Française) 0355
- Germanique 0311
- Latino-américaine 0312
- Moyen-orientale 0315
- Romane 0313
- Slave et est-européenne 0314

PHILOSOPHIE, RELIGION ET THÉOLOGIE

Philosophie 0422
Religion
- Généralités 0318
- Clergé 0319
- Études bibliques 0321
- Histoire des religions 0320
- Philosophie de la religion 0322

Théologie 0469

SCIENCES SOCIALES

Anthropologie
- Archéologie 0324
- Culturelle 0326
- Physique 0327

Droit 0398
Économie
- Généralités 0501
- Commerce-Affaires 0505
- Économie agricole 0503
- Économie du travail 0510
- Finances 0508
- Histoire 0509
- Théorie 0511

Études américaines 0323
Études canadiennes 0385
Études féministes 0453
Folklore 0358
Géographie 0366
Gérontologie 0351
Gestion des affaires
- Généralités 0310
- Administration 0454
- Banques 0770
- Comptabilité 0272
- Marketing 0338

Histoire
- Histoire générale 0578
- Ancienne 0579
- Médiévale 0581
- Moderne 0582
- Histoire des noirs 0328
- Africaine 0331
- Canadienne 0334
- États-Unis 0337
- Européenne 0335
- Moyen-orientale 0333
- Latino-américaine 0336
- Asie, Australie et Océanie 0332

Histoire des sciences 0585
Loisirs 0814
Planification urbaine et régionale 0999
Science politique
- Généralités 0615
- Administration publique 0617
- Droit et relations internationales 0616

Sociologie
- Généralités 0626
- Aide et bien-être social 0630
- Criminologie et établissements pénitentiaires 0627
- Démographie 0938
- Études de l' individu et de la famille 0628
- Études des relations interethniques et des relations raciales 0631
- Structure et développement social 0700
- Théorie et méthodes. 0344
- Travail et relations industrielles 0629

Transports 0709
Travail social 0452

SCIENCES ET INGÉNIERIE

SCIENCES BIOLOGIQUES

Agriculture
- Généralités 0473
- Agronomie. 0285
- Alimentation et technologie alimentaire 0359
- Culture 0479
- Élevage et alimentation 0475
- Exploitation des pâturages 0777
- Pathologie animale 0476
- Pathologie végétale 0480
- Physiologie végétale 0817
- Sylviculture et faune 0478
- Technologie du bois 0746

Biologie
- Généralités 0306
- Anatomie 0287
- Biologie (Statistiques) 0308
- Biologie moléculaire 0307
- Botanique 0309
- Cellule 0379
- Écologie 0329
- Entomologie 0353
- Génétique 0369
- Limnologie 0793
- Microbiologie 0410
- Neurologie 0317
- Océanographie 0416
- Physiologie 0433
- Radiation 0821
- Science vétérinaire 0778
- Zoologie 0472

Biophysique
- Généralités 0786
- Medicale 0760

SCIENCES DE LA TERRE

Biogéochimie 0425
Géochimie 0996
Géodésie 0370
Géographie physique 0368
Géologie 0372
Géophysique 0373
Hydrologie 0388
Minéralogie 0411
Océanographie physique 0415
Paléobotanique 0345
Paléoécologie 0426
Paléontologie 0418
Paléozoologie 0985
Palynologie 0427

SCIENCES DE LA SANTÉ ET DE L'ENVIRONNEMENT

Économie domestique 0386
Sciences de l'environnement 0768
Sciences de la santé
- Généralités 0566
- Administration des hôpitaux 0769
- Alimentation et nutrition 0570
- Audiologie 0300
- Chimiothérapie 0992
- Dentisterie 0567
- Développement humain 0758
- Enseignement 0350
- Immunologie 0982
- Loisirs 0575
- Médecine du travail et thérapie 0354
- Médecine et chirurgie 0564
- Obstétrique et gynécologie 0380
- Ophtalmologie 0381
- Orthophonie 0460
- Pathologie 0571
- Pharmacie 0572
- Pharmacologie 0419
- Physiothérapie 0382
- Radiologie 0574
- Santé mentale 0347
- Santé publique 0573
- Soins infirmiers 0569
- Toxicologie 0383

SCIENCES PHYSIQUES

Sciences Pures

Chimie
- Généralités 0485
- Biochimie 487
- Chimie agricole 0749
- Chimie analytique 0486
- Chimie minérale 0488
- Chimie nucléaire 0738
- Chimie organique 0490
- Chimie pharmaceutique 0491
- Physique 0494
- PolymÇres 0495
- Radiation 0754

Mathématiques 0405
Physique
- Généralités 0605
- Acoustique 0986
- Astronomie et astrophysique 0606
- Électronique et électricité 0607
- Fluides et plasma 0759
- Météorologie 0608
- Optique 0752
- Particules (Physique nucléaire) 0798
- Physique atomique 0748
- Physique de l'état solide 0611
- Physique moléculaire 0609
- Physique nucléaire 0610
- Radiation 0756

Statistiques 0463

Sciences Appliqués Et Technologie

Informatique 0984
Ingénierie
- Généralités 0537
- Agricole 0539
- Automobile 0540
- Biomédicale 0541
- Chaleur et ther modynamique 0348
- Conditionnement (Emballage) 0549
- Génie aérospatial 0538
- Génie chimique 0542
- Génie civil 0543
- Génie électronique et électrique 0544
- Génie industriel 0546
- Génie mécanique 0548
- Génie nucléaire 0552
- Ingénierie des systèmes 0790
- Mécanique navale 0547
- Métallurgie 0743
- Science des matériaux 0794
- Technique du pétrole 0765
- Technique minière 0551
- Techniques sanitaires et municipales 0554
- Technologie hydraulique 0545

Mécanique appliquée 0346
Géotechnologie 0428
Matières plastiques (Technologie) 0795
Recherche opérationnelle 0796
Textiles et tissus (Technologie) 0794

PSYCHOLOGIE

Généralités 0621
Personnalité 0625
Psychobiologie 0349
Psychologie clinique 0622
Psychologie du comportement 0384
Psychologie du développement 0620
Psychologie expérimentale 0623
Psychologie industrielle 0624
Psychologie physiologique 0989
Psychologie sociale 0451
Psychométrie 0632

FUNDAMENTAL SOLUTIONS FOR MULTI-LAYERED TRANSVERSELY ISOTROPIC ELASTIC MEDIA AND BOUNDARY ELEMENT APPLICATIONS

BY

YAOPING WANG

A Thesis submitted to the Faculty of Graduate Studies of the University of Manitoba in partial fulfillment of the requirements for the degree of

DOCTOR OF PHILOSOPHY

ABSTRACT

This thesis presents a complete solution package for the analysis of elastostatic and elastodynamic boundary-value problems related to linear elastic multi-layered transversely isotropic materials. Equations governing static and dynamic (time-harmonic and transient) deformations of a transversely isotropic medium are solved by using appropriate integral transform techniques. A set of analytical general solutions for displacements and stresses corresponding to 2-D and 3-D problems are presented explicitly for static and dynamic loading problems. Thereafter, 2-D and 3-D fundamental solutions (Green's functions) corresponding to buried static and dynamic loadings acting inside a homogeneous transversely isotropic half space are derived explicitly. Analytical solutions are also presented for a transient displacement jump located inside a homogeneous transversely isotropic half space. It is noted that by taking appropriate limits fundamental solutions for a transversely isotropic elastic full space can be easily derived from the half space solutions. An exact stiffness matrix method based on analytical general solutions are presented to compute fundamental solutions corresponding to a multi-layered transversely isotropic elastic half space. The stiffness matrix method involves only negative exponential of integral transform parameter and it is found to be free from the numerical deficiencies associated with algorithms reported in the literature. Some characteristics of the fundamental solutions are investigated and the numerical evaluations of the fundamental solutions is also discussed. Selected numerical results for displacements and stresses corresponding to buried loadings are presented to portray the influence of the degree of material anisotropy, configuration of layering and other governing parameters on the response.

A versatile boundary element code based on the Green's functions derived in this study are presented to analyse displacement, traction and mixed boundary-value problems related to homogeneous and multi-layered transversely isotropic

media. Several boundary-value problems (*eg.* statics and dynamics of rigid inclusions, pressurised cavities, non-linear interface problem, load transfer problems *etc.*) are solved to demonstrate the applicability and accuracy of the boundary element code. Selected numerical results for quantities such as stiffness and impedances of embedded inclusions and load transfer profiles along the length of an embedded elastic bar are presented to portray the influence of material anisotropy and other governing parameters on the response of complicated interaction problems.

ACKNOWLEDGEMENTS

I am deeply grateful to my advisor Professor R.K.N.D. Rajapakse for suggesting the topic of this research and for his constant guidance and encouragement throughout all phases of my Ph.D. program.

I convey my thanks to Professor A.H. Shah and Professor B. Stimpson for providing helpful comments and serving the advisory committee. I am grateful to Professor A.P.S. Selvadurai, an eminent authority in Applied Mechanics, for devoting his time to serve as the external examiner.

The assistance received from Dr. Y.M. Desai for helping with UNIX operating system is much appreciated. Thanks are extended to my friends, Dr. U.G.A. Puswewala, Dr. W. Karunasena, Dr. R. Zhang, Mr. N. Rattanawangcharoen and Mr. T. Senjuntichai, for their help and encouragment.

The financial support received in the form of a research assistantship from the NSERC operating grant of Professor Rajapakse and a graduate fellowship from The University of Manitoba is greatly appreciated.

Finally I wish to express my gratitude to my parents, my son Xiaofan and my wife Yi Lin for their understanding, encouragement and support during the course of my Ph.D. program.

November 1992

Yaoping Wang

Winnipeg, Canada.

TABLE OF CONTENTS

LIST OF TABLES

LIST OF FIGURES

Chapter 1

INTRODUCTION

1.1 GENERAL

In recent years, there has been a considerable growth in the use of anisotropic materials for a wide range of advanced engineering applications. Anisotropic materials encountered in engineering applications are either fabricated materials such as fibre-reinforced plastics, Aluminum alloys *etc.* or natural materials such as geomaterials, precious metals *etc.*. Stress analysis problems related to anisotropic materials are encountered in a number of fields ranging from modern technologies such as electronic packaging to traditional fields such as geophysics and engineering seismology. The fundamental characteristic of an anisotropic material is the directional dependence of its material properties. On the other hand, mechanical properties of an isotropic material are directionally independent. The directional dependence of mechanical properties of anisotropic material can be effectively used to achieve an efficient engineering design.

It is noted from a linear stress-strain relationship that an anisotropic material in its most general form has twenty-one independent elastic constants (Gould 1983). However, such a general form of anisotropy has very limited scope in engineering analysis due to the large number of elastic constants required to define the material. On the other hand, most anisotropic materials (fabricated and natural) possess planes and axes of material symmetry which reduces the number of independent elastic constants appearing in the stress-strain relationship. For example, the presence of a single plane of symmetry reduces the number of independent elastic constants to thirteen and the resulting material is identical as an monoclinic material. The presence of two planes of symmetry reduces the number of independent elastic constants to nine and the resulting material is known as an orthotropic material. A material which possesses an axis of symmetry is called a

transversely isotropic material. The number of independent material coefficients in this case is reduced to five. The introduction of a rotational symmetry with respect to two perpendicular axes results in directional independence of material constants and the resulting material is isotropic and has only two independent material constants.

Since the pioneering work of Boussinesq (1895), Lamb (1904) and Mindlin (1936) several researchers have developed analytical and computational methods for linear and non-linear stress analysis of isotropic materials. To provide the improved science base needed for the development of a wide range of applications of anisotropic materials attention has been focused recently on the development of advanced theories and solution algorithms for stress analysis of anisotropic materials under static and dynamic loadings. Among the different types of anisotropic constitutive relations, the transversely isotropic model has received wide attention due to its simplicity and also its ability to model the response of fibre reinforced composites, crystals, metals and geomaterials (material constants for a number of typical transversely isotropic materials are listed in Table 1.1). This thesis is concerned with the static and dynamic stress analysis of homogeneous and multi-layered transversely isotropic materials. In the ensuing sections, a concise review of literature related to stress analysis of transversely isotropic materials is presented in order to define the objectives and the scope of the present thesis.

1.2 LITERATURE REVIEW

1.2.1 **Fundamental Solutions for Homogeneous Transversely Isotropic Materials**

Elliott (1948), Hu (1954), Eubanks and Sternberg (1954), Lekhnitskii (1963) and Green and Zerna (1968) presented the early studies on elastostatics of a transversely isotropic medium. These authors presented potential function representations to derive general solutions for classical elastostatics and also considered

some basic stress analysis problems. Later, Chen (1966) and Pan and Chou (1976, 1979) presented solutions for point forces acting inside a transversely isotropic full space and on the surface of a transversely isotropic half space.

The elastodynamic response of a homogeneous transversely isotropic medium has also received attention. Stoneley (1949) investigated the types of elastic waves propagating in a transversely isotropic medium. Later, Synge (1956) studied the propagation of Rayleigh type surface waves in a transversely isotropic medium and proved that the Rayleigh waves exists only if the free-plane surface of the material is parallel or perpendicular to the material axis of symmetry. Buchwald (1961) derived the displacements in terms of double-Fourier integrals due to surface waves radiating from a given harmonic source on the surface. Asymptotic solutions were also presented by considering the contribution from poles of the integrand of Fourier integrals. Kraut (1962) solved the case of a transversely isotropic elastic half plane subjected to a suddenly applied line load, and studied in details the response of beryl crystals. A book by Payton (1983) refers to the majority of the existing studies related to transversely isotropic media; it also presents an elegant mathematical treatment of transient response due to impulsive point forces applied on the surface of an elastic half plane or inside an elastic full space. In addition to above studies, Barnett and Lothe (1974) and Chadwick and Smith (1977) presented thorough investigation on the nature of governing equation and existence of surface waves in anisotropic materials including the special case of transverse isotropy.

1.2.2 **Fundamental solutions for Layered Transversely Isotropic Systems**

The study of static and dynamic response of multi-layered transversely isotropic media is very useful to several disciplines such as geomechanics, composites, non-destructive testing *etc.*. The consideration of different materials and layers of different thickness in a multi-layered domain results in formidable difficulties in obtaining an explicit analytical solution. A number of semi-analytical

and numerical methods have been developed over the last 40 years to evaluate the response of isotropic multi-layered media. It should be mentioned here that the majority of existing work dealing with multi-layered media are concerned with dynamic problems due to extensive applications found in geophysics and theoretical modelling of non-destructive testing methods. Dynamic problems also involves more complications in the numerical evaluation of the response and the concepts developed for dynamic analysis can be readily extended to static problems. The earliest approach to study dynamics of layered isotropic media is the transfer matrix method developed by Thomson (1950) and Haskell (1953, 1960, 1962). A procedure similar to the transfer matrix method was also reported independently by Pestel and Leckie (1963). The Thomson-Haskell technique has significant drawbacks in the numerical implementation due to the presence of certain exponential terms. Improved formulations were developed later by Knopoff (1964), Gilbert and Backus (1966), Watson (1970) and Schwab (1970). A finite element type approximation has been proposed by Wass (1972, 1980) and Kausel and Peek (1982) to determine the response of an isotropic multi-layered medium. In this approach the medium is divided into a number of thin layers within which the displacements are assumed to vary linearly. In addition the impedance of the underlying half space region is computed by using further approximations. A comprehensive and rigorous treatment of Green's functions of an isotropic layered medium has been presented by Luco and Apsel (1983) and Apsel and Luco (1983). Applicability and accuracy of these Green's functions in boundary element analysis has also been reported in the literature (Apsel and Luco 1987).

It is noted that studies related to the statics and dynamics of multi-layered anisotropic media are very limited. Gerrard and Harrison (1971) used a direct numerical procedure based on analytical general solutions to compute static response of layered transversely isotropic media. Only Seale and Kausel (1989) presented an extension of the thin layer method (Waas 1972, 1980 and Kausel

and Peek 1982) to study the dynamics of a multi-layered transversely isotropic elastic half space.

1.2.3 Boundary-Value Problems

The majority of problems encountered in engineering applications of transversely isotropic materials involve complicated boundary and loading conditions such as the cases of rigid inclusions embedded in anisotropic materials, cavities under arbitrary loading, dynamics of foundations and piles in anisotropic soils and theoretical model used to simulate problems in geophysics and non-destructive testing of materials *etc.* The review of existing literature indicates that only problems involving highly idealised conditions have been treated in the past. For example, Freedman and Keer (1972) extended the dual integral equation formulations presented by Karasudhi *et al* (1968) to study the time-harmonic response of a rigid strip on an orthotropic half plane. Gazetas (1981) analysed the same problems by using a semi-analytical method. Selvadurai (1979, 1980, 1982) has investigated by analytical means a series of problems related to interaction between a statically loaded penny-shaped rigid disc and a transversely isotropic medium. Selvadurai (1984), Tsai (1984) and Saxena and Dhaliwal (1990) considered crack problems related to a transversely isotropic material by using analytical procedures. Zureick and Eubanks (1988), Zureick (1989) and Heinrich (1991) considered problems related to spheroidal inclusions/cavities in a transversely isotropic medium.

As mentioned earlier, above studies are based on analytical techniques that need to be developed separately for each type of problem. Analytical procedures are elegant and insightful when compared to numerical procedures such as the finite element method. In special cases such as wave propagation problems, the finite element solutions are found to be inaccurate and inefficient when compared to analytical solutions (Luco 1982). Analytical techniques, on the other hand, has the disadvantage that the solutions can be developed only under idealised geomet-

ric configuration and boundary and loading conditions which are not very useful in practical situations. The boundary element method (Rizzo 1967; Banerjee and Butterfield 1981; Brebbia *et al.* 1984; Kobayashi 1984; Beskos 1987) can be considered as a good compromise between analytical methods and the finite element technique to special conditions such as radiation conditions for wave propagation problems and singularities in stress fields of fracture mechanics problems. These problems can be treated rigorously in the boundary element method by using appropriate Green's functions. In problems related to layered elastic half spaces the boundary element method is also found to be computationally efficient than the finite element method. Although the boundary element method has been applied very successfully to problems related to isotropic elasticity, heat transfer, fluid flow *etc.*, it has been rarely used to analyse problems in anisotropic elasticity. According to author's knowledge, only two existing studies (Kobayashi *et al* 1986, Vable and Sikarskie 1988) are concerned with boundary element technique for anisotropic materials. Kobayashi *et al* (1986) studied the response of a transversely isotropic elastic half space subjected to transient surface loading by using the full space Green's function given by Payton (1982). Vable and Sikarskie (1988) considered elastostatic stress analysis of orthotropic plane problems by using the boundary element method. In author's opinion, the main reason for the lack of progress in the development of advanced boundary element codes for the analysis of a wide variety of practically useful boundary-value problems is the unavailability of a comprehensive set of Green's functions for transversely isotropic materials.

1.3 OBJECTIVES OF THE PRESENT STUDY

Based on the above literature review it is evident that a comprehensive treatment of static and dynamic Green's functions of homogeneous and multi-layered transversely isotropic media has not been reported in the literature. In addition,

the development of comprehensive boundary element computer codes capable of solving a variety of boundary-value problems related to homogeneous and multi-layered transversely isotropic media has also not been reported in the literature. Only idealised boundary-value problems such as the interaction between rigid disc and homogeneous transversely isotropic media have been considered in the past. In view of these observations the present thesis is directed towards the development of a complete solution package for Green's functions of homogeneous and multi-layered transversely isotropic media and the development of computer codes based on the boundary integral equation method for analysis of a wide variety of boundary-value problems. In order to achieve this goal, the following objectives are defined:

1. Derivation of explicit analytical solution for three-dimensional elastostatic Green's functions of a homogeneous transversely isotropic elastic half space. Implementation of the Green's functions in a computer code based on the indirect boundary element method for analysis of displacement, traction and mixed boundary-value problems.
2. Derivation of explicit analytical solutions for two-dimensional and three-dimensional dynamic (time-harmonic and transient) Green's functions of a homogeneous transversely isotropic elastic half space. Development of accurate numerical procedures for evaluation of Green's functions and the implementation of Green's functions in the boundary element code.
3. Development of a computationally efficient and numerically stable exact stiffness matrix procedure to numerically evaluate two- and three-dimensional Green's functions of multi-layered transversely isotropic half spaces.
4. Solutions of transversely isotropic elastic half spaces under selected internal loadings and the solution of selected boundary-value problems to investigate the influence of degree of anisotropy and other parameters on the response.

Table1.1 : Material constants ($\bar{c}_{ij} = c_{ij}/c_{44}$)

	$\bar{c}_{11}$	$\bar{c}_{12}$	$\bar{c}_{13}$	$\bar{c}_{33}$	$c_{44}(10^4 MN/m^2)$
Silty clay	2.11	0.43	0.47	2.58	2.70
Beryl rock	4.13	1.47	1.01	3.62	1.00
L/S layered soil	4.46	1.56	1.24	3.26	1.40
Clay I	4.70	1.70	1.20	3.30	0.01
Clay II	4.60	1.60	0.90	2.60	0.01
Isotropic[1]	3.00	1.00	1.00	3.00	0.99997
Apatite	2.52	0.20	1.00	2.11	6.63
Beryllium	1.80	0.16	0.09	2.07	16.20
Beryl	4.22	1.49	1.04	3.71	6.68
Cadmium	7.05	2.59	2.46	3.01	1.56
Cobalt	4.07	2.19	1.36	4.74	7.55
Ice(257K)	4.22	2.03	1.62	4.53	0.32
Hafnium	3.25	1.38	1.18	3.54	5.57
Magnesium	3.61	1.57	1.30	3.74	1.64
Rhenium	3.78	1.67	1.27	4.22	16.20
Titanium	3.47	1.97	1.48	3.88	4.67
Thallium	5.59	4.85	3.97	7.23	0.73
Yttrium	3.21	1.20	0.82	3.16	2.43
Zinc	4.17	0.78	1.26	1.57	3.96
E composite[2]	3.17	1.40	1.11	10.04	0.47
G composite[3]	2.02	0.68	0.07	21.17	0.41
Composite 1	1.99	0.99	0.44	11.15	7.80
Composite 2	2.00	1.00	0.86	23.00	0.07
Al_2O_3	6.76	2.86	2.86	4.90	5.0
SiC	2.97	0.56	0.33	3.34	16.9
nylon	2.52	0.90	1.56	7.69	0.0666

1: ν=0.25, μ=1.0
2: E glass/epoxy composite
3: Graphite/epoxy composite

Chapter 2

ELASTOSTATIC GREEN'S FUNCTIONS

2.1 GENERAL

The derivation of displacement and stress Green's functions corresponding to statically applied circular ring loads acting in the interior of a transversely isotropic elastic half space is considered in this Chapter. Initially, a set of general solutions are derived for equations governing elastostatic deformations of a transversely isotropic elastic medium by using Fourier expansion and Hankel integral transform with respect to circumferential and radial coordinates, respectively. These general solutions are used in the solution of boundary-value problems related to Green's functions. In the derivation of Green's functions, ring loads acting in radial, circumferential and vertical directions are considered. The circumferential distribution of the radial and vertical ring loads is of the form $\cos m\theta$ and that of the circumferential load is $\sin m\theta$. Green's function solutions presented in this Chapter appear in terms of Lipschitz-Hankel integrals involving products of Bessel functions of the first kind. These Green's functions will be used as the kernel functions of the boundary integral equation formulation presented in Chapter 3.

2.2 CONSTITUTIVE EQUATION

Consider a transversely isotropic elastic medium, with a Cartesian coordinate system (x, y, z) and a cylindrical polar coordinate system (r, θ, z) chosen such that the z-axis is parallel to the material axis of symmetry and normal to the stress free-surface as shown in Figure 2.1. The mechanical response of a transversely isotropic elastic medium is governed by five elastic constants $c_{11}, c_{12}, c_{13}, c_{33}$ and

c_{44} which relate stresses and strains referred to a rectangular Cartesian coordinate system in the following manner (Lekhnitskii 1963):

$$\sigma_{xx} = c_{11}\epsilon_{xx} + c_{12}\epsilon_{yy} + c_{13}\epsilon_{zz} \tag{2.1a}$$

$$\sigma_{yy} = c_{12}\epsilon_{xx} + c_{11}\epsilon_{yy} + c_{13}\epsilon_{zz} \tag{2.1b}$$

$$\sigma_{zz} = c_{13}\epsilon_{xx} + c_{13}\epsilon_{yy} + c_{33}\epsilon_{zz} \tag{2.1c}$$

$$\sigma_{xy} = (c_{11} - c_{12})\epsilon_{xy} \tag{2.1d}$$

$$\sigma_{yz} = 2c_{44}\epsilon_{yz} \tag{2.1e}$$

$$\sigma_{xz} = 2c_{44}\epsilon_{xz} \tag{2.1f}$$

Alternatively, the stresses and strains referred to a cylindrical polar coordinate system are related in the following manner:

$$\sigma_{rr} = c_{11}\epsilon_{rr} + c_{12}\epsilon_{\theta\theta} + c_{13}\epsilon_{zz} \tag{2.2a}$$

$$\sigma_{\theta\theta} = c_{12}\epsilon_{rr} + c_{11}\epsilon_{\theta\theta} + c_{13}\epsilon_{zz} \tag{2.2b}$$

$$\sigma_{zz} = c_{13}\epsilon_{rr} + c_{13}\epsilon_{\theta\theta} + c_{33}\epsilon_{zz} \tag{2.2c}$$

$$\sigma_{r\theta} = (c_{11} - c_{12})\epsilon_{r\theta} \tag{2.2d}$$

$$\sigma_{\theta z} = 2c_{44}\epsilon_{\theta z} \tag{2.2e}$$

$$\sigma_{rz} = 2c_{44}\epsilon_{rz} \tag{2.2f}$$

In geotechnical engineering practice Young's moduli E_v and E_h, Poisson's ratios ν_{hh}, ν_{hv} and ν_{vh} and the shear modulus G_{vh} are often used (Desai and Christian 1977) in place of the elastic moduli c_{ij} in eqn (2.1) or (2.2). Here, E_h and E_v are Young's moduli with respect to directions lying in the plane of isotropy (xy-plane) and perpendicular to it (z-axis); ν_{hh} is the Poisson's ratio that characterizes the transverse reduction in the plane of isotropy for the tension in the same plane; ν_{hv} is the Poisson's ratio that characterizes the transverse reduction in the plane of isotropy for the tension in a direction normal to it; and

G_{vh} is the shear modulus for the plane normal to the plane of isotropy. The five elastic constants $E_h, E_v, \nu_{hh}, \nu_{hv}$ and G_{vh} are related to c_{ij} in the following manner:

$$E_h = \frac{(c_{11} - c_{12})(c_{11}c_{33} + c_{12}c_{33} - 2c_{13}^2)}{c_{11}c_{33} - c_{13}^2} \tag{2.3a}$$

$$E_v = \frac{c_{11}c_{33} + c_{12}c_{33} - 2c_{13}^2}{c_{11} + c_{12}} \tag{2.3b}$$

$$\nu_{hh} = \frac{c_{12}c_{33} - c_{13}^2}{c_{11}c_{33} - c_{13}^2} \tag{2.3c}$$

$$\nu_{hv} = \frac{c_{13}}{c_{11} + c_{12}} \tag{2.3d}$$

$$G_{vh} = c_{44} \tag{2.3e}$$

and

$$\nu_{vh}/E_h = \nu_{hv}/E_v \tag{2.3f}$$

The positive definiteness of strain energy requires the following constraints (Payton, 1983) on material constants c_{ij}:

$$c_{11} > |c_{12}|, \quad (c_{11} + c_{12})c_{33} > 2c_{13}^2, \quad c_{44} > 0. \tag{2.4}$$

A set of nondimensional material parameters $\alpha, \beta, \kappa, \gamma$ and ς are introduced as defined below to simplify subsequent algebraic manipulations:

$$\alpha = \frac{c_{33}}{c_{44}}, \quad \beta = \frac{c_{11}}{c_{44}}, \quad \kappa = \frac{(c_{13} + c_{44})}{c_{44}}, \tag{2.5a}$$

$$\gamma = 1 + \alpha\beta - \kappa^2, \qquad \varsigma = \frac{(c_{11} - c_{12})}{2c_{44}} \tag{2.5b}$$

2.3 GOVERNING EQUATIONS AND GENERAL SOLUTIONS

It can be shown that (Green and Zerna, 1968), in the absence of body forces, the displacement and stress fields in a transversely isotropic linear elastic medium

subjected to a state of asymmetric deformations about the axis of elastic symmetry can be expressed in terms of three potential functions $\phi_i(r,\theta,z), i = 1,2,3$ which are solutions of

$$[\nabla^2 + \frac{\partial^2}{\partial z_i^2}]\phi_i(r,\theta,z) = 0, \quad i = 1,2,3 \tag{2.6}$$

where ∇^2 is a linear differential operator defined as,

$$\nabla^2 = \frac{\partial^2}{\partial r^2} + \frac{1}{r}\frac{\partial}{\partial r} + \frac{1}{r^2}\frac{\partial^2}{\partial \theta^2} \tag{2.7}$$

and

$$z_i = z/\sqrt{\nu_i}, \quad i = 1,2,3 \tag{2.8}$$

In eqn (2.8), ν_1 and ν_2 are the roots of the following equation

$$\beta\nu^2 - \gamma\nu + \alpha = 0 \tag{2.9a}$$

or

$$\nu_1 = \frac{\gamma + \sqrt{\gamma^2 - 4\alpha\beta}}{2\beta}, \qquad \nu_2 = \frac{\gamma - \sqrt{\gamma^2 - 4\alpha\beta}}{2\beta} \tag{2.9b}$$

and

$$\nu_3 = 1/\varsigma \tag{2.10}$$

The roots ν_1 and ν_2 may be real or complex conjugates depending on the values of the elastic constants c_{11}, c_{13}, c_{33} and c_{44}. Since the displacements and stresses must be real, the potential functions ϕ_1 and ϕ_2 are complex conjugates when ν_1 and ν_2 are complex and in addition it is necessary to specify that $\sqrt{\nu_1}$ and $\sqrt{\nu_2}$ always have positive real parts.

The displacement and stress components referred to a cylindrical polar coordinate system can be given by:

$$u_r = \frac{\partial}{\partial r}(\phi_1 + \phi_2) + \frac{1}{r}\frac{\partial \phi_3}{\partial \theta} \tag{2.11a}$$

$$u_\theta = \frac{1}{r}\frac{\partial}{\partial \theta}(\phi_1 + \phi_2) - \frac{\partial \phi_3}{\partial r} \tag{2.11b}$$

$$u_z = \frac{\partial}{\partial z}(k_1\phi_1 + k_2\phi_2) \tag{2.11c}$$

and

$$\frac{\sigma_{rr}}{c_{44}} = -[\lambda_1 \frac{\partial^2 \phi_1}{\partial z_1^2} + \lambda_2 \frac{\partial^2 \phi_2}{\partial z_2^2}] - \frac{2}{\nu_3}[(\triangle^2 - \frac{\partial^2}{\partial r^2})(\phi_1 + \phi_2) - \frac{\partial}{\partial r}(\frac{1}{r}\frac{\partial \phi_3}{\partial \theta})] \quad (2.12a)$$

$$\frac{\sigma_{\theta\theta}}{c_{44}} = -[\lambda_1 \frac{\partial^2 \phi_1}{\partial z_1^2} + \lambda_2 \frac{\partial^2 \phi_2}{\partial z_2^2}] - \frac{2}{\nu_3}[\frac{\partial^2}{\partial r^2}(\phi_1 + \phi_2) + \frac{\partial}{\partial r}(\frac{1}{r}\frac{\partial \phi_3}{\partial \theta})] \quad (2.12b)$$

$$\frac{\sigma_{zz}}{c_{44}} = \lambda_1 \nu_1 \frac{\partial^2 \phi_1}{\partial z_1^2} + \lambda_2 \nu_2 \frac{\partial^2 \phi_2}{\partial z_2^2} \quad (2.12c)$$

$$\frac{\sigma_{r\theta}}{c_{44}} = \frac{2}{\nu_3}(\frac{1}{r}\frac{\partial^2}{\partial r \partial \theta} - \frac{1}{r^2}\frac{\partial}{\partial \theta})(\phi_1 + \phi_2) + \frac{1}{\nu_3}(\frac{2}{r}\frac{\partial}{\partial r} + \frac{2}{r^2}\frac{\partial^2}{\partial \theta^2} + \frac{\partial^2}{\partial z_3^2})\phi_3 \quad (2.12d)$$

$$\frac{\sigma_{\theta z}}{c_{44}} = \frac{1}{r}\frac{\partial}{\partial \theta}(\lambda_1 \sqrt{\nu_1}\frac{\partial \phi_1}{\partial z_1} + \lambda_2 \sqrt{\nu_2}\frac{\partial \phi_2}{\partial z_2}) - \frac{1}{\sqrt{\nu_3}}\frac{\partial^2 \phi_3}{\partial r \partial z_3} \quad (2.12e)$$

$$\frac{\sigma_{rz}}{c_{44}} = \frac{\partial}{\partial r}(\lambda_1 \sqrt{\nu_1}\frac{\partial \phi_1}{\partial z_1} + \lambda_2 \sqrt{\nu_2}\frac{\partial \phi_2}{\partial z_2}) + \frac{1}{\sqrt{\nu_3}}\frac{1}{r}\frac{\partial^2 \phi_3}{\partial \theta \partial z_3} \quad (2.12f)$$

where

$$k_i = \frac{\beta \nu_i - 1}{\kappa}, \quad \lambda_i = \frac{1 + k_i}{\nu_i}, \qquad i = 1, 2 \quad (2.13)$$

In order to determine general solutions for potential functions $\phi_i(r, \theta, z)$, $i = 1, 2, 3$ governed by eqn(2.6) the following representation is used:

$$\phi_i(r, \theta, z) = \sum_{m=0}^{\infty} [\phi_{im}(r, z) \cos m\theta + \phi_{im}^*(r, z) \sin m\theta], \quad i = 1, 2 \quad (2.14a)$$

$$\phi_3(r, \theta, z) = \sum_{m=0}^{\infty} [\phi_{3m}(r, z) \sin m\theta - \phi_{3m}^*(r, z) \cos m\theta] \quad (2.14b)$$

where $\phi_{im}(i = 1, 2, 3)$ yield deformations which are symmetric with respect to $\theta = 0$ and while $\phi_{im}^*(i = 1, 2, 3)$ correspond to antisymmetric deformations for the mth harmonic. In the subsequent analysis only the symmetric components $\phi_{im}(i = 1, 2, 3)$ are considered without loss of generality. It is noted that the solutions corresponding to $\phi_{im}^*(i = 1, 2, 3)$ can be obtained by making the substitutions $\phi_{im} \rightarrow \phi_{im}^*(i = 1, 2, 3), \cos m\theta \rightarrow \sin m\theta$ and $\sin m\theta \rightarrow -\cos m\theta$, respectively.

Since the problems under consideration involve domains that extend to infinity in the radial direction, it is natural to introduce Hankel integral transform (Sneddon 1951) with respect to the radial coordinate as,

$$\breve{\phi}_{im}(\lambda, z) = \int_0^\infty \phi_{im}(r, z) J_m(\lambda r) r dr \tag{2.15a}$$

$$\phi_{im}(r, z) = \int_0^\infty \breve{\phi}_{im}(\lambda, z) J_m(\lambda r) \lambda d\lambda \qquad i = 1, 2, 3 \tag{2.15b}$$

In eqn (2.15), J_m denotes the Bessel function of the first kind of order m; λ is the Hankel transform parameter.

Substitution of eqn (2.14) and eqn (2.15) to eqn (2.6) together with the orthogonality of trigonometric function result in the following general solutions for the mth Fourier harmonic of the three potential functions:

$$\phi_{im}(r, z) = \int_0^\infty [A_{im}(\lambda) e^{\lambda z_i} + B_{im}(\lambda) e^{-\lambda z_i}] \lambda J_m(\lambda r) d\lambda, \quad i = 1, 2, 3. \tag{2.16}$$

where $A_{im}(\lambda)$ and $B_{im}(\lambda)$ are arbitrary functions to be determined by using given boundary conditions.

Equations (2.11) and (2.12) together with eqns (2.14) and (2.16) represent the complete general solutions of displacements and stresses for arbitrary asymmetric deformations of a transversely isotropic elastic medium.

2.4 BOUNDARY-VALUE PROBLEMS

In the derivation of Green's functions, a set of ring loads with radius 's' acting in radial, circumferential and vertical directions are considered as shown in Figure 2.2. The circumferential distribution of the radial and vertical ring loads is given by $\cos m\theta$ and that of the circumferential load is $\sin m\theta$. The explicit solution for the Green's functions can be derived by defining a fictitious plane at the level of loading ($z = z'$) as shown in Fig 2.1 and treating the internally

loaded half space as a two-domain problem (Chan *et al.* 1974 and Selvadurai and Rajapakse 1985). In view of the prescribed circumferential distribution of the three ring loads only the term corresponding to the mth Fourier harmonic in eqn (2.14) needs to be considered. The general solutions corresponding to each domain are given by eqns (2.11) and (2.12) together with eqn (2.16). The Fourier harmonic of the displacements and stresses in each domain is denoted by $u_{im}^{(j)}(i = r, \theta, z; j = 1, 2)$ and $\sigma_{ilm}^{(j)}(i, l = r, \theta, z; j = 1, 2)$, respectively. The superscript j denotes the domain number where domain '1' is bounded by $0 \leq z \leq z'$ and domain '2' by $z' \leq z < \infty$.

The boundary and continuity conditions corresponding to the three boundary value problems involving the internally-loaded half space can be expressed as,

$$\sigma_{izm}^{(1)}(r, 0) = 0, \qquad i = r, \theta, z \tag{2.17}$$

$$u_{im}^{(1)}(r, z') - u_{im}^{(2)}(r, z') = 0, \quad i = r, \theta, z \tag{2.18}$$

$$\sigma_{izm}^{(1)}(r, z') - \sigma_{izm}^{(2)}(r, z') = F_i, \quad i = r, \theta, z. \tag{2.19}$$

For the radial loading case,

$$F_r = \delta(r - s) \tag{2.20a}$$

$$F_\theta = F_z = 0 \tag{2.20b}$$

where the δ denotes Dirac's delta function. For the circumferential loading,

$$F_r = F_z = 0 \tag{2.21a}$$

$$F_\theta = \delta(r - s) \tag{2.21b}$$

For the vertical loading,

$$F_r = F_\theta = 0 \tag{2.22a}$$

$$F_z = \delta(r - s) \tag{2.22b}$$

Substitution of general solutions for displacements and stresses given by eqns (2.11), (2.12) and (2.16) together with eqns (2.17)-(2.22) yields a set of linear simultaneous algebraic equations to determine the arbitrary functions $A_{im}^{(j)}(\lambda)$ and $B_{im}^{(j)}(\lambda)$ $(i = 1,2,3; j = 1,2)$ corresponding to the two domains. Note that $A_{im}^{(2)}(\lambda) \equiv 0$ to ensure the regularity of displacements and stresses for domain '2' when $z \to \infty$.

2.5 DISPLACEMENT GREEN'S FUNCTIONS

The explicit solutions for displacement Green's function $G_{ij}^{m}(r,z;s,z')$ denoting the mth Fourier harmonic of the displacement in the i-direction $(i = r,\theta,z)$ at the point (r,z) due to a ring load in the j-direction $(j = r,\theta,z)$ through the point (s,z') with circumferential variation $\cos m\theta$ for $j = r,z$ and $\sin m\theta$ for $j = \theta$ can be expressed in the following form:

$$\begin{aligned} G_{rr}^{m}(r,z;s,z') &= \bar{\mu}_1 \sum_{j=1}^{6} d_{3j}[I_j(m-1,m+1;0) - I_j(m+1,m+1;0) \\ &\quad - I_j(m-1,m-1;0) + I_j(m+1,m-1;0)] \\ &\quad + \bar{\mu}_2 \sum_{j=7}^{8} 4m^2 d_{3j} I_j^*(m,m;-2)/s \end{aligned} \tag{2.23a}$$

$$\begin{aligned} G_{\theta r}^{m}(r,z;s,z') &= -\bar{\mu}_1 \sum_{j=1}^{6} 2m d_{3j}[I_j^*(m,m+1;-1) - I_j^*(m,m-1;-1)] \\ &\quad - \bar{\mu}_2 \sum_{j=7}^{8} 2m d_{3j}[\bar{I}_j(m+1,m;-1) - \bar{I}_j(m-1,m;-1)] \end{aligned} \tag{2.23b}$$

$$G_{zr}^{m}(r,z;s,z') = 2\bar{\mu}_1 k_1 k_2 \sum_{j=1}^{6} d_{2j}[I_j(m,m+1;0) - I_j(m,m-1;0)] \tag{2.23c}$$

$$\begin{aligned} G_{r\theta}^{m}(r,z;s,z') &= \bar{\mu}_1 \sum_{j=1}^{6} 2m d_{3j}[\bar{I}_j(m-1,m;-1) - \bar{I}_j(m+1,m;-1)] \\ &\quad + \bar{\mu}_2 \sum_{j=7}^{8} 2m d_{3j}[I_j^*(m,m+1;-1) - I_j^*(m,m-1;-1)] \end{aligned} \tag{2.24a}$$

$$G^m_{\theta\theta}(r,z;s,z') = -\bar{\mu}_1 \sum_{j=1}^{6} 4m^2 d_{3j} I^*_j(m,m;-2)/s - \bar{\mu}_2 \sum_{j=7}^{8} [I_j(m+1,m+1;0)$$
$$- I_j(m-1,m+1;0) - I_j(m+1,m-1;0) + I_j(m-1,m-1;0)] \quad (2.24b)$$

$$G^m_{z\theta}(r,z;s,z') = 2\bar{\mu}_1 k_1 k_2 \sum_{j=1}^{6} 2m d_{2j} \bar{I}_j(m,m;-1) \quad (2.24c)$$

$$G^m_{rz}(r,z;s,z') = 2\bar{\mu}_1 \sum_{j=1}^{6} d_{1j} [I_j(m-1,m;0) - I_j(m+1,m;0) \quad (2.25a)$$

$$G^m_{\theta z}(r,z;s,z') = -2\bar{\mu}_1 \sum_{j=1}^{6} 2m d_{1j} I^*_j(m,m;-1) \quad (2.25b)$$

$$G^m_{zz}(r,z;s,z') = 4\bar{\mu}_1 \sum_{j=1}^{6} \bar{\nu}_j d_{4j} I_j(m,m;0) \quad (2.25c)$$

where

$$\bar{\mu}_1 = \frac{s}{8c_{44}(k_1-k_2)}, \quad \bar{\mu}_2 = \frac{s\sqrt{\nu_3}}{8c_{44}}, \quad \mu_1 = \frac{1}{k_1-k_2}$$
$$\mu_2 = \frac{1}{\sqrt{\nu_2}-\sqrt{\nu_1}}, \quad \mu_3 = \sqrt{\nu_1}+\sqrt{\nu_2}, \quad \mu_4 = \frac{1+k_1}{1+k_2} \quad (2.26)$$

$$d_{11} = d_{21} = -d_{12} = -d_{22} = \frac{z'-z}{|z'-z|} \quad (2.27a)$$

$$d_{13} = d_{14} = -d_{23} = -d_{24} = \mu_2\mu_3 \quad (2.27b)$$

$$d_{15} = -d_{25}k_2/k_1 = -2\mu_2\sqrt{\nu_1}/\mu_4 \quad (2.28a)$$

$$d_{16} = -d_{26}k_1/k_2 = -2\mu_2\mu_4\sqrt{\nu_2} \quad (2.28b)$$

$$d_{31} = k_2\sqrt{\nu_1}, \quad d_{32} = -k_1\sqrt{\nu_2}, \quad d_{33} = \mu_2\mu_3 k_2\sqrt{\nu_1} \quad (2.29a)$$

$$d_{34} = \mu_2\mu_3 k_1\sqrt{\nu_2}, \quad d_{35} = -2\mu_2\sqrt{\nu_1\nu_2}/\mu_4 \quad (2.29b)$$

$$d_{36} = -2\mu_2\mu_4 k_2\sqrt{\nu_1\nu_2}, \quad d_{37} = d_{38} = 1 \quad (2.29c)$$

$$d_{41} = -d_{42} = 1, \quad d_{43} = d_{44} = -\mu_2\mu_3 \quad (2.30a)$$

$$d_{45} = 2\mu_2\sqrt{\nu_1}/\mu_4, \quad d_{46} = 2\mu_2\mu_4\sqrt{\nu_2} \quad (2.30b)$$

$$\bar{\nu}_j = \frac{k_1}{\sqrt{\nu_1}}: \quad j = 1,3,5; \qquad \bar{\nu}_j = \frac{k_2}{\sqrt{\nu_2}}: \quad j = 2,4,6 \quad (2.31)$$

$$I^*_j(m,n;l) = I_j(m,n;l)/r \quad (2.32a)$$

$$\bar{I}_j(m,n;l) = I_j(m,n;l)/s, \quad j = 1,2,...,8 \tag{2.32b}$$

and I_j are in the form of Lipschitz-Hankel integrals involving the product of Bessel functions of the first kind and can be expressed as

$$I_1(m,n;p) = \int_0^\infty J_m(\lambda r)J_n(\lambda s)\lambda^p e^{-\lambda|z_1-z_1'|}d\lambda \tag{2.33a}$$

$$I_2(m,n;p) = \int_0^\infty J_m(\lambda r)J_n(\lambda s)\lambda^p e^{-\lambda|z_2-z_2'|}d\lambda \tag{2.33b}$$

$$I_3(m,n;p) = \int_0^\infty J_m(\lambda r)J_n(\lambda s)\lambda^p e^{-\lambda(z_1+z_1')}d\lambda \tag{2.33c}$$

$$I_4(m,n;p) = \int_0^\infty J_m(\lambda r)J_n(\lambda s)\lambda^p e^{-\lambda(z_2+z_2')}d\lambda \tag{2.33d}$$

$$I_5(m,n;p) = \int_0^\infty J_m(\lambda r)J_n(\lambda s)\lambda^p e^{-\lambda(z_1+z_2')}d\lambda \tag{2.33e}$$

$$I_6(m,n;p) = \int_0^\infty J_m(\lambda r)J_n(\lambda s)\lambda^p e^{-\lambda(z_1'+z_2)}d\lambda \tag{2.33f}$$

$$I_7(m,n;p) = \int_0^\infty J_m(\lambda r)J_n(\lambda s)\lambda^p e^{-\lambda|z_3-z_3'|}d\lambda \tag{2.33g}$$

$$I_8(m,n;p) = \int_0^\infty J_m(\lambda r)J_n(\lambda s)\lambda^p e^{-\lambda(z_3+z_3')}d\lambda \tag{2.33h}$$

For the case where deformations are also axisymmetric (m=0), ring loads are considered only in the r- and z-directions and the displacement in the θ-direction is equal to zero. The relevant displacement Green's functions are given by eqns (2.23) and (2.25) with m=0 and $G_{\theta r} = G_{\theta z} \equiv 0$.

2.6 STRESS GREEN'S FUNCTIONS

Let $\sigma_{ilj}^m(r,z;s,z')$ denotes the mth Fourier harmonic of the stress component $\sigma_{il}(i,l = r,\theta,z)$ at the point (r,z) due to a ring load in the j-direction $(j = r,\theta,z)$ through the point (s,z'). The circumferential variations of the loads are prescribed as in Fig 2.2. The explicit solutions for $\sigma_{ilj}^m(r,z;s,z')$ are given

below:

$$\sigma^m_{rrr}(r,z;s,z') = \bar{\mu}_1 \sum_{j=1}^{6} d_{3j}\{\bar{\lambda}_1(1+m)[I^*_j(m+1,m+1;0)-$$
$$I^*_j(m+1,m-1;0)] + \bar{\lambda}_1(1-m)[I^*_j(m-1,m-1;0) - I^*_j(m-1,m+1;0)]$$
$$+ 2\lambda_j[I_j(m,m-1;1) - I_j(m,m+1;1)]\}-$$
$$\bar{\mu}_2 \sum_{j=7}^{8} 2m\bar{\lambda}_1[(1+m)I^*_j(m+1,m;-1) + (1-m)I^*_j(m-1,m;-1)]/s \quad (2.34a)$$

$$\sigma^m_{\theta\theta r}(r,z;s,z') = \bar{\mu}_1 \sum_{j=1}^{6} d_{3j}\{\bar{\lambda}_1(1+m)[I^*_j(m+1,m-1;0) - I^*_j(m+1,m+1;0)]$$
$$+ \bar{\lambda}_1(1-m)[I^*_j(m-1,m+1;0) - I^*_j(m-1,m-1;0)$$
$$+ 2(\bar{\lambda}_1 - \lambda_j)[I^*_j(m,m+1;1) - I^*_j(m,m-1;1)]\}+$$
$$\bar{\mu}_2 \sum_{j=7}^{8} 2m\bar{\lambda}_1[(1+m)I^*_j(m+1,m;-1) + (1-m)I^*_j(m-1,m;-1)]/s \quad (2.34b)$$

$$\sigma^m_{zzr}(r,z;s,z') = 2\bar{\mu}_1 \sum_{j=1}^{6}(1+\omega_j)d_{3j}[I_j(m,m+1;1) - I_j(m,m-1;1)] \quad (2.34c)$$

$$\sigma^m_{r\theta r}(r,z;s,z') = \bar{\mu}_1 \sum_{j=1}^{6} d_{3j}\{\bar{\lambda}_1(1+m)[I^*_j(m+1,m+1;0)$$
$$- I^*_j(m+1,m-1;0)] + \bar{\lambda}_1(1-m)[I^*_j(m-1,m+1;0)$$
$$- I^*_j(m-1,m-1;0)]\} - \bar{\mu}_2 \sum_{j=7}^{8} 2md_{3j}[\bar{\lambda}_1\bar{I}_j(m,m;0)$$
$$+ \lambda_1(1+m)I^*_j(m+1,m;-1) - \bar{\lambda}_1(1-m)I^*_j(m-1,m;-1)]/s \quad (2.34d)$$

$$\sigma^m_{\theta zr}(r,z;s,z') = 2\bar{\mu}_1 \sum_{j=1}^{6} md_{5j}\beta_j[I^*_j(m,m-1;0) - I^*_j(m,m+1;0)]$$
$$+ \bar{\mu}_1 \sum_{j=7}^{8} 2md_{5j}[\bar{I}_j(m+1,m;0) - \bar{I}_j(m-1,m;0)]/\mu_1 \quad (2.34e)$$

$$\sigma^m_{zrr}(r,z;s,z') = \bar{\mu}_1 \sum_{j=1}^{6} d_{5j}\beta_j[I_j(m-1,m+1;1) - I_j(m+1,m+1;1)$$
$$- I_j(m-1,m-1;1)] + I_j(m+1,m-1;1)+$$

$$\bar{\mu}_1 \sum_{j=7}^{8} 4m^2 d_{5j} I_j^*(m,m;-1)/s\mu_1 \tag{2.34f}$$

$$\sigma_{rr\theta}^m(r,z;s,z') = \bar{\mu}_1 \sum_{j=1}^{6} 2md_{3j}[\bar{\lambda}_1(1+m)I_j^*(m+1,m;-1)/s$$
$$- \bar{\lambda}_1(1-m)I_j^*(m-1,m;-1)/s - 2\lambda_j \bar{I}_j(m,m;0)]$$
$$+ \bar{\mu}_2 \sum_{j=7}^{8} 2m\bar{\lambda}_1\{(1+m)[I_j^*(m+1,m-1;0) - I_j^*(m+1,m+1;0)]$$
$$+ (1-m)[I_j^*(m-1,m-1;0) - I_j^*(m-1,m+1;0)]\} \tag{2.35a}$$

$$\sigma_{\theta\theta\theta}^m(r,z;s,z') = \bar{\mu}_1 \sum_{j=1}^{6} 2md_{3j}[\bar{\lambda}_1(1-m)I_j^*(m-1,m;-1)/s$$
$$- \bar{\lambda}_1(1+m)I_j^*(m+1,m;-1)/s + 2(\bar{\lambda}_1 - \lambda_j)\bar{I}_j(m,m;0)]$$
$$+ \bar{\mu}_2 \sum_{j=7}^{8} \lambda_1\{(1+m)[I_j^*(m+1,m+1;0) - I_j^*(m+1,m-1;0)]$$
$$+ (1-m)[I_j^*(m-1,m+1;0) - I_j^*(m-1,m-1;0)]\} \tag{2.35b}$$

$$\sigma_{zz\theta}^m(r,z;s,z') = 2\bar{\mu}_1 \sum_{j=1}^{6} 2m(1+\omega_j)d_{3j}\bar{I}_j(m,m;0) \tag{2.35c}$$

$$\sigma_{r\theta\theta}^m(r,z;s,z') = \bar{\mu}_1 \sum_{j=1}^{6} 2md_{3j}[\bar{\lambda}_1(1+m)I_j^*(m+1,m;-1)/s + \bar{\lambda}_1(1-m)$$
$$I_j^*(m-1,m;-1)/s] + \bar{\mu}_2 \sum_{j=7}^{8} d_{3j}\{\bar{\lambda}_1[I_j(m,m+1;1) - I_j(m,m-1;1)]$$
$$+ \bar{\lambda}_1(1+m)[I_j^*(m+1,m-1;0) - I_j^*(m+1,m+1;0)]$$
$$+ \bar{\lambda}_1(1-m)[I_j^*(m-1,m+1;0) - I_j^*(m-1,m-1;0)]\} \tag{2.35d}$$

$$\sigma_{\theta z\theta}^m(r,z;s,z') = -\bar{\mu}_1 \sum_{j=1}^{6} 4m^2 d_{5j}\lambda_j I_j^*(m,m;-1)/s + \bar{\mu}_1 \sum_{j=7}^{8} d_{5j}[I_j(m+1,m+1;1)$$
$$+ I_j(m-1,m-1;1) - I_j(m+1,m-1;1) - I_j(m-1,m+1;1)]/\mu_1 \tag{2.35e}$$

$$\sigma_{zr\theta}^m(r,z;s,z') = \bar{\mu}_1 \sum_{j=1}^{6} 2md_{5j}\lambda_j[\bar{I}_j(m-1,m;0) - \bar{I}_j(m+1,m;0)]$$
$$+ \bar{\mu}_1 \sum_{j=7}^{8} 2md_{5j}[I_j^*(m,m+1;0) - I_j^*(m,m-1;0)]/\mu_1 \tag{2.35f}$$

$$\sigma^m_{rrz}(r,z;s,z') = 2\bar{\mu}_1 \sum_{j=1}^{6} d_{1j}[\bar{\lambda}_1(1+m)I^*_j(m+1,m;0)$$
$$- \bar{\lambda}_1(1-m)I^*_j(m-1,m;0) - 2\lambda_j I_j(m,m;1)] \tag{2.36a}$$

$$\sigma^m_{\theta\theta z}(r,z;s,z') = 2\bar{\mu}_1 \sum_{j=1}^{6} d_{1j}[2(\bar{\lambda}_1 - \lambda_j)I_j(m,m;1)$$
$$- \bar{\lambda}_1(1+m)I^*_j(m+1,m;0) + \bar{\lambda}_1(1-m)I^*_j(m-1,m;0)] \tag{2.36b}$$

$$\sigma^m_{zzz}(r,z;s,z') = 4\bar{\mu}_1 \sum_{j=1}^{6} d_{1j}(1+\omega_j)I_j(m,m;1) \tag{2.36c}$$

$$\sigma^m_{r\theta z}(r,z;s,z') = 2\bar{\mu}_1 \sum_{j=1}^{6} d_{1j}[\bar{\lambda}_1(1+m)I^*_j(m+1,m;0)$$
$$+ \bar{\lambda}_1(1-m)I^*_j(m-1,m;0)] \tag{2.36d}$$

$$\sigma^m_{\theta zz}(r,z;s,z') = -4\bar{\mu}_1 \sum_{j=1}^{6} m d_{4j}\beta_j I^*_j(m,m;0) \tag{2.36e}$$

$$\sigma^m_{zrz}(r,z;s,z') = 2\bar{\mu}_1 \sum_{j=1}^{6} d_{4j}\beta_j[I_j(m-1,m;1) - I_j(m+1,m;1)] \tag{2.36f}$$

where

$$d_{51} = k_2\alpha\sqrt{\nu_1}, \quad d_{52} = -k_1\alpha\sqrt{\nu_2}, \quad d_{53} = -\mu_2\mu_3 k_2\sqrt{\nu_1} \tag{2.37a}$$

$$d_{54} = -\mu_2\mu_3 k_1\sqrt{\nu_2}, \qquad d_{55} = 2\mu_2 k_1\sqrt{\nu_1\nu_2}/\mu_4 \tag{2.37b}$$

$$d_{56} = 2\mu_2\mu_4 k_2\sqrt{\nu_1\nu_2}, \qquad d_{57} = \frac{z'-z}{|z'-z|}, \qquad d_{58} = -1 \tag{2.37c}$$

$$\bar{\lambda}_1 = \frac{c_{11}-c_{12}}{c_{44}}, \quad \bar{\lambda}_2 = \frac{1+k_1}{\nu_1}, \quad \bar{\lambda}_3 = \frac{1+k_2}{\nu_2} \tag{2.38a}$$

$$\bar{\lambda}_4 = \frac{1+k_1}{\sqrt{\nu_1}}, \qquad \bar{\lambda}_5 = \frac{1+k_2}{\sqrt{\nu_2}} \tag{2.38b}$$

$$\lambda_j = \bar{\lambda}_2, \quad \omega_j = k_1, \quad \beta_j = \bar{\lambda}_4 : \qquad j = 1,3,5 \tag{2.39a}$$

$$\lambda_j = \bar{\lambda}_3, \quad \omega_j = k_2, \quad \beta_j = \bar{\lambda}_5 : \qquad j = 2,4,6 \tag{2.39b}$$

The expressions for stress Green's functions corresponding to axisymmetric deformations can be obtained from eqns (2.34) and (2.36) with $m = 0$ and $\sigma^0_{r\theta j} = \sigma^0_{\theta z j} \equiv 0 \quad (j = r, z)$.

Note that the displacement and stress Green's functions corresponding to a transversely isotropic full space can be directly obtained from eqns (2.23)-(2.25) and (2.34)-(2.36) through an appropriate limit procedure. It is noted that the displacement and stress Green's functions appear in terms of Lipschitz-Hankel type integrals and can be expressed in terms of elliptic integrals (Easton *et al.* 1955) and subsequently evaluated by using special mathmatical software. This procedure greatly enhances the numerical accuracy and efficiency when compared to direct numerical integration of infinite integrals.

2.7 GENERAL SOLUTIONS FOR A DEGENERATE CASE

A degenerate case occurs in the elastostatic solutions of transversely isotropic media when the material constants c_{ij} obey the following relationship:

$$\sqrt{\alpha\beta} - \kappa - 1 = 0 \tag{2.40}$$

resulting in

$$\nu_1 = \nu_2 \tag{2.41}$$

It is noted that solutions given by eqns (2.23)-(2.25) and (2.34)-(2.36) under this degenerate condition would be singular.

In order to derive proper general solutions for a transversely isotropic medium whose elastic constants obey the relation given by eqn (2.40), the following potential function representations are introduced:

$$u_r = \frac{\partial \phi_1}{\partial r} + \frac{\partial^2 \phi_2}{\partial r \partial z} + \frac{1}{r}\frac{\partial \phi_3}{\partial \theta} \tag{2.42a}$$

$$u_\theta = \frac{1}{r}\frac{\partial \phi_1}{\partial \theta} + \frac{1}{r}\frac{\partial^2 \phi_2}{\partial \theta \partial z} - \frac{\partial \phi_3}{\partial r} \tag{2.42b}$$

$$u_z = a_1 \frac{\partial \phi_1}{\partial z} + a_2 \nabla^2 \phi_2 + a_3 \frac{\partial^2 \phi_3}{\partial z^2} \tag{2.42c}$$

where the coefficients a_1, a_2 and a_3 are defined as

$$a_1 = \frac{\beta\nu_1 - 1}{\alpha + 1}, \quad a_2 = -\frac{\beta}{\alpha + 1}, \quad a_3 = -\frac{1}{\alpha + 1} \tag{2.43}$$

and ν_1 is the root of eqn (2.9a); α and β are nondimensional material parameters defined in eqn (2.5) and the differential operator ∇^2 is defined in eqn (2.7). Substitution of eqn (2.42) into the governing equations (2.6) together with the applications of Fourier expansion as defined by eqn (2.14) and Hankel integral transform as defined by eqn (2.15) result in the following general solutions for the mth Fourier harmonic of the potential functions,

$$\phi_{im}(r,z) = \int_0^\infty [A_{im}(\lambda)e^{\lambda z_i} + B_{im}(\lambda)e^{-\lambda z_i}]\lambda J_n(\lambda r)d\lambda \quad i = 1,3 \tag{2.44}$$

$$\phi_{2m}(r,z) = \int_0^\infty \{[A_{2m}(\lambda) + z_1 C_{2m}(\lambda)]e^{\lambda z_1} + [B_{2m}(\lambda) + z_1 D_{2m}(\lambda)]e^{-\lambda z_1}\}\lambda J_n(\lambda r)d\lambda \tag{2.45}$$

where z_i is defined in eqn (2.8) and ν_3 is given by eqn (2.10). $A_{im}(\lambda), B_{im}(\lambda)(i = 1,2,3), C_{2m}(\lambda)$ and $D_{2m}(\lambda)$ denote the arbitrary functions.

The general solutions of displacement and stress components can be obtained by substituting eqns (2.44) and (2.45) into the eqns (2.42) and (2.2). Thereafter the Green's functions of displacement and stress can be derived by using a procedure identical to that described in Sections 2.4-2.6.

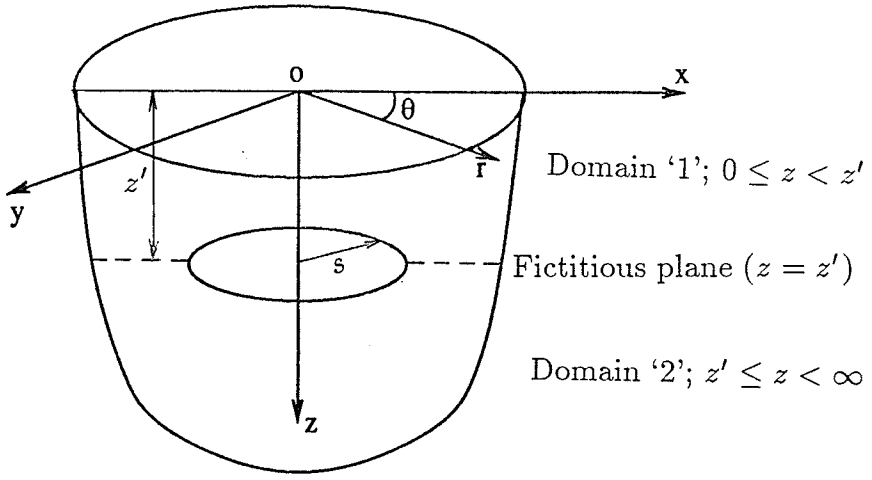

Figure 2.1 Definition of coordinate systems and domains

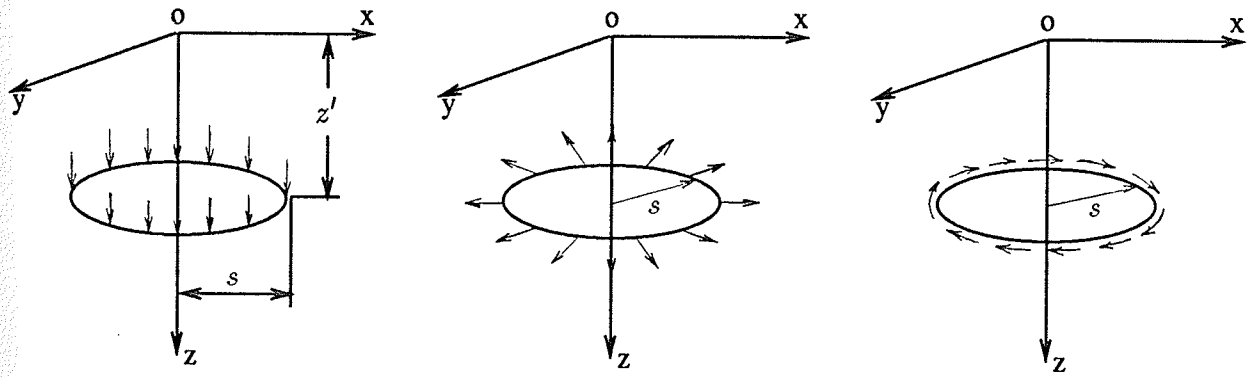

Figure 2.2 Internal loading configuration considered in the derivation of 3-D Green's functions

Chapter 3

ELASTOSTATIC BOUNDARY-VALUE PROBLEMS

3.1 GENERAL

The development of an indirect boundary integral equation method based on Green's functions derived in Chapter 2 is considered in this Chapter for analysis of a variety of three-dimensional elastostatic boundary-value problems related to a homogeneous transversely isotropic elastic half space. Consider a transversely isotropic elastic half space where a volume V bounded by an axisymmetric surface S is defined as shown in Fig 3.1. A cylindrical polar coordinate system (r, θ, z) is defined at the free surface level such that the z-axis coincides with the axis of symmetry of V. If V is a rigid inclusion then displacements on S are prescribed and a displacement boundary-value problem can be defined for the semi-infinite transversely isotropic domain V_c exterior to V. If V is a cavity subjected to pressure then a traction boundary-value problem can be defined for the domain V_c. A more general situation exists when displacements are specified over a part of S denoted by S_1 and tractions are specified over the remainder of S denoted by S_2 (Fig 3.1). In this case a mixed boundary-value problem can be defined for domain V_c. Examples of the mixed problem are situations where loss of contact exists over a portion of the contact surface of an inclusion in an elastic medium or the case of an inclusion where yielding occurs along the contact surface when tractions exceed prescribed limiting values. These boundary-value problems can be formulated in terms of a system of non-singular integral equations by generalizing the indirect boundary integral equation approach proposed by Ohsaki (1973) to study the response of a rigid body embedded in an isotropic elastic medium. The kernel functions of integral equations are displacement and traction Green's functions presented in Chapter 2. A more complicated situation arises when V consists of a different elastic material. For example, the case

of load diffusion from an elastic bar into a transversely isotropic elastic half-space. A solution to this problem is presented by developing a coupled variational-boundary integral equation formulation.

3.2 TRACTION BOUNDARY-VALUE PROBLEMS

3.2.1 Formulation

In the ensuing analysis a detailed solution procedure for a traction boundary-value problem is presented. Consider a situation where tractions are prescribed on a surface S as given below:

$$T_i(r,\theta,z) = \bar{T}_{im}(r,z) f_{im}(\theta), \qquad (r,\theta,z) \in S \tag{3.1}$$

In eqn (3.1), $i = r,\theta,z$ together with $f_{rm}(\theta) = f_{zm}(\theta) = \cos m\theta$ and $f_{\theta m}(\theta) = \sin m\theta$; $\bar{T}_{im}(r,z)$ denotes the prescribed value of traction on the generating curve of S.

An exact solution of domain V_c subjected to the above boundary condition on an arbitrary axisymmetric surface S is mathematically intractable. Alternatively, an indirect approach which exactly satisfies the governing equations of V_c and boundary conditions on S can be developed by considering a uniform (undisturbed) transversely isotropic elastic half space V^* as shown in Fig 3.2. An axisymmetric surface $\bar{S}$ which is identical to S in Fig 3.1 is defined in V^*. Interior to $\bar{S}$, another axisymmetric surface S' is defined. A set of forces with intensity $B_i(r,z) f_{im}(\theta)$ is applied on S' such that tractions on $\bar{S}$ are given by eqn (3.1). Under these conditions the solution of domain V^* exterior to $\bar{S}$ is identical to that of V_c of the original problem. The force intensities $B_i(r,z)$ are governed by the following Fredholm integral equations of the first kind:

$$\int_{S'} H_{ij}^m(r,z;r',z') B_j(r',z') r' dS' = \bar{T}_{im}(r,z), \qquad (r,z) \in S, \quad (r',z') \in S' \tag{3.2}$$

where indices $i,j = r,\theta,z$ and summation is implied on j. In addition, $H_{ij}^m(r,z;r',z')$ denotes the traction Green's function which can be expressed in terms of stress

Green's functions given by eqns (2.34)-(2.36) and unit normals of S. Note that in eqn (3.2) S' refers to the generating curve of the surface S'.

The unknown Fourier component of displacement on $\bar{S}$, denoted by $u_{im}(r,z)$, can be expressed as:

$$\int_{S'} G^m_{ij}(r,z;r',z')B_j(r',z')r'dS' = u_{im}(r,z). \tag{3.3}$$

In view of the complexity of the Green's functions H^m_{ij}, eqns (3.2) are solved numerically. A discrete version of eqn (3.2) with respect to M and M' nodal points on $\bar{S}$ and S', respectively, can be expressed as:

$$\mathbf{QB} = \mathbf{R} \tag{3.4}$$

where

$$\mathbf{Q} = \mathbf{H} \tag{3.5}$$

$$\mathbf{H} = \begin{pmatrix} \bar{\mathbf{H}}_{rr} & \bar{\mathbf{H}}_{r\theta} & \bar{\mathbf{H}}_{rz} \\ \bar{\mathbf{H}}_{\theta r} & \bar{\mathbf{H}}_{\theta\theta} & \bar{\mathbf{H}}_{\theta z} \\ \bar{\mathbf{H}}_{zr} & \bar{\mathbf{H}}_{z\theta} & \bar{\mathbf{H}}_{zz} \end{pmatrix}_{3M\times 3M'} \tag{3.6a}$$

$$\bar{\mathbf{H}}_{pq} = [H^m_{pq}(r,z;r',z')r'\triangle S']_{M\times M'}, \quad p,q = r,\theta,z \tag{3.6b}$$

$$\mathbf{B} = < \mathbf{B}_r(r',z') \quad \mathbf{B}_\theta(r',z') \quad \mathbf{B}_z(r',z') >^T \tag{3.7a}$$

$$\mathbf{R} = < \bar{\mathbf{T}}_{rm}(r',z') \quad \bar{\mathbf{T}}_{\theta m}(r',z') \quad \bar{\mathbf{T}}_{zm}(r',z') >^T \tag{3.7b}$$

In eqn (3.6b), $\bar{\mathbf{H}}_{pq}$ is a matrix whose elements are tractions in the p-direction of the nodes on $\bar{S}$ due to ring loads in the q-direction through node points on S'; $\triangle S'$ is the tributary length corresponding to a node point on S'; $\mathbf{B}_i(r',z')$ is a row vector whose elements are intensities of forces in the i-direction of the node point on S' and the superscript T denotes the transpose of a matrix.

A least-squares solution of eqn (3.4) yields

$$\mathbf{B} = [\mathbf{Q}^T\mathbf{Q}]^{-1}\mathbf{Q}^T\mathbf{R} \tag{3.8}$$

Once $\mathbf{B}$ is determined from eqn (3.8), the Fourier harmonic of displacements on $\bar{S}$ (which are identical to displacements of S of the original problem) can be computed by numerical integration of eqn (3.3).

3.2.2 Numerical Example

The numerical convergence, stability and accuracy of the solution scheme have been investigated with respect to a bench-mark problem for which solutions have been reported in the literature. The problem under consideration corresponds to a spherical cavity of radius 'a' in an isotropic infinite space which is subjected to a uniform radial pressure p_0. An exact analytical solution for this problem is available (Saada 1974). The material isotropy is simulated by setting material constants $c_{11} = 3.0, c_{12} = 1.0, c_{33} = 3.0, c_{13} = 1.0$ and $c_{44} = 0.99997$. This corresponds to an isotropic material with shear modulus and Poisson's ratio equal to 1.0 and 0.25, respectively. Table 3.1 presents a comparison of nondimensional displacement normal to the cavity wall denoted by δ_0, for different locations of inner surfaces S' measured by the distance 'c' (Fig 3.2) and for different number of node points M and M'. The solutions obtained from the present scheme show good convergence and stable behaviour with increasing M and M'. In addition, present solutions are in very close agreement with the analytical solution.

Next a traction boundary-value problem corresponding to a hemispherical cavity of radius 'a' at the surface level of an elastic half space is considered. The cavity is subjected to uniformly distributed normal pressure q_0. The material types considered here are ice, an isotropic material, clay I, magnesium and cadmium and the material constants are given in Table 1.1. The numerical solutions for nondimensional radial displacement $\bar{u}_r$ and vertical displacement $\bar{u}_z$ ($\bar{u}_i = u_i q_0 / a c_{44}$) are presented in Fig 3.3. A surface S' of radius $0.85a$ together with ten and twenty node points on S' and S, respectively are used in the analysis. It is observed from Fig 3.3 that the material anisotropy has significant influence on the displacement profiles. In the case of $\bar{u}_r$, the strongest influence of material

anisotropy is noted in the solution for cadmium followed by clay. The nondimensional radial displacement solutions for magnesium and ice are found to be almost equal to that of the isotropic material. However, a completely different trend is noted for the nondimensional vertical displacement $\bar{u}_z$. The highest influence of material anisotropy is observed in the profiles for ice and cadmium followed by magnesium. The vertical displacement profiles for isotropic material and clay are found to be nearly identical and fall between the vertical displacement profiles for cadmium and magnesium. Comparison of displacement solutions presented in Fig 3.3 with the values of material constants given in Table 1.1 indicates that the normalised constant $\bar{c}_{11}$ dominates the influence of material anisotropy in the case of displacement $\bar{u}_r$ while in the case of $\bar{u}_z$ the influence of anisotropy is mainly governed by $\bar{c}_{33}$. It is also observed that the general shape of displacement profiles along the cavity wall is roughly the same for all five materials although the actual magnitudes are considerably different. In addition, the largest radial displacement is found at a point which is below the free surface of the half space for all materials. It should be mentioned here that the present scheme can be directly applied to analyze a cavity of any arbitrary axisymmetric geometry subjected to an arbitrary variation of pressure over the cavity surface.

3.3 DISPLACEMENT BOUNDARY-VALUE PROBLEMS

3.3.1 **Formulation**

In the case of a displacement boundary-value problem, Fourier harmonic components of displacements on $S(\bar{S})$ are prescribed. The force intensities $B_i(r,z)$ are governed by the following Fredholm integral equation of the first kind:

$$\int_{S'} G_{ij}^{m}(r,z;r',z')B_j(r',z')r'\,dS' = \bar{u}_{im}(r,z) \tag{3.9}$$

where $\bar{u}_{im}(r,z)$ denotes a prescribed displacement on the generating curve of S. A solution for $\mathbf{B}$ is given by (3.8) with

$$\mathbf{Q} = \bar{\mathbf{G}} \tag{3.10}$$

$$\bar{\mathbf{G}} = \begin{pmatrix} \bar{\mathbf{G}}_{rr} & \bar{\mathbf{G}}_{r\theta} & \bar{\mathbf{G}}_{rz} \\ \bar{\mathbf{G}}_{\theta r} & \bar{\mathbf{G}}_{\theta\theta} & \bar{\mathbf{G}}_{\theta z} \\ \bar{\mathbf{G}}_{zr} & \bar{\mathbf{G}}_{z\theta} & \bar{\mathbf{G}}_{zz} \end{pmatrix}_{3M\times 3M'} \tag{3.11a}$$

$$\bar{\mathbf{G}}_{pq} = [G^m_{pq}(r,z;r',z')r'\triangle S']_{M\times M'}, \quad p,q = r,\theta,z \tag{3.11b}$$

and

$$\mathbf{R} =< \bar{\mathbf{u}}_{rm}(r',z') \quad \bar{\mathbf{u}}_{\theta m}(r',z'), \quad \bar{\mathbf{u}}_{zm}(r',z') >^T \tag{3.12}$$

The solution for traction components $T_{im}(r,z)$ is given by the following integral equation:

$$T_{im}(r,z) = \int_{S'} H^m_{ij}(r,z;r',z')B_j(r',z')r'dS' \tag{3.13}$$

3.3.2 Numerical Examples

The example problem used to verify the solution scheme corresponds to an asymmetric displacement boundary-value problem related to a rigid cylinder of radius 'a' and height 'h' partially embedded in an isotropic elastic half space (Fig 3.4). The force-displacement relationship of the cylinder can be expressed in the form:

$$\begin{pmatrix} F_0 \\ M_0/a \end{pmatrix} = c_{44}a \begin{pmatrix} K_h & K_{hm} \\ K_{mh} & K_m \end{pmatrix} \begin{pmatrix} \triangle_x \\ a\phi_y \end{pmatrix} \tag{3.14}$$

In eqn (3.14), K_h, K_m and $K_{hm}(= K_{mh})$ denote the non-dimensional horizontal, rocking and coupled stiffnesses of the rigid cylinder; $\triangle_x$ and ϕ_y denote the horizontal displacement (x-direction) of the bottom and rotation about the y-axis of the cylinder, respectively; F_0 and M_0 denote the resultant force in the x-direction and bending moment about the y-axis with respect to the point A shown in Fig 3.4 respectively.

Apsel and Luco (1987) presented solutions of stiffnesses for rigid cylinders with various h/a ratios embedded in an isotropic elastic half space (Poisson's ratio equal to 0.25) by numerically solving a formulation based on the integral representation theorems (Eringen and Suhubi, 1975). Table 3.2 presents solutions for K_h, K_m and K_{hm} of a rigid cylinder with h/a=1 for two location of surface

S' [considered as a cylinder of radius $(a-c)$ and height $(h-c)$] and for four different discretizations of $\bar{S}$ and S'. The convergence and the stability of the present solutions are clearly evident. Table 3.2 also presents a comparison with the solution presented by Apsel and Luco (1987). The above comparison confirms the accuracy, convergence and stability of numerical solutions obtained from the present analysis.

Next, the asymmetric displacement boundary-value problem related to a rigid cylinder bonded to a transversely isotropic elastic half space is considered (Fig 3.4). The problem under consideration has useful applications in geomechanics and in the analysis and design of composite mechanical components. The quantity of primary interest is the global stiffness of the cylinder-half-space system. Tables 3.3 and 3.4 present non-dimensional axial (K_v), horizontal (K_h), rocking (K_m) and coupled $(K_{mh} = K_{hm})$ stiffnesses of a rigid cylinder bonded to ice, two types of clay and an isotropic medium. Note that $K_v = P_0/(c_{44}a\triangle_z)$, where $\triangle_z$ is the displacement of the cylinder in the z-direction and P_0 is the axial force. The stiffness K_h, K_m, K_{hm} are defined by eqn (3.14). Solutions are presented for rigid cylinders with $h/a = 0.5, 1.0, 2.0$ and 4.0. As expected, all stiffness parameters increase considerably with increasing values of the ratio h/a for all types of materials. The values of K_h, K_m and K_{hm} corresponding to the two clays are quite close to each other which indicates that the differences in $\bar{c}_{13}$ and $\bar{c}_{33}$ observed in Table 1.1 for the two types of clays do not have a significant influence on the stiffness parameters. Further comparisons of the values of material constants $\bar{c}_{ij}$ in Table 1.1 with the values of stiffness parameters in Tables 3.3 and 3.4 indicate that the order of K_v for different materials is identical to that of $\bar{c}_{33}$ and the order of K_h and K_m is identical to that of $\bar{c}_{11}$. However the influence of anisotropy on stiffness K_{hm} is appeared to be governed by more than one value of $\bar{c}_{ij}$.

3.4 A MIXED BOUNDARY-VALUE PROBLEM

3.4.1 Formulation

In the case of mixed boundary-value problems tractions are prescribed over the part S_1 of S (Fig 3.1) and displacements are prescribed over the remaining part S_2. Considering the system shown in Fig 3.2, the force intensities $B_i(r', z')$ on S' are governed by the following dual integral equation system:

$$\int_{S'} H_{ij}^m(r, z; r', z') B_j(r', z') r' dS' = \bar{T}_{im}(r, z), \quad (r, z) \in \bar{S}_1 \tag{3.15a}$$

$$\int_{S'} G_{ij}^m(r, z; r', z') B_j(r', z') r' dS' = \bar{u}_{im}(r, z), \quad (r, z) \in \bar{S}_2 \tag{3.15b}$$

A solution of eqn (3.15) to determine $\mathbf{B}$ can be expressed in the form of eqn (3.8) by discretizing S_1 and S_2 by using M_1 and M_2 node points, respectively. The matrix $\mathbf{Q}$ in eqn (3.8) corresponding to the present case can be expressed as:

$$\mathbf{Q} = \begin{pmatrix} \bar{\mathbf{H}} \\ \bar{\mathbf{G}} \end{pmatrix} \tag{3.16}$$

where $\bar{\mathbf{H}}$ and $\bar{\mathbf{G}}$ are the traction and displacement Green's function matrices defined by eqns (3.6) and (3.11), respectively. Note that the orders of $\bar{\mathbf{H}}$ and $\bar{\mathbf{G}}$ are $3M_1 \times 3M'$ and $3M_2 \times 3M'$, respectively. Once $\mathbf{B}$ is known, the unknown displacement on S_1 and the unknown tractions on S_2 can be determined from the eqns (3.3) and (3.13), respectively.

3.4.2 Example

The non-linear mixed boundary-value problem related to a rigid hemisphere of radius 'a' embedded in a transversely isotropic elastic half space with an elastic-perfectly plastic interface is considered. In the absence of relevant experimental data the axisymmetric twisting problem has been simulated where yielding (slipping) occurs only in the θ-direction when contact traction reaches a limiting value. The limiting traction value in the θ-direction, denoted by $\tau_{\theta y}$, is set to $0.01c_{44}$.

In reality the critical value of traction beyond which slipping occurs along the surface should be determined experimentally and depends on several factors such as the surface texture of the interface, the type of bonding, the deformability characteristics of the materials in contact, *etc.*. The torque (T_0) and twist angle (ω_0) relationship is linear until the contact traction in the θ-direction at a point at the interface reaches the limiting value. A displacement boundary-value problem can be defined for domain V_c (Fig 3.5) during the linear region. Let ω_y denote the twist angle (in radians) at the initiation of yielding. For any $\omega_0 > \omega_y$, a mixed boundary-value problem can be defined for V_c; the traction specified over the part where the critical value has been reached and the displacement specified over the remainder. Note that slipping will occur along the portion of the interface where the limiting traction has reached. It can be shown that the torque T_y corresponding to a completely yielded interface is equal to $0.005\pi^2 c_{44} a^3$ for $\tau_{\theta y} = 0.01 c_{44}$. The response of the hemisphere for $\omega_0 > \omega_y$ can be studied by an incremental analysis. In the present study the surface S' was taken as a hemisphere of radius $0.8a$ and M=20 and M'=10. The incremental analysis was performed by using increments of rotation equal to $0.05\omega_y$ for $\omega_0 > \omega_y$.

Figure 3.5 shows the torque-twist relationship after the initiation of interface yielding for a rigid hemisphere embedded in an isotropic material, ice, clay and cadmium (Table 1.1). The point of intersection of the torque-twist curve with the horizontal axis corresponds to the twist angle ω_y at the initiation of interface yielding. The normalized torque $T^* = T_0/T_y$, where T_0 is the torque acting on the hemisphere and $\omega_0^* = \omega_0 c_{44}/\tau_{\theta y}$. The non-linear behaviour of the torque-twist relationship is evident from Fig 3.5. The present analysis can also be used to compute the amount of slip between the rigid hemisphere and surrounding half-space at points along the interface which have reached the limiting traction. The non-dimensional slip at a point (r, z) on the interface is denoted by $\triangle^*$ and defined by $\triangle^*(r, z) = [r\omega_0 - v(r, z)]c_{44}/(a\tau_{\theta y})$, where $v(r, z)$ is the displacement

in the θ-direction of the half-space. Note that for $\omega_0 < \omega_y$, no slip takes place at the interface and $\triangle^* = 0$ for all points on the interface. Figure 3.6 shows the variation of $\triangle^*$ with angle ϕ (Fig 3.5) for normalized rotation $\bar{\omega}_0 = \omega_0/\omega_y$. Yielding is initiated at the free surface level ($\phi = \pi/2$) and gradually progresses downward as ω_0 is increased. Nearly one-half of the interface yields at $\bar{\omega}_0 = 1.30$ for all types of materials. Note that in the present problem, the analytical solution results in zero traction in the θ-direction when $\phi \to 0$. This implies, theoretically, the yielding of the bottom ($\phi = 0$) occurs when $\bar{\omega}_0 \to \infty$. This behaviour is reflected in both Figs 3.5 and 3.6. This example demonstrates the effectiveness of the present scheme in analysing a mixed boundary-value problem related to a rigid inclusion. The analysis can be modified without any fundamental difficulty to simulate an interface with Coulomb friction.

3.5 LOAD TRANSFER PROBLEM

3.5.1 General

The study of load transfer from a partially embedded cylindrical elastic bar of finite length into an elastic medium has useful applications in several engineering problems. In applications related to composite materials and geomechanics, the load is transfered to a medium which is essentially anisotropic. In this section the general elastostatic load transfer from a cylindrical elastic bar which is partially embedded in a transversely isotropic elastic half space is investigated. A coupled variational-boundary integral equation method scheme is used in the analysis by generalising the formulations presented previously by Selvadurai and Rajapakse (1987) and Rajapakse (1988).

3.5.2 Deformation of Elastic Bar

Consider a cylindrical elastic bar of radius 'a' and length 'h' ($h/a >> 1$) partially embedded in a transversely isotropic elastic half space as shown in Fig 3.7. A Cartesian coordinate system (x, y, z) and a cylindrical coordinate system

(r, θ, z) are defined such that z-axis coincides with the centroidal axis of the bar and perpendicular to the stress free surface of the surrounding half space. The Young's modulus of the bar is denoted by E_b (shear modulus μ_b). The bar may be subjected to a torque T_0 about z-axis, an axial force P_0, a horizontal force H_0 along the x-axis (θ=0) or a bending moment M_0 about the y-axis ($\theta = \pi/2$). In view of the assumption that $h/a >> 1$, the deformation of the bar is assumed to be governed by an appropriate one-dimensional theory. Let $w_i(r, \theta, z)$ denote the displacement of the bar in the i-direction ($i = r, \theta, z$). It is assumed that the displacement of the bar can be represented by an admissible function indeterminate with respect to a set of generalized coordinates. In the case where the bar is subjected to an axisymmetric torque, the following representation is used:

$$w_\theta(r, \theta, z) = \sum_{n=1}^{N} \alpha_n r \phi_n(z) \tag{3.17a}$$

$$w_r(r, \theta, z) = w_z(r, \theta, z) = 0 \tag{3.17b}$$

where, $\alpha_1, \alpha_2 ..., \alpha_N$ are generalized coordinates to be determined and $\phi_n(z)$ ($n = 1, 2, ...,N$) is a set of smooth and continuous functions of $z(0 \leq z \leq h)$.

For the axial load transfer problem,

$$w_z(r, \theta, z) = \sum_{n=1}^{N} \alpha_n \phi_n(z) \tag{3.18a}$$

$$w_r(r, \theta, z) = w_\theta(r, \theta, z) = 0 \tag{3.18b}$$

In eqn (3.18b), consistent with the assumed one-dimensional behaviour, any radial displacement of the bar due to longitudinal straning has been neglected.

For the transverse load (shear force Q_0 or moment M_0) transfer problem,

$$w_x(r, \theta, z) = \sum_{n=1}^{N} \alpha_n \phi_n(z) \tag{3.19a}$$

$$w_y(r, \theta, z) = 0 \tag{3.19b}$$

$$w_z(r, \theta, z) = -\cos\theta \sum_{n=1}^{N} r \alpha_n \frac{d\phi_n}{dz} \tag{3.19c}$$

Note that eqns (3.19a) and (3.19b) yield,

$$w_r(r,\theta,z) = \cos\theta \sum_{n=1}^{N} \alpha_n \phi_n(z) \tag{3.20a}$$

and

$$w_\theta(r,\theta,z) = -\sin\theta \sum_{n=1}^{N} \alpha_n \phi_n(z) \tag{3.20b}$$

A variety of admissible functions can be selected for $\phi_n(z)$. It is important that the selected function set includes the appropriate rigid body displacement mode of the bar for the load type under consideration. In the present analysis the following choice is made for $\phi_n(z)$:

$$\phi_n(z) = (z/h)^{n-1} \tag{3.21}$$

3.5.3 Coupled Variational-Boundary Integral Equation Formulation

Using the displacement representations given by eqns (3.17)-(3.20), the strain energy U_b of the elastic bar can be expressed as

$$U_b = \sum_{n=1}^{N} \sum_{m=1}^{N} \alpha_n \alpha_m D_{nm} \tag{3.22}$$

For the torsion load transfer problem,

$$D_{nm} = \begin{cases} \pi \mu_b a^4 (n-1)(m-1)/[4h(n+m-3)] & n+m \neq 3 \\ 0 & n+m = 3 \end{cases} \tag{3.23a}$$

For the axial load transfer problem,

$$D_{nm} = \begin{cases} \pi E_b a^2 (n-1)(m-1)/[2h(n+m-3)] & n+m \neq 3 \\ 0 & n+m = 3 \end{cases} \tag{3.23b}$$

For the transverse load transfer problem,

$$D_{nm} = \begin{cases} \pi E_b a^4 (n-1)(n-2)(m-1)(m-2)/[8h^3(n+m-5)] & n+m \neq 5 \\ 0 & n+m = 5 \end{cases} \tag{3.23c}$$

The displacement compatibility between the bar and the half space along the contact surface S can be expressed as,

$$w_i(r,\theta,z) = u_i(r,\theta,z), \quad i = r,\theta,z; \quad (r,\theta,z) \in S \tag{3.24}$$

where $u_i(r,\theta,z)$ denotes the displacement in the i-direction of the elastic half space.

The strain energy of the surrounding half space region denoted by U_h can be expressed as

$$U_h = \frac{1}{2}\int_S T_i u_i dS \tag{3.25}$$

In eqn (3.25), $T_i(r,\theta,z)$ denote the traction in the i-direction $(i = r,\theta,z)$ at a point on the contact surface S and summation is implied over the legal range of i corresponding to each load transfer problem.

In view of eqn (3.24), a displacement component $u_i(r,\theta,z)$ at a point (r,θ,z) on the contact surface S can be expressed as

$$u_i(r,\theta,z) = \sum_{n=1}^{N} \alpha_n u_{in}(r,z) f_i(\theta) \tag{3.26}$$

The explicit form of $u_{in}(r,z)$ appearing in eqn (3.26) can be obtained from eqn (3.24) together with eqns (3.17)-(3.21) for different loading cases.

Let $T_{in}(r,z)f_i(\theta)$ denote components of traction at a point (r,θ,z) on the contact surface due to a displacement field $u_{in}(r,z)f_i(\theta)$ imposed on S. Then traction T_i due to displacement field u_i can be expressed as,

$$T_i(r,\theta,z) = \sum_{n=1}^{N} \alpha_n T_{in}(r,z) f_i(\theta) \tag{3.27}$$

In view of eqns (3.21), (3.22) and (3.25)-(3.27), a constraint energy functional (Washizu 1982) of the bar-half space system which takes into consideration the bar top boundary conditions can be expressed as

$$\bar{\pi} = \sum_{n=1}^{N}\sum_{m=1}^{N} \alpha_n \alpha_m [D_{nm} + F_{nm}] - W \tag{3.28}$$

where,

$$F_{nm} = \frac{\eta}{2} \int_S T_{in}(r,z) u_{im}(r,z) r dS \tag{3.29}$$

For the torsion transfer problem

$$W = T_0 \alpha_1 + \lambda_1 (\frac{J\mu}{2h} \alpha_2 - T_0) \tag{3.30a}$$

for the axial load transfer problem

$$W = P_0 \alpha_1 + \lambda_1 (\frac{EA}{h} \alpha_2 - P_0) \tag{3.30b}$$

for the transverse load transfer problem

$$W = M_0 \frac{\alpha_2}{h} + Q_0 \alpha_1 + \lambda_1 (\frac{2EI}{h^2} \alpha_3 - M_0) + \lambda_2 (\frac{6EI}{h^3} \alpha_4 + Q_0) \tag{3.30c}$$

and

$$\eta = \begin{cases} 2\pi & \text{torsion} \\ \pi & \text{axial and transverse} \end{cases} \tag{3.31}$$

Note that summation is implied over the index $i (i = r, \theta, z)$ in eqn (3.29) and the integration is taken over the generating curve of S. In eqns (3.30), A, I and J denote cross-sectional area, moment of inertia and polar moment of inertia of the elastic bar respectively, and $\lambda_i (i = 1, 2)$ denotes a Lagrange multiplier.

At equilibrium, the generalized principle of minimum potential energy states that $\bar{\pi}$ is stationary. The relevant stationary conditions yield a set of linear simultaneous equations to determine $\alpha_i (i = 1, 2, ..., N)$. For example, the set of equations corresponding to the transverse loading problem can be expressed as,

$$\sum_{n=1}^{N} \alpha_n [2D_{nm} + F_{nm} + F_{mn}] + \lambda_1 \frac{EI\delta_{m3}}{h^2} + \lambda_2 \frac{EI\delta_{m4}}{h^3}$$

$$= H_0 \delta_{1m} + \frac{M_0}{h} \delta_{2m} \quad m = 1, 2, ..., N \tag{3.32}$$

$$\frac{2EI\alpha_3}{h^2} = M_0, \quad \frac{6EI\alpha_4}{h^3} = -Q_0 \tag{3.33}$$

where δ_{mn} denotes Kronecker's delta function.

The numerical solution of linear equation systems yields the solutions for generalized coordinates $\alpha_i (i = 1, 2, ..., N)$ corresponding to the three different types of load transfer problems. The solutions for bar displacements and stress resultants can be determined by using one of the eqns (3.17)-(3.21) and an appropriate one-dimensional continuum theory. It is noted from eqns (3.32) that the coefficients of the linear simultaneous equation system involve the the term F_{nm} defined by eqn (3.29). The evaluation of F_{nm} corresponding to different types of load transfer problems is discussed in the following section.

3.5.4 Evaluation of Term F_{mn}

The evaluation of F_{nm} given by eqn (3.29) reduces mainly to the computation of traction components $T_{in}(r, z)$ on S since $u_{in}(r, z)$ can be obtained from eqns (3.24) and (3.17)-(3.21). Note $T_{in}(r, z)$ denotes traction components on the cavity surface of an elastic half space with a cavity identical to the bar when the cavity surface is subjected to a displacement field with components $u_{in}(r, z)$. It is evident that an analytical solution for $T_{in}(r, z)$ cannot be derived. However, a numerical solution for $T_{in}(r, z)$ which satisfies all the governing equations of the half space region can be derived by using an indirect boundary integral equation scheme given in section 3.3.

Consider an uniform half-space region without a cavity. A fictitious surface $\bar{S}$ identical to the bar-half-space contact surface S is defined. A set of forces with components $B_{in}(r', z')f_i(\theta)$ are applied on a cylindrical surface S', interior to $\bar{S}$ such that displacements on $\bar{S}$ are equal to $u_{in}(r, z)f_i(\theta)$. The force components $B_{in}(r, z)$ are governed by the nonsingular integral equation (3.9). Note in eqn (3.9), indices i and j take the range of values defined previously for different load-transfer problems, and summation is implied on index j. In addtion, $G^m_{ij}(r, z; r', z')$ corresponding to each load-transfer problem is presented in Chap-

ter 2. The traction components on $\bar{S}$ that are equal to $T_{in}(r,z)$ can be expressed as in eqn (3.13). The explicit solutions for $H_{ij}^{m}(r,z;r',z')$ corresponding to various types of load-transfer problems can be derived by using the solutions presented in Chapter 2. A solution for $T_{in}(r,z)$ can be obtained by discretizing S' and $\bar{S}$ with a set of node points and solving eqns (3.9) and (3.13) numerically. Details of the numerical solution procedure is presented in Sections 3.2 and 3.3. Alternatively, a numerical solution for $T_{in}(r,z)$ can be obtained from direct boundary integral equation method (Apsel and Luco 1987).

3.5.5 **Numerical Solutions**

3.5.5.1 Numerical Scheme

In the numerical study, the response of elastic bars subjected to different types of loading is investigated. The values of normalized material constants $\bar{c}_{ij}(=c_{ij}/c_{44})$ of ice, cadimium, magnesium, a clay soil and an isotropic medium are given in Table 1.1. The selection of the above set of anisotropic materials among several others is based on their relevance to applications related to composite materials (magnesium, cadmium and isotropic) and geomechanics (clay, ice and isotropic). The convergence and numerical stability of the solution scheme with respect to the number of terms N in eqns (3.17)-(3.19) and number of node points N' and $\bar{N}$ on generating curves S' and $\bar{S}$, respectively, have been investigated. It is found that the solution of elastic bar converges for $N \geq 8$ and $\bar{N} = 30$ and 40 are sufficient for bars with $h/a = 5$ and 10.

3.5.5.2 Bar Stiffness

The stiffness of the bar is expressed in terms of a set of nondimensional stiffness parameters as defined below

$$K_V = \frac{P_0}{c_{44}a\triangle_z}; \qquad K_T = \frac{T_0}{c_{44}a^3\phi_z}; \qquad K_H = \frac{Q_0}{c_{44}a\triangle_{xQ}}; \tag{3.34a}$$

$$K_M = \frac{M_0}{c_{44}a^3\phi_{yM}}; \qquad K_{HM} = \frac{Q_0}{c_{44}a^2\phi_{yQ}}; \qquad K_{MH} = \frac{M_0}{c_{44}a^2\triangle_{xM}} \tag{3.34b}$$

where K_V, K_T, K_H, K_M and $K_{MH}(= K_{HM})$ denote axial, torsional, horizontal, rotational and coupled stiffnesses of the bar, respectively. In addition $\triangle_z, \phi_z, \triangle_x$ and ϕ_y denote the vertical displacement, twist angle, lateral displacement and rotation of the top end of the bar, respectively. $\triangle_{xQ}$ and $\triangle_{xM}$ denote the horizontal displacements due to Q_0 and M_0 applied at the top end of the bar, respectively; ϕ_{yQ} and ϕ_{yM} denote the rotation due to Q_0 and M_0, respectively.

Figures 3.8 and 3.9 show the variation of stiffness parameters with moduli ratio $\bar{E}_b(= E_b/c_{44})$ for bars with $h/a = 5$ and 10, respectively. Note that for bars subjected to torsion the moduli ratio $\bar{\mu}_b = \mu_b/c_{44}$ is used. All stiffness parameters increase rapidly with $\bar{E}_b$ and approaches a limiting value beyond which the bar exhibits characteristics of a rigid bar. The value of $\bar{E}_b$ beyond which the bar behaves perfectly rigid depends on the degree of anisotropy of the surrounding material, type of loading and the bar length-radius ratio.

It is noted from Figs 3.8 and 3.9 that the torsional, horizontal, rotational and coupled stiffnesses of bars embedded in an isotropic medium and magnesium are nearly equal and solutions corresponding to bars embedded in ice are slightly higher. Therefore, magnesium and ice can be considered isotropic and slightly anisotropic, respectively, for transverse load and torque transfer problems. The solutions for transverse (K_H, K_M, K_{MH}) and torsional stiffnesses of bars embedded in clay and cadmium show a considerable influence of the material anisotropy. It is also noted that the influence of material anisotropy, if any, is more pronounced for stiffer bars when compared to very flexible bars (lower values of $\bar{E}_b$). Based on the solutions presented in Figs 3.8 and 3.9 for transverse and torsional stiffnesses, cadmium is found to possess the highest degree of anisotropy followed in the order of decreasing degree of anisotropy by clay, ice and magnesium.

It is useful to relate the influence of the material anisotropy observed in the numerical study for transverse and torsional stiffnesses to the magnitudes

of normalized material constant $\bar{c}_{ij}$ in Table 1.1. Comparison of the values in Table 1.1 indicates that magnesium and isotropic material have relatively closer $\bar{c}_{ij}$ values and this is consistent with the close agreement of stiffness parameters observed in Figs 3.8 and 3.9. The $\bar{c}_{ij}$ values of of clay are also closer to isotropic values except in the case of $\bar{c}_{11}$. In addition, $\bar{c}_{ij}$ values of ice are greater than clay except in the case of $\bar{c}_{11}$. However, in Figs 3.8 and 3.9, transverse and torsional stiffnesses of bars embedded in clay are greater than the corresponding solutions for ice. In addition, cadmium, which shows the highest influence of anisotropy in Figs 3.8 and 3.9 also has the highest values of $\bar{c}_{11}, \bar{c}_{12}$ and $\bar{c}_{13}$ when compared to other materials. These comparisons indicate that the transverse stiffness is governed mainly by the value of $\bar{c}_{11}$ and to a lesser degree by $\bar{c}_{12}$ and $\bar{c}_{13}$. In the case of torsional load transfer, the torsional response equation indicates that the dependence of material anisotropy can be related only to the value of $(\bar{c}_{11} - \bar{c}_{12})$. A comparison of $(\bar{c}_{11} - \bar{c}_{12})$ values from Table 1.1 is in agreement with the order of the influence of material anisotropy observed in Figs 3.8 and 3.9 for K_T.

The solutions for axial stiffness K_V presented in Figs 3.8 and 3.9 indicate that the influence of material anisotropy is relatively lesser when compared to transverse and torsional stiffnesses. The axial stiffness of bars embedded in cadmium and the isotropic medium is nearly identical. In addition, bars embedded in ice have the largest axial stiffness. Solutions corresponding to clay and magnesium are nearly identical and are in between solutions for ice and the isotropic material. Comparison of $\bar{c}_{ij}$ values in Table 1.1 and the numerical solutions in Figs 3.8 and 3.9 indicate that in the case of axial stiffness the influece of anisotropy is primarily governed by the value of $\bar{c}_{33}$. It is noted that the magnitude of K_V in Figs 3.8 and 3.9 for different materials is in the same order as the magnitude of $\bar{c}_{33}$ in Table 1.1.

3.5.5.3 Load Transfer Curves

Fig 3.10 shows the axial load transfer curves of an elastic bar $(h/a = 10)$

with moduli ratio $\bar{E}_b = 50$ and 100 embedded in cadmium and an isotropic solid. The numerical results for other materials fall within the two load transfer curves shown in Fig 3.10. These solutions indicate that the influence of material anisotropy on axial load transfer along the bar is negligible. Comparison were also made for nearly rigid bars and found that the axial load transfer curves are not significantly influenced by the degree of anisotropy of the half space materials. Additional numerical solutions indicate that the moduli ratio $\bar{E}_b$ and the length-radius ratio significantly influence the load transfer profiles. For a bar of given length-radius ratio, the load diffuses rapidly with increasing bar flexibility (*i.e.*, decreasing values of $\bar{E}_b$). Fig 3.11 shows the torque transfer curves of an elastic bar ($b/a = 10, \bar{\mu}_b = 50$ and 100). The influence of material anisotropy is clearly visible in these curves when compared to axial load transfer curves shown in Fig 3.10. The torque transfer curves for elastic bars embedded in clay and cadmium indicate a higher rate of diffusion of bar torque with depth when compared to an isotropic medium. Additional numerical solutions indicate that as $\bar{\mu}_b$ increases, the influence of material anisotropy on bar torque profiles decrease and in the case of rigid bars the torque profiles are nearly independent of the degree of anisotropy of the half space. In general, the torque transfer along the bar length is more rapid when compared to axial load transfer and the rate of torque diffusion increase with decreasing values of moduli ratio $\bar{\mu}_b$.

Fig 3.12 shows the shear force profiles of a bar ($h/a = 10, \bar{E}_b = 50$ and 100) subjected to a horizontal force Q_0 at the top end. The solutions are found to be negligibly influenced by the degree of anisotropy of the surrounding half space. Similar behaviour is also observed for rigid bars. It is also noted that shear force diffuses rapidly and shows a reversal in sign within the top portion of the bar. In addition, some minor oscillations within the lower portion of the bar are noticed for very flexible bars. This behaviour is different to that observed previously for the axial load and torque. It should be mentioned here that a long flexible beam

on a Winkler medium and subjected to a concentrated load at one end shows qualitatively similar shear force profiles. As the bar becomes rigid ($\bar{E}_b \to \infty$), the oscillation vanishes and the shear force reduces gradually with a change in sign within the top portion and thereafter increases linearly in the bottom portion.

Fig 3.13 shows the bending moment profiles of elastic bars ($\bar{E}_b = 50$ and 100) subjected to a horizontal force Q_0 at the top end. These profiles show an influence of anisotropy which is similar to that observed previously for torque transfer profiles. It is also observed that for a bar of given length-radius ratio, the shape of the bending moment profiles is significantly influenced by the bar moduli ratio $\bar{E}_b$. For low values of $\bar{E}_b$, the magnitude of maximum bending moment is smaller and the bending moment decreases rapidly along the bar. As the bar becomes more stiffer, the magnitude of maximum bending moment increases and the profiles show more gradual decreases of bending moment along the lower portion of the bar. Some oscillations in the profiles are observed within the lower portion of the bar for very flexible bars.

Fig 3.14 shows the bending moment profiles of bars of three different length-radius ratios ($h/a = 5, 10, 20$) embedded in ice and subjected to a bending moment M_0 at the top end. Solutions are presented for a bar with $\bar{E}_b = 100$ and a rigid bar $\bar{E}_b \to \infty$. These profiles clearly indicate the influence of bar length on the relative flexibility of the bar-elastic medium system. For a short bar ($h/a = 5$) the profiles corresponding to $\bar{E}_b = 100$ and ∞ are quite close indicating that even at low values of $\bar{E}_b$, short bars behave nearly rigid. For longer bars ($h/a = 10$ and 20) the profiles for $\bar{E}_b = 100$ and ∞ show considerable differences both in magnitude and in shape. Changes in sign and oscillations are observed in bending moment profiles of flexible bars ($\bar{E}_b = 100$) for $h/a = 10$ and 20. These features do not appear in bending moment profiles of rigid bars of same length-radius ratio. The oscillations observed in bending moment profiles are found to be also influenced by the length-radius ratio and the moduli ratio of the bar. It is

interesting to note here that a long elastic beam on a Winkler medium and subjected to a bending moment at one end shows bending moment profiles which are qualitatively similar to that observed in Fig 3.14 for flexible bars.

3.6 CONCLUSIONS

It can be concluded at this stage that an accurate boundary integral formulation has been presented to analyze a general (displacement, traction and mixed) boundary-value problem related to a transversely isotropic elastic medium. The kernels are the Green's functions derived explicitly in Chapter 2. The numerical examples have demonstrated the accuracy, flexibility and versatility of the solution scheme in analyzing a variety of problems. The boundary integral scheme of domain V_c can be coupled to a finite element representation of the near field domain V to develop a hybrid scheme (Zienkiewicz *et al.* 1977) which can be used to model a variety of linear and nonlinear problems related to transversely isotropic elastic media. The present methodology can be used to solve general boundary-value problems related to a multilayered transversely isotropic elastic medium without any fundamental difficulty. In the case of layered media, however, the Green's functions can not be derived explicitly and have to be constructed by using accurate numerical techniques. The development of an exact stiffness matrix method for computation of Green's functions of layered media is presented in Chapter 7. It should be mentioned here that the above boundary-value problems can also be analyzed by using the integral representation theorems (Rizzo 1967, Eringen and Suhubi 1975). The kernel functions of the resulting integral equations are again the displacement and traction Green's functions, given by eqns (2.23)-(2.25) and (2.34)-(2.36), respectively.

A coupled variational-boundary integral equation scheme is introduced to analyze the load transfer from a cylindrical elastic bar to a transversely isotropic elastic half space. The displacement compatibility between the bar and the half

space is satisfied at nodal locations defined along the real contact surface. In all cases, as the bar becomes rigid, the method yields a solution for the exact boundary value problem corresponding to the surrounding half space. To the writer's knowledge, the present solution is the first treatment of the transverse load-transfer problem with full displacement compatibility on real bar-half space interface. The boundary integral scheme adopted for the surrounding half space is rigorous and satisfies all governing equations and boundary value conditions. The solutions for axial, torsional, horizontal, rotational, and coupled stiffnesses indicate that the degree of anisotropy of the medium has a significant influence on the stiffness parameters. It is found that normalized axial stiffness is influenced mainly by the material constants $\bar{c}_{33}$. Transverse stiffnesses are influenced primarily by $\bar{c}_{11}$, and to a lesser degree by $\bar{c}_{12}$ and $\bar{c}_{13}$, and the normalized torsional stiffness depends on the value of $(\bar{c}_{11} - \bar{c}_{12})$. In addition, the length-radius ratio and the bar moduli ratio $\bar{E}_b$ significantly influence the stiffness parameters and the load transfer profiles. The influence of material anisotropy is found to be negligible for axial and shear force profiles of both elastic and rigid bars. However, torque and bending moment profiles show a dependence on the degree of anisotropy of the surrounding medium for low values of $\bar{E}_b$. The shear force and bending moment profiles of flexible bars display changes in sign and oscillations. This is qualitatively similar to that observed in the analytical solutions for semi-infinite elastic beams on a Winkler medium subjected to a concentrated load or moment at the origin. It is also noted that the relative flexibility of the bar-half space system is governed by both the length-radius ratio and moduli ratio of the bar.

Table 3.1 Variation of normal displacement of cavity wall for different locations of S' and discretization of S and S'

(M', M)	c=0.25	c=0.15
(5, 10)	0.2120	0.1441
(6, 12)	0.2287	0.1718
(8, 12)	0.2438	0.2184
(8, 16)	0.2455	0.2241
(8, 18)	0.2459	0.2293
(10, 20)	0.2490	0.2319
(15, 30)	0.2499	0.2482
(20, 40)	0.2500	0.2497
Analytical	0.2500	

Table 3.2 Convergence of cylinder stiffnesses for various discretizations and locations of surface S'

	c=0.1			c=0.15		
(M, M')	K_h	$K_{mh} = K_{hm}$	K_m	K_h	$K_{mh} = K_{hm}$	K_m
(16, 8)	9.46	-2.87	13.48	9.49	-2.83	13.59
(24, 12)	9.51	-2.79	13.80	9.48	-2.81	13.75
(28, 14)	9.52	-2.78	13.88	9.51	-2.77	13.85
(32, 20)	9.52	-2.75	13.93	9.51	-2.77	13.92
Case 1	9.52	-2.75	13.94			

Case 1: Apsel and Luco (1987)

Table 3.3: Axial and horizontal stiffness of a rigid cylinder embedded in transversely isotropic elastic half space

	K_v				K_h			
h/a	Ice	Clay I	Clay II	Isotropic	Ice	Clay I	Clay II	Isotropic
0.5	9.30	7.74	6.77	7.10	8.59	10.00	10.32	7.50
1.0	10.27	9.03	8.06	8.35	10.93	12.90	12.90	9.52
2.0	12.28	10.97	10.00	10.32	14.80	18.06	18.06	12.87
4.0	16.16	14.84	13.87	13.92	21.20	22.58	22.90	17.50

Table 3.4: Rocking and coupled stiffness of a rigid cylinder embedded in transversely isotropic elastic half space

	K_m				K_{hm}			
h/a	Ice	Clay I	Clay II	Isotropic	Ice	Clay I	Clay II	Isotropic
0.5	9.37	8.06	7.74	7.56	0.93	1.29	0.97	0.73
1.0	16.40	16.45	15.81	13.93	3.31	3.87	3.87	2.75
2.0	42.08	46.77	46.13	36.37	10.59	12.58	12.58	9.06
4.0	160.28	178.39	179.35	131.04	33.65	44.19	44.19	25.76

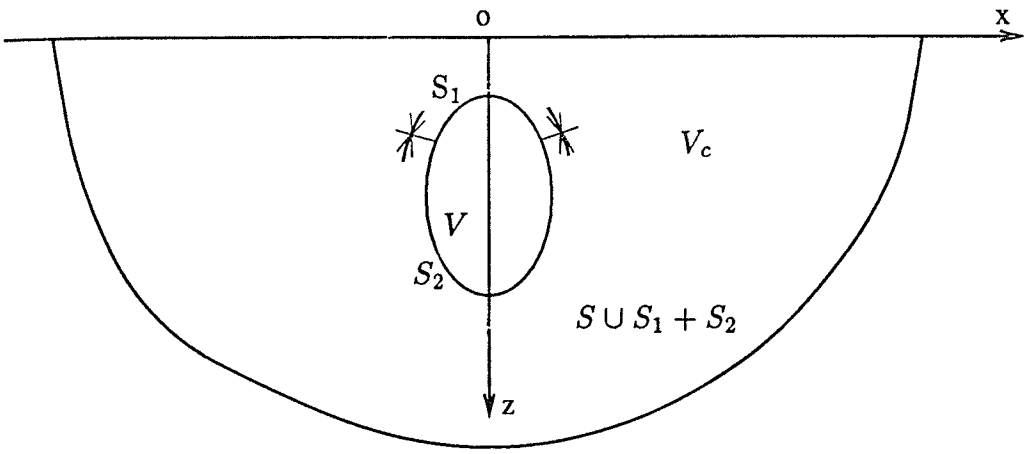

Figure 3.1 Domains and surfaces related to boundary value problems

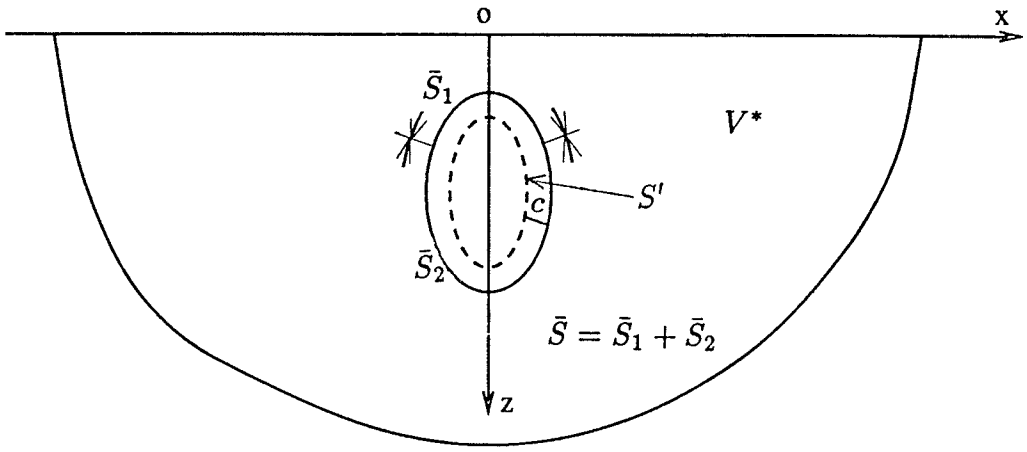

Figure 3.2 Equivalent domain considered in the indirect boundary integral method

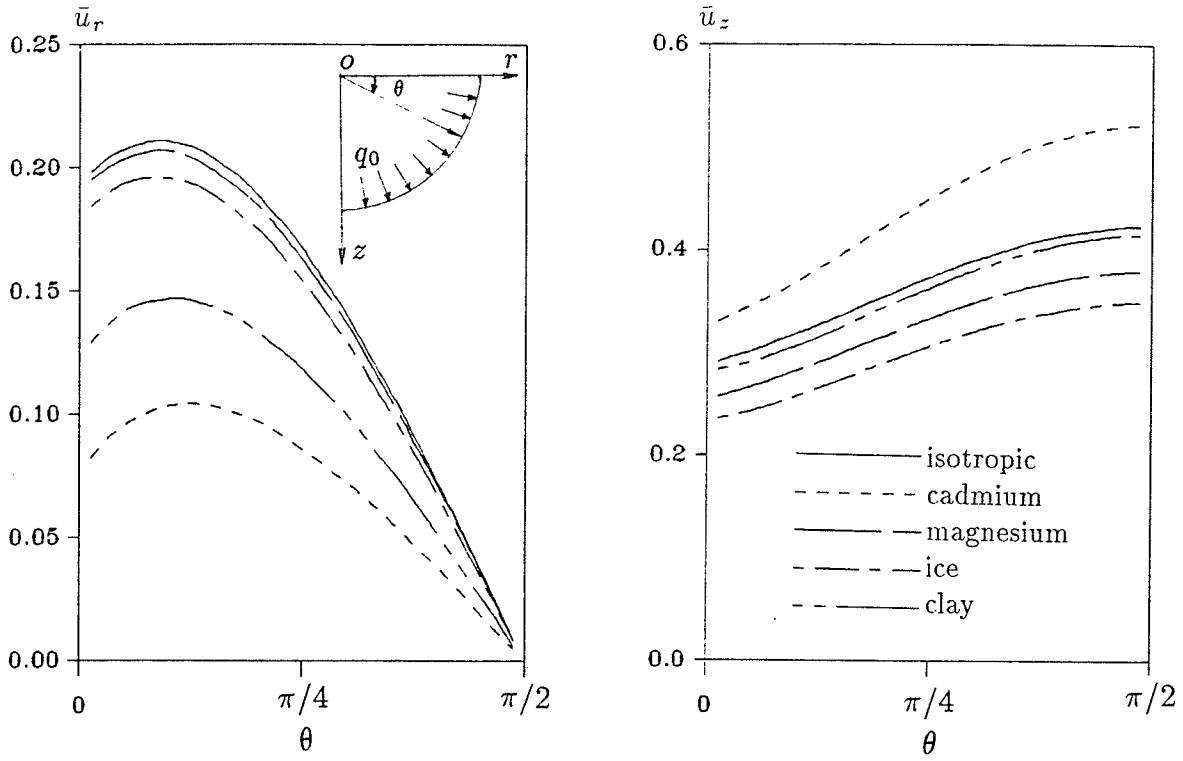

Figure 3.3 Displacement profiles along hemispherical cavity surface

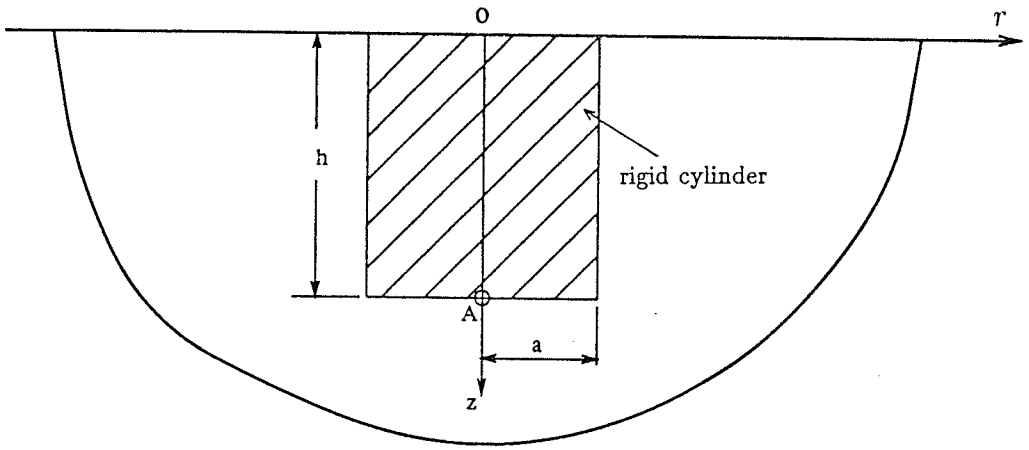

Figure 3.4 Geometry of rigid cylinder embedded in a half space

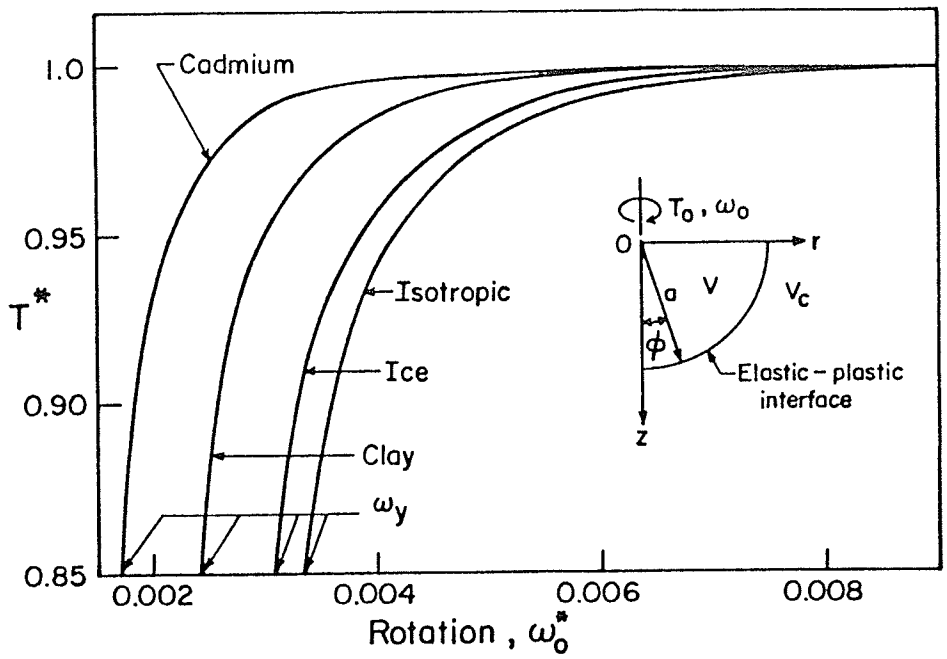

Figure 3.5 Torque-twist relationship after initiation of interface yielding

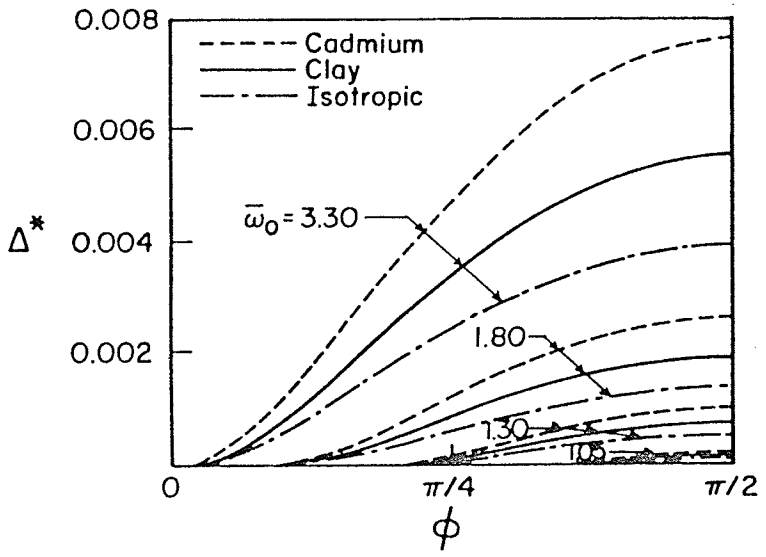

Figure 3.6 Slip along the interface after initiation of interface yielding

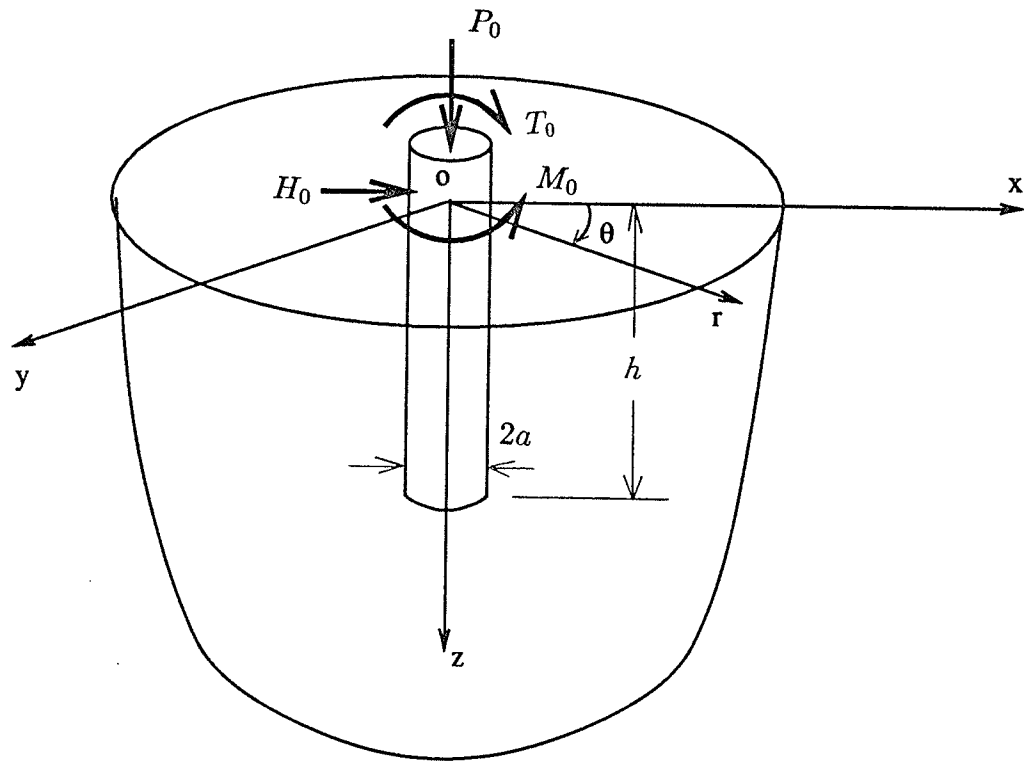

Figure 3.7 Elastic bar embedded in transversely isotropic half space

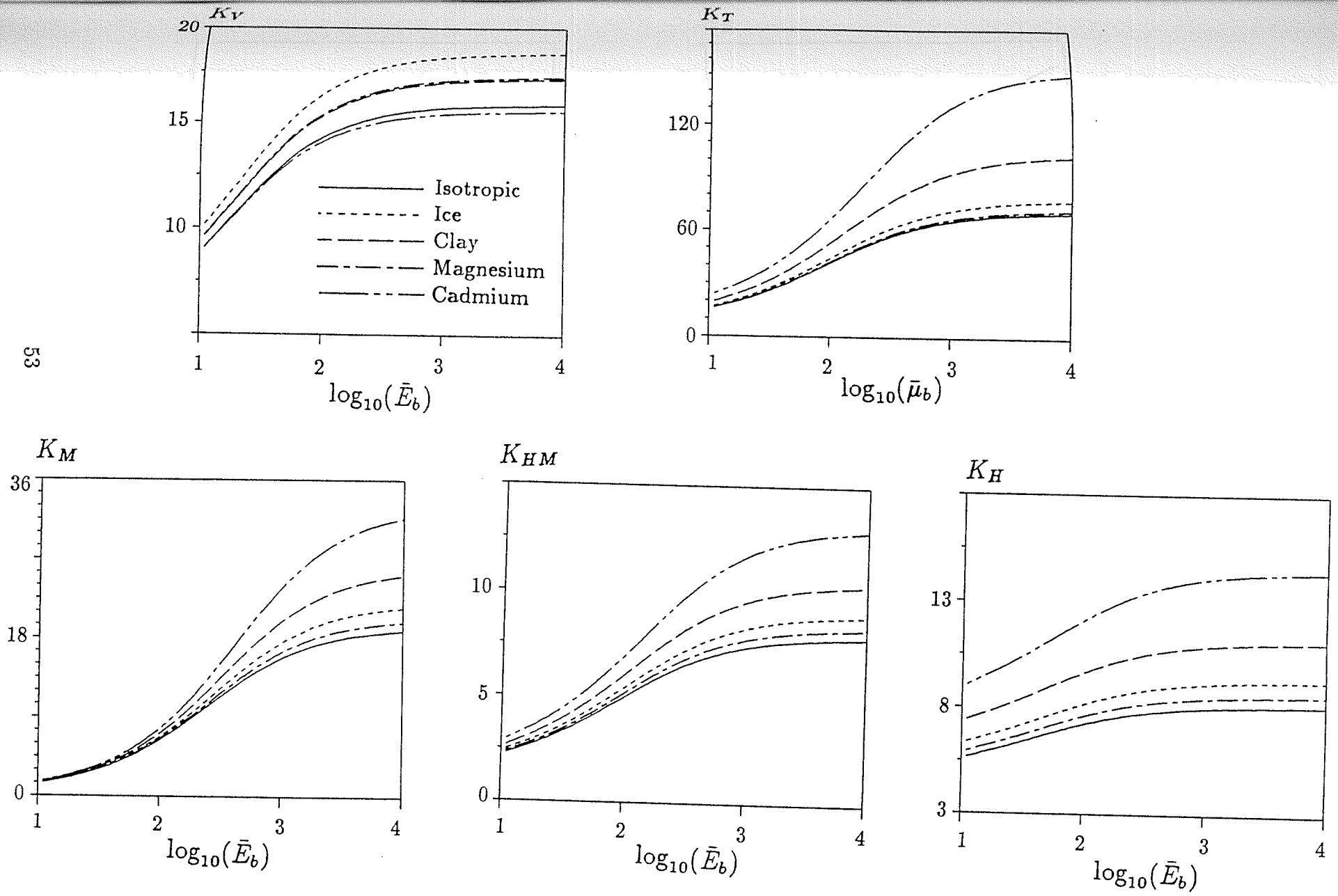

Figure 3.8 Stiffness parameters of elastic bars embedded in different anisotropic media ($h/a = 5$)

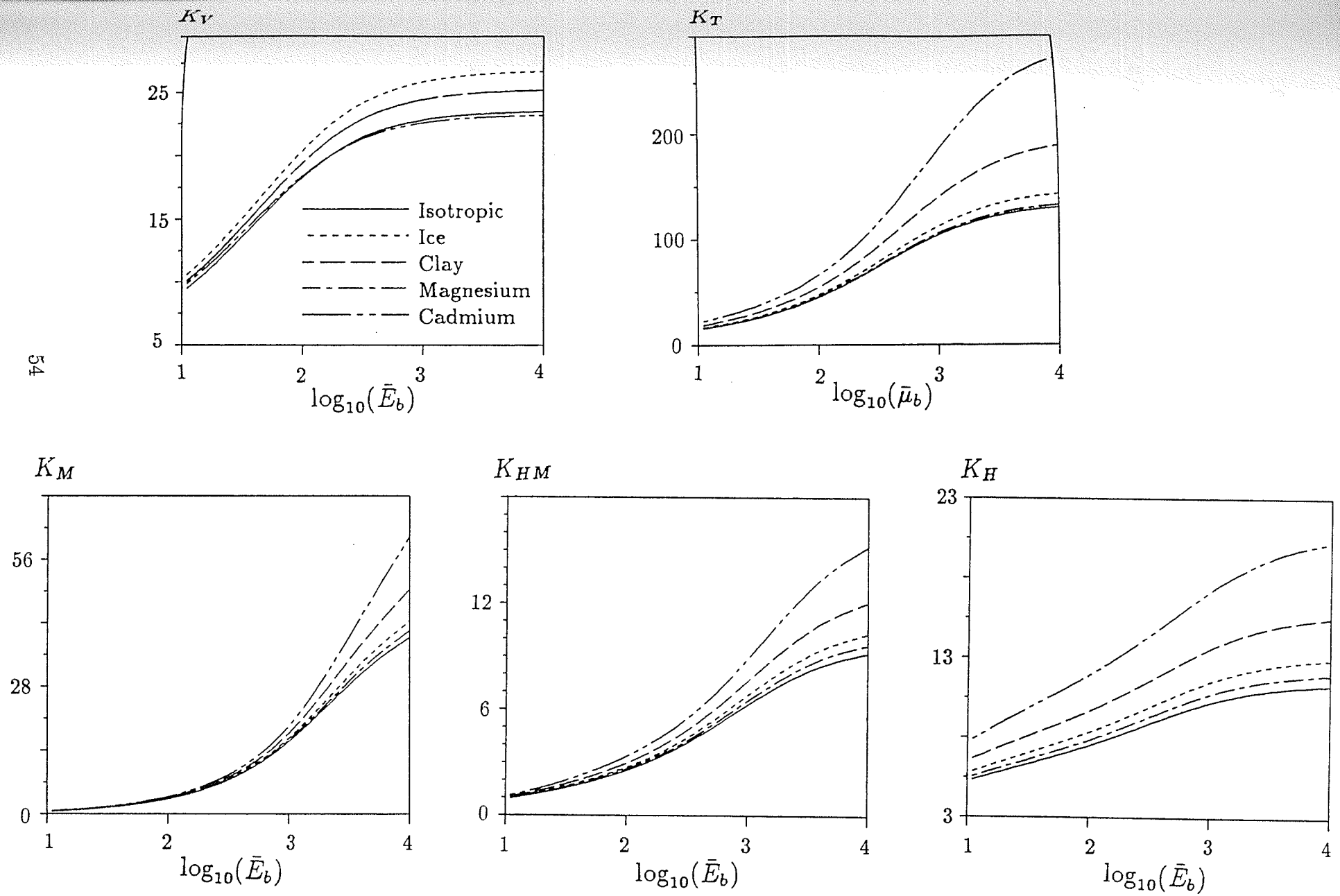

Figure 3.9 Stiffness parameters of elastic bars embedded in different anisotropic media ($h/a = 10$)

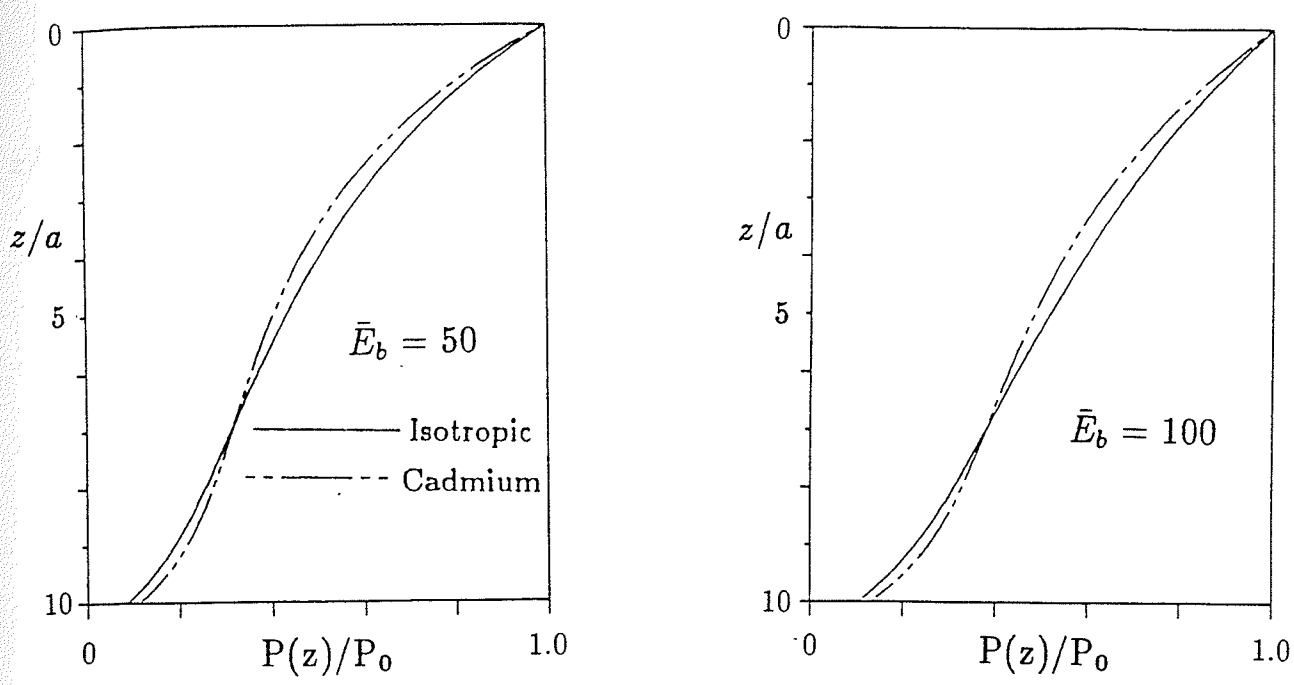

Figure 3.10 Axial load profile of elastic bars ($h/a = 10$)

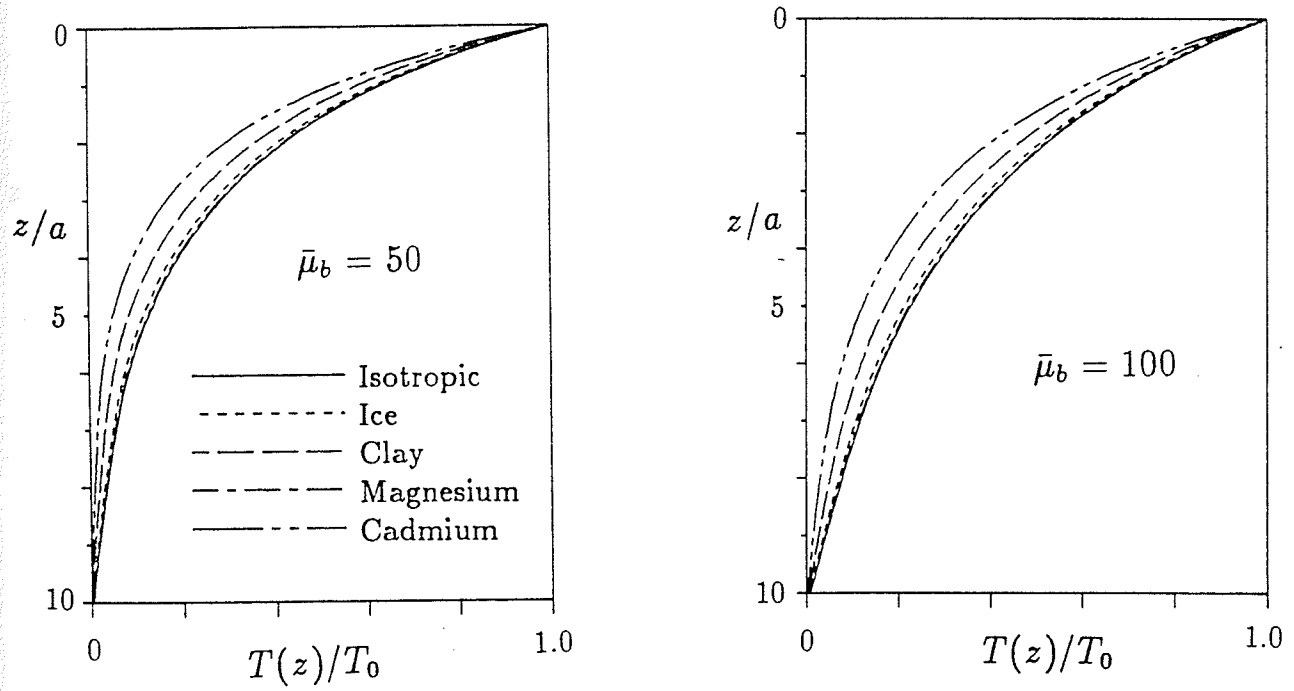

Figure 3.11 Torque profiles of Elastic bars ($h/a = 10$)

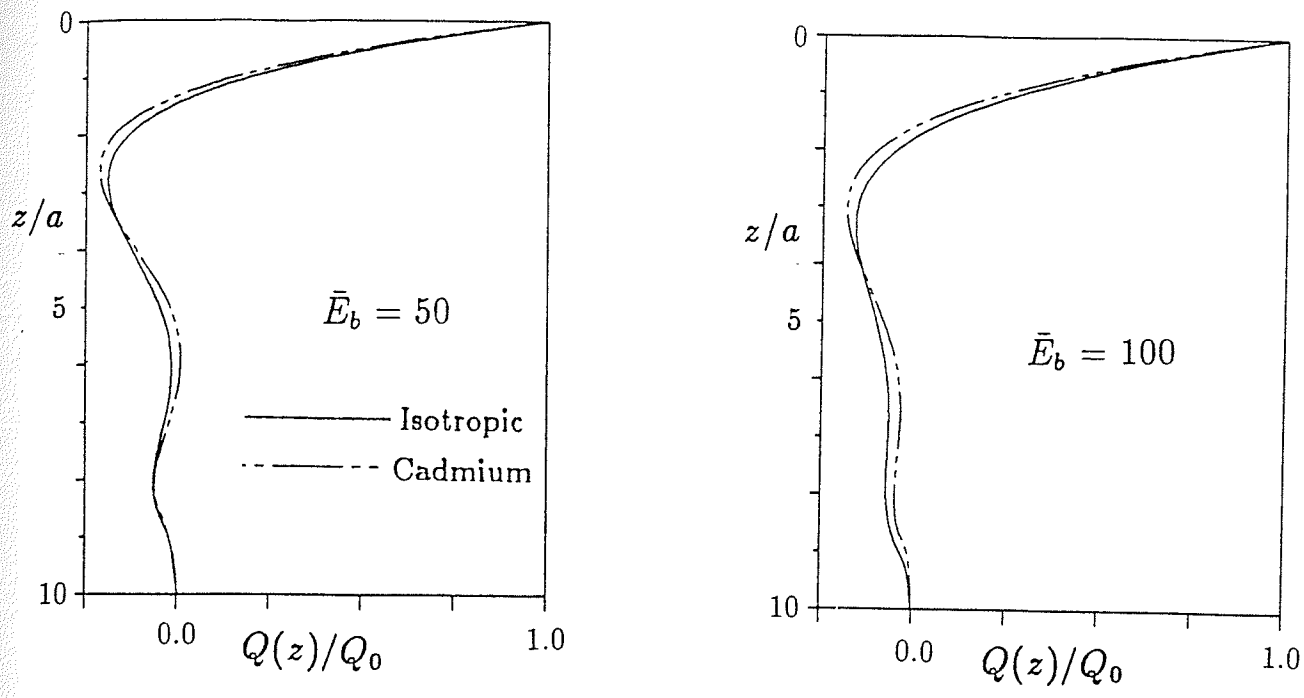

Figure 3.12 Shear force profiles of elastic bars under horizontal load ($h/a = 10$)

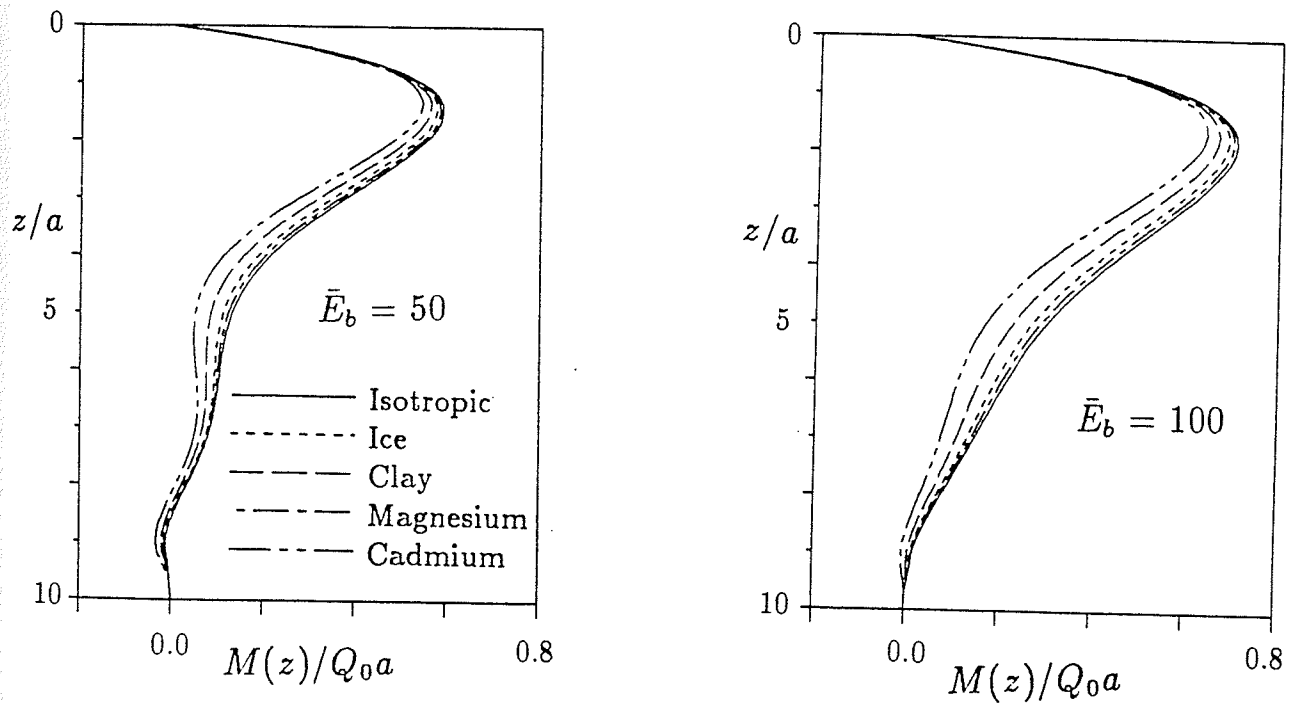

Figure 3.13 Bending moment profiles of elastic bars under horizontal load ($h/a = 10$)

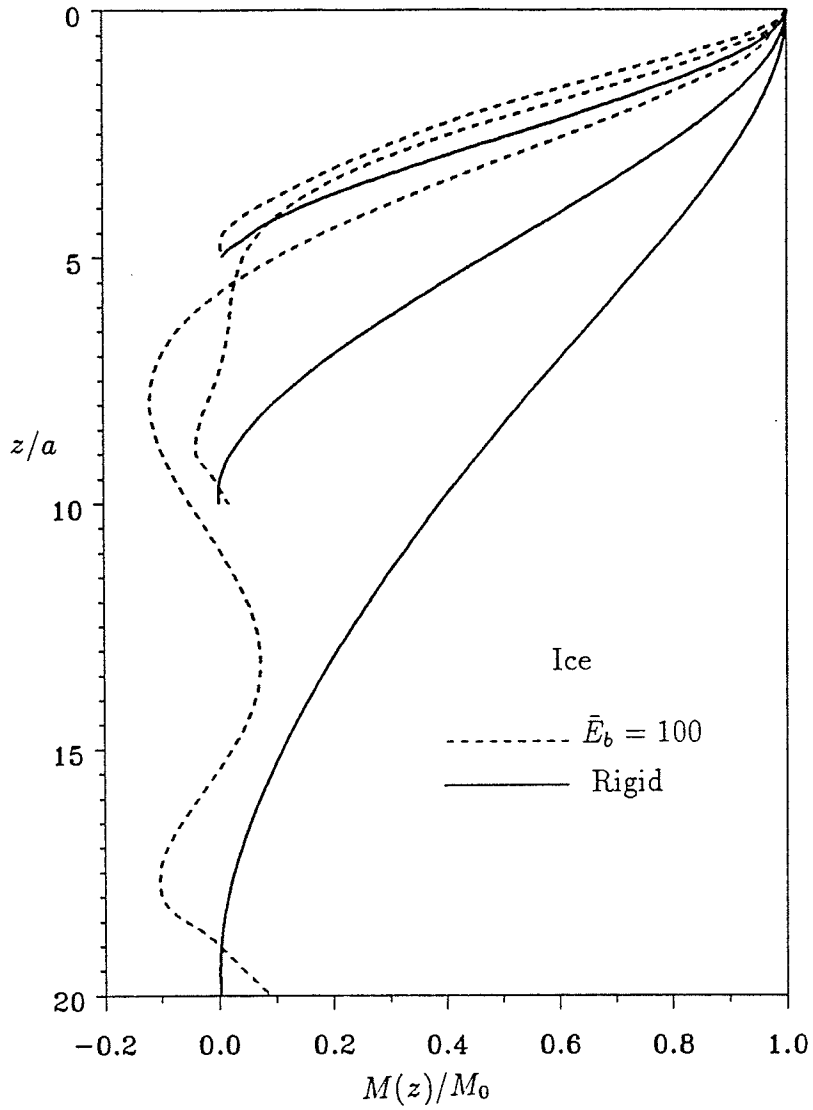

Figure 3.14 Bending moment profiles of elastic and rigid bars with different length radius radio under moment loading ($h/a = 5, 10, 20$)

Chapter 4

2-D ELASTODYNAMIC GREEN'S FUNCTIONS

4.1 GENERAL

In this chapter, explicit analytical solutions for displacement and stress Green's functions of a homogeneous orthotropic elastic half-plane are presented. Fourier integral transforms and Laplace transforms are employed to solve the governing equations corresponding to time-harmonic and transient problems. General solutions for displacements and stresses are presented. Thereafter solutions for displacement and stress Green's functions corresponding to a set of time-harmonic and transient internal vertical and horizontal loadings and transient displacement discontinuities are derived explicitly. Selected numerical results for displacements and stresses are also presented to portray the influence of various parameters on the response. The availability of an exact analytical solution for elastodynamic Green's functions and an accurate numerical procedure for its evaluation enables the solution of more complicated problems related to dynamic soil-structure interaction, elastic wave scattering, fracture mechanics *etc.* by using the boundary integral equation method and other techniques as demonstrated in Chapter 6.

4.2 GOVERNING EQUATIONS

Consider a homogeneous orthotropic elastic medium with Cartesian coordinate system (x, y, z) defined as shown in Fig 4.1. The stress-strain relationship of a homogeneous orthotropic elastic material can be expressed as (Lekhnitskii 1963)

$$\sigma_{xx} = c_{11}\varepsilon_{xx} + c_{12}\varepsilon_{yy} + c_{13}\varepsilon_{zz} \qquad (4.1a)$$

$$\sigma_{yy} = c_{12}\varepsilon_{xx} + c_{22}\varepsilon_{yy} + c_{23}\varepsilon_{zz} \tag{4.1b}$$

$$\sigma_{zz} = c_{13}\varepsilon_{xx} + c_{23}\varepsilon_{yy} + c_{33}\varepsilon_{zz} \tag{4.1c}$$

$$\sigma_{xy} = 2c_{55}\varepsilon_{xy} \tag{4.1d}$$

$$\sigma_{xz} = 2c_{44}\varepsilon_{xz} \tag{4.1e}$$

$$\sigma_{yz} = 2c_{66}\varepsilon_{yz} \tag{4.1f}$$

where $c_{11}, c_{12}, c_{13}, c_{22}, c_{23}, c_{33}, c_{44}, c_{55}$ and c_{66} are material constants. It is assumed that the deformations are plane strain in the xz plane. Therefore $\varepsilon_{yy} = \varepsilon_{yz} = \varepsilon_{xy} = 0$ and $c_{12}, c_{22}, c_{23}, c_{55}$ and c_{66} do not appear in subsequent manipulations. It is noted that constitutive equations for plane strain problems corresponding to orthotropic materials are identical to those corresponding to a transversely isotropic material with xy plane as the plane of isotropy [eqn (2.1)].

The equations of motion in the absence of body forces can be expressed in terms of displacements $u_x(x,z,t)$ and $u_z(x,z,t)$ as

$$c_{11}\frac{\partial^2 u_x}{\partial x^2} + c_{44}\frac{\partial^2 u_x}{\partial z^2} + (c_{13}+c_{44})\frac{\partial^2 u_z}{\partial x \partial z} = \rho\frac{\partial^2 u_x}{\partial t^2} \tag{4.2a}$$

$$c_{44}\frac{\partial^2 u_z}{\partial x^2} + c_{33}\frac{\partial^2 u_z}{\partial z^2} + (c_{13}+c_{44})\frac{\partial^2 u_x}{\partial x \partial z} = \rho\frac{\partial^2 u_z}{\partial t^2} \tag{4.2b}$$

where ρ is the mass density of the orhtotropic medium.

4.3 TIME-HARMONIC GENERAL SOLUTIONS

It is assumed that the motion is time-harmonic of the form $e^{i\omega t}$, where $i = \sqrt{-1}$ and ω is the circular frequency. An uncoupled version of eqns (4.2a) and (4.2b) can be written as

$$Lu_x(x,z) = 0, \qquad Lu_z(x,z) = 0 \tag{4.3}$$

where L is a linear differential operator defined by

$$L = \beta\frac{\partial^4}{\partial x^4} + \alpha\frac{\partial^4}{\partial z^4} + \gamma\frac{\partial^4}{\partial x^2 \partial z^2} + (1+\beta)\delta^2\frac{\partial^2}{\partial x^2} + (1+\alpha)\delta^2\frac{\partial^2}{\partial z^2} + \delta^4 \tag{4.4}$$

where α, β and γ are defined in eqn (2.5) and

$$\delta^2 = \rho \frac{\omega^2}{c_{44}} \tag{4.5}$$

In two-dimensional elastodynamic problems related to unbounded domains it is natural to introduce Fourier integral transforms (Sneddon 1951) with respect to the x-coordinate defined as

$$\tilde{f}(\lambda, z) = \frac{1}{\sqrt{2\pi}} \int_{-\infty}^{\infty} f(x, z) e^{-i\lambda x} dx \tag{4.6a}$$

and the inverse formula is defined by

$$f(x, z) = \frac{1}{\sqrt{2\pi}} \int_{-\infty}^{\infty} \tilde{f}(\lambda, z) e^{i\lambda x} d\lambda \tag{4.6b}$$

The application of Fourier integral transforms to eqn (4.3) results in

$$\bar{L}\tilde{u}_x(\lambda, z) = 0, \qquad \bar{L}\tilde{u}_z(\lambda, z) = 0 \tag{4.7}$$

where $\tilde{u}_x$ and $\tilde{u}_z$ denote Fourier transforms of u_x and u_z and

$$\bar{L} = \beta\lambda^4 + \alpha \frac{d^4}{dz^4} - \gamma\lambda^2 \frac{d^2}{dz^2} - (1+\beta)\lambda^2\delta^2 + (1+\alpha)\delta^2 \frac{d^2}{dz^2} + \delta^4 \tag{4.8}$$

The ordinary differential equations for $\tilde{u}_x$ and $\tilde{u}_z$ given by eqn (4.7) can be solved analytically and the following general solutions are obtained for displacements and stresses

$$u_l = \frac{\delta}{\sqrt{2\pi}} \int_{-\infty}^{\infty} \tilde{u}_l e^{i\delta\zeta x} d\zeta; \qquad l = x, z \tag{4.9a}$$

$$\sigma_{lj} = \frac{\delta}{\sqrt{2\pi}} \int_{-\infty}^{\infty} \tilde{\sigma}_{lj} e^{i\delta\zeta x} d\zeta; \qquad l, j = x, z \tag{4.9b}$$

where $\tilde{\sigma}_{xx}, \tilde{\sigma}_{xz}$ and $\tilde{\sigma}_{zz}$ are the Fourier transforms of σ_{xx}, σ_{xz} and σ_{zz} respectively, and

$$\tilde{u}_x = \varpi_1 A e^{-\delta\xi_1 z} - \varpi_1 B e^{\delta\xi_1 z} + \varpi_2 C e^{-\delta\xi_2 z} - \varpi_2 D e^{\delta\xi_2 z} \tag{4.10a}$$

$$\tilde{u}_z = A e^{-\delta\xi_1 z} + B e^{\delta\xi_1 z} + C e^{-\delta\xi_2 z} + D e^{\delta\xi_2 z} \tag{4.10b}$$

$$\tilde{\sigma}_{xx} = c_{44}\delta(\eta_1 A e^{-\delta\xi_1 z} - \eta_1 B e^{\delta\xi_1 z} + \eta_2 C e^{-\delta\xi_2 z} - \eta_2 D e^{\delta\xi_2 z}) \tag{4.10c}$$

$$\tilde{\sigma}_{xz} = c_{44}\delta(\eta_3 A e^{-\delta\xi_1 z} + \eta_3 B e^{\delta\xi_1 z} + \eta_4 C e^{-\delta\xi_2 z} + \eta_4 D e^{\delta\xi_2 z}) \tag{4.10d}$$

$$\tilde{\sigma}_{zz} = c_{44}\delta(\eta_5 A e^{-\delta\xi_1 z} - \eta_5 B e^{\delta\xi_1 z} + \eta_6 C e^{-\delta\xi_2 z} - \eta_6 D e^{\delta\xi_2 z}) \tag{4.10e}$$

where $A(\zeta), B(\zeta), C(\zeta)$ and $D(\zeta)$ are arbitrary functions and a normalised Fourier transform parameter ζ defined by $\zeta = \lambda/\delta$ is used in eqns (4.9)-(4.10) instead of λ. In addition,

$$\eta_1 = \frac{1}{\kappa\xi_1}[(\gamma - 1 + \kappa)\xi_1^2 + \beta(1-\zeta^2)]; \quad \eta_2 = \frac{1}{\kappa\xi_2}[(\gamma - 1 + \kappa)\xi_2^2 + \beta(1-\zeta^2)] \tag{4.11a}$$

$$\eta_3 = \frac{i}{\kappa\zeta}[(\alpha\xi_1^2 + 1) + (\kappa - 1)\zeta^2]; \quad \eta_4 = \frac{i}{\kappa\zeta}[(\alpha\xi_2^2 + 1) + (\kappa - 1)\zeta^2] \tag{4.11b}$$

$$\eta_5 = \frac{1}{\kappa\xi_1}[(\kappa - 1)(1-\zeta^2) - \alpha\xi_1^2]; \quad \eta_6 = \frac{1}{\kappa\xi_2}[(\kappa - 1)(1-\zeta^2) - \alpha\xi_2^2] \tag{4.11c}$$

$$\varpi_1 = \frac{\alpha\xi_1^2 + 1 - \zeta^2}{i\kappa\xi_1\zeta}; \quad \varpi_2 = \frac{\alpha\xi_2^2 + 1 - \zeta^2}{i\kappa\xi_2\zeta} \tag{4.11d}$$

In eqns (4.10) and (4.11), ξ_1^2 and ξ_2^2 are the roots of the following equation

$$\alpha\xi^4 - (\gamma\zeta^2 - 1 - \alpha)\xi^2 + [\beta\zeta^4 - (1+\beta)\zeta^2 + 1] = 0 \tag{4.12}$$

Therefore,

$$\xi_1(\zeta) = \frac{(\gamma\zeta^2 - 1 - \alpha + \sqrt{\Phi})^{\frac{1}{2}}}{\sqrt{2\alpha}} \tag{4.13a}$$

$$\xi_2(\zeta) = \frac{(\gamma\zeta^2 - 1 - \alpha - \sqrt{\Phi})^{\frac{1}{2}}}{\sqrt{2\alpha}} \tag{4.13b}$$

and

$$\Phi(\zeta) = (\gamma\zeta^2 - 1 - \alpha)^2 - 4\alpha(\beta\zeta^4 - \beta\zeta^2 - \zeta^2 + 1) \tag{4.14}$$

The radicals ξ_1 and ξ_2 are selected such that $Re(\xi_1, \xi_2) \geq 0$. With this definition the radiation condition at infinity is satisfied and $B(\zeta) = D(\zeta) \equiv 0$ for a domain where $z \to \infty$. It can be shown that in the case of an isotropic material, $\alpha = \beta = \gamma/2 = (\bar{\lambda} + 2\bar{\mu})/\bar{\mu}$, where $\bar{\lambda}$ and $\bar{\mu}$ are Lame constants, and the eqn (4.13) reduces to $\xi_1 = (\zeta^2 - \alpha^{-1})^{\frac{1}{2}}$ and $\xi_2 = (\zeta^2 - 1)^{\frac{1}{2}}$, respectively.

4.4 TRANSIENT GENERAL SOLUTIONS

In the case of an orthotropic elastic medium subjected to transient dynamic loadings, it is convenient to employ Laplace transform to obtain the general solutions. Laplace transform of function $F(t)$ is defined by (Sneddon 1951)

$$\bar{F}(p) = \int_0^\infty F(t) e^{-pt} dt \tag{4.15a}$$

and the inverse formula is defined by

$$F(t) = \frac{i}{2\pi} \int_{d-i\infty}^{d+i\infty} \bar{F}(p) e^{pt} dp \tag{4.15b}$$

where p is the transform parameter defined as

$$p = d + i\varrho \tag{4.16}$$

and the line $p = d$ is to the right of all singularities of $\bar{F}(p)$.

The application of Laplace transforms to the equations of motion corresponding to a medium which is at rest for $t \leq 0$ and subsequent manipulations result in the following uncoupled form of the eqn (4.2).

$$L^* \bar{u}_x(x, z, p) = 0, \qquad L^* \bar{u}_z(x, z, p) = 0 \tag{4.17}$$

where $\bar{u}_x$ and $\bar{u}_z$ are the Laplace transforms of horizontal and vertical displacements and L^* is a linear differential operator defined by

$$L^* = \beta \frac{\partial^4}{\partial x^4} + \alpha \frac{\partial^4}{\partial z^4} + \gamma \frac{\partial^4}{\partial x^2 \partial z^2} - (1+\beta)\mu^2 \frac{\partial^2}{\partial x^2} - (1+\alpha)\mu^2 \frac{\partial^2}{\partial z^2} + \mu^4 \tag{4.18}$$

and

$$\mu^2 = \rho\frac{p^2}{c_{44}} = p^2/\vartheta^2 \tag{4.19}$$

The application of Fourier integral transforms to eqn (4.17) results in

$$\tilde{L}\tilde{u}_x(\lambda, z, \mu) = 0, \qquad \tilde{L}\tilde{u}_z(\lambda, z, \mu) = 0 \tag{4.20}$$

where $\tilde{u}_x$ and $\tilde{u}_z$ are the Fourier transforms of $\bar{u}_x$ and $\bar{u}_z$ and

$$\tilde{L} = \beta\lambda^4 + \alpha\frac{d^4}{dz^4} - \gamma\lambda^2\frac{d^2}{dz^2} + (1+\beta)\lambda^2\mu^2 - (1+\alpha)\mu^2\frac{d^2}{dz^2} + \mu^4 \tag{4.21}$$

The ordinary differential equations for $\tilde{u}_x$ and $\tilde{u}_z$ given by eqn (4.20) can be solved analytically and the following general solutions are obtained for displacements and stresses

$$u_l = \frac{i\vartheta}{\sqrt{8\pi^3}}\int_{d-i\infty}^{d+i\infty}\int_{-\infty}^{\infty}\tilde{u}_l e^{i\lambda x+\vartheta\mu t}d\lambda d\mu; \qquad l = x, z \tag{4.22a}$$

$$\sigma_{lj} = \frac{i\vartheta}{\sqrt{8\pi^3}}\int_{d-i\infty}^{d+i\infty}\int_{-\infty}^{\infty}\tilde{\sigma}_{lj} e^{i\lambda x+\vartheta\mu t}d\lambda d\mu; \quad l, j = x, z \tag{4.22b}$$

where $\tilde{\sigma}_{xx}, \tilde{\sigma}_{xz}$ and $\tilde{\sigma}_{zz}$ are the Laplace-Fourier transforms of stresses σ_{xx}, σ_{xz} and σ_{zz} respectively, and the expressions for $\tilde{u}_i$ and $\tilde{\sigma}_{ij}(i, j = x, z)$ are identical to those given by eqn (4.10) for the time-harmonic case with the following definition of parameters $\eta_i(i = 1, 2, ..., 6), \varpi_1, \varpi_2, \xi_1$ and ξ_2.

$$\eta_1 = \frac{1}{\kappa\xi_1}[(\gamma-1+\kappa)\xi_1^2-\beta(\mu^2+\lambda^2)]; \quad \eta_2 = \frac{1}{\kappa\xi_2}[(\gamma-1+\kappa)\xi_2^2-\beta(\mu^2+\lambda^2)] \tag{4.23a}$$

$$\eta_3 = \frac{i}{\kappa\lambda}[(\alpha\xi_1^2+\mu^2)+(\kappa-1)\lambda^2]; \qquad \eta_4 = \frac{i}{\kappa\lambda}[(\alpha\xi_2^2+\mu^2)+(\kappa-1)\lambda^2] \tag{4.23b}$$

$$\eta_5 = \frac{-1}{\kappa\xi_1}[(\kappa-1)(\mu^2+\lambda^2)+\alpha\xi_1^2]; \qquad \eta_6 = \frac{-1}{\kappa\xi_2}[(\kappa-1)(\mu^2+\lambda^2)+\alpha\xi_2^2] \tag{4.23c}$$

$$\varpi_1 = \frac{\alpha\xi_1^2 - \mu^2 - \lambda^2}{i\kappa\xi_1\lambda}; \qquad \varpi_2 = \frac{\alpha\xi_2^2 - \mu^2 - \lambda^2}{i\kappa\xi_2\lambda} \tag{4.24}$$

In addition, ξ_1^2 and ξ_2^2 are the roots of the following equation

$$\alpha\xi^4 - (\gamma\lambda^2 + \mu^2 + \alpha\mu^2)\xi^2 + [\beta\lambda^4 + (\mu^2 + \beta\mu^2)\lambda^2 + \mu^4] = 0 \tag{4.25}$$

in which

$$\xi_1(\lambda) = \frac{(\gamma\lambda^2 + \mu^2 + \alpha\mu^2 + \sqrt{\Phi})^{\frac{1}{2}}}{\sqrt{2\alpha}} \tag{4.26a}$$

$$\xi_2(\lambda) = \frac{(\gamma\lambda^2 + \mu^2 + \alpha\mu^2 - \sqrt{\Phi})^{\frac{1}{2}}}{\sqrt{2\alpha}} \tag{4.26b}$$

and

$$\Phi(\zeta) = (\gamma\lambda^2 + \mu^2 + \alpha\mu^2)^2 - 4\alpha(\beta\lambda^4 + \beta\lambda^2\mu^2 + \lambda^2\mu^2 + \mu^4) \tag{4.27}$$

The radicals ξ_1 and ξ_2 are selected such that $Re(\xi_1, \xi_2) \geq 0$. Again with this definition the radiation condition at infinity is satisfied, and $B(\lambda) = D(\lambda) \equiv 0$ for a domain where $z \to \infty$. It can be shown that in the case of an isotropic material eqn (4.26) reduces to $\xi_1 = (\lambda^2 + \mu^2/\alpha)$ and $\xi_2 = (\lambda^2 + \mu^2)$ where $\alpha = 2(1-\nu)/(1-2\nu)$ and ν is the Poisson's ratio.

4.5 TIME-HARMONIC GREEN'S FUNCTIONS

Consider an orthotropic elastic half plane region subjected to buried time-harmonic loadings in the vertical z- and horizontal x-directions as shown in Figure 4.1. The loading is assumed to be distributed over a strip of width $2a$ located at a depth z' below the free surface. The loading is uniform in the y-direction so that the resulting deformations are of plane strain type. The boundary-value problem associated with the internally loaded half plane can be solved by defining a fictitious horizontal plane at $z = z'$ and considering a two-domain boundary-value problem (Fig 4.1). The domain '1' is defined by $|x| < \infty, 0 \leq z \leq z'$ and for the domain '2', $|x| < \infty$, and $z' \leq z < \infty$. The general solution for displacements and

stresses of each domain is given by eqn (4.9) together with (4.10) with each arbitrary function incorporated with a subscript 'j', ($j = 1, 2$) to denote the domain number. It is evident that $B_2(\zeta) = D_2(\zeta) \equiv 0$ to satisfy radiation condition at infinity. The boundary-value problem corresponding to the loaded half plane can be described by

$$\sigma_{zi}^{(1)}(x, 0) = 0, \qquad i = x, z \tag{4.28a}$$

$$u_i^{(1)}(x, z') - u_i^{(2)}(x, z') = 0; \quad i = x, z \tag{4.28b}$$

$$\sigma_{zi}^{(1)}(x, z') - \sigma_{zi}^{(2)}(x, z') = p_i(x)[H(x + a) - H(x - a)], \quad i = x, z \tag{4.28c}$$

In eqn (4.28), $H(x)$ denotes the unit step function. The intensity of distributed load acting in the i-direction over a strip of width $2a$ is denoted by $p_i (i = x, z)$. The solution of eqn (4.28) with the aid of general solutions given by eqns (4.9) and (4.10) results in the solutions for arbitrary coefficients corresponding to the two domains.

It is convenient to present solutions corresponding to horizontal and vertical loadings separately. Let $G_{ij}(x, z; 0, z')$ denote the displacement in the i-direction ($i = x, z$) at the point (x, z) due to a symmetrically distributed load p_j acting in the j-direction ($j = x, z$) over a strip of width $2a$ located at the depth z' (Fig 4.1) and $\sigma_{ilj}(x, z; 0, z')$ denote the stress component σ_{il} ($i, l = x, z$) at the point (x, z) due to the same loading configuration. The following analytical solutions are obtained for $G_{ij}(x, z; 0, z')$ and $\sigma_{ilj}(x, z; 0, z')$ from the analysis.

$$G_{ij}(x, z; 0, z') = \frac{1}{\pi c_{44}} \int_0^\infty G_{ij}^* d\zeta, \qquad i, j = x, z \tag{4.29a}$$

$$\sigma_{ilj}(x, z; 0, z') = \frac{\delta}{\pi} \int_0^\infty \sigma_{ilj}^* d\zeta, \qquad i, l, j = x, z \tag{4.29b}$$

where

$$G_{xx}^* = \frac{-\tilde{p}_x}{KE}(g_1 e_1 + g_1 e_2 + g_2 e_3 - g_2 e_4 - g_1 e_5 - g_2 e_6) \cos(\delta\zeta x) \tag{4.30a}$$

$$G^*_{zx} = \frac{\tilde{p}_x}{KE}(-e_1 + Ie_2 - e_3 - Ie_4 + e_5 + e_6)\sin(\delta\zeta x) \tag{4.30b}$$

$$\sigma^*_{xxx} = \frac{-\tilde{p}_x}{KE}(\eta_1 e_1 + \eta_1 e_2 + \eta_2 e_3 - \eta_2 e_4 - \eta_1 e_5 - \eta_2 e_6)\sin(\delta\zeta x) \tag{4.31a}$$

$$\sigma^*_{xzx} = \frac{\tilde{p}_x}{KE}(-\bar{\eta}_3 e_1 + I\bar{\eta}_3 e_2 - \bar{\eta}_4 e_3 - I\bar{\eta}_4 e_4 + \bar{\eta}_3 e_5 + \bar{\eta}_4 e_6)\cos(\delta\zeta x) \tag{4.31b}$$

$$\sigma^*_{zzx} = \frac{-\tilde{p}_x}{KE}(\eta_5 e_1 + \eta_5 e_2 + \eta_6 e_3 - \eta_6 e_4 - \eta_5 e_5 - \eta_6 e_6)\sin(\delta\zeta x) \tag{4.31c}$$

$$G^*_{xz} = \frac{\tilde{p}_z}{KG}(g_1 g_2 e_1 + Ig_1 g_2 e_2 + g_1 g_2 e_3 - Ig_1 g_2 e_4 - g_1^2 e_5 - g_2^2 e_6)\sin(\delta\zeta x) \tag{4.32a}$$

$$G^*_{zz} = \frac{\tilde{p}_z}{KG}(g_2 e_1 - g_2 e_2 + g_1 e_3 + g_1 e_4 - g_1 e_5 - g_2 e_6)\cos(\delta\zeta x) \tag{4.32b}$$

$$\sigma^*_{xxz} = \frac{\tilde{p}_z}{KG}(f_1 e_1 + If_1 e_2 + f_2 e_3 - If_2 e_4 - \eta_1 g_1 e_5 - \eta_2 g_2 e_6)\cos(\delta\zeta x) \tag{4.33a}$$

$$\sigma^*_{xzz} = \frac{\tilde{p}_z}{KG}(f_3 e_1 - f_3 e_2 + f_4 e_3 + f_4 e_4 - \bar{\eta}_3 g_1 e_5 - \bar{\eta}_4 g_2 e_6)\sin(\delta\zeta x) \tag{4.33b}$$

$$\sigma^*_{zzz} = \frac{\tilde{p}_z}{KG}(f_5 e_1 + If_5 e_2 + f_6 e_3 - If_6 e_4 - \eta_5 g_1 e_5 - \eta_6 g_2 e_6)\cos(\delta\zeta x) \tag{4.33c}$$

in which

$$I = \frac{(z' - z)}{|z' - z|} \tag{4.34}$$

and

$$K = [2(1-\kappa)\zeta^2 - \gamma\zeta^2 + \alpha](1 - \zeta^2) - \alpha\xi_1\xi_2 \tag{4.35}$$

$$Q = \frac{K(\xi_2 - \xi_1)}{\kappa\zeta\xi_1\xi_2} \tag{4.36a}$$

$$E = \frac{\alpha(\xi_1^2 - \xi_2^2)(\xi_2 - \xi_1)}{\kappa^2\zeta^2\xi_1\xi_2}; \qquad G = \frac{\alpha^2(\xi_1^2 - \xi_2^2)(\xi_2 - \xi_1)}{\kappa^2\zeta^2(1 - \beta\zeta^2)} \tag{4.36b}$$

$$\bar{\eta}_3 = i\eta_3; \quad \bar{\eta}_4 = i\eta_4; \quad f_1 = \eta_1 g_2; \quad f_2 = \eta_2 g_1; \quad f_3 = \bar{\eta}_3 g_2 \tag{4.37a}$$

$$f_4 = \bar{\eta}_4 g_1; \quad f_5 = \eta_5 g_2; \quad f_6 = \eta_6 g_1; \quad g_1 = i\varpi_1; \quad g_2 = i\varpi_2 \tag{4.37b}$$

$$h_1 = \bar{\eta}_3\eta_6 + \bar{\eta}_4\eta_5; \quad h_2 = 2\bar{\eta}_3\eta_5; \quad h_3 = 2\bar{\eta}_4\eta_6 \tag{4.37c}$$

$$e_1 = h_1 e^{-\delta\xi_1(z'+z)}; \quad e_2 = Qe^{-\delta\xi_1|z'-z|}; \quad e_3 = h_1 e^{-\delta\xi_2(z'+z)} \tag{4.38a}$$

$$e_4 = Qe^{-\delta\xi_2|z'-z|}; \quad e_5 = h_3 e^{-\delta(\xi_1 z + \xi_2 z')}; \quad e_6 = h_2 e^{-\delta(\xi_1 z' + \xi_2 z)} \tag{4.38c}$$

In eqns (4.30)-(4.33), $\tilde{p}_x$ and $\tilde{p}_z$ are related to the Fourier integral transform

of the applied loading. It is noted that if $p_i(x) = q_0$, (*i.e.*, uniform load) then,

$$\tilde{p}_i(\zeta) = \frac{\sin(\delta\zeta a)}{\delta\zeta} q_0; \qquad i = x, z \tag{4.39}$$

In the case of a concentrated line load of magnitude P_0 acting through the point $(0, z')$, $\tilde{p}_i$ is given by

$$\tilde{p}_i(\zeta) = \frac{P_0}{2}; \qquad i = x, z \tag{4.40}$$

Note that the solutions corresponding to nonuniformly distributed loading can be derived through the integration of point load solutions.

The solution corresponding to a load acting inside an elastic full plane can be derived from eqns (4.29) together with (4.30)-(4.33) through a limit procedure. For example, the solutions for an orthotropic elastic full plane subjected to a concentrated line load P_0 in the x-direction and applied at the coordinate origin can be expressed as in eqn (4.29) with the following solutions for G^*_{ij} and σ^*_{ilj}.

$$G^*_{xx}(x, z; 0, 0) = \frac{P_0}{2H}[g_1 e^{I'\delta\xi_1 z} - g_2 e^{I'\delta\xi_2 z}] \cos(\delta\zeta x) d\zeta \tag{4.41a}$$

$$G^*_{zx}(x, z; 0, 0) = \frac{I' P_0}{2H}[e^{I'\delta\xi_1 z} - e^{I'\delta\xi_2 z}] \sin(\delta\zeta x) d\zeta \tag{4.41b}$$

$$\sigma^*_{xxx}(x, z; 0, 0) = \frac{-P_0}{2H}[\eta_1 e^{I'\delta\xi_1 z} - \eta_2 e^{I'\delta\xi_2 z}] \sin(\delta\zeta x) d\zeta \tag{4.42a}$$

$$\sigma^*_{xzx}(x, z; 0, 0) = \frac{I' P_0}{2H}[\bar{\eta}_3 e^{I'\delta\xi_1 z} - \bar{\eta}_4 e^{I'\delta\xi_2 z}] \cos(\delta\zeta x) d\zeta \tag{4.42b}$$

$$\sigma^*_{zzx}(x, z; 0, 0) = \frac{-P_0}{2H}[\eta_5 e^{I'\delta\xi_1 z} - \eta_6 e^{I'\delta\xi_2 z}] \sin(\delta\zeta x) d\zeta \tag{4.42c}$$

where $g_1, g_2, \eta_1, \eta_2, \bar{\eta}_3, \bar{\eta}_4, \eta_5$ and η_6 are given in eqns (4.37) and (4.23) and

$$I' = \frac{-z}{|z|} \tag{4.43}$$

$$H = \frac{\alpha(\xi_1^2 - \xi_2^2)}{\kappa\zeta} \tag{4.44}$$

4.6 TRANSIENT GREEN'S FUNCTIONS

Let $G_{ij}(x,z,t;0,z')$ denote the displacement in the i-direction ($i=x,z$) at the point (x,z) at the time instant 't' due to a symmetrically distributed load p_j with a time history $F(t)$ acting in the j-direction ($j=x,z$) over a strip of width $2a$ located at a depth z' (Fig 4.1) and $\sigma_{ilj}(x,z,t;0,z')$ denote the stress component σ_{il} ($l=x,z$) at the point (x,z) at the time instant 't' due to the same loading configuration. The analytical solutions are obtained for $G_{ij}(x,z,t;0,z')$ and $\sigma_{ilj}(x,z,t;0,z')$ following procedures similar to that used in Section 4.5 for time-harmonic problems.

$$G_{ij}(x,z,t;0,z') = \frac{i\vartheta}{2\pi^2 c_{44}} \int_{d-i\infty}^{d+i\infty} \bar{F} \int_0^\infty G^*_{ij} e^{\vartheta\mu t} d\lambda d\mu \quad i,j = x,z \tag{4.45a}$$

$$\sigma_{ilj}(x,z,t;0,z') = \frac{i\vartheta}{2\pi^2} \int_{d-i\infty}^{d+i\infty} \bar{F} \int_0^\infty \sigma^*_{ilj} e^{\vartheta\mu t} d\lambda d\mu \quad i,l,j = x,z \tag{4.45b}$$

The solutions for G^*_{ij} and σ^*_{ilj} are identical to G^*_{ij} and σ^*_{ilj} given by eqns (4.30)-(4.33) with the replacement of parameter $\delta\zeta$ by λ, $\delta\xi_i$ by $\xi_i (i=1,2)$ which is defined by eqn (4.26) and the following definitions of parameters K, Q, E, G, g_1 and g_2 appearing in eqns (4.30)-(4.33).

$$K = [2(\kappa-1)\lambda^2 + \gamma\lambda^2 + \alpha\mu^2](\mu^2+\lambda^2) + \alpha\xi_1\xi_2\mu^2 \tag{4.46}$$

$$Q = \frac{K(\xi_2-\xi_1)}{\kappa\lambda\xi_1\xi_2} \tag{4.47a}$$

$$E = \frac{\alpha(\xi_1^2-\xi_2^2)(\xi_2-\xi_1)}{\kappa^2\lambda^2\xi_1\xi_2}; \qquad G = \frac{\alpha^2(\xi_1^2-\xi_2^2)(\xi_2-\xi_1)}{\kappa^2\lambda^2(\mu^2-\beta\lambda^2)} \tag{4.47b}$$

$$g_1 = \frac{\alpha\xi_1^2-\lambda^2-\mu^2}{\kappa\lambda\xi_1}; \qquad g_2 = \frac{\alpha\xi_2^2-\lambda^2-\mu^2}{\kappa\lambda\xi_2} \tag{4.48}$$

In addition, the other related parameters $\eta_1, \eta_2, \eta_3, \eta_4, \eta_5$ and η_6 are as given in eqns (4.23). The Laplace transform $\bar{F}$ of $F(t)$ is given by

$$\bar{F} = 1; \qquad \text{for an impulse load} \tag{4.49a}$$

$$\bar{F} = 1/p; \qquad \text{for a step load} \tag{4.49b}$$

The solutions given by eqns (4.45) are the required kernel functions in the development of boundary element methods for transient problems involving an orthotropic elastic half-plane. The transient Green's functions of an orthotropic full plane can be obtained from the time-harmonic full space Green's functions [*ie.*, eqns (4.29), (4.41) and (4.42)] with appropriate replacements of parameters as in the case of half plane Green's functions.

4.7 FUNDAMENTAL SOLUTIONS FOR TRANSIENT DISPLACEMENT JUMPS

The boundary-value problems involving transient displacement discontinuities (jumps) inside an orthotropic half plane are investigated. Crouch and Starfield (1983) have shown that fundamental solutions for displacement jumps can be used to develop boundary element methods to analyse crack problems. Consider a half space V and an internal surface S defined as in Fig 4.2 across which a displacement discontinuity may exists. Let S^+ and S^- are opposite faces of the fault. A boundary-value problem similar to the applied internal loading problem considered in Sections 4.5 and 4.6 can be formulated for the displacement discontinuity problem by realizing the fact that the displacement is now discontinuious whereas the traction is continuious over the fictitious interface at $z = z'$. In this study the displacement jumps are assumed to be located at a depth z' below the free surface and over a strip of width $2a$. The boundary-value problem corresponding to an internal displacement jump (discontinuity) can be expressed as

$$\sigma_{zi}^{(1)}(x,0,t) = 0, \qquad i = x,z \tag{4.50a}$$

$$u_i^{(1)}(x,z',t) - u_i^{(2)}(x,z',t) = u_i^0(x)[H(x+a) - H(x-a)]F(t); \quad i = x,z \tag{4.50b}$$

$$\sigma_{zi}^{(1)}(x,z',t) - \sigma_{zi}^{(2)}(x,z',t) = 0, \quad i = x,z \tag{4.50c}$$

where u_x^0 and u_z^0 are the absolute values of the displacement jump in x- and z-directions, respectively. In addition, $H(x)$ denotes the unit step function and $F(t)$ is the time history of the displacement jumps which can be usually treated as a step function $H(t)$ to depict the spontaneous behaviour of a displacement discontinuty such as the slip across a rupturing fault surface. The solutions to the boundary-value problems can be obtained by applying Laplace-Fourier transform in eqn (4.50) and substituting the two-dimensional transient general solutions given by eqn (4.22) into (4.50).

Let $G_{ij}(x,z,t;0,z')$ denote the displacement in the i-direction ($i=x,z$) at the point (x,z) at the time instant 't' due to a symmetrically distributed displacement jump in the j-direction ($j=x,z$) over a strip of width $2a$ (Fig 4.1) located at a depth z' and $\sigma_{ilj}(x,z,t;0,z')$ denotes the stress component σ_{il} ($l=x,z$) at the point (x,z) at the time instant 't' due to the same dynamic excitation. The analytical solutions for displacements $G_{ij}(x,z,t;\ 0,z')$ and stresses $\sigma_{ilj}(x,z,t;\ 0,z')$ can be expressed in the forms of eqns (4.45), respectively with G_{ij}^* and σ_{ilj}^* defined by

$$G_{xx}^* = \frac{\tilde{u}_x^0}{QH}(g_1\eta_6 e_1 + Ig_1\eta_6 e_2 + g_2\eta_5 e_3 - Ig_2\eta_5 e_4 - g_1\eta_5 e_5 - g_2\eta_6 e_6)\cos(\lambda x) \quad (4.51a)$$

$$G_{zx}^* = \frac{-\tilde{u}_x^0}{QH}(\eta_6 e_1 - \eta_6 e_2 + \eta_5 e_3 + \eta_5 e_4 - \eta_5 e_5 - \eta_6 e_6)\sin(\lambda x) \quad (4.51b)$$

$$\sigma_{xxx}^* = \frac{-c_{44}\tilde{u}_x^0}{QH}(\gamma_{11} e_1 + I\gamma_{11} e_2 + \gamma_{12} e_3 - I\gamma_{12} e_4 - \eta_1\eta_5 e_5 - \eta_2\eta_6 e_6)\sin(\lambda x) \quad (4.52a)$$

$$\sigma_{zzx}^* = \frac{c_{44}\tilde{u}_x^0}{QH}(\gamma_{21} e_1 - \gamma_{21} e_2 + \gamma_{22} e_3 + \gamma_{22} e_4 - \bar{\eta}_3\eta_5 e_5 - \bar{\eta}_4\eta_6 e_6)\cos(\lambda x) \quad (4.52b)$$

$$\sigma_{zzx}^* = \frac{-c_{44}\tilde{u}_x^0}{QH}(\gamma_3 e_1 + I\gamma_3 e_2 + \gamma_3 e_3 - I\gamma_3 e_4 - \eta_5\eta_5 e_5 - \eta_6\eta_6 e_6)\sin(\lambda x) \quad (4.52c)$$

$$G_{xz}^* = \frac{\tilde{u}_z^0}{QE}(g_1\bar{\eta}_4 e_1 + g_1\bar{\eta}_4 e_2 + g_2\bar{\eta}_3 e_3 - g_2\bar{\eta}_3 e_4 - g_1\bar{\eta}_3 e_5 - g_2\bar{\eta}_4 e_6)\sin(\lambda x) \quad (4.53a)$$

$$G_{zz}^* = \frac{\tilde{u}_z^0}{QE}(\bar{\eta}_4 e_1 - I\bar{\eta}_4 e_2 + \bar{\eta}_3 e_3 + I\bar{\eta}_4 e_3 - \bar{\eta}_3 e_5 - \bar{\eta}_4 e_6)\cos(\lambda x) \quad (4.53b)$$

$$\sigma_{xxz}^* = \frac{c_{44}\tilde{u}_z^0}{QE}(\gamma_{41} e_1 + \gamma_{41} e_2 + \gamma_{42} e_3 - \gamma_{42} e_4 - \eta_1\bar{\eta}_3 e_5 - \eta_2\bar{\eta}_4 e_6)\cos(\lambda x) \quad (4.54a)$$

$$\sigma^*_{xzz} = \frac{c_{44}\tilde{u}^0_z}{QE}(\gamma_5 e_1 - I\gamma_5 e_2 + \gamma_5 e_3 + I\gamma_5 e_4 - \bar{\eta}_3\bar{\eta}_3 e_5 - \bar{\eta}_4\bar{\eta}_4 e_6)\sin(\lambda x) \qquad (4.54b)$$

$$\sigma^*_{zzz} = \frac{c_{44}\tilde{u}^0_z}{QE}(\gamma_{22} e_1 + \gamma_{22} e_2 + \gamma_{21} e_3 - \gamma_{21} e_4 - \eta_5\bar{\eta}_3 e_5 - \eta_6\bar{\eta}_4 e_6)\cos(\lambda x) \qquad (4.54c)$$

where $\tilde{u}^0_x$ and $\tilde{u}^0_z$ are the Fourier transforms of $u^0_x(x)[H(x+a) - H(x-a)]$ and $u^0_z(x)[H(x+a) - H(x-a)]$, respectively. Note that $g_1, g_2, \eta_1, \eta_2, \bar{\eta}_3, \bar{\eta}_4, \eta_5, \eta_6$, $e_1, e_2, e_3, e_4, e_5, e_6, I, Q$ and $\bar{F}$ are defined by eqns (4.48), (4.23), (4.38), (4.34), (4.47a) and (4.49) together with the replacement of $\delta\xi_i (i = 1, 2)$ by ξ_i which is defined in eqn (4.26). In addition,

$$H = g_1\eta_6 - g_2\eta_5; \qquad E = \bar{\eta}_3 - \bar{\eta}_4 \qquad (4.55)$$

$$\gamma_{11} = \eta_1\eta_6; \quad \gamma_{12} = \eta_2\eta_5; \quad \gamma_{21} = \bar{\eta}_3\eta_6; \quad \gamma_{22} = \bar{\eta}_4\eta_5 \qquad (4.56a)$$

$$\gamma_3 = \eta_5\eta_6; \quad \gamma_{41} = \eta_1\bar{\eta}_4; \quad \gamma_{42} = \eta_2\bar{\eta}_3; \quad \gamma_5 = \bar{\eta}_3\bar{\eta}_4 \qquad (4.56b)$$

Note that a solution corresponding to an arbitrary distribution of $u^0_x(x)$ and $u^0_z(x)$ can be obtained by the superposition of the solutions given above and shifting of the origin of x-axis.

4.8 NUMERICAL SOLUTIONS FOR TIME-HARMONIC PROBLEMS

4.8.1 **Numerical Scheme**

The solutions for displacements and stresses given by eqn (4.29) appear in terms of infinite integrals with a complex-valued integrand. As in the case of an isotropic medium, these integrals cannot be evaluated analytically for both surface and interior loadings. However, in the case of a surface loading the solutions may be reduced to a form containing a set of finite integrals by performing an integration along a closed contour in the complex-plane similar to that used by Lamb (1904). Since our objective is to apply these Green's functions to solve complex problems related to anisotropic media through a numerical solution based on the

boundary integral equation method, it is natural to develop accurate numerical integration schemes to evaluate both time-harmonic and transient Green's functions. The numerical evaluation of eqn (4.29) requires careful consideration due to the presence of singularities within the range of integration and the oscillatory nature of the integrand due to the trigonometric terms. The oscillatory nature of the integrand can be accounted by using Filon's integration scheme (Tranter 1956). The singularities of the integrals of eqn (4.29) also need to be examined prior to the establishment of a numerical integration procedure.

An understanding of the singularities of the integrands of eqn (4.29) together with (4.30)-(4.33) can be obtained by treating ζ as a complex-variable. It is noted that due to the presence of radicals ξ_1 and ξ_2 the Riemann surface of the integrand of each integral has four sheets. However, the condition $Re(\xi_1, \xi_2) \geq 0$ which is required to satisfy regularity conditions at infinity implies that only the sheet in which radicals ξ_1 and ξ_2 have positive real parts everywhere is relevant. The important singularities of the integrand are the branch points of the radicals ξ_1 and ξ_2 as defined by eqn (4.13) and poles of the function K defined by eqn (4.35). The branch points of ξ_1 and ξ_2 are given by

$$\xi_1 = 0, \quad \xi_2 = 0 \tag{4.57}$$

The substitution of eqns (4.57) in eqn (4.13) leads to the following branch points.

$$\zeta_p = \pm 1/\sqrt{\beta}, \qquad \zeta_s = \pm 1 \tag{4.58}$$

For an isotropic solid, the eqn (4.58) reduces to $\zeta_s = \pm 1$ and $\zeta_p = \pm\sqrt{\bar{\mu}/(\bar{\lambda} + 2\bar{\mu})}$. It can be shown (Stoneley 1949) that in a two-dimensional orthotropic material there are two kinds of waves. The wave numbers of these waves are equal to $\delta/\sqrt{\beta}$ and δ. The motion associated with these waves is neither purely dilatational nor purely distortional. However, noting that branch points ζ_p and ζ_s in an isotropic case correspond to purely dilatational and distortional waves (Lamb 1904), the

waves corresponding to these branch points in an anisotropic case are called quasi-dilatational and quasi-distortional.

The denominator of the integrand of the integrals given by eqns (4.29)-(4.33) yields poles and their locations are given by K in eqn (4.35). The eqn (4.35) reduces to the classical Rayleigh equation (Lamb 1904) in the case of an isotropic solid. It is also noted that through appropriate manipulation the eqn (4.35) can be transformed into a form identical to the eqn (30) of the paper by Stoneley (1949) where it is shown that the eqn (4.35) has only two roots $\pm\zeta_R$ along the real axis. These roots cannot be determined explicitly due to the complex nature of eqn (4.35) and an appropriate numerical procedure is required. In the present study, four different materials, namely, an isotropic material, cadmium, ice, and a layered soil are considered. The choice of the above set of anisotropic materials among several others is based on their relevance to applications related to earthquake engineering, dynamics of foundation and composite materials. Table 1.1 presents the values of material constants $\bar{c}_{11}, \bar{c}_{12}, \bar{c}_{13}, \bar{c}_{33}$ and c_{44} where $\bar{c}_{ij} = c_{ij}/c_{44}$. Table 4.1 presents the values of ζ_R and branch points ζ_s, ζ_p for each of the four materials. Note that the location of singularities is independent of the frequency of excitation ω since the Fourier transform parameter ζ is normalised with respect to δ.

The integrals in eqns (4.29)-(4.33) can be evaluated accurately by using a direct numerical integration technique provided the positive real axis is free from any singularities . It is noted from Table 4.1 that this is not the case for the four materials under consideration when there is no attenuation in materials. However the introduction of a small attenuation (*ie.*, $\bar{c}_{44} = 1 + 0.01i$) results in complex values for α, β and γ and singularities are shifted away from the real axis. This technique which is consistent with the reality that all physical materials display some amount of attenuation (damping) has been used successfully to numerically evaluate infinite integrals related to Green's functions of a layered isotropic medium (Apsel and Luco 1983). Alternatively, it is possible to deviate

the integration contour initially into the first quadrant of the complex plane to avoid the singularities on the real axis and then fall back to an integration along the real axis. The deviated portion of the contour should be selected in light of the location of singularities of the integrand as given in Table 4.1. In the present study, both procedures mentioned above are used to evaluate eqn (4.29) and obtained numerical solutions agree with each other very closely. All numerical results presented in the ensuing section is based on the technique where the material is assumed to possess negligible attenuation.

4.8.2 **Numerical Solutions**

The dynamic response of elastic half plane regions of different materials is considered in this section. The loading is assumed to be uniformly distributed over a width of dimension '$2a$' with intensity q_0, and acting at a depth $z'/a = 1.0$. The numerical results are presented in terms of normalised displacement and stress Green's functions $\bar{G}_{ij} = G_{ij}c_{44}/(aq_0)$ and $\bar{\sigma}_{ijk} = \sigma_{ijk}/q_0$ respectively. In addition, a nondimensional frequency a_0 defined as $a_0 = a\delta = a\omega(\rho/c_{44})^{1/2}$ is used in the present study.

Figure 4.3 shows the variation of $\bar{G}_{xx}$ and $\bar{G}_{zz}$ along the z axis for the four different materials at frequency $a_0 = 1.0$. The real part of $\bar{G}_{xx}$ and $\bar{G}_{zz}$ show a kink at $z'/a = 1.0$ which is consistent with the fact that the loading is applied at this level. The influence of material anisotropy is clearly noted in the case of imaginary part of $\bar{G}_{xx}$ and for both real and imaginary part of $\bar{G}_{zz}$. Figure 4.4 shows the variation of $\bar{G}_{xx}$ and $\bar{G}_{zz}$ at the surface level ($z = 0$) with the horizontal distance x. It is noted that $\bar{G}_{xx}$ shows strong dependence on the degree of anisotropy at the surface level when compared to its behaviour along the z-axis. In the case of $\bar{G}_{zz}$ the influence of the anisotropy is found to be comparatively lesser. This is in contrast to the strong influence observed in Fig 4.3 for $\bar{G}_{zz}$ along the z-axis. It is useful to relate the influence of material anisotropy observed in

Figs 4.3 and 4.4 to the values of $\bar{c}_{ij}$ given in Table 1.1. The solutions for $\bar{G}_{zz}$ indicate that the highest influence of anisotropy is observed in solutions for ice and followed by layered soil, the isotropy and cadmium. Comparison of values of $\bar{c}_{ij}$ in Table 1.1 in light of the solutions in Figs 4.3 and 4.4 indicates that in the case of $\bar{G}_{zz}$ the influence of material anisotropy is mainly governed by the value of $\bar{c}_{33}$. Solutions for $\bar{G}_{xx}$ in Figs 4.3 and 4.4 show an influence which is different to that observed for $\bar{G}_{zz}$. For example, solutions for cadmium show the highest influence of anisotropy and $\bar{G}_{xx}$ of layered soil and ice are nearly equal. Comparison of the above features of the solution and $\bar{c}_{ij}$ values in Table 1.1 indicate that the influence of anisotropy on $\bar{G}_{xx}$ is mainly controlled by the value of $\bar{c}_{11}$.

Figure 4.5 shows the variation of normalised stress Green's functions $\bar{\sigma}_{xzx}$ and $\bar{\sigma}_{zzz}$ along the z-axis at $a_0 = 1.0$. The real part of $\bar{\sigma}_{xzx}$ profile shows a negligible influence of material anisotropy and a discontinuity equal to a unit value at $z'/a = 1.0$ due to the applied loading. The influence of material anisotropy is clearly noted in the solutions for both real and imaginary part of $\bar{\sigma}_{zzz}$. In the case of $\bar{\sigma}_{zzz}$, the solutions for cadmium and ice show the highest influence of anisotropy. The general shape of stress profiles is somewhat similar for all four materials. Figures 4.6 and 4.7 show the influence of normalised frequency a_0 ($a_0 = 0.5$ and 3.0) on displacement and stress profiles along the z-axis respectively. The materials considered are isotropic, layered soil and cadmium. These solutions together with that given in Figs 4.3-4.5 for a_0=1.0, indicate a complicated dependence of response on the frequency. At low frequencies ($a_0 = 0.5, 1.0$), both displacement and stress profiles show a gradual variation with the depth. However at the high frequency ($a_0 = 3.0$), the solutions for $\bar{G}_{xx}, \bar{\sigma}_{xzx}$ and $\bar{\sigma}_{zzz}$ show considerable waviness with the depth. In general the real part of the displacement is found to decrease with increasing frequency whereas the imaginary part shows an increase in magnitude with increasing a_0. It is also noted that the

general trend of the variation of solutions with the frequency is somewhat similar for all three materials within the frequency range $a_0 = 0.0 - 3.0$.

4.9 NUMERICAL SOLUTIONS FOR TRANSIENT PROBLEMS

4.9.1 Numerical Scheme

The evaluation of explicit analytical solutions for transient displacements and stresses presented in Sections 4.6 and 4.7 is considered here. It is noted that all solutions appear in terms of an infinite integral with respect to the Laplace transform parameter 'p' [or μ, see eqn (4.19)] and a semi-infinite integral with respect to the Fourier integral transfer parameter λ. Due to the presence of double integrals involving highly complex integrands the evaluation of displacements and stresses requires special consideration. One of the standard methods of dealing with the infinite integrals encountered in transient wave propagation problems is to apply the method proposed by Cagniard (1962). This method involves a complicated transformation of the variables of integration. Mitra (1963) applied Cagniard's technique to obtain the transient response due to an impulsive disc of pressure applied to the surface of an isotropic elastic half space. Another method (Eason 1966) to evaluate the Laplace inversion integral is to take the integral around a suitable contour in the complex-p plane and to apply the residue theorem with due consideration given to branch points and poles of the integrand. The review of existing literature reveals that Cagniard's method has been applied to evaluate the response due to an impulsive surface load on a transversely isotropic elastic half plane (Kraut 1962, Payton 1983) whereas a direct contour integration method similar to that used by Eason (1966) has not been applied to evaluate the transient response of transversely isotropic materials. As stated by Payton (1983) the application of analytical procedures to evaluate the integrals corresponding to the response at an arbitrary point is very complicated even in the case of surface loading.

The application of analytical procedures become almost impossible when the excitation is also inside the medium as in the case of the solutions derived in Sections 4.6 and 4.7. In addition the analytical inversion requires certain restrictions on parameters α, β and γ. It is noted from the transient solutions presented by Eason (1966) for an isotropic medium that even after the analytical inversion of Laplace transform, the solution still involves semi-infinite integrals with respect to Fourier transform and Hankel transform parameters for 2-D and 3-D problems, respectively. These semi-infinite integrals are somewhat similar to the integrals associated with solutions corresponding to time-harmonic vibration of an elastic half-plane and cannot be evaluated analytically to determine the response at an arbitrary point due to an internal loading. However, asymptotic solutions valid for far-field observation points can be obtained in some cases. In the application of the boundary integral equation method to analyse complicated transient wave propagation problems it is required to compute displacements and stresses at all boundary node points due to transient dynamic excitations applied at each and every boundary node point. Therefore a substantial amount of response calculation are required at near-field points. In view of the complexity of the integrands of the integrals associated with the solutions presented in Sections 4.6 and 4.7 and the formidable difficulties involved in the application of analytical procedures to evaluate these integrals it is author's opinion that the use of an accurate numerical quadrature technique would be the most efficient way to compute the transient solutions. This is further validated by the fact that the final solution to boundary integral equation also has to be obtained numerically.

In the development of a numerical quadrature method to evaluate the transient response it is necessary to consider integrals of the following form for 2-D problems

$$I(x,z,t) = \int_{d-i\infty}^{d+i\infty} \int_0^{\infty} \chi(z,\lambda,\mu) e^{i\mu t} \{\cos(\lambda x) or \sin(\lambda x)\} d\lambda d\mu \qquad (4.59)$$

The review of literature indicates that several methods are currently available for numerical inversion of Laplace transform. Piessens (1975) and Davies and Martin (1979) presented a review of numerical Laplace inversion techniques. It should be noted that numerical inversion of Laplace transform solutions related to transient wave propagation problems requires special attention when compared to the numerical Laplace inversion of solutions encountered in heat transfer, diffusion and consolidation problems. Based on a study of different numerical algorithms available in the literature it is found that the numerical algorithm presented by Hosono (1979) provides accurate numerical solutions for transient wave propagation problems.

The numerical algorithm proposed by Hosono (1979) is based on an approximation of the exponential function and Euler transformation. It determines the transient solution $f(t)$ in terms of $(N+M)$ values of the Laplace transform $\bar{f}(\mu)$ sampled at $(N+M)$ complex values of μ. The inversion formula is given by

$$f(t) = \frac{e^{0.5}}{t}[\sum_{n=1}^{N-1} f_n(\mu) + \frac{1}{2^{M+1}} \sum_{m=0}^{M} A_{M,m} f_{N+m}(\mu)] \tag{4.60}$$

where

$$A_{M,M} = 1, \quad A_{M,m-1} = A_{M,m} + \frac{(M+1)!}{M!(M-m+1)!} \tag{4.61a}$$

$$\mu_n = \frac{1}{t}[a + i(n - \pi/2)] \tag{4.61b}$$

$$f_n(\mu) = (-1)^n Im[\bar{f}(\mu_n)] \tag{4.61c}$$

In addition, the values of N, M and a in eqns (4.60) and (4.61b) are determined on the basis of a convergence study.

The application of eqn (4.60) to evaluate the integrals given by eqn (4.59) involves the numerical evaluation of semi-infinite integrals with respect to λ for $(N+M)$ complex values of μ. Since μ is complex in eqn (4.59) it is noted that integrand $\chi(z, \lambda, \mu)$ for 2-D does not have any branch points or poles along the

real λ-axis. Therefore the semi-infinite integral with respect to λ can be evaluated accurately by applying a direct numerical quadrature scheme. Since trigonometric functions in eqn (4.59) are oscillatory it is necessary to select a sufficiently small value for the integration interval $\triangle\lambda$. It is found that $\triangle\lambda = 0.1$ is accurate enough in the present case. In addtion, N=15 and M=5 in eqn (4.60) are found to yield converged numerical solutions.

4.9.2 **Numerical Results**

The accuracy of the numerical algorithm used in the present study to evaluate transient solutions presented in Sections 4.6 and 4.7 is first investigated in this section. As mentioned earlier, Mansur (1983) presented transient solutions for an elastic half plane subjected to a uniform step load of intensity q_0 applied over a surface strip of width $2a$. The loading is uniform in the y-direction resulting in plane strain deformations. Figure 4.8 presents a comparison of numerical solutions for normalised vertical displacement $G^*_{zz}(G^*_{zz} = \frac{\bar{\mu}G_{zz}}{q_0 a}$, where $\bar{\mu}$ is the shear modulus of the half space) at three points on the x-axis obtained from the present numerical integration scheme with the results presented by Mansur (1983). Note that a nondimensional time τ defined by $\tau = \frac{t}{a}(\frac{\bar{\mu}}{\rho})^{1/2}$ is used in the numerical study. It is evident from Fig 4.8 that the numerical algorithm used in the present study results in very accurate numerical solutions.

Isotropic, layered soil, glass/epoxy composite and graphite/epoxy composite half planes are considered in the numerical study. The related material constants are given in Table 1.1. Figures 4.10a and 4.10b show the normalised displacement $G^*_{zz}(= \frac{c_{44}G_{zz}}{p_0 a}$, where $2a$ is the width of the load and p_0 is the intensity of the load) at three points $(x/a = 0, 1, 5)$ on the surface of the half plane due to vertical loading histories shown in Figs 4.9a and 4.9b. These loadings are applied at a depth $z'/a = 1.0$ below the surface of the half plane. It can be seen from the Fig 4.10 that the degree of anisotropy of the material and the time history of the

excitation have a significant influence on the response. Composite material shows the lowest displacements whereas the layered soil has the highest displacements. Displacements increase more rapidly at near-field points under the rectangular pulse excitation when compared to displacements due to the triangle pulse. The peak displacements are also higher in the case of the rectangular pulse. The ascending parts of the response curves indicate the presence of a constant velocity period at early time where as velocity decreases rapidly over the descending part of the response.

Figure 4.11 shows the vertical displacement $\bar{G}_{zz}(=\frac{G_{zz}}{w_0})$ due to a displacement jump in the vertical direction over a strip of width $2a$ located at a depth $z'/a = 1.0$ below the surface of the half plane. The time history of the displacement jump is shown in Fig 4.9c and the displacement jump has the distribution $w(x) = w_0 \cos(\pi x/2a)$. The response at near-field indicates the presence of an initial constant velocity period for all three materials followed by transition to the static displacements. Both composites are more stiffer than the isotropic material. Response at far-field shows the presence of negative displacements at early time of response histories and rapidly varying velocities. In addition the response decays rapidly with the distance.

4.10 CONCLUSIONS

A solution scheme to derive Green's functions for an orthotropic elastic half plane subjected to buried dynamic loadings is presented. The governing equations are solved by applying Fourier and Laplace-Fourier integral transforms for time-harmonic and transient problems, respectively. The analytical general solutions for displacement and stress are then used to solve the boundary-value problems corresponding to buried time-harmonic loads, buried transient loads and displacement jumps. The explicit analytical solutions for dynamic Green's functions of displacement and stress are presented. It is found that Green's func-

tions appear in terms of complex-valued infinite integrals. Numerical solutions for displacements and stresses corresponding to time-harmonic excitations are computed by direct numerical integration of the infinite integrals by introducing negligible material attenuation. In the case of transient problems, the response is again evaluated by using an approximate Laplace inversion technique together with direct numerical integration of semi-infinite integrals. Comparison with existing solutions for isotropic materials confirms the accuracy of the numerical scheme. As in the case of static problems, solutions for displacements and stresses indicate that the degree of anisotropy of the material significantly influences the dynamic response. It is found that in the case of displacement Green's functions G_{xx} and G_{zz} the influence of material anisotropy is mainly reflected by the value of $\bar{c}_{11}$ and $\bar{c}_{33}$ respectively. The solutions for displacements and stresses also show a strong dependence on the frequency and time history of the excitations. The availability of an exact analytical solution for Green's functions and an accurate numerical procedure for evaluation enables the solution for more complicated problems related to dynamic soil-structure interaction, seismic wave scattering, composite materials, *etc.* by using the boundary integral equation method and other techniques. The present solutions can also serve as the basis for estimating the accuracy of approximate numerical algorithms that could be used to evaluate the dynamic response of an anisotropic medium. The present solution scheme is extended to derive Green's functions for three-dimensional elastodynamic problems in Chapter 5. In addition, the general solutions expressed in eqns (4.9) and (4.10) are used in Chapter 7 to develop an exact stiffness matrix method to compute Green's functions of multi-layered orthotropic half spaces.

Table 4.1: Location of Singularities on real ζ-axis

	ζ_R	ζ_p	ζ_s
Isotropic	1.088	0.577	1.0
Ice	1.043	0.485	1.0
Layered soil	1.051	0.473	1.0
Cadmium	1.052	0.377	1.0

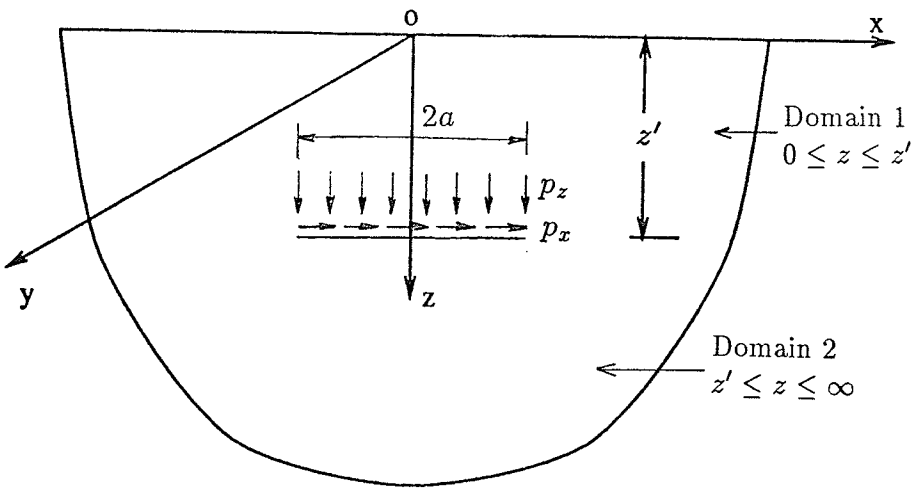

Figure 4.1 The geometry considered for two dimensional dynamics

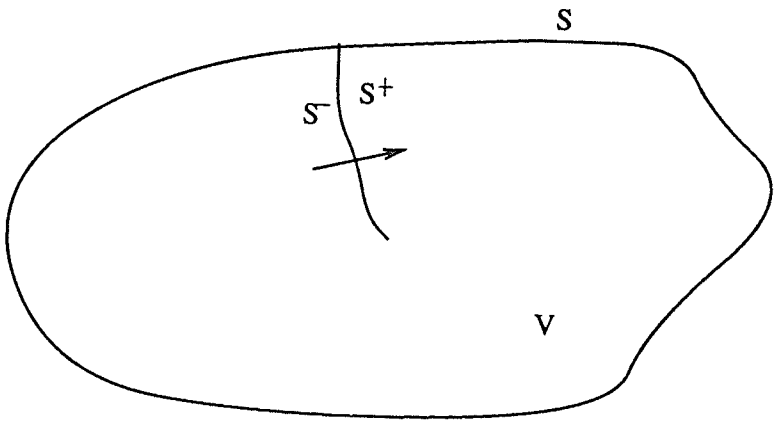

Figure 4.2 Geometry of considered displacement discontinuity problem

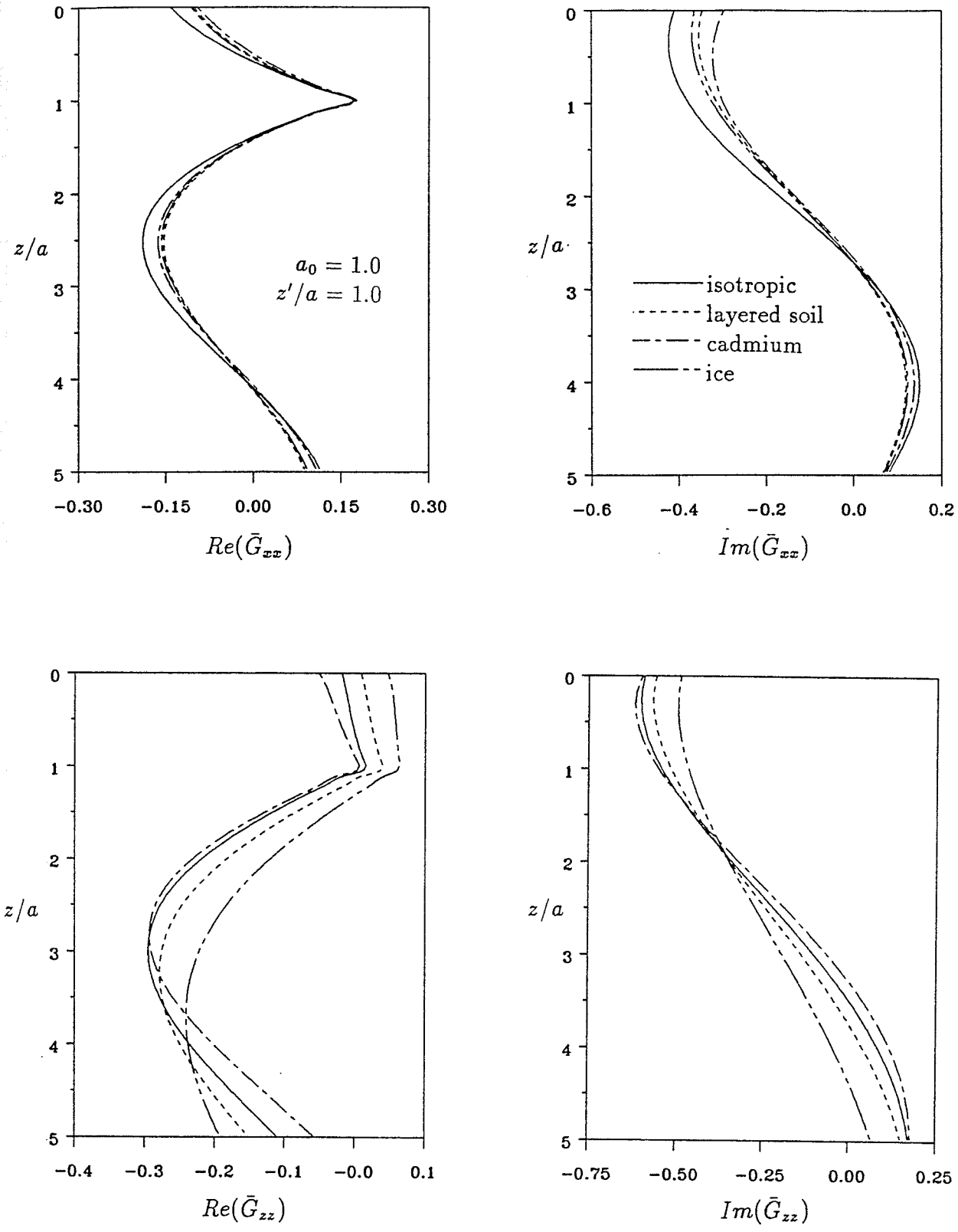

Figure 4.3 Normalized displacement Green's function $\bar{G}_{xx}$ and $\bar{G}_{zz}$ along z-axis for different orthotropic materials

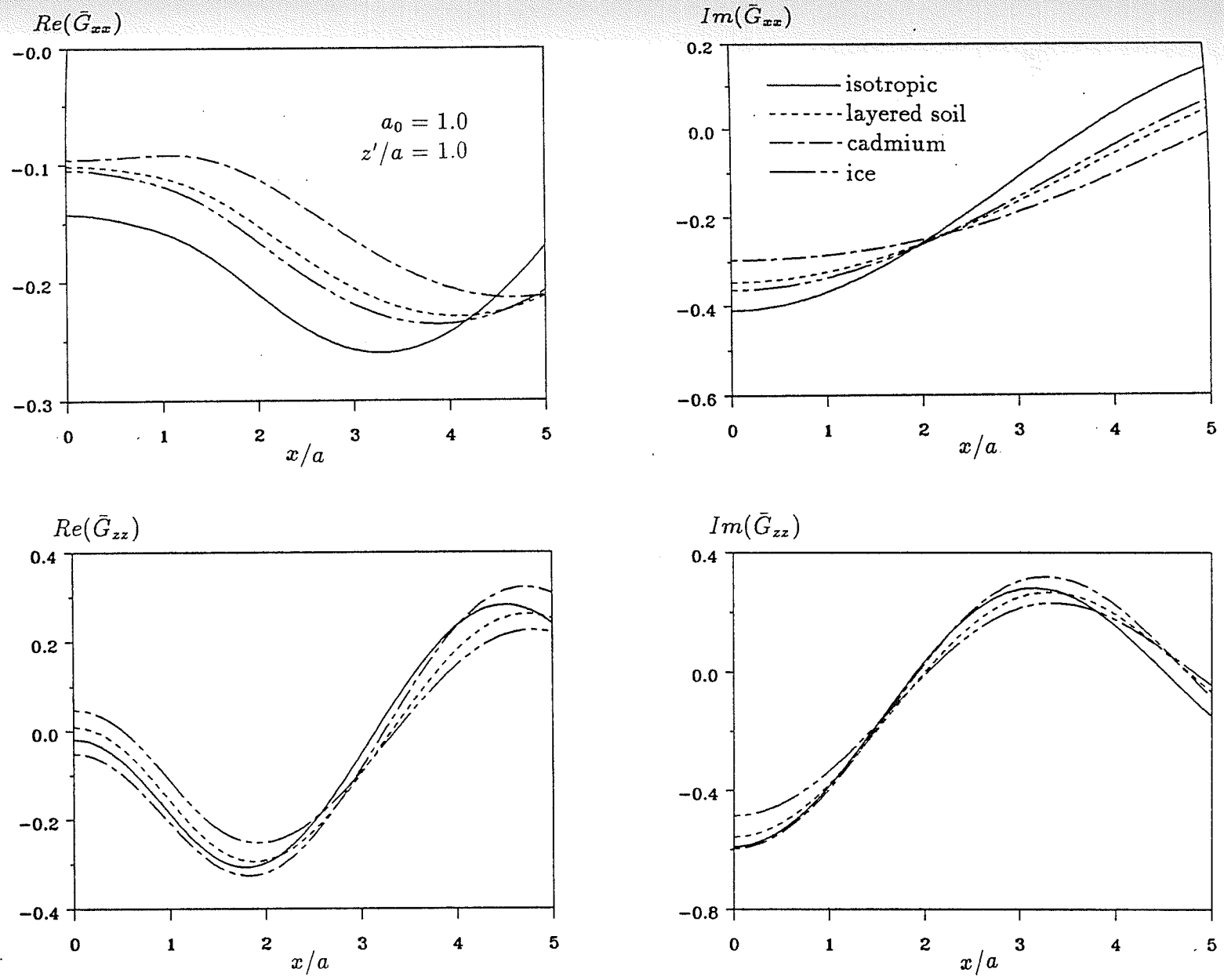

Figure 4.4 Normalized displacement Green's function $\bar{G}_{xx}$ and $\bar{G}_{zz}$ along free surface (z-axis) for different orthotropic materials

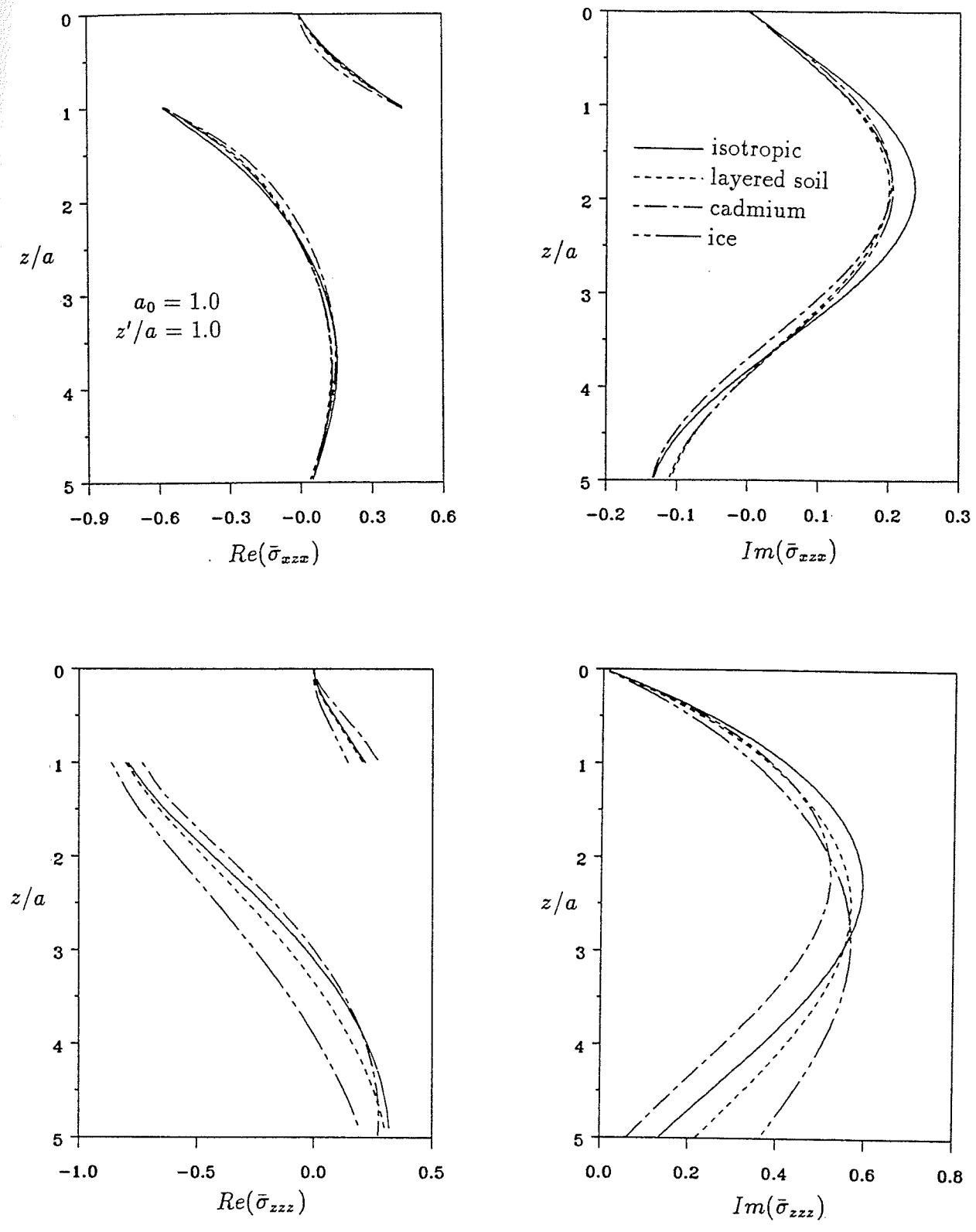

Figure 4.5 Normalized stress Green's function $\bar{\sigma}_{xzx}$ and $\bar{\sigma}_{zzz}$ along z-axis for different orthotropic materials

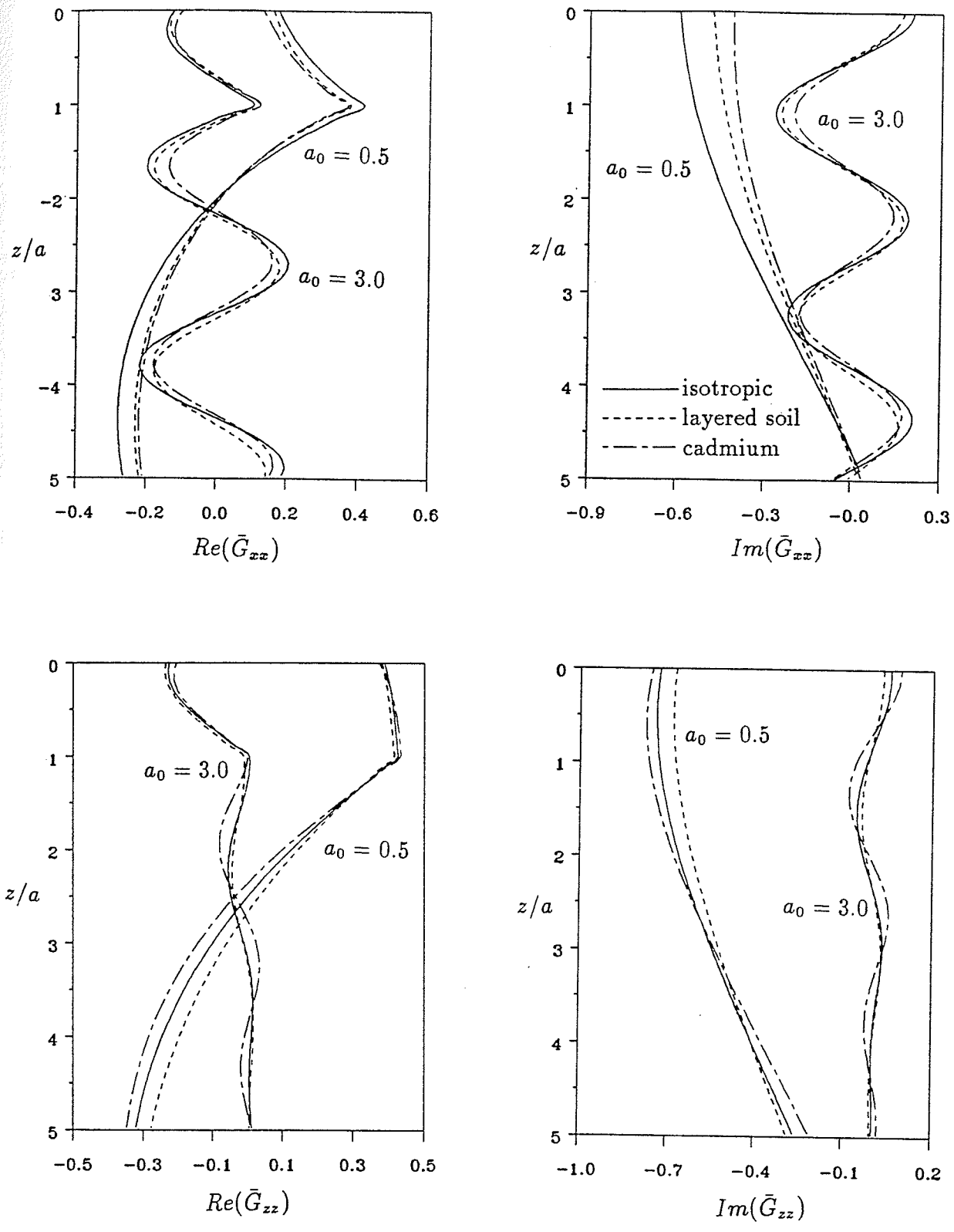

Figure 4.6 Effects of frequency on displacement Green's functions $\bar{G}_{xx}$ and $\bar{G}_{zz}$ along z-axis for different orthotropic materials ($z'/a = 1.0$)

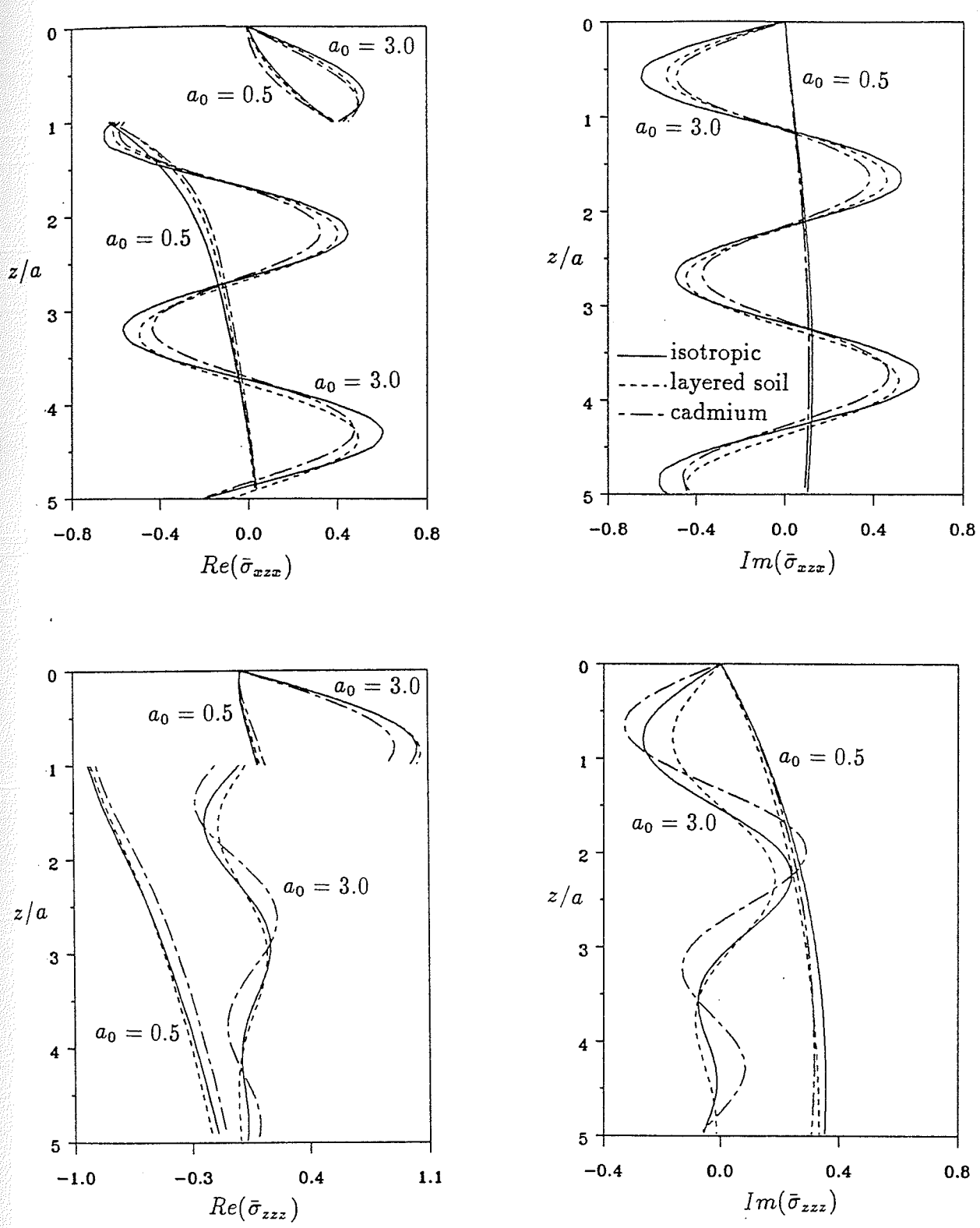

Figure 4.7 Effects of frequency on stress Green's functions $\bar{\sigma}_{xzx}$ and $\bar{\sigma}_{zzz}$ along z-axis for different orthotropic materials ($z'/a = 1.0$)

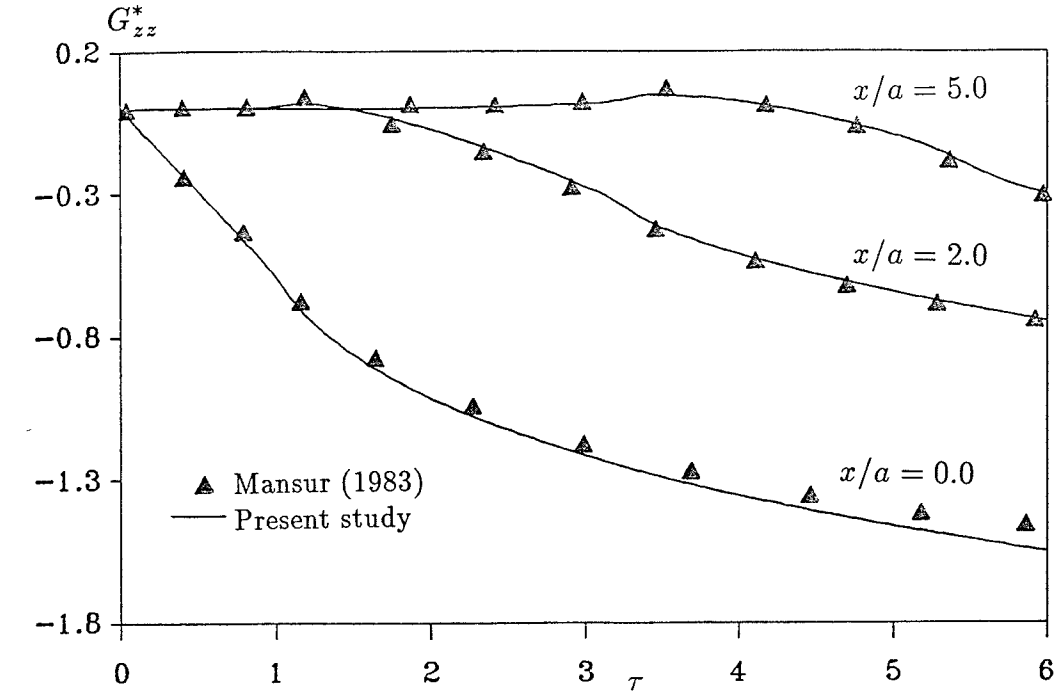

Figure 4.8 Vertical displacement on surface points due to uniform step load on the surface of an isotropic half plane (Poisson's ratio=0.25)

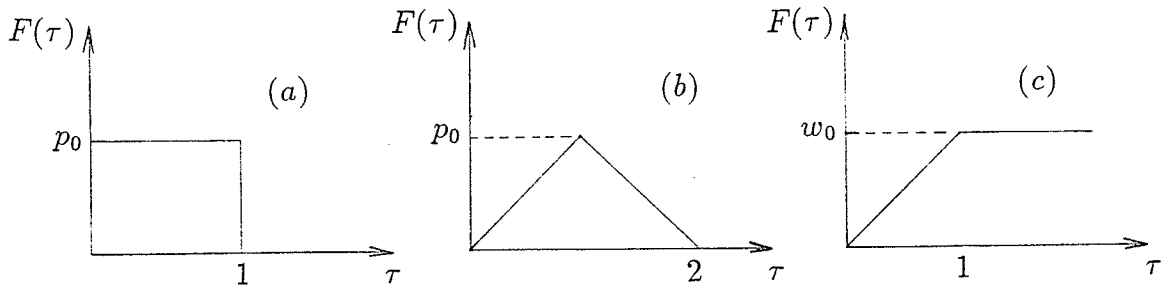

Figure 4.9 Time history of applied excitations

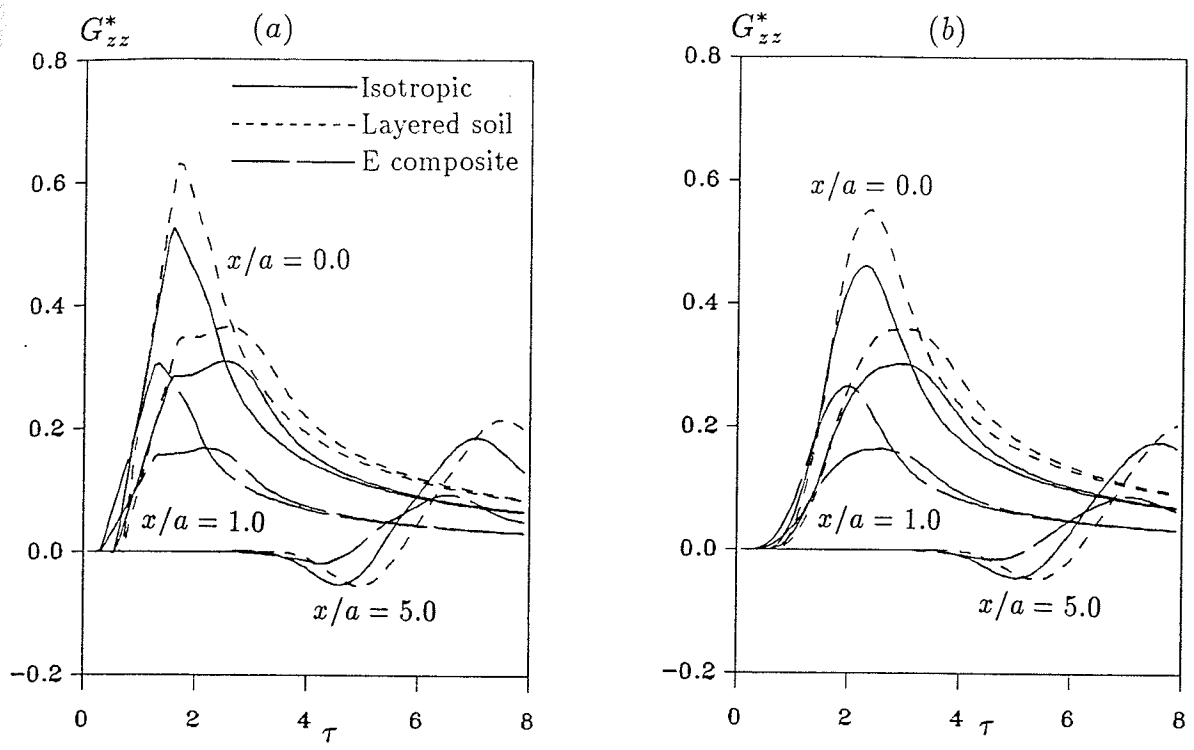

Figure 4.10 Vertical displacements at surface due to an internal load

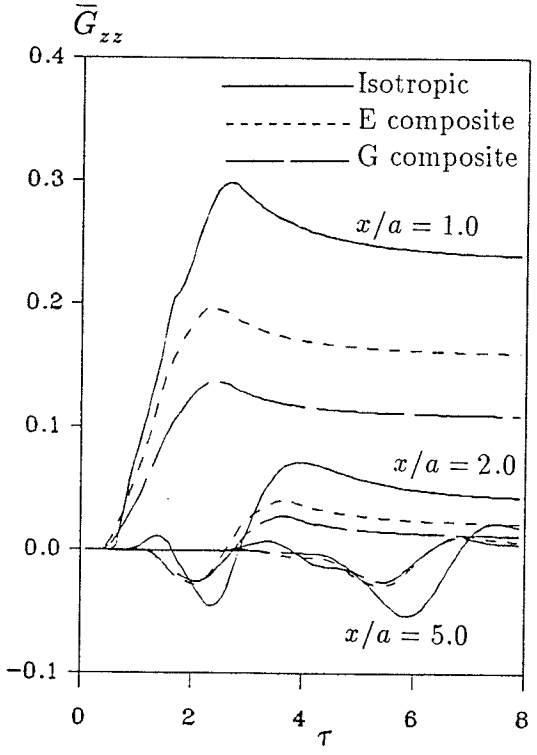

Figure 4.11 Vertical displacements at surface due to an internal displacement jump

Chapter 5

3-D ELASTODYNAMIC GREEN'S FUNCTIONS

5.1 GENERAL

This Chapter is concerned with the derivation of three-dimensional dynamic Green's functions of a homogeneous transversely isotropic elastic half space. Governing equations corresponding to three-dimensional time-harmonic and transient wave propagation problems are solved by using integral transform techniques. Explicit general solutions for displacements and stresses corresponding to time-harmonic and transient problems are presented. Thereafter boundary-value problems corresponding to internal time-harmonic and transient loadings and transient displacement discontinuities are solved. Explicit analytical solutions for dynamic Green's functions corresponding to internal loadings and displacement discontinuities are presented. Numerical evaluation of the Green's functions expressed in terms of infinite and semi-infinite integrals is also discussed. Selected numerical results for displacements and stresses due to a buried circular patch load are presented to portray the effects of anisotropy on the response of the medium. The fundamental solutions (Green's functions) presented in this Chapter can be used to develop solution algorithms based on the boundary integral equation method for the analysis of a variety of 3-D wave propagation problems involving transversely isotropic materials.

5.2 GOVERNING EQUATIONS

In many engineering and geophysical applications involving three-dimensional domains and loadings it is convenient to adopt a cylindrical coordinate system in the analysis. Consider a transversely isotropic elastic half space with a cylindrical coordinate system (r, θ, z) chosen such that the z-axis is parallel to

the material axis of symmetry and normal to the stress free-surface of the half space as shown in Fig 2.1. Let $u_r(r,\theta,z,t), u_\theta(r,\theta,z,t)$ and $u_z(r,\theta,z,t)$ denote the displacements in the r-, θ- and z- directions respectively. The equations of motion of a transversely isotropic elastic half space in the absence of body forces can be expressed in terms of displacements as

$$c_{11}(\frac{\partial^2 u_r}{\partial r^2}+\frac{1}{r}\frac{\partial u_r}{\partial r}-\frac{u_r}{r^2})+\frac{c_{11}-c_{12}}{2}\frac{1}{r^2}\frac{\partial^2 u_r}{\partial \theta^2}+c_{44}\frac{\partial^2 u_r}{\partial z^2}$$

$$+\frac{c_{11}+c_{12}}{2}(\frac{1}{r}\frac{\partial^2 u_\theta}{\partial r\partial\theta}+\frac{1}{r^2}\frac{\partial u_\theta}{\partial\theta})-2c_{11}\frac{1}{r^2}\frac{\partial u_\theta}{\partial\theta}+(c_{13}+c_{44})\frac{\partial^2 u_z}{\partial r\partial z}=\rho\frac{\partial^2 u_r}{\partial t^2} \quad (5.1a)$$

$$\frac{c_{11}-c_{12}}{2}(\frac{\partial^2 u_\theta}{\partial r^2}+\frac{1}{r}\frac{\partial u_\theta}{\partial r}-\frac{u_\theta}{r^2})+c_{11}\frac{1}{r^2}\frac{\partial^2 u_\theta}{\partial\theta^2}+c_{44}\frac{\partial^2 u_\theta}{\partial z^2}$$

$$+\frac{c_{11}+c_{12}}{2}(\frac{1}{r}\frac{\partial^2 u_r}{\partial r\partial\theta}-\frac{1}{r^2}\frac{\partial u_r}{\partial\theta})+2c_{11}\frac{1}{r^2}\frac{\partial u_r}{\partial\theta}+(c_{13}+c_{44})\frac{1}{r}\frac{\partial^2 u_z}{\partial\theta\partial z}=\rho\frac{\partial^2 u_\theta}{\partial t^2} \quad (5.1b)$$

$$c_{44}(\frac{\partial^2 u_z}{\partial r^2}+\frac{1}{r}\frac{\partial u_z}{\partial r}+\frac{1}{r^2}\frac{\partial^2 u_z}{\partial\theta^2})+c_{33}\frac{\partial^2 u_z}{\partial z^2}$$

$$+(c_{13}+c_{44})(\frac{\partial^2 u_r}{\partial r\partial z}+\frac{1}{r}\frac{\partial u_r}{\partial z}+\frac{1}{r}\frac{\partial^2 u_\theta}{\partial\theta\partial z})=\rho\frac{\partial^2 u_z}{\partial t^2} \quad (5.1c)$$

Equation (5.1) can be solved (Buchwald 1961) by introducing three potential functions ϕ, ψ and χ which are related to the displacements u_r, u_θ and u_z by

$$u_r=\frac{\partial\phi}{\partial r}+\frac{1}{r}\frac{\partial\psi}{\partial\theta} \quad (5.2a)$$

$$u_\theta=\frac{1}{r}\frac{\partial\phi}{\partial\theta}-\frac{\partial\psi}{\partial r} \quad (5.2b)$$

$$u_z=\frac{\partial\chi}{\partial z} \quad (5.2c)$$

5.3 TIME-HARMONIC GENERAL SOLUTIONS

Substitution of eqn (5.2) into eqn (5.1) together with the assumption that motion is time-harmonic with circular frequency ω indicates that the equations

of motion are satisfied if the potential functions ψ, ϕ and χ are governed by the follwing differential equations.

$$\kappa\nabla^2\frac{\partial^2\chi}{\partial z^2} + (\beta\nabla^2 + \frac{\partial^2}{\partial z^2} + \delta^2)\nabla^2\phi = 0 \tag{5.3a}$$

$$\kappa\nabla^2\frac{\partial^2\phi}{\partial z^2} + (\nabla^2 + \alpha\frac{\partial^2}{\partial z^2} + \delta^2)\frac{\partial^2\chi}{\partial z^2} = 0 \tag{5.3b}$$

$$(\varsigma\nabla^2 + \frac{\partial^2}{\partial z^2} + \delta^2)\nabla^2\psi = 0 \tag{5.3c}$$

where ∇^2 is a differential operator defined in eqn (2.7) and the dimensionless parameters $\alpha, \beta, \kappa, \gamma$ and ς are defined as in eqn (2.5). In addition, the parameter δ in eqn (5.3) is defined in eqn (4.5).

Application of the Fourier expansion defined in eqn (2.14) to the potential functions ϕ, ψ and χ and Hankel integral transform in the radial direction as defined in eqn (2.15) results in the following governing equations

$$\kappa\frac{d^2\breve{\chi}_m}{dz^2} + \frac{d^2\breve{\phi}_m}{dz^2} - (\beta\lambda^2 - \delta^2)\breve{\phi}_m = 0 \tag{5.4a}$$

$$-\kappa\lambda^2\breve{\phi}_m + \alpha\frac{d^2\breve{\chi}_m}{dz^2} - (\lambda^2 - \delta^2)\breve{\chi}_m = 0 \tag{5.4b}$$

$$\frac{d^2\breve{\psi}_m}{dz^2} - (\varsigma\lambda^2 - \delta^2)\breve{\psi}_m = 0 \tag{5.4c}$$

where $\breve{\psi}_m, \breve{\phi}_m$ and $\breve{\chi}_m$ are the m-th order Hankel integral transform of the mth symmetric Fourier components ψ_m, ϕ_m and χ_m of the three potential functions and λ is the Hankel transform parameter. It is noted from the above equations that $\breve{\psi}_m$ is independent of other two potential functions, whilst $\breve{\phi}_m$ and $\breve{\chi}_m$ still are coupled in (5.4a) and (5.4b).

The coupled partial differential equations (5.4a) and (5.4b) can be solved by assuming

$$\breve{\phi}_m = Pe^{\delta\xi z}, \qquad \breve{\chi}_m = Qe^{\delta\xi z}. \tag{5.5}$$

Substitution of the above expressions into eqns (5.4a) and (5.4b) yields the following coupled homogeneous algebraic equation system to determine the coefficients

P and Q,

$$(\xi^2 - \beta\zeta^2 + 1)P + \kappa\xi^2 Q = 0 \tag{5.6a}$$

$$-\kappa\zeta^2 P + (\alpha\xi^2 - \zeta^2 + 1)Q = 0 \tag{5.6b}$$

where the parameter $\zeta = \lambda/\delta$. For a non-trivial solution of P and Q the parameter ξ in eqn (5.6) should satisfy the equation (4.12). Therefore the roots ξ_1 and ξ_2 of eqn (5.6) resulting in non-trivial solutions for P and Q can be given by eqns (4.13a) and (4.13b), respectively.

In view of eqn (5.4c), the solution of $\breve{\psi}_m$ can be expressed as

$$\breve{\psi}_m = Ce^{\delta\xi z} \tag{5.7}$$

where ξ is the root of the following equation

$$\xi^2 - (\varsigma\zeta^2 - 1) = 0 \tag{5.8}$$

and this root can be given as

$$\xi_3 = \pm\sqrt{\varsigma\zeta^2 - 1} \tag{5.9}$$

In view of eqns (5.5)-(5.9) the general solutions for the mth Fourier harmonic of the potential functions ϕ, ψ and χ can be expressed as

$$(\phi_m, \psi_m, \chi_m) = \int_0^\infty (\breve{\phi}_m, \breve{\psi}_m, \breve{\chi}_m) J_m(\delta\zeta r)\delta^2\zeta d\zeta \tag{5.10}$$

where

$$\breve{\phi}_m = \varrho_1 A_m e^{-\delta\xi_1 z} + \varrho_1 B_m e^{\delta\xi_1 z} + \varrho_2 C_m e^{-\delta\xi_2 z} + \varrho_2 D_m e^{\delta\xi_2 z} \tag{5.11a}$$

$$\breve{\psi}_m = E_m e^{-\delta\xi_3 z} + F_m e^{\delta\xi_3 z} \tag{5.11b}$$

$$\breve{\chi}_m = A_m e^{-\delta\xi_1 z} + B_m e^{\delta\xi_1 z} + C_m e^{-\delta\xi_2 z} + D_m e^{\delta\xi_2 z} \tag{5.11c}$$

in which

$$\varrho_1 = \frac{\alpha\xi_1^2 - \zeta^2 + 1}{\kappa\zeta^2}, \quad \varrho_2 = \frac{\alpha\xi_2^2 - \zeta^2 + 1}{\kappa\zeta^2} \tag{5.12}$$

and $A_m, B_m, C_m, D_m, E_m, F_m$ are arbitrary functions to be determined by suitable boundary and continuity conditions. Radicals $\xi_i (i = 1, 2, 3)$ are selected such that $Re(\xi_i) \geq 0$. With this definition the radiation condition at infinity is satisfied and $B_m = D_m = F_m \equiv 0$ for a domain where $z \to \infty$.

In view of eqns (5.10), (5.11) and (5.2), the general solution for mth symmetric Fourier component of displacements and stresses can be expressed as

$$u_{im} = \delta^2 \int_0^\infty u^*_{im} \zeta d\zeta, \qquad i = r, \theta, z \tag{5.13a}$$

$$\sigma_{ijm} = \delta^2 \int_0^\infty \sigma^*_{ijm} \zeta d\zeta, \qquad i, j = r, \theta, z \tag{5.13b}$$

Note that u_{im} and σ_{ijm} in eqn (5.13) denote the mth symmetric components of u_i and σ_{ij} expanded in the form of eqn (2.14). The solutions for u^*_{im} and σ^*_{ijm} can be expressed as

$$u^*_{rm} = (a_1 \bar{A}_m + a_1 \bar{B}_m + a_2 \bar{C}_m + a_2 \bar{D}_m + a_3 \bar{E}_m + a_3 \bar{F}_m) \tag{5.14a}$$

$$u^*_{\theta m} = -(a_4 \bar{A}_m + a_4 \bar{B}_m + a_5 \bar{C}_m + a_5 \bar{D}_m + a_6 \bar{E}_m + a_6 \bar{F}_m) \tag{5.14b}$$

$$u^*_{zm} = -(a_7 \bar{A}_m - a_7 \bar{B}_m + a_8 \bar{C}_m - a_8 \bar{D}_m) \tag{5.14c}$$

$$\sigma^*_{rrm} = c_{44}(b_{11} \bar{A}_m + b_{11} \bar{B}_m + b_{12} \bar{C}_m + b_{12} \bar{D}_m + b_{13} \bar{E}_m + b_{13} \bar{F}_m) \tag{5.15a}$$

$$\sigma^*_{\theta\theta m} = c_{44}(b_{61} \bar{A}_m + b_{61} \bar{B}_m + b_{62} \bar{C}_m + b_{62} \bar{D}_m - b_{13} \bar{E}_m - b_{13} \bar{F}_m) \tag{5.15b}$$

$$\sigma^*_{zzm} = c_{44}(b_{21} \bar{A}_m + b_{21} \bar{B}_m + b_{22} \bar{C}_m + b_{22} \bar{D}_m) \tag{5.15c}$$

$$\sigma^*_{r\theta m} = c_{44}(b_{31} \bar{A}_m + b_{31} \bar{B}_m + b_{32} \bar{C}_m + b_{32} \bar{D}_m + b_{33} \bar{E}_m + b_{33} \bar{F}_m) \tag{5.15d}$$

$$\sigma^*_{\theta zm} = c_{44}(b_{41} \bar{A}_m - b_{41} \bar{B}_m + b_{42} \bar{C}_m - b_{42} \bar{D}_m + b_{43} \bar{E}_m - b_{43} \bar{F}_m) \tag{5.15e}$$

$$\sigma^*_{rzm} = -c_{44}(b_{51} \bar{A}_m - b_{51} \bar{B}_m + b_{52} \bar{C}_m - b_{52} \bar{D}_m + b_{53} \bar{E}_m - b_{53} \bar{F}_m) \tag{5.15f}$$

where

$$\bar{A}_m = A_m e^{-\delta \xi_1 z}, \quad \bar{B}_m = B_m e^{\delta \xi_1 z}, \quad \bar{C}_m = C_m e^{-\delta \xi_2 z} \tag{5.16a}$$

$$\bar{D}_m = D_m e^{\delta \xi_2 z}, \quad \bar{E}_m = E_m e^{-\delta \xi_3 z}, \quad \bar{F}_m = F_m e^{\delta \xi_3 z} \tag{5.16b}$$

and, for $i = 1, 2$,

$$b_{1i} = \frac{\varsigma\varrho_i\delta\zeta}{2r}[(m-1)J_{m-1}(\delta\zeta r) - (m+1)J_{m+1}(\delta\zeta r)] - [\delta^2\zeta^2\beta\varrho_i - (\kappa-1)\delta^2\xi_i^2]J_m(\delta\zeta r) \tag{5.17a}$$

$$\frac{b_{13}}{\varsigma} = \frac{2b_{3i}}{\varrho_i\varsigma\delta\zeta} = \frac{2b_{33}}{[1+(\delta^2\zeta^2r^2/2m)]\varsigma\delta\zeta} = [(m-1)J_{m-1}(\delta\zeta r) - (m+1)J_{m+1}(\delta\zeta r)] \tag{5.17b}$$

$$b_{6i} = -\frac{\varsigma\varrho_i\delta\zeta}{2r}[(m-1)J_{m-1}(\delta\zeta r) - (m+1)J_{m+1}(\delta\zeta r)] - [\delta^2\zeta^2\beta\varrho_i - (\kappa-1)\delta^2\xi_i^2]J_m(\delta\zeta r) \tag{5.17c}$$

$$b_{2i} = [\alpha\delta^2\xi_i^2 - (\kappa-1)\delta^2\zeta^2\varrho_i]J_m(\delta\zeta r), \quad a_7/\delta\xi_1 = a_8/\delta\xi_2 = J_m(\delta\zeta r) \tag{5.17d}$$

$$a_3 = \frac{a_4}{\varrho_1} = \frac{a_5}{\varrho_2} = \frac{b_{4i}}{(1+\varrho_i)\delta\xi_i} = \frac{b_{53}}{\delta\xi_3} = \frac{\delta\zeta[J_{m-1}(\delta\zeta r) + J_{m+1}(\delta\zeta r)]}{2} \tag{5.17e}$$

$$a_6 = \frac{a_1}{\varrho_1} = \frac{a_2}{\varrho_2} = \frac{b_{5i}}{(1+\varrho_i)\delta\xi_i} = \frac{b_{43}}{\delta\xi_3} = \frac{\delta\zeta[J_{m-1}(\delta\zeta r) - J_{m+1}(\delta\zeta r)]}{2} \tag{5.17f}$$

5.4 TRANSIENT GENERAL SOLUTIONS

For a transversely isotropic elastic medium subjected to transient excitations, the governing equations in eqn (5.1) can be solved by employing the potential functions defined in eqn (5.2) and applying Laplace transform, Hankel transform and Fourier expansion with respect to time, radial and circumferential coordinates, respectively. The governing equations are found to be

$$\kappa\frac{d^2\breve{\chi}_m}{dz^2} + \frac{d^2\breve{\phi}_m}{dz^2} - (\beta\lambda^2 + \mu^2)\breve{\phi}_m = 0 \tag{5.18a}$$

$$-\kappa\lambda^2\breve{\phi}_m + \alpha\frac{d^2\breve{\chi}_m}{dz^2} - (\lambda^2 + \mu^2)\breve{\chi}_m = 0 \tag{5.18b}$$

$$\frac{d^2\breve{\psi}_m}{dz^2} - (\varsigma\lambda^2 + \mu^2)\breve{\psi}_m = 0 \tag{5.18c}$$

where $\breve{\phi}_m, \breve{\psi}_m$ and $\breve{\chi}_m$ are the Laplace-Hankel integral transforms of the mth symmetric components of the Fourier expansion of ϕ, ψ and χ, respectively. In addition λ is the Hankel transform parameter and μ is defined by eqn (4.19).

Following a solution procedure identical to that presented in Section 5.3 for time-harmonic excitations, the general solutions for the mth symmetric Fourier component of the potential functions for transient excitations can be expressed as,

$$(\phi_m, \psi_m, \chi_m) = \frac{i\vartheta}{2\pi} \int_{d-i\infty}^{d+i\infty} \int_0^{\infty} (\breve{\phi}_m, \breve{\psi}_m, \breve{\chi}_m) J_m(\lambda r) e^{\mu\vartheta t} \lambda d\lambda d\mu \tag{5.19}$$

where ϑ is defined in eqn (4.19) and

$$\breve{\phi}_m = \varrho_1 A_m e^{-\xi_1 z} + \varrho_1 B_m e^{\xi_1 z} + \varrho_2 C_m e^{-\xi_2 z} + \varrho_2 D_m e^{\xi_2 z} \tag{5.20a}$$

$$\breve{\psi}_m = E_m e^{-\xi_3 z} + F_m e^{\xi_3 z} \tag{5.20b}$$

$$\breve{\chi}_m = A_m e^{-\xi_1 z} + B_m e^{\xi_1 z} + C_m e^{-\xi_2 z} + D_m e^{\xi_2 z} \tag{5.20c}$$

in which

$$\varrho_1 = \frac{\alpha\xi_1^2 - \lambda^2 - \mu^2}{\kappa\lambda^2}, \quad \varrho_2 = \frac{\alpha\xi_2^2 - \lambda^2 - \mu^2}{\kappa\lambda^2} \tag{5.21}$$

ξ_1 and ξ_2 are given in eqn (4.26),

$$\xi_3 = (\varsigma\lambda^2 + \mu^2)^{\frac{1}{2}} \tag{5.22}$$

and A_m, B_m, C_m, D_m, E_m and F_m are arbitrary functions to be determined by suitable boundary and continuity conditions. The radicals $\xi_i (i = 1, 2, 3)$ are selected such that $Re(\xi_i) \geq 0$. With this definition the radiation condition at infinity is satisfied and $B_m = D_m = F_m \equiv 0$ for a domain where $z \to \infty$.

In view of eqn (5.2), (5.19) and eqn (5.20), the general solutions for mth symmetric Fourier component of displacements and stresses for a three-dimensional transient problem can be expressed as

$$u_{im} = \frac{i\vartheta}{2\pi} \int_{d-i\infty}^{d+i\infty} \int_0^{\infty} u_{im}^* e^{\vartheta\mu t} \lambda d\lambda d\mu \quad i = r, \theta, z \tag{5.23a}$$

$$\sigma_{ijm} = \frac{i\vartheta}{2\pi} \int_{d-i\infty}^{d+i\infty} \int_0^{\infty} \sigma_{ijm}^* e^{\vartheta\mu t} \lambda d\lambda d\mu \quad i, j = r, \theta, z. \tag{5.23b}$$

The expressions for u^*_{im} and σ^*_{ijm} are identical to that of u^*_{im} and σ^*_{ijm} of time-harmonic response in eqns (5.14) and (5.15), respectively. However, the replacement of $\delta\xi_i (i = 1,2,3)$ by ξ_i which are defined by eqns (4.26) and (5.22) and $\delta\zeta$ by λ should be made for the coefficients $a_i (i = 1,2,...,8)$ and $b_{ij} (i = 1,2,...,6; j = 1,2,3)$. The parameters $\varrho_i (i = 1,2)$ corresponding to transient excitations are defined in (5.21).

5.5 TIME-HARMONIC GREEN'S FUNCTIONS

5.5.1 **Boundary-Value Problem**

Boundary-value problems related to time harmonic loadings applied in the interior of a transversely isotropic elastic half space are considered in this Section. The dynamic excitations are applied at a depth z' below the free surface of the half space and over a ciruclar ring of radius 's' as shown in Fig 2.2. Again as in the elastostatic problem of a transversely isotropic half space, the intensities of applied loadings vary in the θ-direction according to $\cos m\theta$ for ring loadings in the radial and vertical directions and $\sin m\theta$ for a ring load in the circumferential direction, respectively. Once the solutions for excitations of the above types are derived, solutions corresponding to excitations applied over an axisymmetric domain with arbitrary intensities can be obtained through appropriate integrations and Fourier expansion with respect to the circumferential coordinate.

A solution to the boundary-value problem can be derived by defining a fictitious plane at $z = z'$ and considering the problem as a two-domain problem as in Chapter 2 for a three-dimensional elastostatic problem. The boundary conditions for a transversely isotropic half space subjected to buried time-harmonic loadings can be expressed as

$$\sigma^{(1)}_{izm}(r,0) = 0; \quad i = r,\theta,z \tag{5.24a}$$

$$u^{(1)}_{im}(r,z') - u^{(2)}_{im}(r,z') = 0, \qquad i = r,\theta,z \tag{5.24b}$$

$$\sigma^{(1)}_{izm}(r,z') - \sigma^{(2)}_{izm}(r,z') = p_0\delta(r-s); \quad i = r,\theta,z \tag{5.24c}$$

where p_0 are the specified loading densities, δ is the Dirac's delta function and the superscript '1' and '2' are used to denote the domain numbers (Fig 2.1). The existance of regularity conditions for domain '2' implies that $B_2 = D_2 = F_2 \equiv 0$. The substitution of general solutions for displacements and stresses given by eqns (5.13)-(5.15) in eqn (5.24) results in solutions for arbitrary coefficients of the two domains.

5.5.2 **Green's Functions**

Let the displacement Green's function $G^m_{ij}(r,\theta,z;s,z')$ denote the displacement component in the i-direction $(i = r,\theta,z)$ at the point (r,θ,z) due to a time-harmonic circular ring load in the j-direction $(j = r,\theta,z)$ through the point (s,z') with a circumferential dependence as prescribed earlier and the stress Green's function $\sigma^m_{ilj}(r,\theta,z;s,z')$ denote the stress component σ_{il} $(l = r,\theta,z)$ at the point (r,θ,z) due to the same excitation. The solutions for G^m_{ij} and σ^m_{ilj} can be expressed as

$$G^m_{ij}(r,\theta,z;s,z') = \frac{\delta^2}{c_{44}} \int_0^\infty \hat{G}^m_{ij}\zeta d\zeta \quad i,j = r,\theta,z \tag{5.25a}$$

$$\sigma^m_{ilj}(r,\theta,z;s,z') = \delta^2 \int_0^\infty \hat{\sigma}^m_{ilj}\zeta d\zeta \quad i,l,j = r,\theta,z \tag{5.25b}$$

where

$$\begin{aligned}\hat{G}^m_{rz} =& \cos m\theta \frac{p_1}{RV}(a_1\varrho_2\bar{e}_1 + Ia_1\varrho_2\bar{e}_2 + a_2\varrho_1\bar{e}_3 - Ia_2\varrho_1\bar{e}_4 \\ & - a_1\varrho_1\bar{e}_5 - a_2\varrho_2\bar{e}_6)\end{aligned} \tag{5.26a}$$

$$\begin{aligned}\hat{G}^m_{\theta z} =& -\sin m\theta \frac{p_1}{RV}(a_4\varrho_2\bar{e}_1 - Ia_4\varrho_2\bar{e}_2 + a_5\varrho_1\bar{e}_3 + Ia_5\varrho_1\bar{e}_4 \\ & - a_4\varrho_1\bar{e}_5 - a_5\varrho_2\bar{e}_6)\end{aligned} \tag{5.26b}$$

$$\begin{aligned}\hat{G}^m_{zz} =& \cos m\theta \frac{p_1}{RV}(a_7\varrho_2\bar{e}_1 - a_7\varrho_2\bar{e}_2 + a_8\varrho_1\bar{e}_3 + a_8\varrho_1\bar{e}_4 \\ & - a_7\varrho_1\bar{e}_5 - a_8\varrho_2\bar{e}_6)\end{aligned} \tag{5.26c}$$

$$\hat{G}^m_{r\theta} = \cos m\theta[\frac{(p_2+p_3)}{RS}(a_1\xi_2\bar{e}_1 - a_1\xi_2\bar{e}_2 + a_2\xi_1\bar{e}_3 + a_2\xi_1\bar{e}_4$$

$$- a_1\xi_1\bar{e}_5 - a_2\xi_2\bar{e}_6) - \frac{(p_2-p_3)}{\xi_3}a_3(\bar{e}_7+\bar{e}_8)] \tag{5.27a}$$

$$\hat{G}^m_{\theta\theta} = -\sin m\theta[\frac{(p_2+p_3)}{RS}(a_4\xi_2\bar{e}_1 - a_4\xi_2\bar{e}_2 + a_5\xi_1\bar{e}_3 + a_5\xi_1\bar{e}_4$$
$$- a_4\xi_1\bar{e}_5 - a_5\xi_2\bar{e}_6) - \frac{(p_2-p_3)}{\xi_3}a_6(\bar{e}_7+\bar{e}_8)] \tag{5.27b}$$

$$\hat{G}^m_{z\theta} = \cos m\theta\frac{(p_2+p_3)}{RS}(a_7\xi_2\bar{e}_1 - Ia_7\xi_2\bar{e}_2 + a_8\xi_1\bar{e}_3 + Ia_8\xi_1\bar{e}_4$$
$$- a_7\xi_1\bar{e}_5 - a_8\xi_2\bar{e}_6) \tag{5.27c}$$

$$\hat{G}^m_{rr} = -\cos m\theta[\frac{(p_2-p_3)}{RS}(a_1\xi_2\bar{e}_1 - a_1\xi_2\bar{e}_2 + a_2\xi_1\bar{e}_3 + a_2\xi_1\bar{e}_4$$
$$- a_1\xi_1\bar{e}_5 - a_2\xi_2\bar{e}_6) + \frac{(p_2+p_3)}{\xi_3}a_3(\bar{e}_7+\bar{e}_8)] \tag{5.28a}$$

$$\hat{G}^m_{\theta r} = \sin m\theta[\frac{(p_2-p_3)}{RS}(a_4\xi_2\bar{e}_1 - a_4\xi_2\bar{e}_2 + a_5\xi_1\bar{e}_3 + a_5\xi_1\bar{e}_4$$
$$- a_4\xi_1\bar{e}_5 - a_5\xi_2\bar{e}_6) + \frac{(p_2+p_3)}{\xi_3}a_6(\bar{e}_7+\bar{e}_8)] \tag{5.28b}$$

$$\hat{G}^m_{zr} = -\cos m\theta\frac{(p_2-p_3)}{RS}(a_7\xi_2\bar{e}_1 - Ia_7\xi_2\bar{e}_2 + a_8\xi_1\bar{e}_3 + Ia_8\xi_1\bar{e}_4$$
$$- a_7\xi_1\bar{e}_5 - a_8\xi_2\bar{e}_6) \tag{5.28c}$$

$$\hat{\sigma}^m_{rrz} = \cos m\theta\frac{p_1}{RV}(b_{11}\varrho_2\bar{e}_1 + Ib_{11}\varrho_2\bar{e}_2 + b_{12}\varrho_1\bar{e}_3 - Ib_{12}\varrho_1\bar{e}_4$$
$$- b_{11}\varrho_1\bar{e}_5 - b_{12}\varrho_2\bar{e}_6) \tag{5.29a}$$

$$\hat{\sigma}^m_{\theta\theta z} = \cos m\theta\frac{p_1}{RV}(b_{61}\varrho_2\bar{e}_1 + Ib_{61}\varrho_2\bar{e}_2 + b_{62}\varrho_1\bar{e}_3 - Ib_{62}\varrho_1\bar{e}_4$$
$$- b_{61}\varrho_1\bar{e}_5 - b_{62}\varrho_2\bar{e}_6) \tag{5.29b}$$

$$\hat{\sigma}^m_{zzz} = \cos m\theta\frac{p_1}{RV}(b_{21}\varrho_2\bar{e}_1 + Ib_{21}\varrho_2\bar{e}_2 + b_{22}\varrho_1\bar{e}_3 - Ib_{22}\varrho_1\bar{e}_4$$
$$- b_{21}\varrho_1\bar{e}_5 - b_{22}\varrho_2\bar{e}_6) \tag{5.29c}$$

$$\hat{\sigma}^m_{r\theta z} = -\sin m\theta\frac{p_1}{RV}(b_{31}\varrho_2\bar{e}_1 + Ib_{31}\varrho_2\bar{e}_2 + b_{32}\varrho_1\bar{e}_3 - Ib_{32}\varrho_1\bar{e}_4$$
$$- b_{31}\varrho_1\bar{e}_5 - b_{32}\varrho_2\bar{e}_6) \tag{5.29d}$$

$$\hat{\sigma}^m_{\theta zz} = \sin m\theta\frac{p_1}{RV}(b_{41}\varrho_2\bar{e}_1 - b_{41}\varrho_2\bar{e}_2 + b_{42}\varrho_1\bar{e}_3 + b_{42}\varrho_1\bar{e}_4$$
$$- b_{41}\varrho_1\bar{e}_5 - b_{42}\varrho_2\bar{e}_6) \tag{5.29e}$$

$$\hat{\sigma}^m_{rzz} = -\cos m\theta\frac{p_1}{RV}(b_{51}\varrho_2\bar{e}_1 - b_{51}\varrho_2\bar{e}_2 + b_{52}\varrho_1\bar{e}_3 + b_{52}\varrho_1\bar{e}_4$$

$$- b_{51}\varrho_1\bar{e}_5 - b_{52}\varrho_2\bar{e}_6) \tag{5.29f}$$

$$\hat{\sigma}^m_{rr\theta} = \cos m\theta[\frac{(p_2+p_3)}{RS}(b_{11}\xi_2\bar{e}_1 - b_{11}\xi_2\bar{e}_2 + b_{12}\xi_1\bar{e}_3 + b_{12}\xi_1\bar{e}_4$$
$$- b_{11}\xi_1\bar{e}_5 - b_{12}\xi_2\bar{e}_6) - \frac{(p_2-p_3)}{\xi_3}b_{13}(\bar{e}_7+\bar{e}_8)] \tag{5.30a}$$

$$\hat{\sigma}^m_{\theta\theta\theta} = \cos m\theta[\frac{(p_2+p_3)}{RS}(b_{61}\xi_2\bar{e}_1 - b_{61}\xi_2\bar{e}_2 + b_{62}\xi_1\bar{e}_3 + b_{62}\xi_1\bar{e}_4$$
$$- b_{61}\xi_1\bar{e}_5 - b_{62}\xi_2\bar{e}_6) + \frac{(p_2-p_3)}{\xi_3}b_{13}(\bar{e}_7+\bar{e}_8)] \tag{5.30b}$$

$$\hat{\sigma}^m_{zz\theta} = \cos m\theta\frac{(p_2+p_3)}{RS}(b_{21}\xi_2\bar{e}_1 - b_{21}\xi_2\bar{e}_2 + b_{22}\xi_1\bar{e}_3 + b_{22}\xi_1\bar{e}_4$$
$$- b_{21}\xi_1\bar{e}_5 - b_{22}\xi_2\bar{e}_6) \tag{5.30c}$$

$$\hat{\sigma}^m_{r\theta\theta} = -\sin m\theta[\frac{(p_2+p_3)}{RS}(b_{31}\xi_2\bar{e}_1 - b_{31}\xi_2\bar{e}_2 + b_{32}\xi_1\bar{e}_3 + b_{32}\xi_1\bar{e}_4$$
$$- b_{31}\xi_1\bar{e}_5 - b_{32}\xi_2\bar{e}_6) - \frac{(p_2-p_3)}{\xi_3}b_{33}(\bar{e}_7+\bar{e}_8)] \tag{5.30d}$$

$$\hat{\sigma}^m_{\theta z\theta} = \sin m\theta[\frac{(p_2+p_3)}{RS}(b_{41}\xi_2\bar{e}_1 - Ib_{41}\xi_2\bar{e}_2 + b_{42}\xi_1\bar{e}_3 + Ib_{42}\xi_1\bar{e}_4$$
$$- b_{41}\xi_1\bar{e}_5 - b_{42}\xi_2\bar{e}_6) - \frac{(p_2-p_3)}{\xi_3}b_{43}(\bar{e}_7 - I\bar{e}_8)] \tag{5.30e}$$

$$\hat{\sigma}^m_{rz\theta} = -\cos m\theta[\frac{(p_2+p_3)}{RS}(b_{51}\xi_2\bar{e}_1 - Ib_{51}\xi_2\bar{e}_2 + b_{52}\xi_1\bar{e}_3 + Ib_{52}\xi_1\bar{e}_4$$
$$- b_{51}\xi_1\bar{e}_5 - b_{52}\xi_2\bar{e}_6) - \frac{(p_2-p_3)}{\xi_3}b_{53}(\bar{e}_7 - I\bar{e}_8)] \tag{5.30f}$$

$$\hat{\sigma}^m_{rrr} = -\cos m\theta[\frac{(p_2-p_3)}{RS}(b_{11}\xi_2\bar{e}_1 - b_{11}\xi_2\bar{e}_2 + b_{12}\xi_1\bar{e}_3 + b_{12}\xi_1\bar{e}_4$$
$$- b_{11}\xi_1\bar{e}_5 - b_{12}\xi_2\bar{e}_6) + \frac{(p_2+p_3)}{\xi_3}b_{13}(\bar{e}_7+\bar{e}_8)] \tag{5.31a}$$

$$\hat{\sigma}^m_{\theta\theta r} = -\cos m\theta[\frac{(p_2-p_3)}{RS}(b_{61}\xi_2\bar{e}_1 - b_{61}\xi_2\bar{e}_2 + b_{62}\xi_1\bar{e}_3 + b_{62}\xi_1\bar{e}_4$$
$$- b_{61}\xi_1\bar{e}_5 - b_{62}\xi_2\bar{e}_6) - \frac{(p_2+p_3)}{\xi_3}b_{13}(\bar{e}_7+\bar{e}_8)] \tag{5.31b}$$

$$\hat{\sigma}^m_{zzr} = -\cos m\theta\frac{(p_2-p_3)}{RS}(b_{21}\xi_2\bar{e}_1 - b_{21}\xi_2\bar{e}_2 + b_{22}\xi_1\bar{e}_3 + b_{22}\xi_1\bar{e}_4$$
$$- b_{21}\xi_1\bar{e}_5 - b_{22}\xi_2\bar{e}_6) \tag{5.31c}$$

$$\hat{\sigma}^m_{r\theta r} = \sin m\theta[\frac{(p_2-p_3)}{RS}(b_{31}\xi_2\bar{e}_1 - b_{31}\xi_2\bar{e}_2 + b_{32}\xi_1\bar{e}_3 + b_{32}\xi_1\bar{e}_4$$
$$- b_{31}\xi_1\bar{e}_5 - b_{32}\xi_2\bar{e}_6) + \frac{(p_2+p_3)}{\xi_3}b_{33}(\bar{e}_7+\bar{e}_8)] \tag{5.31d}$$

$$\hat{\sigma}^m_{\theta zr} = -\sin m\theta[\frac{(p_2-p_3)}{RS}(b_{41}\xi_2\bar{e}_1 - Ib_{41}\xi_2\bar{e}_2 + b_{42}\xi_1\bar{e}_3 + Ib_{42}\xi_1\bar{e}_4$$
$$- b_{41}\xi_1\bar{e}_5 - b_{42}\xi_2\bar{e}_6) + \frac{(p_2+p_3)}{\xi_3}b_{43}(\bar{e}_7 - I\bar{e}_8)] \tag{5.31e}$$

$$\hat{\sigma}^m_{zrr} = \cos m\theta[\frac{(p_2-p_3)}{RS}(b_{51}\xi_2\bar{e}_1 - Ib_{51}\xi_2\bar{e}_2 + b_{52}\xi_1\bar{e}_3 + Ib_{52}\xi_1\bar{e}_4$$
$$- b_{51}\xi_1\bar{e}_5 - b_{52}\xi_2\bar{e}_6) + \frac{(p_2+p_3)}{\xi_3}b_{53}(\bar{e}_7 - I\bar{e}_8)] \tag{5.31f}$$

where

$$R = \frac{K(\xi_1-\xi_2)}{\kappa\delta^2\zeta^2} \tag{5.32}$$

$$V = \alpha(\xi_1^2-\xi_2^2)(\zeta^2+1)/\kappa\zeta^2, \quad S = \alpha\delta^2\xi_1\xi_2(\xi_1^2-\xi_2^2)/\kappa\zeta^2 \tag{5.33}$$

$$p_1 = \frac{p_0 s J_m(\delta\zeta s)}{2}, \quad p_2 = \frac{p_0 s J_{m-1}(\delta\zeta s)}{4}, \quad p_3 = \frac{p_0 s J_{m+1}(\delta\zeta s)}{4} \tag{5.34}$$

$$f_1 = \xi_1(1+\varrho_1)[\alpha\xi_1^2 - (\kappa-1)\zeta^2\varrho_1] \tag{5.35}$$

$$f_2 = \xi_2(1+\varrho_2)[\alpha\xi_2^2 - (\kappa-1)\zeta^2\varrho_2] \tag{5.36}$$

$$f_3 = \xi_2(1+\varrho_2)[\alpha\xi_1^2 - (\kappa-1)\delta^2\varrho_1] + \xi_1(1+\varrho_1)[\alpha\xi_2^2 - (\kappa-1)\delta^2\varrho_2] \tag{5.37}$$

$$\bar{e}_1 = f_3 e^{-\delta\xi_1(z'+z)}; \quad \bar{e}_2 = Re^{-\delta\xi_1|z'-z|}; \quad \bar{e}_3 = f_3 e^{-\delta\xi_2(z'+z)} \tag{5.38a}$$

$$\bar{e}_4 = Re^{-\delta\xi_2|z'-z|}; \quad \bar{e}_5 = 2f_1 e^{-\delta(\xi_1 z+\xi_2 z')}; \quad \bar{e}_6 = 2f_2 e^{-\delta(\xi_1 z'+\xi_2 z)} \tag{5.38b}$$

$$\bar{e}_7 = e^{-\xi_3(z'+z)}; \quad \bar{e}_8 = e^{-\xi_3|z'-z|} \tag{5.38c}$$

and I, K, a_i and b_{ij} are defined in eqns (4.34), (4.35) and (5.17), respectively.

The displacements and stresses of a transversely isotropic full space subjected to time-harmonic ring loads can be obtained by taking the limit $z' \to \infty$, and $|z'-z| = z^*$, where z^* is the vertical distance between the load and the observation point.

5.6 TRANSIENT GREEN'S FUNCTIONS

The boundary-value problem corresponding to a transversely isotropic elastic half space subjected to buried transient loadings located at a depth z' below the

free surface can be described by a set of equations similar to eqn (5.24). A function $F(t)$ is used to describe the time history of the applied transient loadings. The substitution of general solutions in the corresponding boundary and continuity conditions results in a system of linear algebraic equations for the solutions of arbitrary functions associated with the two domains. Thereafter, the analytical solutions of transient Green's functions of displacement and stress can be derived explicitly.

Let $G_{ij}^m(r,\theta,z,t;s,z')$ denote the displacement in the i-direction $(i=r,\theta,z)$ at the point (r,θ,z) and at the time instant 't' due to a transient ring load of intensity p_0 per unit arc length and time history $F(t)$ acting in the j-direction $(j=r,\theta,z)$ through the point (s,z'), and $\sigma_{ilj}^m(r,\theta,z,t;s,z')$ denote the stress component σ_{il} $(l=r,\theta,z)$ at the point (r,θ,z) due to the same loading configuration. The following analytical solutions are obtained for G_{ij}^m and σ_{ilj}^m

$$G_{ij}^m(r,\theta,z,t;s,z') = \frac{i\vartheta}{2\pi c_{44}} \int_{d-i\infty}^{d+i\infty} \bar{F} \int_0^\infty \hat{G}_{ij}^m \lambda e^{\vartheta\mu t} d\lambda d\mu \quad i,j=r,\theta,z \quad (5.39a)$$

$$\sigma_{ilj}^m(r,\theta,z,t;s,z') = \frac{i\vartheta}{2\pi} \int_{d-i\infty}^{d+i\infty} \bar{F} \int_0^\infty \hat{\sigma}_{ilj}^m \lambda e^{\vartheta\mu t} d\lambda d\mu \quad i,l,j=r,\theta,z \quad (5.39b)$$

where the expressions of $\hat{G}_{ij}^m$ and $\hat{\sigma}_{ilj}^m$ are identical to that of $\hat{G}_{ij}^m$ and $\hat{\sigma}_{ilj}^m$ given in eqns (5.26)-(5.31) for a time-harmonic response with the replacement of $\delta\zeta \to \lambda$ and $\delta\xi_i \to \xi_i$. The corresponding parameters $\xi_i (i=1,2), \xi_3$ and $\varrho_i (i=1,2)$ are given by (4.26), (5.22) and (5.21), respectively. In addition, $\bar{F}$ is the Laplace transform of $F(t)$.

5.7 GREEN'S FUNCTIONS FOR DISPLACEMENT JUMPS

The boundary-value problems corresponding to transient displacement discontinuities (jumps) inside a transversely isotropic half space are considered. The displacement jumps are assumed to occur at a depth z' below the free surface and

over a circular disk of radius s. The intensities of the radial and vertical displacement discontinuities vary in the θ-direction according to $\cos m\theta$. The intensity of the displacement discontinuity in the circumferential direction varies with θ according to $\sin m\theta$. The time history of the excitation is denoted by $F(t)$. The boundary-value problems corresponding to internal displacement discontinuities can be expressed as

$$\sigma^{(1)}_{zim}(r,0,t) = 0; \quad i = r,\theta,z \tag{5.40a}$$

$$u^{(1)}_{im}(r,z',t) - u^{(2)}_{im}(r,z',t) = u^{0}_{im}(r)H(s-r)F(t); \qquad i = r,\theta,z \tag{5.40b}$$

$$\sigma^{(1)}_{zim}(r,z',t) - \sigma^{(2)}_{zim}(r,z',t) = 0; \quad i = r,\theta,z \tag{5.40c}$$

where the superscripts '1' and '2' denote the domain numbers and $u^{0}_{im}(r)$ denotes the radial variation of the absolute value of the displacement jump at $z = z'$ in the i- direction $(i = r,\theta,z)$. The application of Laplace-Hankel transform in eqn (5.40) together with the substitution of transient general solutions results in a system of linear algebraic equations to determine the arbitrary functions associated with the two domains.

Let $G^m_{ij}(r,\theta,z,t;s,z')$ denote the displacement in the i-direction $(i = r,\theta,z)$ at the point (r,θ,z) and at the time instant 't' due to a transient displacement discontinuity in the j-direction $(j = r,\theta,z)$ over a disk of radius 's' located at $z = z'$, and $\sigma^m_{ilj}(r,\theta,z,t;s,z')$ denote the stress component σ_{il} $(l = r,\theta,z)$ at the point (r,θ,z) due to the same excitation. The fundamental solutions $G^m_{ij}(x,\theta,z,t;s,z')$ and $\sigma^m_{ilj}(r,\theta,z,t;s,z')$ corresponding to transient displacement jumps can be expressed in the forms of eqns (5.39a) and (5.39b), respectively, with $\hat{G}^m_{ij}$ and $\hat{\sigma}^m_{ilj}$ defined by

$$\begin{aligned}\hat{G}^m_{rz} = &\cos m\theta \frac{\bar{u}^o_z}{RS}(a_1 w_4 \bar{e}_1 - a_1 w_4 \bar{e}_2 + a_2 w_3 \bar{e}_3 + a_2 w_3 \bar{e}_4 \\ &- a_1 w_3 \bar{e}_5 - a_2 w_4 \bar{e}_6)\end{aligned} \tag{5.41a}$$

$$\hat{G}^m_{\theta z} = -\sin m\theta \frac{\bar{u}^o_z}{RS}(a_4 w_4 \bar{e}_1 - a_4 w_4 \bar{e}_2 + a_5 w_3 \bar{e}_3 + a_5 w_3 \bar{e}_4$$

$$- a_4 w_3 \bar{e}_5 - a_5 w_4 \bar{e}_6) \tag{5.41b}$$

$$\hat{G}^m_{zz} = - \cos m\theta \frac{\bar{u}^o_z}{RS}(a_7 w_4 \bar{e}_1 - I a_7 w_4 \bar{e}_2 + a_8 w_3 \bar{e}_3 + I a_8 w_3 \bar{e}_4$$
$$- a_7 w_3 \bar{e}_5 - a_8 w_4 \bar{e}_6) \tag{5.41c}$$

$$\hat{G}^m_{r\theta} = \cos m\theta [\frac{(\bar{u}^0_{\theta 1} + \bar{u}^o_{\theta 2})}{RV}(a_1 w_2 \bar{e}_1 - I a_1 w_2 \bar{e}_2 + a_2 w_1 \bar{e}_3 + I a_2 w_1 \bar{e}_4$$
$$- a_1 w_1 \bar{e}_5 - a_2 w_2 \bar{e}_6) - a_3 (\bar{u}^0_{\theta 1} - \bar{u}^0_{\theta 2})(\bar{e}_7 + I \bar{e}_8)] \tag{5.42a}$$

$$\hat{G}^m_{\theta\theta} = - \sin m\theta [\frac{(\bar{u}^0_{\theta 1} + \bar{u}^o_{\theta 2})}{RV}(a_4 w_2 \bar{e}_1 - I a_4 w_2 \bar{e}_2 + a_5 w_1 \bar{e}_3 + I a_5 w_1 \bar{e}_4$$
$$- a_4 w_1 \bar{e}_5 - a_5 w_2 \bar{e}_6) - a_6 (\bar{u}^0_{\theta 1} - \bar{u}^0_{\theta 2})(\bar{e}_7 + I \bar{e}_8)] \tag{5.42b}$$

$$\hat{G}^m_{z\theta} = - \cos m\theta \frac{(\bar{u}^0_{\theta 1} + \bar{u}^o_{\theta 2})}{RV}(a_7 w_2 \bar{e}_1 + a_7 w_2 \bar{e}_2 + a_8 w_1 \bar{e}_3 - a_8 w_1 \bar{e}_4$$
$$- a_7 w_1 \bar{e}_5 - a_8 w_2 \bar{e}_6) \tag{5.42c}$$

$$\hat{G}^m_{rr} = - \cos m\theta [\frac{(\bar{u}^0_{r1} - \bar{u}^o_{r2})}{RV}(a_1 w_2 \bar{e}_1 - I a_1 w_2 \bar{e}_2 + a_2 w_1 \bar{e}_3 + I a_2 w_1 \bar{e}_4$$
$$- a_1 w_1 \bar{e}_5 - a_2 w_2 \bar{e}_6) + a_3 (\bar{u}^0_{r1} + \bar{u}^0_{r2})(\bar{e}_7 + I \bar{e}_8)] \tag{5.43a}$$

$$\hat{G}^m_{\theta r} = \sin m\theta [\frac{(\bar{u}^0_{r1} - \bar{u}^o_{r2})}{RV}(a_4 w_2 \bar{e}_1 - I a_4 w_2 \bar{e}_2 + a_5 w_1 \bar{e}_3 + I a_5 w_1 \bar{e}_4$$
$$- a_4 w_1 \bar{e}_5 - a_5 w_2 \bar{e}_6) + a_6 (\bar{u}^0_{r1} + \bar{u}^0_{r2})(\bar{e}_7 + I \bar{e}_8)] \tag{5.43b}$$

$$\hat{G}^m_{zr} = \cos m\theta \frac{(\bar{u}^0_{r1} - \bar{u}^o_{r2})}{RV}(a_7 w_2 \bar{e}_1 + a_7 w_2 \bar{e}_2 + a_8 w_1 \bar{e}_3 - a_8 w_1 \bar{e}_4$$
$$- a_7 w_1 \bar{e}_5 - a_8 w_2 \bar{e}_6) \tag{5.43c}$$

$$\hat{\sigma}^m_{rrz} = \cos m\theta \frac{c_{44} \bar{u}^o_z}{RS}(b_{11} w_4 \bar{e}_1 - b_{11} w_4 \bar{e}_2 + b_{12} w_3 \bar{e}_3 + b_{12} w_3 \bar{e}_4$$
$$- b_{11} w_3 \bar{e}_5 - b_{12} w_4 \bar{e}_6) \tag{5.44a}$$

$$\hat{\sigma}^m_{\theta\theta z} = \cos m\theta \frac{c_{44} \bar{u}^o_z}{RS}(b_{61} w_4 \bar{e}_1 - b_{61} w_4 \bar{e}_2 + b_{62} w_3 \bar{e}_3 + b_{62} w_3 \bar{e}_4$$
$$- b_{61} w_3 \bar{e}_5 - b_{62} w_4 \bar{e}_6) \tag{5.44b}$$

$$\hat{\sigma}^m_{zzz} = \cos m\theta \frac{c_{44} \bar{u}^o_z}{RS}(b_{21} w_4 \bar{e}_1 - b_{21} w_4 \bar{e}_2 + b_{22} w_3 \bar{e}_3 + b_{22} w_3 \bar{e}_4$$
$$- b_{21} w_3 \bar{e}_5 - b_{22} w_4 \bar{e}_6) \tag{5.44c}$$

$$\hat{\sigma}^m_{r\theta z} = \sin m\theta \frac{c_{44} \bar{u}^o_z}{RS}(b_{31} w_4 \bar{e}_1 - b_{31} w_4 \bar{e}_2 + b_{32} w_3 \bar{e}_3 + b_{32} w_3 \bar{e}_4$$
$$- b_{31} w_3 \bar{e}_5 - b_{32} w_4 \bar{e}_6) \tag{5.44d}$$

$$\hat{\sigma}^m_{\theta zz} = \sin m\theta \frac{c_{44} \bar{u}^o_z}{RS}(b_{41} w_4 \bar{e}_1 - I b_{41} w_4 \bar{e}_2 + b_{42} w_3 \bar{e}_3 + I b_{42} w_3 \bar{e}_4$$

$$- b_{41}w_3\bar{e}_5 - b_{42}w_4\bar{e}_6) \tag{5.44e}$$

$$\hat{\sigma}^m_{rzz} = -\cos m\theta \frac{c_{44}\bar{u}^o_z}{RS}(b_{51}w_4\bar{e}_1 - Ib_{51}w_4\bar{e}_2 + b_{52}w_3\bar{e}_3 + Ib_{52}w_3\bar{e}_4$$
$$- b_{51}w_3\bar{e}_5 - b_{52}w_4\bar{e}_6) \tag{5.44f}$$

$$\hat{\sigma}^m_{rr\theta} = \cos m\theta[\frac{c_{44}(\bar{u}^0_{r1} + \bar{u}^0_{r2})}{RV}(b_{11}w_2\bar{e}_1 - Ib_{11}w_2\bar{e}_2 + b_{12}w_1\bar{e}_3 + Ib_{12}w_1\bar{e}_4$$
$$- b_{11}w_1\bar{e}_5 - b_{12}w_2\bar{e}_6) - b_{13}(\bar{u}^0_{r1} - \bar{u}^0_{r2})(\bar{e}_7 + I\bar{e}_8)] \tag{5.45a}$$

$$\hat{\sigma}^m_{\theta\theta\theta} = \cos m\theta[\frac{c_{44}(\bar{u}^0_{r1} + \bar{u}^0_{r2})}{RV}(b_{61}w_2\bar{e}_1 - Ib_{61}w_2\bar{e}_2 + b_{62}w_1\bar{e}_3 + Ib_{62}w_1\bar{e}_4$$
$$- b_{61}w_1\bar{e}_5 - b_{62}w_2\bar{e}_6) + b_{13}(\bar{u}^0_{r1} - \bar{u}^0_{r2})(\bar{e}_7 + I\bar{e}_8)] \tag{5.45b}$$

$$\hat{\sigma}^m_{zz\theta} = \cos m\theta \frac{c_{44}(\bar{u}^0_{r1} + \bar{u}^0_{r2})}{RV}(b_{21}w_2\bar{e}_1 - Ib_{21}w_2\bar{e}_2 + b_{22}w_1\bar{e}_3 + Ib_{22}w_1\bar{e}_4$$
$$- b_{21}w_1\bar{e}_5 - b_{22}w_2\bar{e}_6) \tag{5.45c}$$

$$\hat{\sigma}^m_{r\theta\theta} = \sin m\theta[\frac{c_{44}(\bar{u}^0_{\theta1} + \bar{u}^0_{\theta2})}{RV}(b_{31}w_2\bar{e}_1 - Ib_{31}w_2\bar{e}_2 + b_{32}w_1\bar{e}_3 + Ib_{32}w_1\bar{e}_4$$
$$- b_{31}w_1\bar{e}_5 - b_{32}w_2\bar{e}_6) - b_{33}(\bar{u}^0_{\theta1} - \bar{u}^0_{\theta2})(\bar{e}_7 + I\bar{e}_8)] \tag{5.45d}$$

$$\hat{\sigma}^m_{\theta z\theta} = \sin m\theta[\frac{c_{44}(\bar{u}^0_{\theta1} + \bar{u}^0_{\theta2})}{RV}(b_{41}w_2\bar{e}_1 + b_{41}w_2\bar{e}_2 + b_{42}w_1\bar{e}_3 - b_{42}w_1\bar{e}_4$$
$$- b_{41}w_1\bar{e}_5 - b_{42}w_2\bar{e}_6) - b_{43}(\bar{u}^0_{\theta1} - \bar{u}^0_{\theta2})(\bar{e}_7 - \bar{e}_8)] \tag{5.45e}$$

$$\hat{\sigma}^m_{rz\theta} = -\cos m\theta[\frac{c_{44}(\bar{u}^0_{\theta1} + \bar{u}^0_{\theta2})}{RV}(b_{51}w_2\bar{e}_1 + b_{51}w_2\bar{e}_2 + b_{52}w_1\bar{e}_3 - b_{52}w_1\bar{e}_4$$
$$- b_{51}w_1\bar{e}_5 - b_{52}w_2\bar{e}_6) - b_{53}(\bar{u}^0_{\theta1} - \bar{u}^0_{\theta2})(\bar{e}_7 - \bar{e}_8)] \tag{5.45f}$$

$$\hat{\sigma}^m_{rrr} = -\cos m\theta[\frac{c_{44}(\bar{u}^0_{r1} - \bar{u}^0_{r2})}{RV}(b_{11}w_2\bar{e}_1 - Ib_{11}w_2\bar{e}_2 + b_{12}w_1\bar{e}_3 + Ib_{12}w_1\bar{e}_4$$
$$- b_{11}w_1\bar{e}_5 - b_{12}w_2\bar{e}_6) + b_{13}(\bar{u}^0_{r1} + \bar{u}^0_{r2})(\bar{e}_7 + I\bar{e}_8)] \tag{5.46a}$$

$$\hat{\sigma}^m_{\theta\theta r} = -\cos m\theta[\frac{c_{44}(\bar{u}^0_{r1} - \bar{u}^0_{r2})}{RV}(b_{61}w_2\bar{e}_1 - Ib_{61}w_2\bar{e}_2 + b_{62}w_1\bar{e}_3 + Ib_{62}w_1\bar{e}_4$$
$$- b_{61}w_1\bar{e}_5 - b_{62}w_2\bar{e}_6) - b_{13}(\bar{u}^0_{r1} + \bar{u}^0_{r2})(\bar{e}_7 + I\bar{e}_8)] \tag{5.46b}$$

$$\hat{\sigma}^m_{zzr} = -\cos m\theta \frac{c_{44}(\bar{u}^0_{r1} - \bar{u}^0_{r2})}{RV}(b_{21}w_2\bar{e}_1 - Ib_{21}w_2\bar{e}_2 + b_{22}w_1\bar{e}_3 + Ib_{22}w_1\bar{e}_4$$
$$- b_{21}w_1\bar{e}_5 - b_{22}w_2\bar{e}_6) \tag{5.46c}$$

$$\hat{\sigma}^m_{r\theta r} = -\sin m\theta[\frac{c_{44}(\bar{u}^0_{r1} - \bar{u}^0_{r2})}{RV}(b_{31}w_2\bar{e}_1 - Ib_{31}w_2\bar{e}_2 + b_{32}w_1\bar{e}_3 + Ib_{32}w_1\bar{e}_4$$
$$- b_{31}w_1\bar{e}_5 - b_{32}w_2\bar{e}_6) + b_{33}(\bar{u}^0_{r1} + \bar{u}^0_{r2})(\bar{e}_7 + I\bar{e}_8)] \tag{5.46d}$$

$$\hat{\sigma}^m_{\theta zr} = -\sin m\theta[\frac{c_{44}(\bar{u}^0_{r1} - \bar{u}^0_{r2})}{RV}(b_{41}w_2\bar{e}_1 + b_{41}w_2\bar{e}_2 + b_{42}w_1\bar{e}_3 - b_{42}w_1\bar{e}_4$$

$$- b_{41}w_1\bar{e}_5 - b_{42}w_2\bar{e}_6) + b_{43}(\bar{u}^0_{r1} + \bar{u}^0_{r2})(\bar{e}_7 - \bar{e}_8)] \tag{5.46e}$$

$$\hat{\sigma}^m_{rzr} = \cos m\theta[\frac{c_{44}(\bar{u}^0_{r1} - \bar{u}^0_{r2})}{RV}(b_{51}w_2\bar{e}_1 + b_{51}w_2\bar{e}_2 + b_{52}w_1\bar{e}_3 - b_{52}w_1\bar{e}_4$$
$$- b_{51}w_1\bar{e}_5 - b_{52}w_2\bar{e}_6) + b_{53}(\bar{u}^0_{r1} + \bar{u}^0_{r2})(\bar{e}_7 - \bar{e}_8)] \tag{5.46f}$$

in which

$$\bar{u}^0_z = \frac{1}{2}\int_0^s u^0_{zm}(r)J_m(\lambda r)rdr \tag{5.47a}$$

$$\bar{u}^0_{\theta 1} = \frac{1}{4}\int_0^s u^0_{\theta m}(r)J_{m-1}(\lambda r)rdr; \quad \bar{u}^0_{\theta 2} = \frac{1}{4}\int_0^s u^0_{\theta m}(r)J_{m+1}(\lambda r)rdr \tag{5.47b}$$

$$\bar{u}^0_{r1} = \frac{1}{4}\int_0^s u^0_{rm}(r)J_{m-1}(\lambda r)rdr; \quad \bar{u}^0_{r2} = \frac{1}{4}\int_0^s u^0_{rm}(r)J_{m+1}(\lambda r)rdr \tag{5.47c}$$

$$w_1 = (1 + \varrho_1)\xi_1; \qquad w_2 = (1 + \varrho_2)\xi_2 \tag{5.48a}$$

$$w_3 = \alpha\xi_1^2 - (\kappa - 1)\lambda^2\varrho_1; \qquad w_4 = \alpha\xi_2^2 - (\kappa - 1)\lambda^2\varrho_2 \tag{5.48b}$$

and $\bar{u}^0_{im}(i = r, \theta, z)$ denote the mth order Hankel transform of $u^0_{im}H(s - r)$. The other parameters $R, V, S, \bar{e}_i, a_i, b_{ij}$ are defined by eqns (5.32), (5.33), (5.38) and (5.17) together with the replacement of $\delta\xi_i$ by ξ_i of eqns (4.26) and (5.22) and $\delta\zeta$ by λ. The solution corresponding to a displacement discontinuity over an annular region can be obtained by replacing $u^0_{im}H(s - r)$ in eqn (5.40) by $u^0_{im}[H(s_1 - r) - H(s_2 - r)]$ where s_1 and s_2 are outer and inner radii of the annular region, respectively.

5.8 NUMERICAL SOLUTIONS FOR TIME-HARMONIC PROBLEMS

5.8.1 Numerical Scheme

The solutions for displacements and stresses given by eqns (5.25)-(5.31) appear in terms of semi-infinite integrals with a complex-valued integrand. As in the case of an isotropic medium and 2-D orthotropic half-plane solutions, these integrals cannot be evaluated analytically for both surface and interior loadings. In view of the complexity of the integrands, it is natural to employ a suitable

numerical quadrature scheme to evaluate the Green's functions. The numerical evaluation of solutions given by eqns (5.25)-(5.31) requires careful consideration due to the presence of singularities within the range of integration and the oscillatory nature of the integrands involving product of Bessel functions. The singularities of the integrands of eqns (5.25)-(5.31) also need to be examined prior to the establishment of a numerical integration procedure. An understanding of the singularities of the integrands of eqns (5.25)-(5.31) can be obtained by treating ζ as a complex variable similar to the case of 2-D problems considered in subsection 4.8.1. It is noted that due to the presence of radicals $\xi_i (i = 1, 2, 3)$ the Riemann surface of the integrand of each integrals has eight sheets. However, the condition $Re(\xi_i) \geq 0$, which is required to satisfy regularity conditions at infinity, implies that only the sheet in which radicals $\xi_i (i = 1, 2, 3)$ have positive real parts everywhere is relevant. The important singularities of the integrands are the branch points of the radicals $\xi_i (i = 1, 2, 3)$ and poles of the function K. The branch points of $\xi_i (i = 1, 2, 3)$ are given by

$$\xi_i = 0, \qquad i = 1, 2, 3 \tag{5.49}$$

and the eqn (5.49) results in,

$$\zeta_p = \pm \frac{1}{\sqrt{\beta}} \tag{5.50a}$$

$$\zeta_{s_1} = \pm 1; \qquad \zeta_{s_2} = \pm \frac{1}{\sqrt{\varsigma}} \tag{5.50b}$$

For an isotropic solid, the eqns (5.50) reduce to $\zeta_p = \pm\sqrt{\bar{\mu}/(\bar{\lambda} + 2\bar{\mu})}$ and $\zeta_{s_1} = \zeta_{s_2} = \pm 1$. It can be shown (Buchwald 1961) that in a three-dimensional orthotropic material there are three kinds of body waves. The wave numbers of these waves are equal to $\delta/\sqrt{\beta}$, δ and $\delta/\sqrt{\varsigma}$. The motion associated with these waves is neither purely dilatational nor purely distortional. However, at the limit of isotropy, the above three waves correspond to P, SV and SH waves associated with an isotropic medium. It is noted that in plane strain problems considered in Chapter

4 the integrands of the integrals appearing in the Green's function solutions have only two branch points. These are ζ_p and ζ_{s_1} and the solutions are independent of the material constant c_{12} [*ie* the nondimensional constant ς]. The poles of the factor K in the denominator of the integrand of 3-D problems are identical to those of a two-dimensional time-harmonic problem. The numerical evaluation of the integrals encountered in 3-D time-harmonic problems are carried out by using a direct numerical quadrature scheme similar to that used in Section 4.8 for 2-D problems. Negligible material attenuation is considered to shift all singularities of the integrands from the real ζ-axis.

5.8.2 Numerical Solutions

In the numerical study the response of five different transversely isotropic materials, namely, an isotropic material, layered soil, beryl rock, E composite and G composite are considered and the values of material constants of these materials are given in Table 1.1. The loading is assumed to be uniformly distributed over a circular area of radius a with intensity q_0 and acting at a depth a as shown in Fig 5.1. The numerical solutions are presented in terms of normalised displacement and stress Green's functions $\bar{G}_{ij} = G_{ij}c_{44}/aq_0$ and $\bar{\sigma}_{ijk} = \sigma_{ijk}/q_0$. In addition, a nondimensional frequency a_0 defined as $a_0 = a\delta = a\omega(\rho/c_{44})^{1/2}$ is used.

Figure 5.2 shows the variation of normalised displacement Green's function $\bar{G}_{zz}$ along the z-axis of the half space for the five different materials. Solutions are presented for three different frequencies ($a_0 = 0.5, 1.0$ and 3.0) and the loading configuation is shown in Fig $5.1(a)$. Comparison of solutions presented in Fig $5.2(a)$ indicates that the degree of anisotropy of the materials has a significant influence on both real and imaginary parts of the displacements. The variation of the displacements along the z-axis is more gradual for E composite and G composite when compared to isotropic material, layered soil and beryl rock. The real parts of the displacements have a kink at $z/a = 1.0$ which is consistent with

the discontinuity of stress at this level due to the applied loading. Note that the kink at $z = a$ is not much visible in the case of the two composite materials since these materials are much stiffer than the other three materials. Imaginary parts of the displacements are smooth along the z-axis. In all cases, the displacement profiles, except that for G composite, show changes in sign with increasing depth. Comparison of Figs 5.2(a) and 5.2(b) indicates that the influence of frequency on $\bar{G}_{zz}$ is also very significant. It is noted that $Re(\bar{G}_{zz})$ generally decreases with a_0 whereas the variation of $Im(\bar{G}_{zz})$ with a_0 is more complicated. As frequency increases (*eg.* a_0=3.0), both real and imaginary parts show oscillatory variation with the depth. At low frequencies ($a_0 \leq 1.0$) the highest magnitude of $Re(\bar{G}_{zz})$ is noted at the level of loading. However at high frequencies, maximum values are noted at other depths.

Figure 5.3 shows the variation of $\bar{G}_{zz}$ at the free surface. These solutions also confirm the significant dependence of the response on the degree of anisotropy of the material and the frequency of excitation. Displacements are generally more smoother at the surface level when compared to those along the z-axis. In addition, both real and imaginary parts of the displacements decay quite rapidly with the radial distance and the largest magnitude is noted at $r = 0$ for most cases. Comparison of displacement profiles in Figs 5.2 and 5.3 indicates that the highest influence of anisotropy is noted in the case of G composite followed by E composite and beryl rock. It is found that the solutions for layered soil are generally closer to isotropic solutions within the frequency range $0 \leq a_0 \leq 2.0$. Comparison of the solutions for $\bar{G}_{zz}$ with the coefficients $\bar{c}_{ij}$ indicates that the behaviour of solutions noted in Figs 5.2 and 5.3 at low frequencies ($a_0 < 1.5$) can be related to the order of the magnitude of $\bar{c}_{33}$ and the influence of other values of $\bar{c}_{ij}$ on $\bar{G}_{zz}$ is relatively small. Note that c_{33} corresponds to a Young's modulus in the vertical direction and in the present case the loading is also applied in the same direction.

Figure 5.4 shows the normalised stress Green's function $\bar{\sigma}_{zzz}$ along the z-axis. The influence of the degree of material anisotropy as well as the frequency of excitation is clearly evident on these solutions. $Re(\bar{\sigma}_{zzz})$ decays rapidly with z for $z/a > 1.0$ whereas at high frequencies a gradually decaying oscillatory variation is noted. The variation of $Im(\bar{\sigma}_{zzz})$ with z is smooth except at higher frequencies (*eg.* $a_0 = 3.0$). $Re(\bar{\sigma}_{zzz})$ shows a discontinuity equal to unity at $z/a = 1.0$ due to the applied loading but no discontinuity exists in $Im(\bar{\sigma}_{zzz})$ profiles. Comparison of stress profiles corresponding to different materials indicates that the influence of material anisotropy is similar to that observed earlier for displacements. Stresses coressponding to G composite shows the highest influence of material anisotropy followed by E composite, beryl rock and layered soil. It was observed in Section 4.8 that the influence of material anisotropy on σ_{zz} is relatively less in the case of 2-D problems.

Figure 5.5 shows the normalised displacement $\bar{G}_{xx}$ along the z-axis for different materials. The loading configuration is shown in Fig 5.1*b* and the solutions are presented for three frequencies. It is noted that the influence of material anisotropy is much less than that observed earlier for $\bar{G}_{zz}$ due to a vertical loading. Generally the imaginary part of the solution shows more dependence on material anisotropy when compared to the real part of the solution. The influence of frequency of excitation on the profiles are quite similar to those observed earlier in Fig 5.2 except that at higher frequency ($a_0 = 3.0$) more prominent oscillatory variations are observed with depth. The kink at $z/a = 1.0$ in $Re(\bar{G}_{xx})$ is much sharper than that of $\bar{G}_{zz}$ and it is due to the loading applied at this level. $Im(\bar{G}_{xx})$ is smooth at this point. Fig 5.6 shows the variation of normalised displacement Green's function $\bar{G}_{xx}$ at the surface level with the horizontal distance for different materials. The influence of degree of anisotropy on these solutions is more prominent when compared to the solutions along the z-axis. In addition, the dependence of these profiles on a_0 is quite similar to that observed earlier for

$\bar{G}_{zz}$ in Fig 5.3. It is useful to relate the behaviour of displacements observed in Figs 5.5 and 5.6 to the material constants presented in Table 1.1. It is noted that the normalised in-plane Young's modulus $\bar{c}_{11}$ for all five materials are relatively closer to each other when compared to $\bar{c}_{33}$. Note that both the direction of the loading and the displacement are in-plane and it is reasonable to expect that at least within the low frequency range ($a_0 < 1.5$) the main influence of anisotropy would arise from $\bar{c}_{11}$. Since $\bar{c}_{11}$ for these five materials are quite closer to each other the influence of anisotropy on $\bar{G}_{xx}$ is relatively less. The difference observed in surface displacements may be due to the fact that at surface level both surface and body waves contribute to the displacements and interaction between the two systems of waves are more complicated. In fact, in all cases it is observed that at high frequencies (*eg.* $a_0 = 3.0$) the influence of anisotropy cannot be related to a single material constant. Figure 5.7 shows the variation of normalised stress Green's function $\bar{\sigma}_{zxx}$ along the z-axis for different materials. The influence of material anisotropy is negligible on $Re(\bar{\sigma}_{zxx})$. However, $Im(\bar{\sigma}_{zxx})$ is more dependent on the material anisotropy especially at high frequencies. At low frequencies, maximum $Re(\bar{\sigma}_{zxx})$ is observed at the level of loading and $Re(\bar{\sigma}_{zxx})$ decays rapidly with the depth. On the other hand, at high frequencies, maximum $Re(\bar{\sigma}_{zxx})$ is not at the level of loading and slowly decaying oscillatory variations are observed. $Im(\bar{\sigma}_{zxx})$ also shows oscillatory variations with the depth at high frequencies.

5.9 NUMERICAL SOLUTIONS FOR TRANSIENT PROBLEMS

5.9.1 **Numerical Scheme**

The numerical algorithm used in Section 4.9 to evaluate the transient response of a half-plane is also employed here to obtain numerical solutions for the transient response of a transversely isotropic elastic half space. The accuracy of the numerical algorithm for 3-D problems is first investigated by considering an

isotropic half space subjected to a surface step loading. As mentioned earlier, Eason (1966) presented numerical solutions for transient response of an isotropic elastic half space subjected to a vertical step load of intensity q_0 applied uniformly over a circular disk of radius 'a' located at the surface. Eason (1966) used contour integration to invert Laplace transform and thereafter reduced the semi-infinite integral with respect to Hankel transform parameter to a set of finite integrals and expressions in terms of complete elliptic integrals. Fig 5.8 presents a comparison of numerical solutions for normalised vertical displacement G^*_{zz} (G^*_{ij} is defined in Section 4.9) at five points along the z-axis obtained from the present numerical integration scheme with the results reported by Eason (1966). It is evident from Fig 5.8 that the numerical algorithm used in the present study also results in very accurate numerical solutions for 3-D problems.

5.9.2 Numerical Solutions

At this stage attention is focused to Fig 5.9 where normalised vertical displacement $G^*_{zz}(r,0)$ at three surface points (r/a= 0,1,5) is plotted with the nondimensional time τ (τ is defined in Section 4.9). These displacements correspond to layered soil, isotropic and beryl rock half spaces subjected to a rectangular pulse load (see Fig 5.9) in the vertical direction acting uniformly over a circular area of radius a located at depth $z'/a = 1.0$. Comparison of solutions for layered soil and beryl rock with the isotropic material solution indicates that the degree of anisotropy of the material has a visible influence on the transient response. Since the normalised material coefficients and normalised displacements are used in the analysis any difference in the solutions for different materials indicates the influence of material anisotropy. Solutions at $r/a = 0$ and 1.0 indicate the existence of an approximately constant velocity period during $0.5 < \tau < 1.5$. This velocity is nearly identical for the isotropic material and beryl rock but it is smaller than that corresponding to a layered soil. In general, layered soil has the largest surface displacements followed by the isotropic material and beryl rock. It

is also noted that transient waves arrive at the observation point slightly later in the case of layered soil half space. Displacements continue to increase at $r/a = 0$ and 1.0 after the removal of the load (*i.e.* $\tau > 1$) and reach its peak value near $\tau = 1.5$ for both points and for all three materials. The retarding velocities are found to decrease rapidly with increasing r/a. At far field, *i.e.* $r/a = 5.0$, a minor negative displacement is initially observed and the excitation is observed during the interval $4.5 < \tau < 9.0$. Far-field displacements also show the influence of anisotropy of the medium.

Selected numerical solutions for stresses are presented next. Figure 5.10 presents a comparison of solution for $\sigma^*_{zzz}(= \frac{\sigma_{ijk}}{\sigma_0})$ at two interior points on the z-axis due to a uniform disc pressure of radius 'a' applied at the surface (Laturelle 1990). The time dependence of the loading is denoted by $H(t)$. It is evident from Fig 5.10 that the present numerical solutions agree closely with those reported in literature for stresses as well. Figure 5.11 presents numerical solutions for σ^*_{zzz} due to a uniform disc pressure of radius 'a' applied at $z'/a = 1.0$. It is noted that the numerical solutions for stresses due to internal loadings have not been reported in literature even for an isotropic half space. Comparison of solutions in Fig 5.11 indicates that the stresses at internal points due to buried loadings show characteristics which are quite different from surface loadings. It is also noted that beryl rock experiences high peak stresses when compared to isotropic material. However, the general trend of the variation of transient stress solutions for both materials are similar. The initial transient disturbances arrive observation points at nearly identical nondimentional time instants for both materials. Static stresses (long term solutions) are also found to be nearly identical for both materials. It is very important to note that the peak transient stresses at both observation points are nearly twice of the corresponding static solutions. As in the case of elastostatic solutions presented in Chapter 3 the influence of material anisotropy is more prominent in displacements when compared to stresses.

5.10 CONCLUSIONS

The three-dimensional dynamic response of a transversely isotropic elastic half space is studied. Analytical general solutions for displacements and stresses are obtained by applying Fourier expansion together with Hankel integral transform for time-harmonic three-dimensional problems and Laplace-Hankel integral transform for transient three-dimensional problems. These general solutions are then used to solve the boundary-value problems corresponding to internal time-harmonic and transient loads and displacement discontinuities in a transversely isotropic elastic half space. Analytical solutions for displacements and stresses corresponding to the above boundary-value problems are presented explicitly. It is noted that solutions corresponding to arbitrary loadings and displacement discontinuities can be derived through the application of superposition and standard analytical procedures to the fundamental solutions presented in this Chapter. Numerical quadrature schemes are used to obtain numerical solutions for displacements and stresses. The accuracy of the numerical schemes employed in this study is confirmed by comparison with existing solutions for isotropic materials. Selected numerical solutions for displacements and stresses corresponding to buried patch loads are presented to illustrate influence of material anisotropy. Numerical solutions for displacements and stresses show significant dependence on the degree of anisotropy of the materials in both time-harmonic and transient responses. It is found that in the case of dynamic Green's functions $\bar{G}_{zz}$, G^*_{zz} and $\bar{G}_{xx}$ the influence of the material anisotropy is mainly reflected by the values of $\bar{c}_{33}$ and $\bar{c}_{11}$, respectively. In addition, the availability of explicit analytical solutions for different transient source configurations (Sections 5.6 and 5.7) would enable a rigorous interpretation of the various characteristics of transient solutions and their relationship to the interpretation of geophysical observations. This lengthy and tedious exercise is not attempted here.

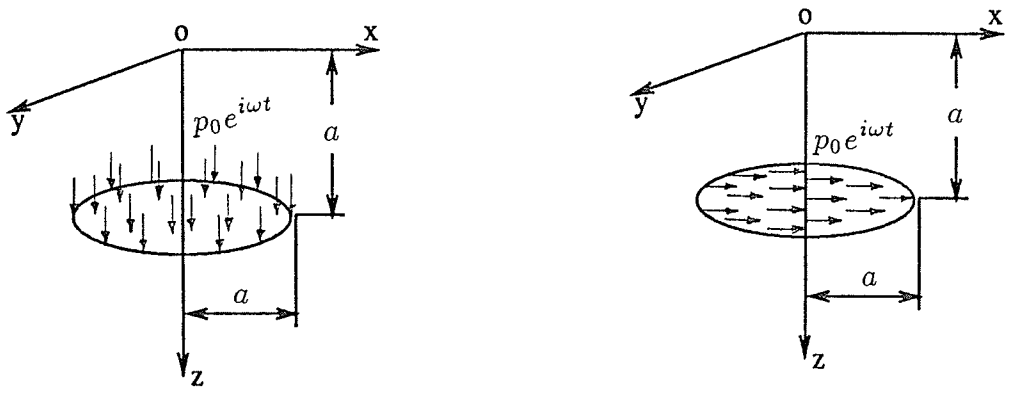

(a) Vertical patch load

(b) Horizontal patch load

Figure 5.1 Loading configurations considered in numerical study

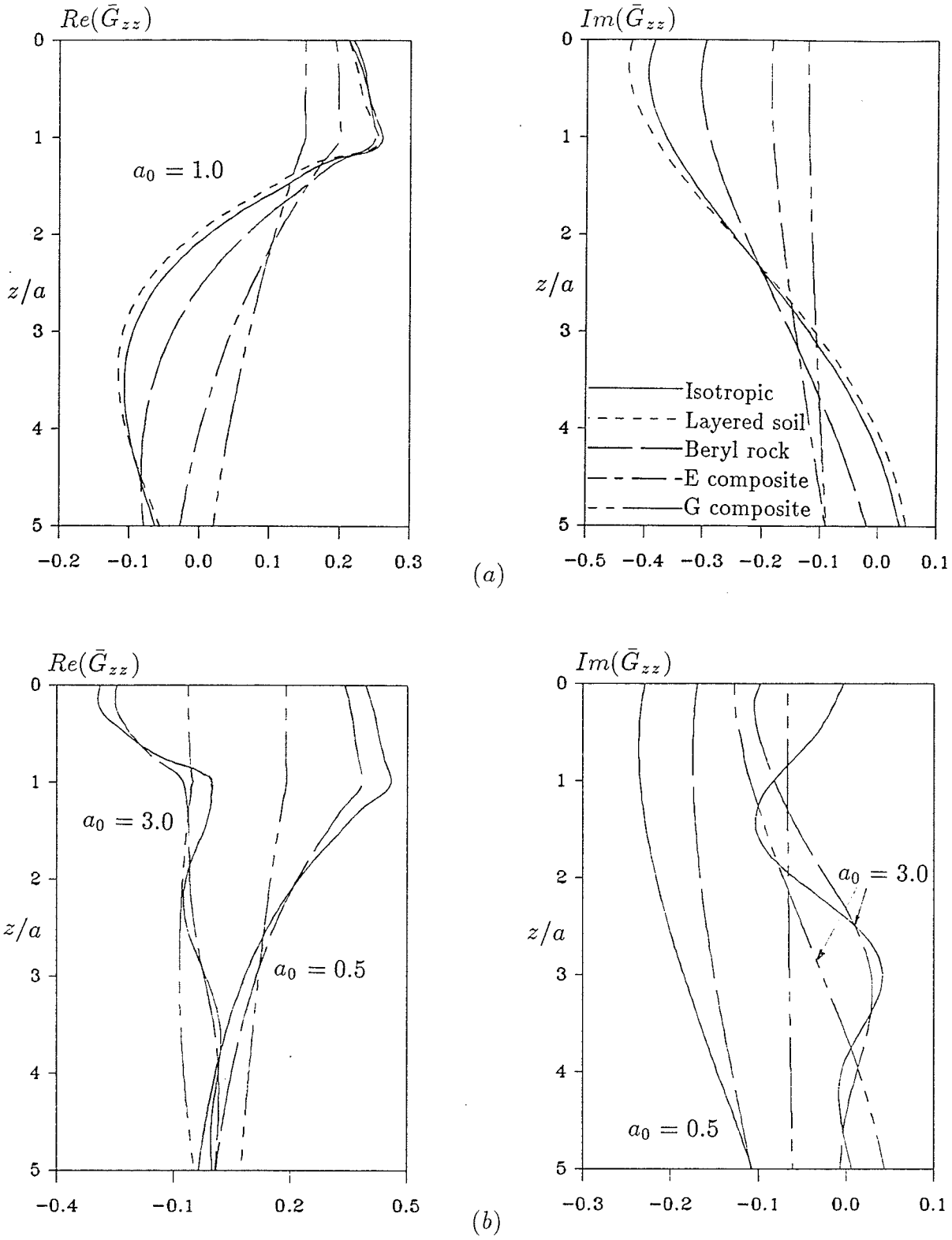

Figure 5.2 Normalised displacement Green's function $\bar{G}_{zz}$ along the z-axis for different materials and frequencies (loading case shown in Fig 5.1a)

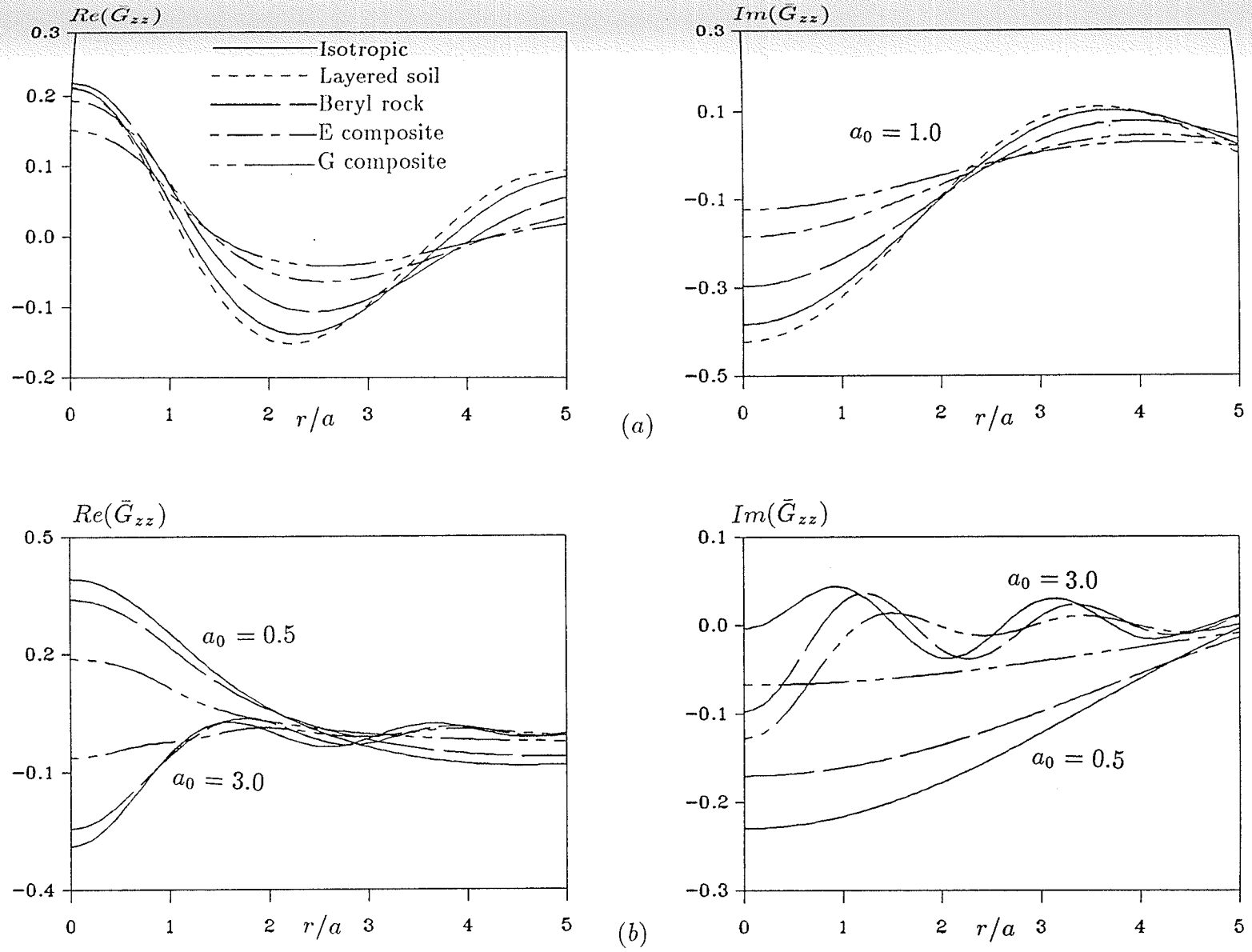

Figure 5.3 Normalised displacement Green's function $\bar{G}_{zz}$ along the free surface for different materials and frequencies (loading case shown in Fig 5.1*a*)

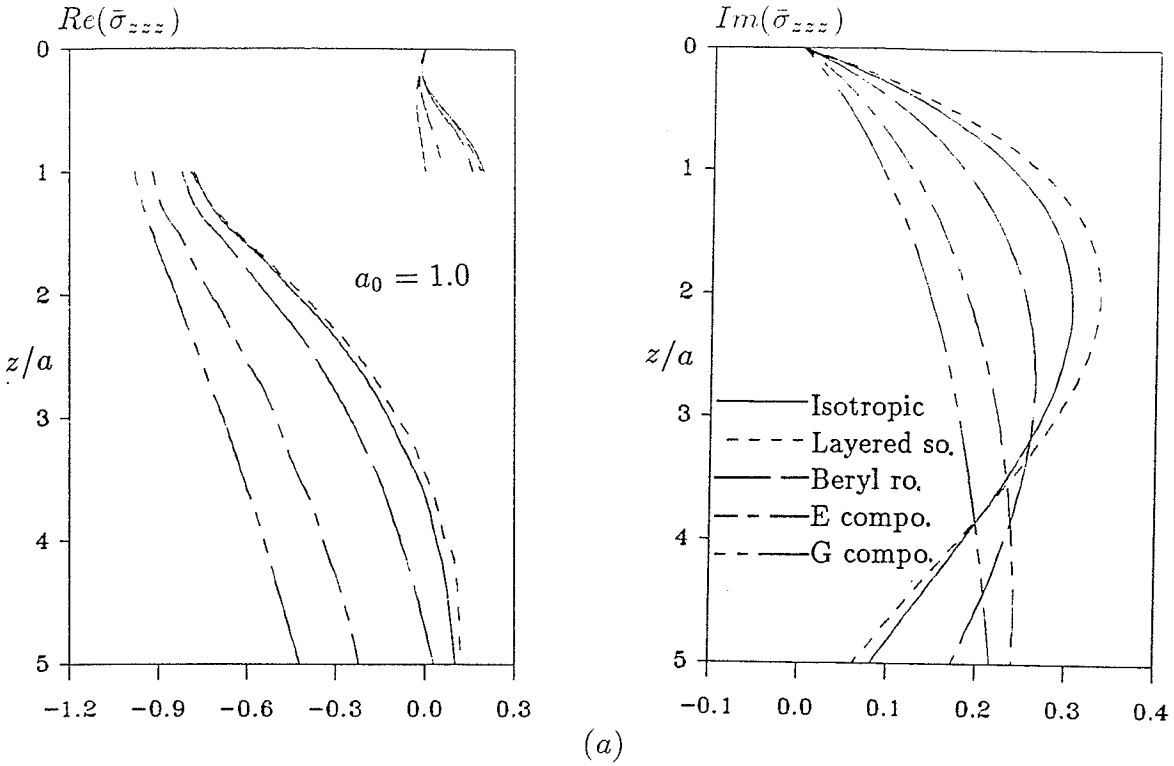

(a)

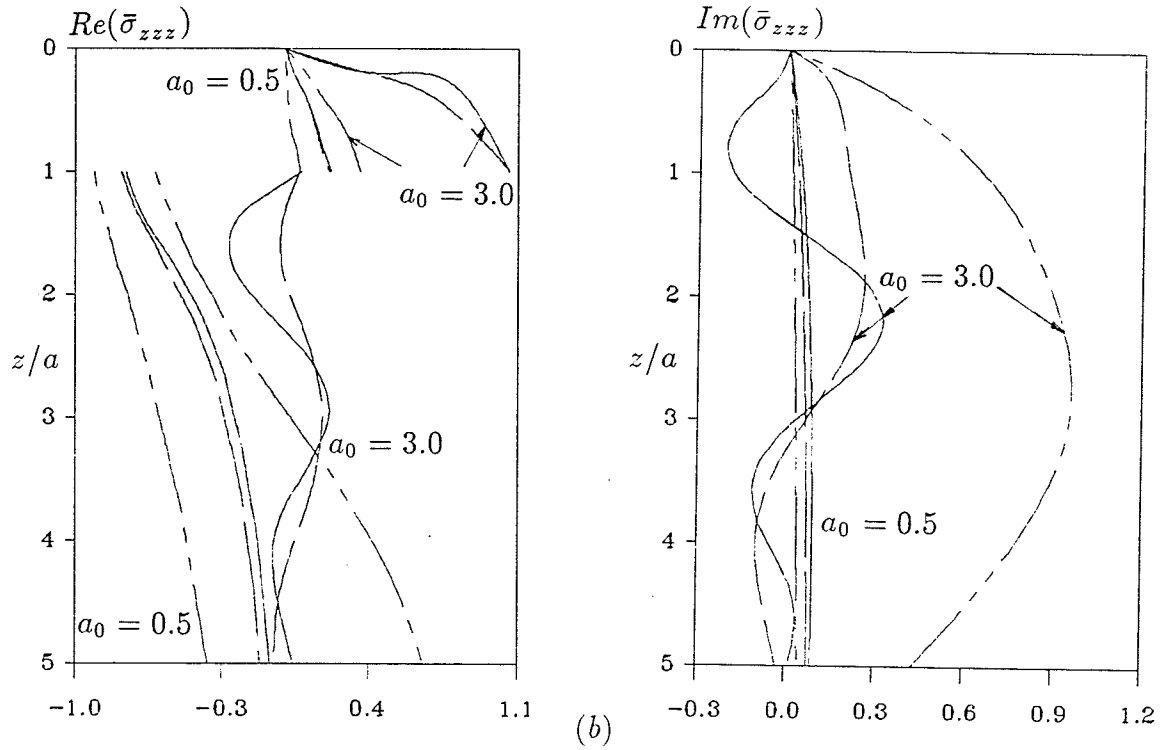

(b)

Figure 5.4 Normalised stress Green's function $\bar{\sigma}_{zzz}$ along the z-axis for different materials and frequencies (loading case shown in Fig 5.1a)

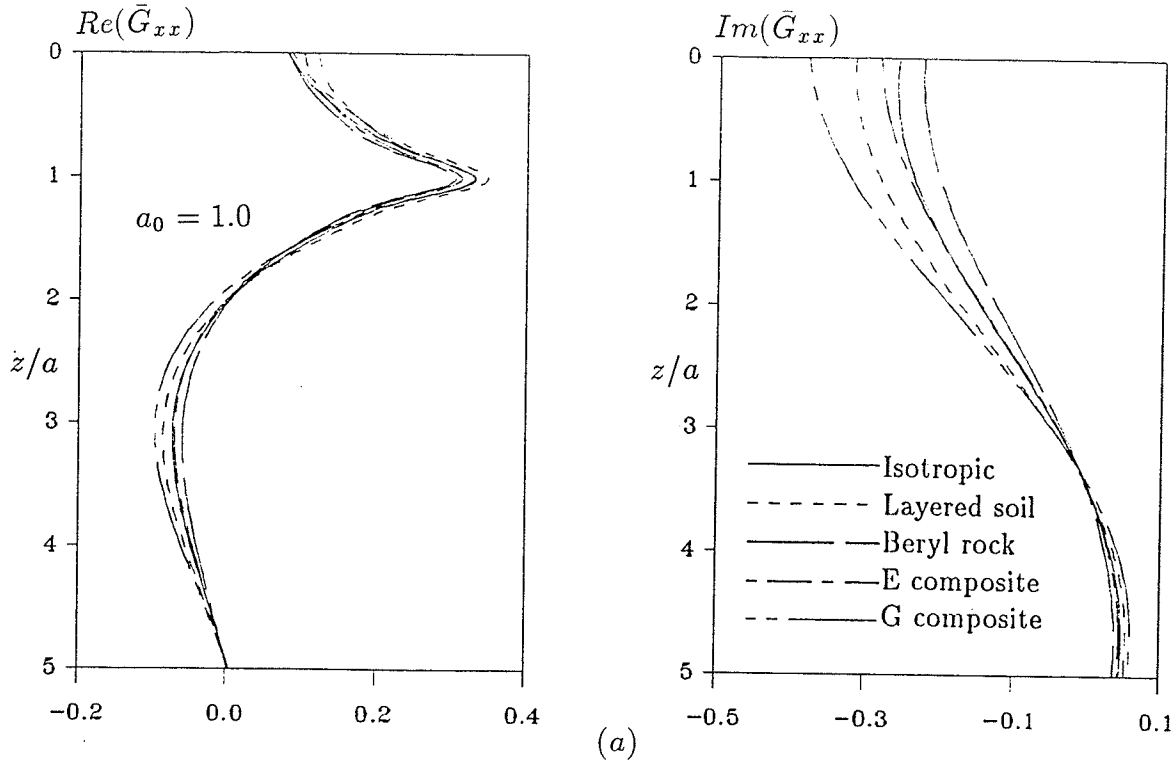

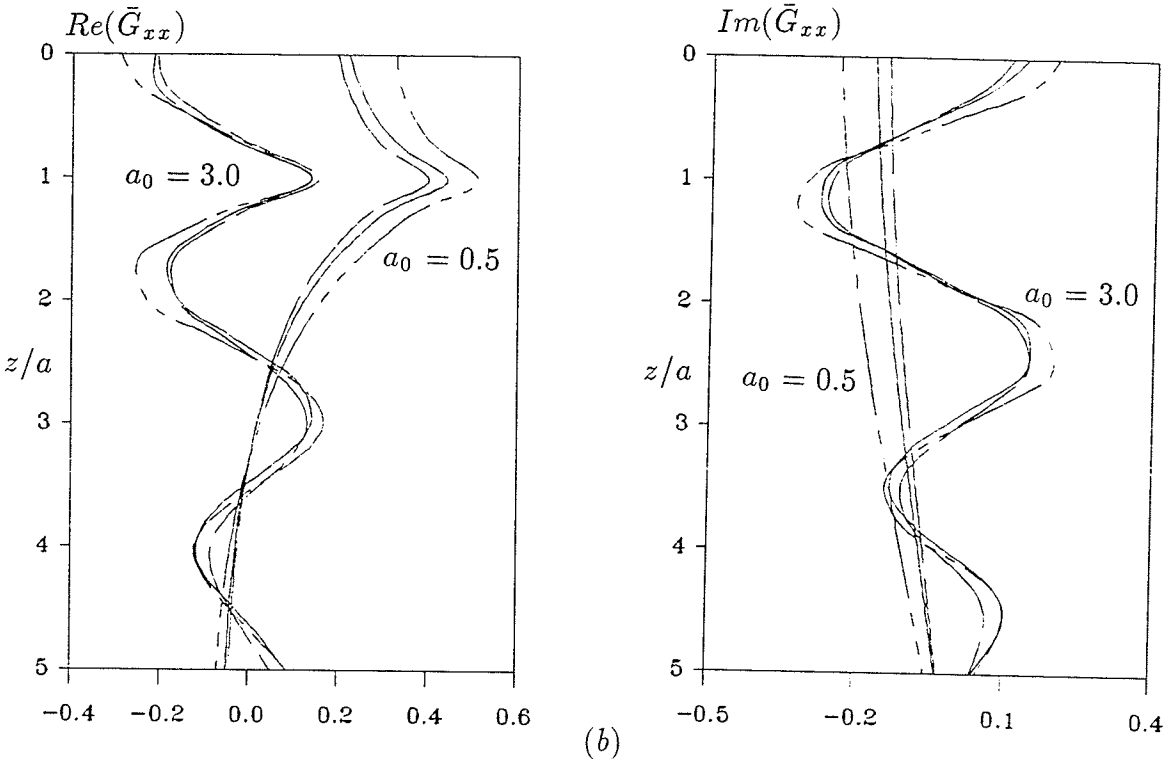

Figure 5.5 Normalised displacement Green's function $\bar{G}_{xx}$ along the z-axis for different materials and frequencies (loading case shown in Fig 5.1*b*)

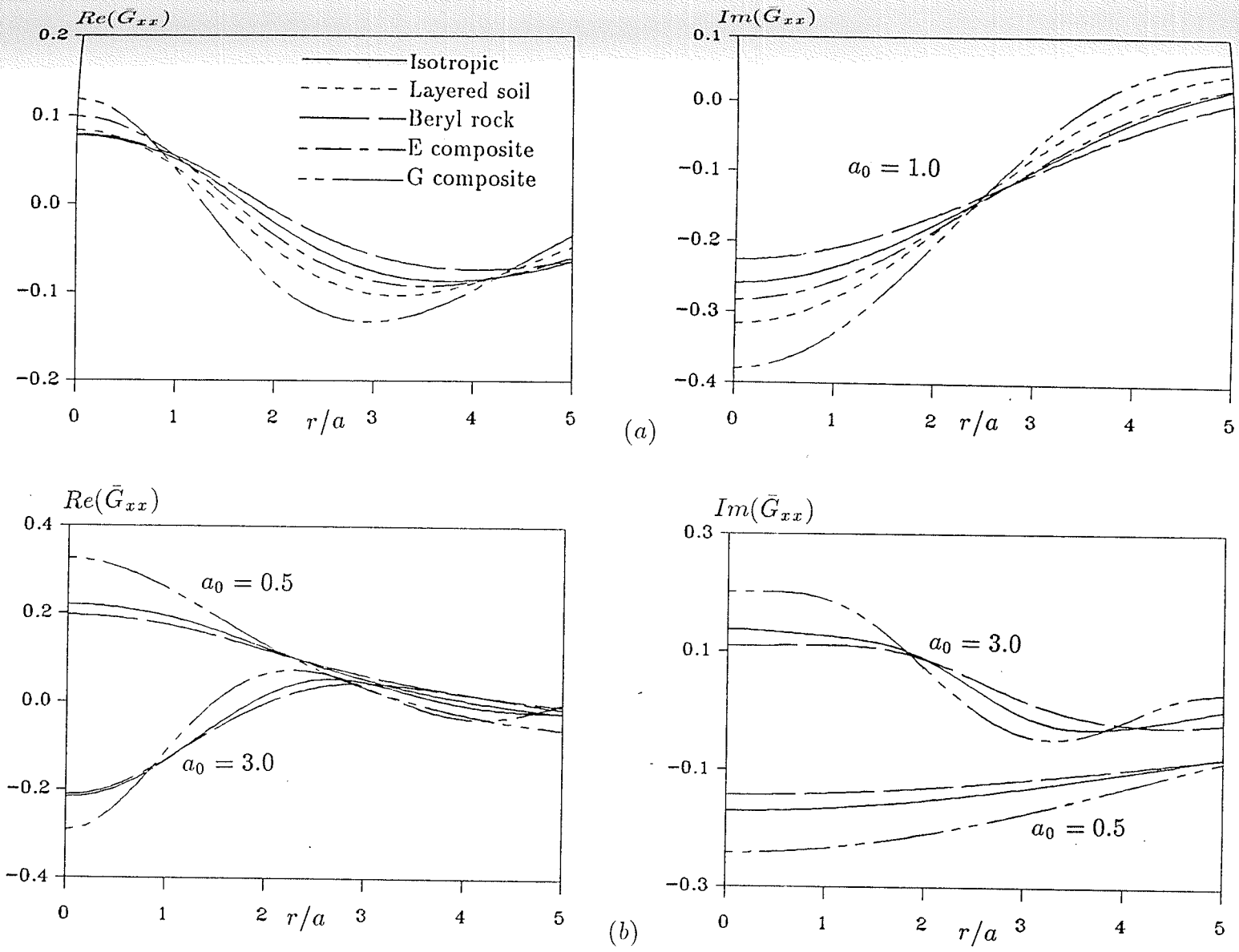

Figure 5.6 Normalised displacement Green's function $\bar{G}_{xx}$ along the free surface for different materials and frequencies (loading case shown in Fig 5.1*b*)

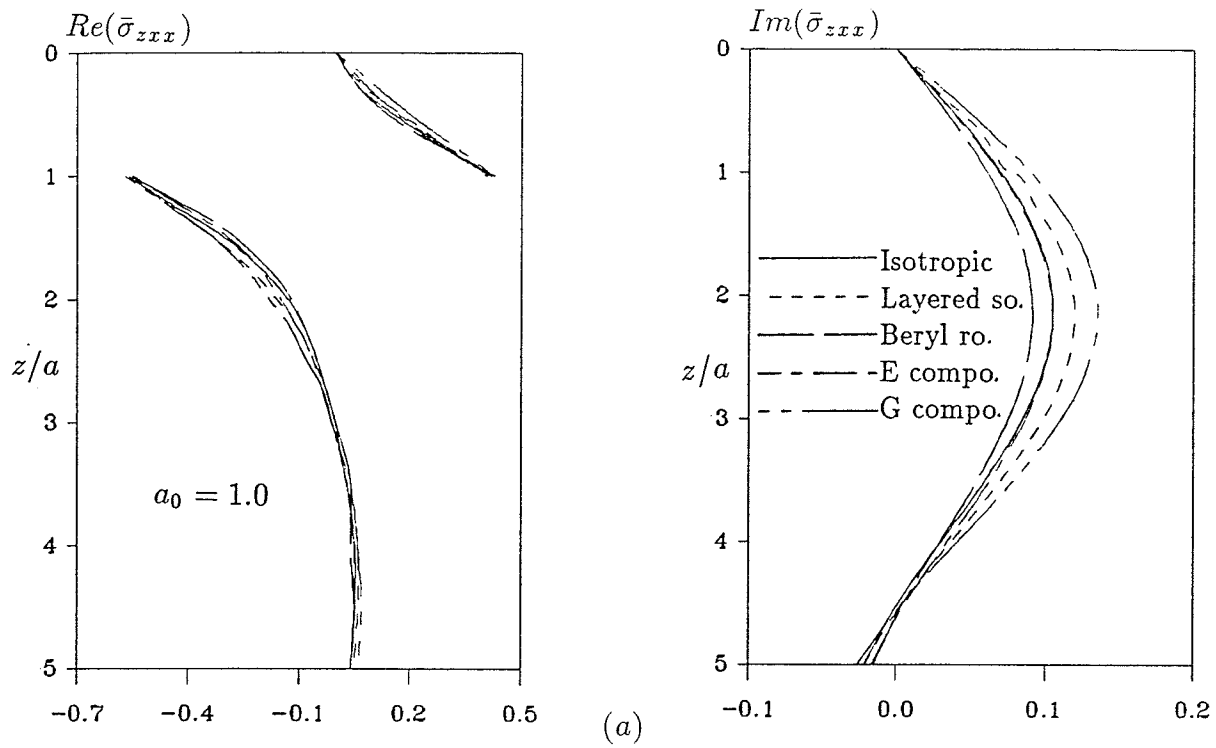

Figure 5.7 Normalised stress Green's function $\bar{\sigma}_{zxx}$ along the z-axis for different materials and frequencies (loading case shown in Fig 5.1*b*)

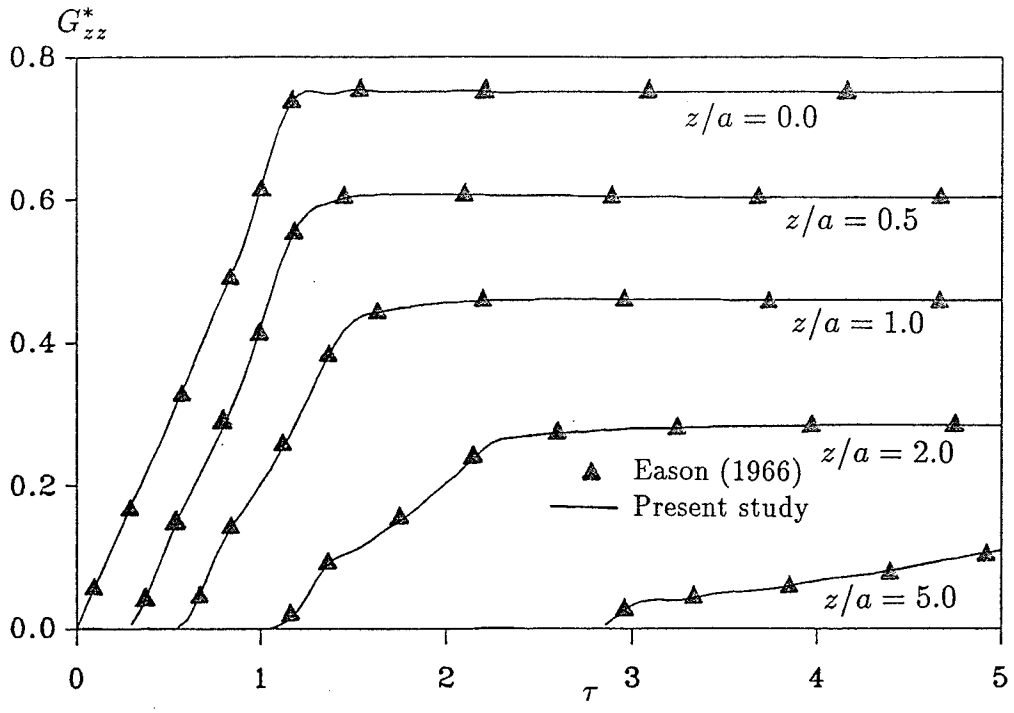

Figure 5.8 Vertical displacement on the z-axis due to uniform step load on the surface of an isotropic half space (Poisson's ratio=0.25)

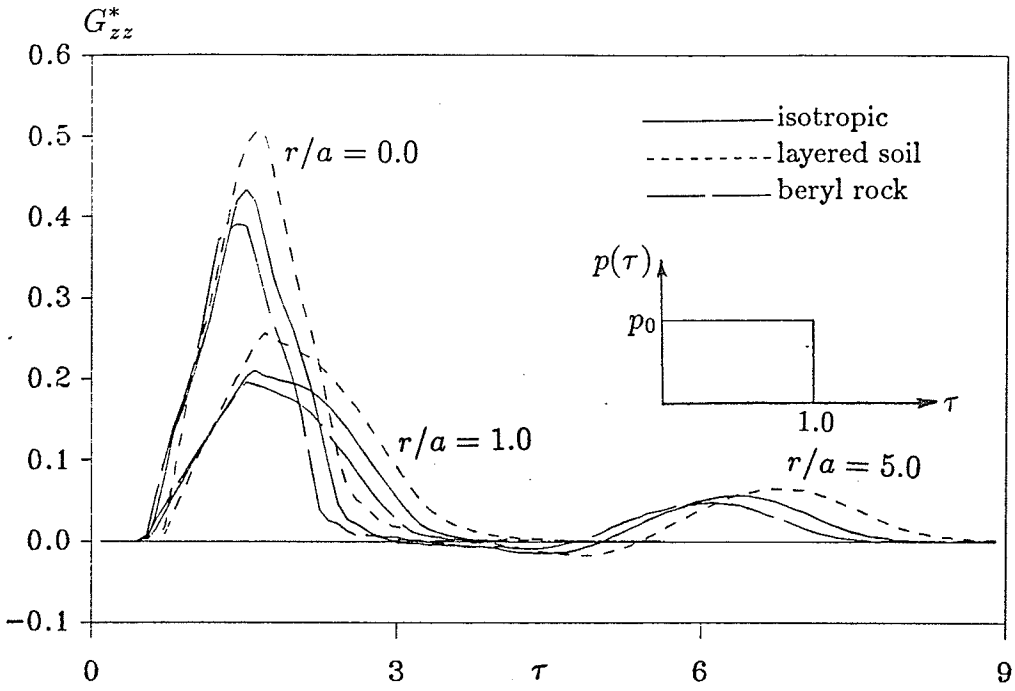

Figure 5.9 Vertical displacements at the surface due to an internal uniform disc pressure applied at $z'/a = 1.0$

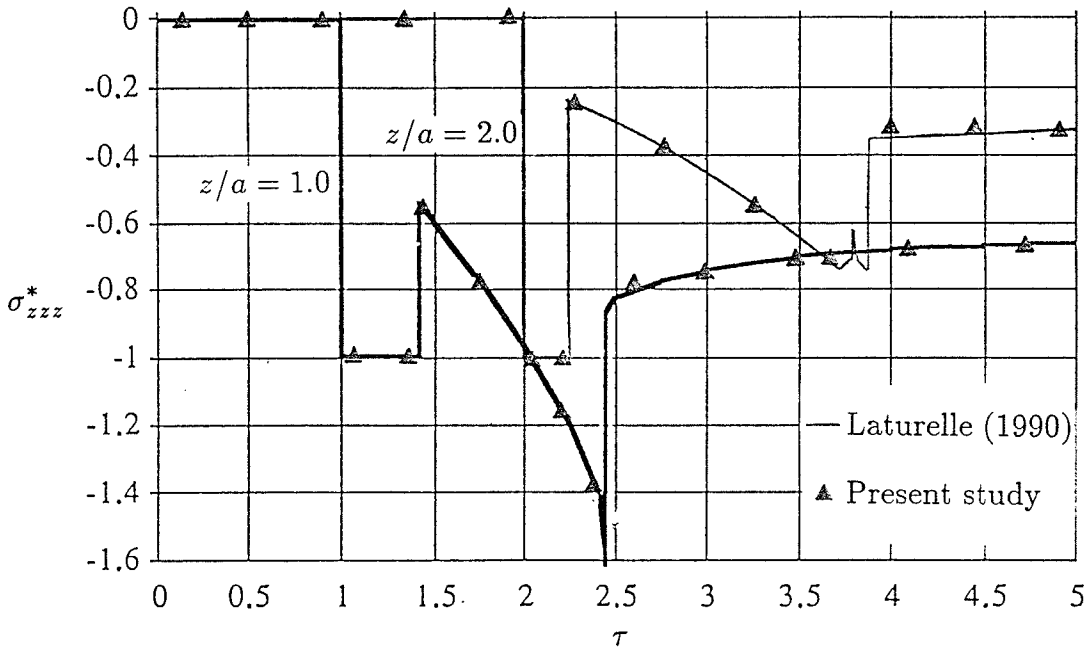

Figure 5.10 Stress σ_{zz} on the z-axis due to uniform step load (Poisson's ratio=0.25)

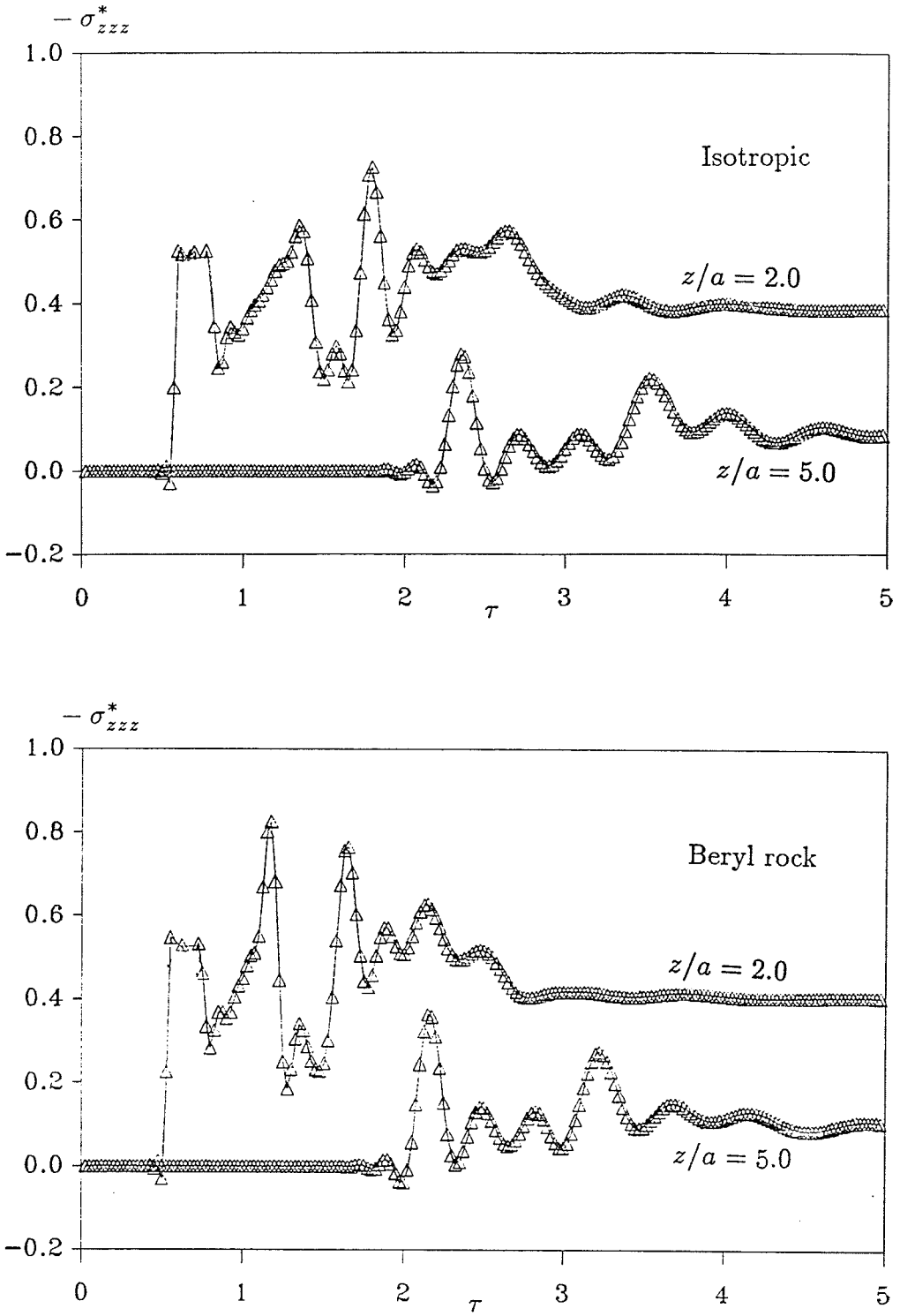

Figure 5.11 Stress $\bar{\sigma}_{zz}$ on the z-axis due to an internal uniform disc pressure applied at $z'/a = 1.0$

Chapter 6

ELASTODYNAMIC BOUNDARY-VALUE PROBLEMS

6.1 GENERAL

The primary objective of this Chapter is to demonstrate the application of elastodynamic Green's functions derived in Chapters 4 and 5 in the analysis of some useful dynamic boundary-value problems. Attention is particularly focused on elastodynamic boundary-value problems related to embedded rigid inclusions due to the relationship of these problems to the analysis of foundation structures in civil engineering projects. First, the dynamic response of rigid strip foundations embedded in orthotropic elastic materials is investigated. The indirect boundary integral equation method based on elastodynamic Green's functions presented in Chapter 4 is used for the analysis of this dynamic boundary-value problem. Numerical solutions for vertical, horizontal, rocking and coupled impedances of embedded strip foundations with rectangular and semi-circular cross-sections are presented. The versatility of the analysis is demonstrated by considering the through soil interaction between two foundations. The other problem considered in this Chapter corresponds to the three-dimensional dynamic response of a rigid cylindrical foundation embedded in a transversely isotropic soil half space. However, the direct boundary integral equation method is used to solve this boundary-value problem. The kernel functions of the boundary integral equations are the 3-D elastodynamic Green's functions derived in Chapter 5. Numerical convergence and accuracy of the solution scheme are investigated by considering rigid cylinders with different length/radius ratio embedded in an isotropic elastic half space. Numerical solutions are presented to portray the influence of material anisotropy, frequency of excitation and length/radius ratio on the vertical, horizontal, rocking and coupled impedances of rigid cylinders embedded in selected

transversely isotropic materials. Given the fact that almost every soil exhibits a certain degree of anisotropic behaviour the present solutions can be considered as a more realistic simulation of a fundamental soil-structure interaction problem. The concepts developed in this Chapter can be extended to study dynamics of single piles and pile groups, transient soil-structure interaction problems as well as problems involving layered media by using appropriate Green's functions.

6.2 DYNAMIC ANALYSIS OF EMBEDDED RIGID STRIP FOUNDATIONS

Fig 6.1 shows a massless rigid strip foundation, occupying a region V bounded by the surface S embedded in an orthotropic elastic medium. It is assumed that the rigid foundation is perfectly bonded to the surrounding material along the contact surface S. The foundation is subjected to time harmonic vertical, horizontal and moment loadings $F_z e^{i\omega t}, F_x e^{i\omega t}$ and $M_y e^{i\omega t}$, per unit length respectively. The displacements of the foundation, under the applied loadings, can be expressed in terms of vertical displacement $\triangle_V e^{i\omega t}$, horizontal displacement $\triangle_H e^{i\omega t}$ and rotation $\phi_y e^{i\omega t}$ about the y-axis of a point A with coordinate $(\bar{x}, \bar{z})$ as shown in Fig 6.1.

The displacement at a point (x, z) on the contact surface can be expressed in terms of $\triangle_V, \triangle_H$ and ϕ_y as

$$u_x(x,z) = \triangle_H + (\bar{z} - z)\phi_y \tag{6.1a}$$

$$u_z(x,z) = \triangle_V + (x - \bar{x})\phi_y \quad x, z \in S \tag{6.1b}$$

The resultant forces and moment acting on the massless foundation can be expressed in terms of traction components $T_i(x, z)$ as

$$F_z = \int_S T_z dS \tag{6.2}$$

$$F_x = \int_S T_x dS \tag{6.3}$$

$$M_y = \int_S T_z(x - \bar{x})dS + \int_S T_x(\bar{z} - z)dS \tag{6.4}$$

The indirect boundary integral equation approach used in chapter 3 to analyze the elastostatic boundary-value problems is extended here to analyse the dynamic response of the embedded rigid strip foundation. In the analysis, an undisturbed orthotropic elastic half plane V' with a surface $\bar{S}$ in it (which is identical to S) is considered. A set of forces with intensity $f_i(x,z)$ is applied on a surface S' interior to $\bar{S}$ such that the displacements on $\bar{S}$ are equal to that given by eqn (6.1) and the traction resultants on $\bar{S}$ satisfy eqns (6.2)-(6.4). The force intensities $f_i(x,z)$ are governed by the following Fredholm integral equations of the first kind.

$$\int_{S'} G_{ij}(x,z;x',z')f_j(x',z')dS' = \bar{u}_i(x,z) \qquad (x,z) \in \bar{S}, \quad (x',z') \in S' \qquad (6.5)$$

where indices $i,j = x,z$ and summation is implied on j; $G_{ij}(x,z;x',z')$ denotes the displacement Green's function defined by eqns (4.29), (4.30) and (4.32) for an orthotropic elastic half plane subjected to buried time-harmonic loadings. In addition, $\bar{u}_i(x,z)$ denotes the displacement component in the i direction ($i = x,z$) on the surface $\bar{S}$ as given by eqn (6.1).

The components of traction on $\bar{S}$, denoted by $T_i(x,z)$, can be expressed as

$$T_i(x,z) = \int_{S'} H_{ij}(x,z;x',z')f_j(x',z')dS' \qquad (x,z) \in \bar{S}, \quad (x',z') \in S' \qquad (6.6)$$

where

$$H_{ij}(x,z;x',z') = \sigma_{ilj}(x,z;x',z')n_l(x,z) \qquad (6.7)$$

and $\sigma_{ilj}(x,z;x',z')$ denotes the stress Green's function defined in eqns (4.29), (4.31) and (4.33). In addition, $n_l(l = x,z)$ denotes the components of the unit outward normal vector to the surface $\bar{S}$.

A discrete version of eqns (6.5) and (6.6) can be obtained by discretizing $\bar{S}$ and S' using M and M' nodal points, respectively as illustrated in Chapter 3. A solution for force intensities at nodal locations on S' can be obtained in terms

of $\triangle_V, \triangle_H$ and ϕ_y by a least square solution of eqn (6.5) as shown in eqn (3.8). Thereafter solutions for nodal tractions are expressed in terms of $\triangle_V, \triangle_H$ and ϕ_y from eqn (6.6). Substitution of the solutions for nodal tractions in a discrete version of eqns (6.2)-(6.4) written with respect to nodal points on S yields a relationship between applied forces and displacements $\triangle_V, \triangle_H$ and ϕ_y.

The response of an embedded rigid strip foundation is characterized by the following nondimensional impedance matrix

$$\begin{pmatrix} F_z \\ F_x \\ M_y \end{pmatrix} = \pi c_{44} \begin{pmatrix} K_V & 0 & 0 \\ 0 & K_H & K_{HM} \\ 0 & K_{MH} & K_M \end{pmatrix} \begin{pmatrix} \triangle_V \\ \triangle_H \\ b\phi_y \end{pmatrix} \tag{6.8}$$

where $K_V, K_H, K_{MH}(= K_{HM})$ and K_M are the vertical, horizontal, coupled and rocking impedances; and b is the half width of the strip foundation at the surface level.

In the case of a system of N foundations, the above procedure can be extended by considering several fictitious surfaces $\bar{S}_i, S_i'$ $(i = 1, ..., N)$ and applying forces on S_i' to satisfy appropriate rigid body deformations and equilibrium conditions of each foundation. In this study only two rigid strip foundations are investigated to show some factors of through soil interaction between a multi-strip foundation system. In this case owing to the symmetry of the foundations arrangement, a total of twelve components of impedances are necessary to define the complete dynamic response of the two foundation system. Impedance matrix corresponding to the present case can be defined as

$$\begin{pmatrix} F_z^1 \\ F_x^1 \\ M_y^1 \\ F_z^2 \\ F_x^2 \\ M_y^2 \end{pmatrix} = \pi c_{44} \begin{pmatrix} K_{11} & K_{12} & K_{13} & K_{14} & K_{15} & K_{16} \\ & K_{22} & K_{23} & -K_{15} & K_{25} & K_{26} \\ & & K_{33} & -K_{16} & K_{26} & K_{36} \\ & & & K_{11} & -K_{12} & -K_{13} \\ & & symm & & K_{22} & K_{23} \\ & & & & & K_{33} \end{pmatrix} \begin{pmatrix} \triangle_V^1 \\ \triangle_H^1 \\ b\phi_y^1 \\ \triangle_V^2 \\ \triangle_H^2 \\ b\phi_y^2 \end{pmatrix} \tag{6.9}$$

In eqn (6.9), superscripts '1' and '2' are used to denote the forces and rigid body displacements of the first and the second foundations, respectively. It is

important to note that each column of the impedance matrix defined by eqn (6.9) corresponds to forces acting on the foundations when the corresponding element of the degree of freedom vector in eqn (6.9) is equal to unity and the remaining five elements of the degree of freedom vector are set to zero.

6.3 IMPEDANCES OF EMBEDDED RIGID STRIP FOUNDATIONS

Table 6.1 presents a convergence study of numerical solutions for vertical, horizontal and rocking impedances of a strip foundation of rectangular cross-section (width $2b$ and depth h) embedded in an isotropic medium. The parameters tested for convergence in Table 6.1 are the impedances of the foundation with respect to the number of nodal points M and M' used to discretise surfaces $\bar{S}$ and S', respectively. Table 6.2 presents a convergence study of impedances with respect to the location of the source contour S' (*i.e.* distance c shown in Fig 3.2) for a foundation with $h/b = 1.0$ and $M = 32$ and $M' = 16$. Table 6.3 presents a comparison of impedances of a rigid strip foundation ($h/b = 0.5$) in the presence of another identical unloaded foundation with the results reported earlier by Rajapakse and Shah (1988). The impedances of the loaded foundation presented in Table 6.3 are obtained by a relation identical to eqn (6.8) and the unloaded foundation is not restrained. It is evident from numerical results presented in Tables 6.1-6.3 that the present solution scheme is stable and converges closely to numerical results for impedances reported elsewhere (Rajapakse and Shah 1988) by using a different solution scheme for strip foundations embedded in isotropic soils.

6.3.1 **Single Rigid Strip Foundation**

The range of the non-dimensional frequency $0.0 < a_0 \leq 2.0$ is considered in the numerical study since most forced vibrations of machine foundations are within this range (Gazetas 1983). An isotropic soil and three transversely isotropic

soils, namely, clay I, silty clay and a beryl rock are considered in the numerical study. The material constants for these soils are listed in Table 1.1.

Figures 6.2-6.4 show the impedances K_V, K_H, K_M and K_{HM} of a single rigid massless rectangular strip foundation of width $2b$ and height h. Solutions are presented for h/b=0.25, 0.5 and 1.0. It is observed that the real part of the vertical impedance shows minor dependence on the h/b ratio of a rectangular foundation. For all values of h/b considered in this study, the real part of K_V increases rapidly with frequency in the range $0 < a_0 < 0.6$ and thereafter decreases gradually with increasing a_0. This behaviour is observed for all types of soils. Comparison of $Re(K_V)$ for different types of soils indicates that the influence of degree of anisotropy of soil is significant. Within the frequency range $0 < a_0 < 1.8$, it is noted that the highest magnitude of $Re(K_V)$ corresponds to foundations embedded in beryl rock and followed in the order of magnitude by foundations embedded in clay I, isotropic soil and silty clay. Comparison of values of $\bar{c}_{ij}$ in Table 1.1 and the order of magnitudes of solutions for $Re(K_V)$ indicate that the influence of anisotropy is mainly governed by the value of $\bar{c}_{33}$. The influence of other $\bar{c}_{ij}$ is found to be negligible. Solutions in Figs 6.2-6.4 also show a tendency that for $a_0 > 1.8$ the value of $Re(K_V)$ of a foundation embedded in silty clay may be greater than that corresponding to an isotropic soil. This indicates that at high frequencies impedances may show a more complicated dependence on the degree of anisotropy. Comparison of solutions for imaginary part of K_V indicates that its dependence on a_0 is nearly linear for all h/b ratios and for different types soils. The magnitude of $Im(K_V)$ is found to increase gradually with increasing h/b ratios. The influence of soil anisotropy follows the same trend as in the case of $Re(K_V)$ and governed mainly by the value of $\bar{c}_{33}$. However, the influence of degree of anisotropy of embedding medium on $Im(K_V)$ is found to be significant only at higher frequencies ($a_0 > 1.0$).

Comparison of solution for the real part of horizontal impedance K_H in-

dicates that $Re(K_H)$ increases rapidly with a_0 in the range $0 < a_0 < 0.75$ and shows a tendency to gradually increase or decrease beyond $a_0 = 0.75$ depending on the type of soil and the h/b ratio. The magnitude of $Re(K_H)$ is found to be in the same range for all h/b ratios. The influence of the degree of anisotropy of the soil on $Re(K_H)$ is significant as in the case of $Re(K_V)$ except that the values corresponding to clay I is higher than those for beryl rock. Comparison of the order of magnitude of $Re(K_H)$ with the values of $\bar{c}_{ij}$ in Table 1.1 indicates that the influence of the degree of anisotropy of the surrounding medium is governed mainly by $\bar{c}_{11}$ in the case of $Re(K_H)$. It is noted that $Im(K_H)$ varies linearly with a_0 for all h/b ratios and soil types. This behaviour is similar to that observed previously for $Im(K_V)$. The magnitude of $Im(K_H)$ is also found to increase with h/b and the influence of degree of anisotropy of soil is more visible with increasing h/b ratio especially at high frequencies ($a_0 > 1.0$). The order of magnitude of $Im(K_H)$ for different soils is identical to that observed earlier for $Re(K_H)$.

The real part of rocking impedance K_M is found to decrease gradually with the frequency a_0. The magnitude of $Re(K_M)$ increases with increasing h/b ratios for all types of soils. The influence of soil anisotropy on $Re(K_M)$ is found to be similar to that observed earlier for $Re(K_V)$. The imaginary part of K_M varies linearly with a_0 except for $a_0 < 0.3$ and its magnitude increases with increasing h/b ratio. The influence of the degree of anisotropy of the soil on $Im(K_M)$ is found to be comparatively lesser when compared to the case of $Re(K_M)$ and similar to that observed earlier for $Im(K_V)$. The real part of coupled impedance K_{HM} is found to decrease with increasing h/b ratio. For lower ratios of h/b ($h/b < 0.5$), $Re(K_{HM})$ initially increases with a_0 for low frequencies and thereafter decreases gradually with increasing a_0. For h/b=1.0, $Re(K_{HM})$ shows more complicated variation with a_0. The influence of degree of anisotropy of soil on $Re(K_{HM})$ is also found to be rather complicated. For example in the case of a foundation with h/b=0.5, the $Re(K_{HM})$ for the isotropic soil is always greater than that

for clay I. However, for h/b=1.0, $Re(K_{HM})$ for clay I is higher than the values corresponding to the isotropic soil within the range $1.6 < a_0 < 2.0$. Therefore it is difficult to directly relate the influence of soil anisotropy on $Re(K_{HM})$ to any specific $\bar{c}_{ij}$ term. The variation of imaginary part of K_{HM} with frequency a_0 is found to be nearly linear for all h/b ratios and for the different types of soils. The values of $Im(K_{HM})$ decrease with increasing h/b ratios. In addition the solution for silty clay is always the largest and followed by the isotropic soil, beryl rock and clay I.

Figure 6.5 shows the impedances of a single rigid massless strip footing with a semi-circular cross section of radius b. It is noted that within the frequency range $0 < a_0 < 2.0$, both $Re(K_V)$ and $Re(K_H)$ increase with a_0. This behaviour is different to that observed earlier for a rectangular foundation with h/b=1.0. The values of $Re(K_V)$ and $Re(K_H)$ of a semi-circular foundation at low frequencies ($a_0 < 0.25$) are lower than the corresponding solutions for a rectangular foundation with $h/b = 1.0$. The solution for $Re(K_M)$ of a semi-circular foundation decreases with a_0 showing a behaviour similar to that observed earlier for rectangular foundations. The imaginary parts of K_V, K_H and K_M of a semi-circular foundation show a linear variation with a_0 and the values are always less than the corresponding values for a rectangular foundation with h/b=1.0. The influence of the degree of anisotropy of soil on impedances K_V, K_H and K_M is similar to that observed earlier for rectangular foundations. The solutions for $Re(K_{HM})$ show a decrease in value with increasing a_0 and this is contrast to the behaviour observed earlier for a rectangular foundation with $h/b = 1.0$. The magnitude for $Re(K_{HM})$ is also found to be lower than the corresponding solution for a rectangular foundation with $h/b = 1.0$. The solutions for $Im(K_{HM})$ show a linear variation with a_0 and the values are quite close to the corresponding solutions for a rectangular foundation with $h/b = 1.0$. The appreciable differences noted in the solutions for a rectangular foundation with $h/b = 1.0$ and a semi-circular foundation indicate

that eventhough the depth of embedment is same in both cases the solution for impedances are quite different indicating that the exact geometry of the footing also has a significant influence on the response.

6.3.2 Two Semi-circular Rigid Strip Foundations

The dynamic interaction between two embedded rigid massless strip foundations with identical semi-circular cross-sections (radius=b) is considered in this section. The distance between the centres of the foundations is denoted by d ($\bar{d} = d/b$). In the present study, only the diagonal impedances K_{11}, K_{22} and K_{33} and the coupling impedances K_{14}, K_{25} and K_{36} defined in eqn (6.9) are presented for brevity. These components could demonstrate some features of the dynamic interaction between foundations embedded in anisotropic soils.

Figure 6.6 presents the solutions for diagonal impedances K_{11}, K_{22} and K_{33} of the two foundations system for $\bar{d}$=3.0. It is noted that at small frequencies ($a_0 < 0.2$) and $\bar{d}$=3.0, the real parts of K_{11} and K_{22} are much larger (nearly twice) than the corresponding values for a single foundation. However as a_0 increases both $Re(K_{11})$ and $Re(K_{22})$ decrease, showing a behaviour which is in contrast to the behaviour observed earlier for a single footing. The values of $Re(K_{33})$ are somewhat closer to the solutions corresponding to a single footing. The solution for imaginary parts of K_{11}, K_{22} and K_{33} are relatively closer both in shape and magnitude to the corresponding diagonal impedances of a single foundation. It is also noted that the influence of anisotropy of soil on the response of the active foundation follows a trend similar to that of a single foundation. The distance $\bar{d}$ has a very significant influence on the response and the dependence of impedances on $\bar{d}$ is quite complicated as in the case of rectangular three-dimensional foundations (Apsel and Luco 1987).

Figure 6.7 shows the coupling impedances K_{14}, K_{25} and K_{36}. It is noted that these impedances depend significantly on the frequency. At low frequencies

($a_0 < 1.0$) the influence of anisotropy of soil on coupling impedances are found to be negligible except for real parts of K_{24} and K_{36}. However as a_0 increases ($a_0 > 1.0$) the influence of soil anisotropy becomes more significant but the order of the influence of the degree of anisotropy of soil on these coupling impedances is found to be in contrast to that observed earlier for the diagonal impedances and also for impedances of a single foundation. Both the real and imaginary parts of the coupling impedances show notable differences in magnitude and shape to that observed earlier for the diagonal impedances. The solutions for coupling impedances are generally smaller than the diagonal impedances or impedances of a single foundation and show changes in sign within the frequency range under consideration. Given the fact that in most practical situations, the study of dynamic response of structures involves more than a single foundation the above results confirm the complex nature of the through soil interaction between foundations reported earlier (Warburton *et al* 1971, Wong and Luco 1986, Rajapakse and Shah 1988, Wang *et al* 1991). In addition, these results also highlight the importance of soil anisotropy in the analysis of dynamic response of foundations.

6.4 DYNAMIC ANALYSIS OF EMBEDDED RIGID CYLINDRICAL FOUNDATIONS

This Section is concerned with the dynamic response of a massless rigid cylindrical foundation embedded in a transversely isotropic elastic half space as shown in Fig 6.8. The foundation is subjected to time-harmonic vertical, horizontal and moment loadings $F_z e^{i\omega t}, F_x e^{i\omega t}$ and $M_y e^{i\omega t}$, at the point O as shown in Fig 6.8. With the assumption that the rigid foundation is perfectly bonded to the surrounding material along the contact surface S the problem under consideration can be described as a displacement boundary-value problem. Therefore the displacement at the contact surface S can be expressed in terms of the displacements at the point O. For example in the case of a transversely loaded rigid cylinder, the

displacements at an arbitrary point on the generating curve of S can be expressed as

$$\begin{aligned} u_r(r,z) &= \Delta_H - z\phi_y \\ u_\theta(r,z) &= -\Delta_H + z\phi_y; \qquad r,z \in S \\ u_z(r,z) &= r\phi_y \end{aligned} \tag{6.10}$$

where Δ_H and ϕ_y are the horizontal (x-direction) displacement and rotation about the y-axis of the point O respectively.

The dynamic response of a rigid cylindrical foundation embedded in a transversely isotropic elastic half space can be expressed by the nondimensional impedance matrix defined below.

$$\begin{pmatrix} F_z \\ F_x \\ M_y \end{pmatrix} = ac_{44} \begin{pmatrix} K_V & 0 & 0 \\ 0 & K_H & K_{HM} \\ 0 & K_{MH} & K_M \end{pmatrix} \begin{pmatrix} \triangle_V \\ \triangle_H \\ a\phi_y \end{pmatrix} \tag{6.11}$$

where $K_V, K_H, K_{MH}(= K_{HM})$ and K_M are the vertical, horizontal, coupled and rocking impedances respectively. This displacement boundary-value problem can be readily solved by using the indirect boundary integral equation method presented in Section 3.3. The kernel corresponding to the present problem are the 3-D dynamic Green's functions presented in Section 5.5. However, in this Section the application of direct boundary integral equation method is illustrated as an alternative to the indirect method to compute the impedances of rigid cylindrical inclusions.

In the direct boundary integral equation approach, an elastic half space with a cavity which is identical to the embedded inclusion is considered as shown in Fig 6.8. A displacement field with components $u_i(r,z)$ as given by eqn (6.10) is imposed on the generating curve of S. The direct boundary (integral representation theorem) of domain V can be expressed as (Eringen and Suhubi 1975)

$$c_{ij}(\mathbf{x})u_j(\mathbf{x}) + \int_S H_{ij}(\mathbf{x},\bar{\mathbf{x}})u_j(\bar{\mathbf{x}})dS = \int_S G_{ij}(\mathbf{x},\bar{\mathbf{x}})t_j(\mathbf{u})dS \quad (i,j,=r,\theta,z) \tag{6.12}$$

where $\mathbf{x}$ and $\bar{\mathbf{x}}$ denote position vectors and $\bar{\mathbf{x}} \in S$. In addition S denotes the generating curve of the contact surface S. The coefficients $c_{ij}(\mathbf{x})$ can be given as

$$c_{ij}(\mathbf{x}) = \begin{cases} 1, & \mathbf{x} \text{ inside } V \\ 1/2, & \mathbf{x} \text{ on } S \\ 0 & \mathbf{x} \text{ outside } V \end{cases} \tag{6.13}$$

In the present problem we select $\mathbf{x}$ such that $\mathbf{x} \in S$, *ie.*, $\mathbf{x}$ is located on the generating curve S, and c_{ij} is equal to $1/2$. Note that G_{ij} and H_{ij} in eqn (6.12) are the Fourier harmonic of the displacement and traction Green's functions of an undisturbed transversely isotropic elastic half space as expressed by eqns (5.25)-(5.31) when $m = 1$; u_i is the specified Fourier harmonic of displacements on the curve S as given by eqn (6.10) and t_i denotes the Fourier harmonic of the corresponding tractions.

To compute t_i corresponding to displacements u_i from the boundary integral equation (6.12), the curve S is discretized into M equal intervals. It is assumed that the displacements and tractions are constant within a discretized segment. In view of the above assumption, the integrals involving the Green's functions in eqn (6.12) can be integrated analytically with respect to $\mathbf{x}$ over a discretized interval of S. Then, the equaion (6.12) can be expressed in the following matrix form

$$\frac{1}{2}\mathbf{Iu} + \mathbf{Hu} = \mathbf{GT} \tag{6.14}$$

where $\mathbf{I}$ is a unit matrix; $\mathbf{u}$ denotes the displacement vector with its elements being the displacements at M node points on S as specified in eqn (6.10). In addition, $\mathbf{T}$ denotes the nodal traction vector corresponding to the specified nodal displacement vector. The elements of the matrix $\mathbf{H}$ and $\mathbf{G}$ are obtained by integrating the traction and displacement Green's functions over discretized intervals of S. The size of $\mathbf{H}$ and $\mathbf{G}$ matrices is $3M \times 3M$ for the transverse problem. A solution for $\mathbf{T}$ can be obtained from eqn (6.14) as

$$\mathbf{T} = \mathbf{G}^{-1}(\frac{1}{2}\mathbf{I} + \mathbf{H})\mathbf{u} \tag{6.15}$$

It is noted that the displacement vector $\mathbf{u}$ in above equation can be easily expressed in terms of the displacement $\triangle_H$ and rotation ϕ_y of the point O. Once the traction vector $\mathbf{T}$ is obtained from eqn (6.15) in terms of $\triangle_H$ and ϕ_y, the impedances of a rigid cylindrical inclusion can be calculated by using appropriate equilibrium equations similar to those given by eqns (6.2)-(6.4) for the 2-D problems.

6.5 IMPEDANCES OF RIGID CYLINDRICAL FOUNDATIONS

First, the numerical stability and accuracy of the direct boundary integral equation method are studied by varing the number of nodal points M on the generating surface S. The evaluation of elements of Green's function matrices $\mathbf{H}$ and $\mathbf{G}$ appearing in the eqn (6.15) follows procedures identical to that presented in Section 5.8. Table 6.4 presents a convergence study of numerical solutions for impedances K_V, K_H and K_M of a rigid cylindrical foundation with respect to the number of node points M. A cylindrical foundation with a length-radius ratio $h/a = 1.0$ embedded in an isotropic half space is considered. The convergence test is conducted at normalised frequency a_0=1.0. Table 6.4 also presents the solutions of impedances reported previously by Apsel and Luco (1987) by solving eqn (6.12) with $\bar{\mathbf{x}}$ selected on a contour S' which is outside V (Fig 6.8). It is evident that the results obtained by the present solution scheme are numerically very stable and are in close agreement with those reported by Apsel and Luco (1987). Next, the accuracy of the present numerical solutions for impedances K_V, K_H and K_M is investigated by considering different h/a ratios and a_0 values. For example, Table 6.5 presents numerical solutions for impedances of a cylinder with h/a =1.0 at frequency a_0=0.25,0.75,1.5,2.0 and corresponding solutions given by Apsel and Luco (1987). Table 6.6 presents the impedances of rigid cylinders with h/a=0.25,0.5 and 2.0 at frequency a_0=1.0 and corresponding solutions given by Apsel and Luco (1987). Comparison of the numerical results presented in Tables

6.5 and 6.6 further confirms the numerical accuracy, stability and reliability of the present boundary element scheme in the analysis of soil-structure interaction problems.

Numerical solutions for impedances of rigid cylindrical foundations embedded in selected anisotropic elastic soils are presented in Figs 6.9-6.12. The materials considered in this study are silty clay, beryl rock, clay I and an isotropy. The relevant material constants are given in Table 1.1.

It is noted that the real part of vertical impedance, *ie.* $Re(K_V)$, decreases smoothly as the frequency a_0 increases ($0 < a_0 < 2.0$) for rigid cylinders with h/a=0.25, 0.5 and 1.0. However, for the cylinder with h/a=2.0, $Re(K_V)$ decreases in the range $0 \leq a_0 \leq 0.8$ and thereafter increases with increasing frequency. The general trend of variation of $Re(K_V)$ with a_0 is found to be similar for all four materials although the actual magnitudes of $Re(K_V)$ are considerably different for different types of soils. The influence of the degree of material anisotropy is also clearly evident on the profiles of $Re(K_V)$. The largest $Re(K_V)$ is found for a cylinder embedded in beryl rock followed by cylinders embedded in clay, isotropic material and silty clay. The profiles of imaginary part of K_V show a linear variation with a_0 within the range $0.0 \leq a_0 \leq 2.0$. The influence of the material anisotropy on $Im(K_V)$ is found to be relatively smaller but has the same order as $Re(K_V)$. In fact the influence of material anisotropy on $Im(K_V)$ can be ignored if $h/a \geq 1.0$. A comparison of the order of magnitudes of K_V with the values of material constants given in Table 1.1 indicates that the influence of material anisotropy is mainly reflected by the value of the normalised material constant $\bar{c}_{33}$.

The real part of horizontal impedance K_H is found to be almost independent of a_0 in the case of rigid cylinders with $h/a \leq 0.5$ embedded in the four types of materials. However in the case of rigid cylinders with $h/a \geq 1.0$, $Re(K_H)$ gradually decreases with a_0 in the range $0.0 \leq a_0 \leq 2.0$. The imaginary part

of K_H shows a near linear variation with a_0 within the frequency range under consideration. This behaviour is similar to that observed earlier for $Im(K_V)$. The influence of material anisotropy is clearly noted in both real and imaginary parts of K_H. The largest influence of anisotropy is found on $Re(K_H)$ of a cylinder embedded in silty clay followed by $Re(K_H)$ corresponding to cylinders embedded in clay, isotropic material and beryl rock. However, $Im(K_H)$ shows lesser dependence on the degree of material anisotropy than $Re(K_H)$ eventhough the influence of material anisotropy on $Im(K_H)$ follows the same order as that for $Re(K_H)$. It is found from a comparison of the order of the profiles of K_H and the values of normalised material constants in Table 1.1 that the nondimensional material constants $\bar{c}_{11}$ controls the influence of material anisotropy on K_H.

It is noted from Figs 6.9-6.12 that the $Re(K_M)$ decreases gradually with a_0 within the range $0.0 \leq a_0 \leq 2.0$ for rigid cylinders with $h/a \leq 2.0$. The shape of the profiles of $Re(K_M)$ are almost identical for the four materials. The influence of material anisotropy is clearly noted on the profiles of $Re(K_M)$ and shows a behaviour similar to that of $Re(K_V)$ for shorter cylinders ($h/a \leq 0.5$). For $h/a \geq 1.0$, the $Re(K_M)$ of a cylinder embedded in silty clay shows a trend which would result in a value larger than the corresponding value for a cylinder embedded in beryl rock. Therefore it is noted that for $h/a > 1.0$, the influence of material anisotropy on $Re(K_M)$ cannot be related to a particular value of $\bar{c}_{ij}$. A linear variation with the frequency is observed for the profiles of $Im(K_M)$ for $a_0 > 0.6$. $Im(K_M)$ shows a non-linear variation with a_0 if $a_0 < 0.6$. It is also observed that $Im(K_M)$ of short cylinders ($h/a \leq 1.0$) shows lesser dependence on the degree of material anisotropy. Generally the order of magnitudes of $Im(K_M)$ profiles is found to be similar to that for $Re(K_M)$.

It is noted that in the case of shorter cylinders ($h/a \leq 0.5$), $Re(K_{HM})$ initially increase with a_0 in the range of $0 \leq a_0 \leq 1.0$ and then decreases with increasing a_0. However for $h/a \geq 1.0$, $Re(K_{HM})$ is found to gradually increase

with a_0 within the frequency range under consideration. $Re(K_{HM})$ also shows a strong dependence on the degree of material anisotropy. The highest influence of material anisotropy on $Re(K_{HM})$ is noted for a cylinder embedded in silty clay and followed by cylinders embedded in an isotropic material, beryl rock and clay. The same order of influence of the material anisotropy is also observed on the profiles of $Im(K_{HM})$ eventhough the influence is much less visible in this case. In addition $Im(K_{HM})$ decreases linearly with a_0 in frequency range under consideration. Comparison of the order of magnitude of the profiles of K_{HM} and the normalised material values in Table 1.1 indicates that the influence of material anisotropy on K_{HM} is governed by the ratio $1/(\bar{c}_{11} - \bar{c}_{12})$.

6.6 CONCLUSIONS

A solution scheme is presented for the analysis of dynamic response of rigid strip foundations and rigid cylindrical foundations embedded in anisotropic elastic soils. The indirect boundary integral equation method based on exact elastodynamic Green's functions of an undisturbed orthotropic soil is used in the analysis of rigid strip foundations. However, the direct boundary integral equation method is used in the case of rigid cylindrical foundations to demonstrate the applicability of the direct method. Numerical solutions for vertical, horizontal, rocking and coupled impedances of embedded strip foundations with rectangular and semi-circular cross-sections and rigid cylindrical foundations are presented. These solutions indicate that the impedances significantly depend on the frequency of excitation, degree of anisotropy of soil and the geometry of the foundation. The variation of real part of impedance with the frequency is gradual and non-oscillatory whereas the imaginary part shows near linear variation with the frequency for all types of soils. Naturally the magnitudes of real and imaginary parts of impedances of the foundations are found to increase with increasing depth of embedment. Within the frequency range $0.0 < a_0 < 2.0$, the influence of

degree of anisotropy of soil on the vertical and rocking impedances is found to be controlled mainly by the normalised elastic modulus $\bar{c}_{33}$. In the case of horizontal impedance the influence of soil anisotropy is governed mainly by $\bar{c}_{11}$. It can be also concluded that the degree of material anisotropy has lesser influence on the imaginary parts of impedances when compared to the real parts. Solutions for impedances also indicate that at high frequencies the influence of anisotrpy on impedances could not be related to a single elastic modulus. Impedances of the active foundation of two semi-circular strip foundation system show that the presence of an adjacent foundation significantly changes the response. These solutions indicate significant differences in magnitude and shape of impedance profiles when compared to single foundation solutions. It is also noted that the influence of soil anisotropy on impedances is very complicated in this case and cannot be related to a single elastic modulus.

The solutions presented in this study clearly indicate the importance of the consideration of soil anisotropy in the analysis of dynamic response of foundations. The methodologies used in this study can be extended to study the dynamic response of rigid foundations embedded in layered anisotropic media without any fundamental difficulty.

Table 6.1 Convergence of impedance of a rigid strip with number of node points ($h/b = 1.0, c/b = 0.1, a_0 = 1.5, \nu = 0.3$)

(M', M)	K_V	K_H	K_M
(16, 24)	(0.45, 2.59)	(0.64, 2.54)	(1.49, 1.58)
(16, 32)	(0.45, 2.59)	(0.64, 2.53)	(1.48, 1.58)
(20, 40)	(0.46, 2.60)	(0.63, 2.52)	(1.47, 1.58)
case *I*	(0.47, 2.60)	(0.66, 2.41)	(1.44, 1.51)

case *I*: Apsel and Luco (1987)

Table 6.2 Convergence of impedance of a rigid strip foundation with the location of source contour S' ($h/b = 1.0, a_0 = 1.5, \nu = 0.3, M' = 16, M = 32$)

$(\bar{c} = c/b)$	K_V	K_H	K_M
0.075	(0.42, 2.52)	(0.59, 2.43)	(1.37, 1.51)
0.10	(0.45, 2.59)	(0.64, 2.53)	(1.48, 1.58)
0.125	(0.45, 2.62)	(0.62, 2.54)	(1.45, 1.59)
0.150	(0.45, 2.62)	(0.62, 2.55)	(1.45, 1.57)

Table 6.3 Comparison of impedance of a rigid strip foundation in the presence of another identical unloaded foundation ($h/b = 0.5, \bar{d} = 6.0, c/b = 0.1$, $\nu = 0.3$, $M' = 16, M = 32$)

	$a_0 = 0.1$	$a_0 = 0.1$	$a_0 = 1.0$	$a_0 = 1.0$	$a_0 = 1.5$	$a_0 = 1.5$
	case *I*	case *II*	case *I*	case *II*	case *I*	case *II*
K_V	(0.41, 0.31)	(0.41, 0.29)	(0.60, 1.42)	(0.55, 1.37)	(0.34, 2.28)	(0.37, 2.23)
K_H	(0.43, 0.29)	(0.42, 0.27)	(0.62, 1.25)	(0.66, 1.21)	(0.68, 1.79)	(0.65, 1.71)
K_M	(1.15, 0.01)	(1.11, 0.01)	(0.98, 0.58)	(0.99, 0.54)	(0.81, 0.86)	(0.79, 0.80)

case *I*: present study
case *II*: Rajapakse and Shah (1988)

Table 6.4 Convergence and comparison of impedances of a rigid cylinder with number of node points ($h/a = 1.0, a_0 = 1.0, \nu = 0.25$)

(M)	K_V	K_H	K_M
10	(7.52, 10.61)	(9.28, 11.01)	(11.37, 5.16)
13	(7.34, 10.45)	(9.31, 11.01)	(11.37, 5.15)
15	(7.29, 10.40)	(9.29, 10.99)	(11.26, 5.16)
17	(7.25, 10.38)	(9.26, 10.96)	(11.25, 5.16)
20	(7.24, 10.37)	(9.24, 10.94)	(11.25, 5.16)
Apsel & Luco	(7.57, 10.79)	(9.30, 11.13)	(11.31, 5.32)

Table 6.5 Comparison of impedances of a rigid cylinder with different frequencies ($h/a = 1.0, \nu = 0.25, M = 15$)

a_0		0.25	0.75	1.50	2.0
K_V	case I	(8.44,2.68)	(7.82,7.96)	(7.11,16.07)	(6.76,22.01)
	case II	(8.25,2.73)	(7.86,8.02)	((6.94,16.57)	(6.44,22.70)
K_H	case I	(9.73,2.90)	(9.46,8.30)	(8.82,16.49)	(8.39,22.18)
	case II	(9.57,2.96)	(9.46,8.39)	(8.90,16.57)	(8.49,22.70)
K_M	case I	(13.58,0.58)	(11.93,3.35)	(10.57,8.84)	(9.98,12.46)
	case II	(13.44,0.75)	(11.85,3.51)	(10.60,9.03)	(10.11,12.76)

case I: present study; case II: Apsel and Luco (1987).

Table 6.6 Comparison of impedances of a rigid cylinder with varied h/a ($a_0 = 1.0, \nu = 0.25$)

$h/a(M)$		0.25(10)	0.50(12)	2.0(17)
K_V	case I	(5.72,5.87)	(6.34,7.36)	(9.63,17.70)
	case II	(5.99,6.10)	(6.59,7.55)	(9.70,17.92)
K_H	case I	(6.16,5.01)	(7.48,7.02)	(12.37,19.96)
	case II	(6.27,5.14)	(7.47,7.09)	(12.45,20.06)
K_M	case I	(4.46,1.02)	(6.17,1.88)	(28.68,24.22)
	case II	(4.52,1.09)	(6.20,1.96)	(28.69,24.67)

case I: present study; case II: Apsel and Luco (1987).

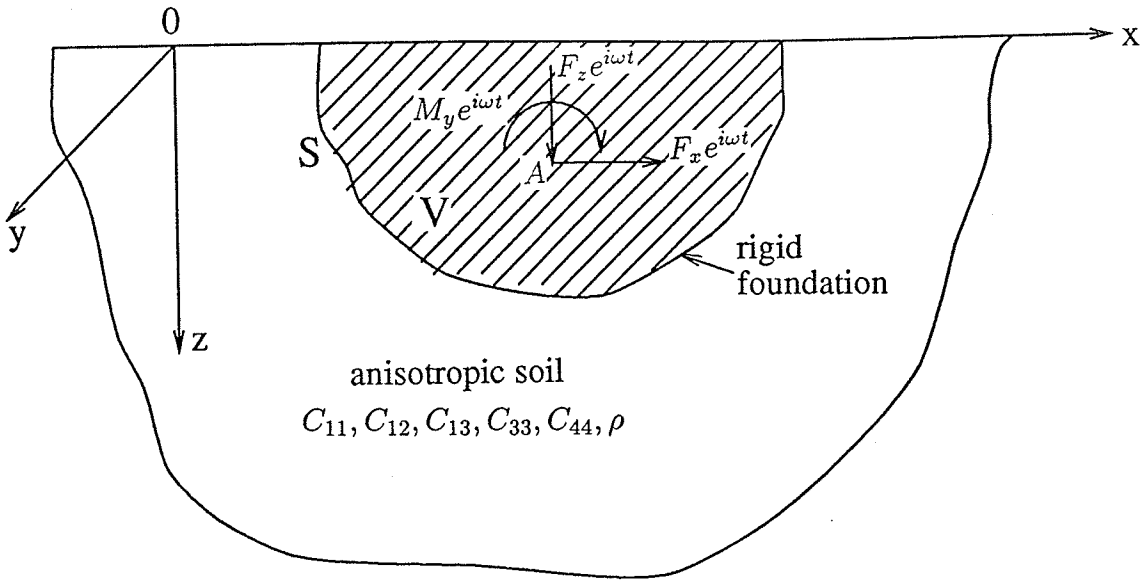

Figure 6.1 Geometry of an arbitrary shaped rigid strip fundation

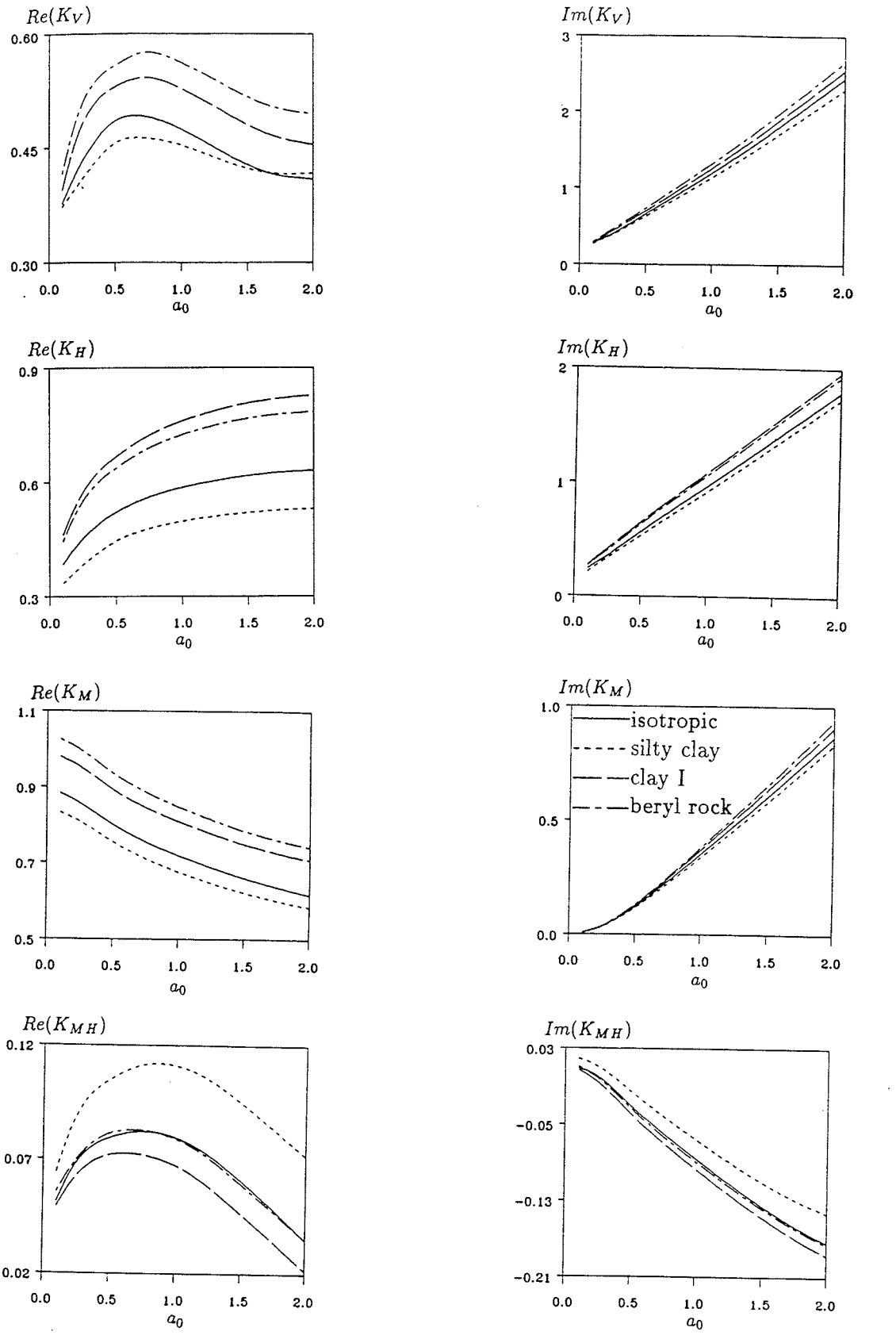

Figure 6.2 Impedances of a rigid strip foundation with rectangular cross-section $(h/b = 0.25, M' = 12, M = 28, \bar{c} = 0.1)$

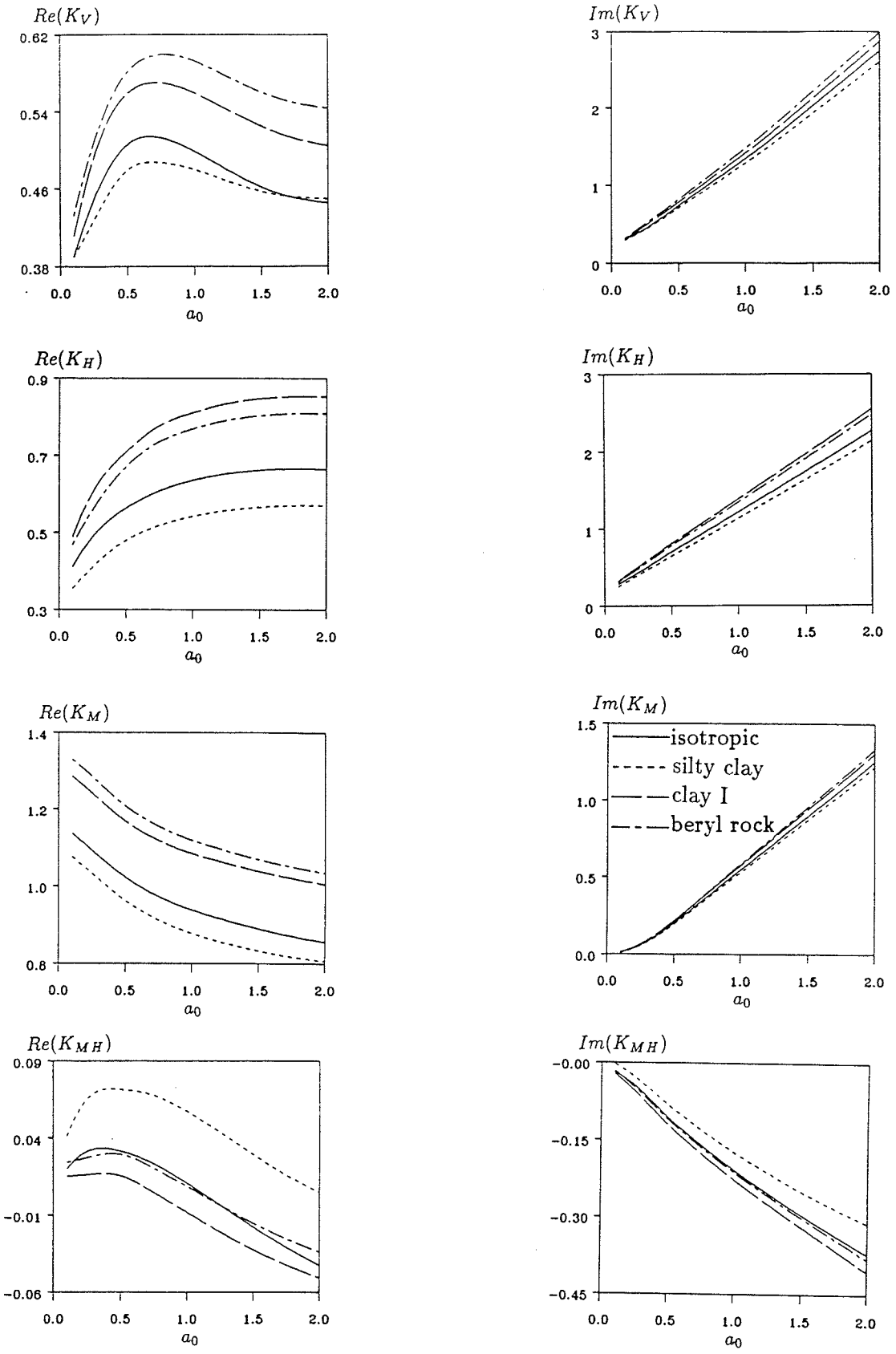

Figure 6.3 Impedances of a rigid strip foundation with rectangular cross-section $(h/b = 0.5, M' = 12, M = 28, \bar{c} = 0.1)$

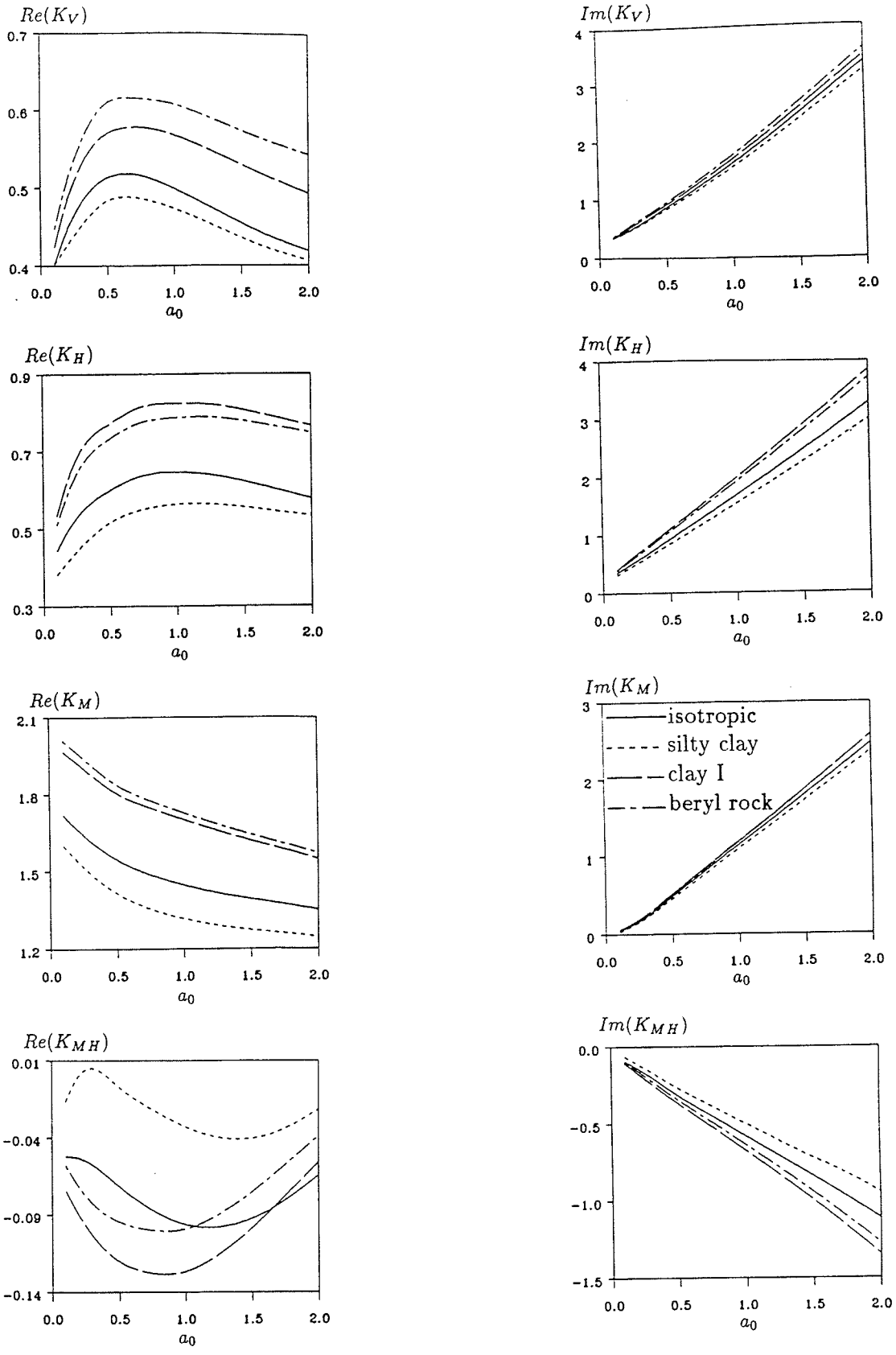

Figure 6.4 Impedances of a rigid strip foundation with rectangular cross-section $(h/b = 1.0, M' = 16, M = 32, \bar{c} = 0.1)$

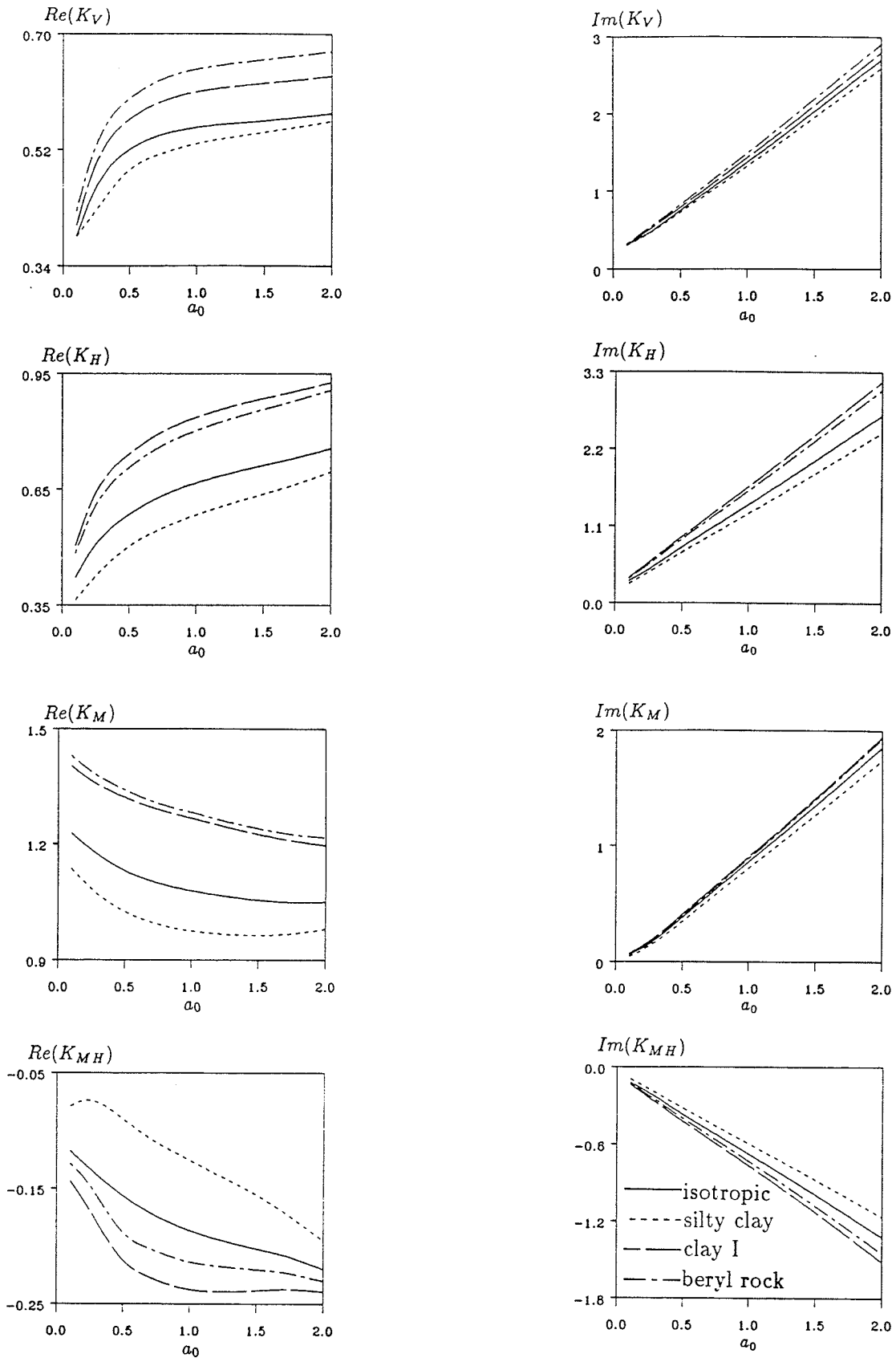

Figure 6.5 Impedances of a rigid strip foundation with semi-circular cross-section ($M' = 15, M = 30, \bar{c} = 0.1$)

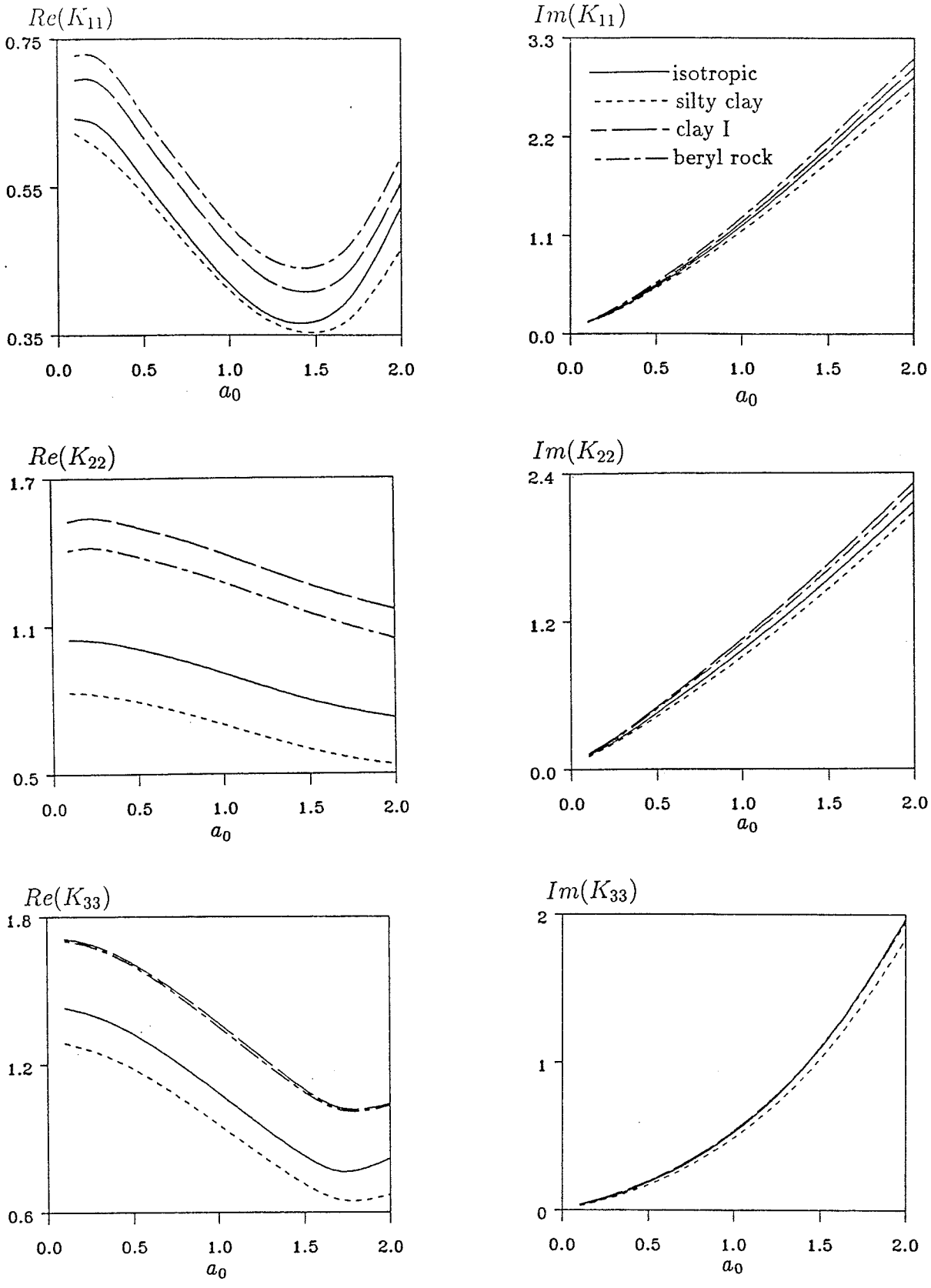

Figure 6.6 Diagonal impedances K_{11}, K_{22} and K_{33} of two identical semi-circular rigid strip foundation system ($M' = 15, M = 30, \bar{d} = 3.0$)

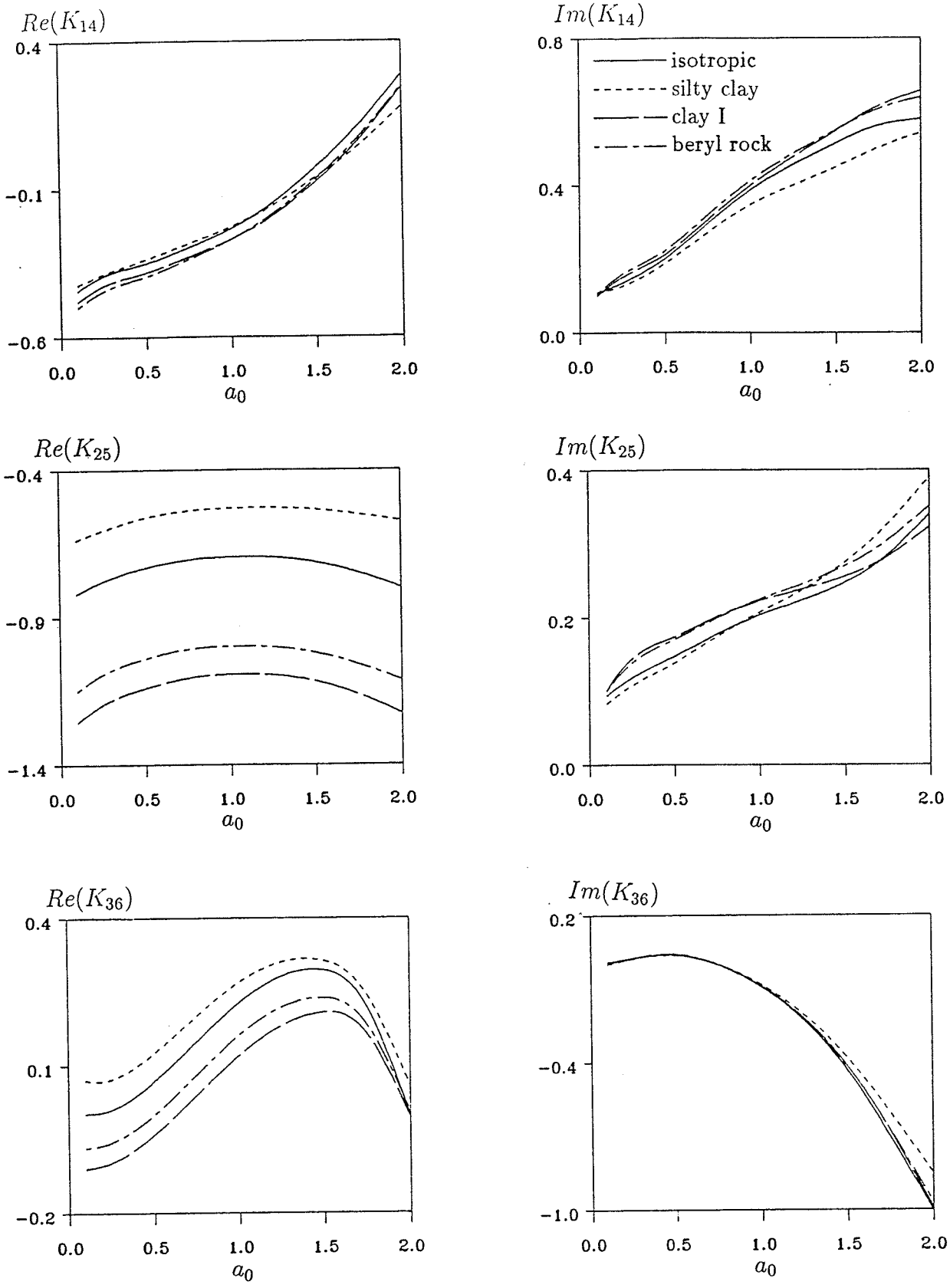

Figure 6.7 Coupling impedances K_{14}, K_{25} and K_{36} of two identical semi-circular rigid strip foundation system ($M' = 15, M = 30, \bar{d} = 3.0$)

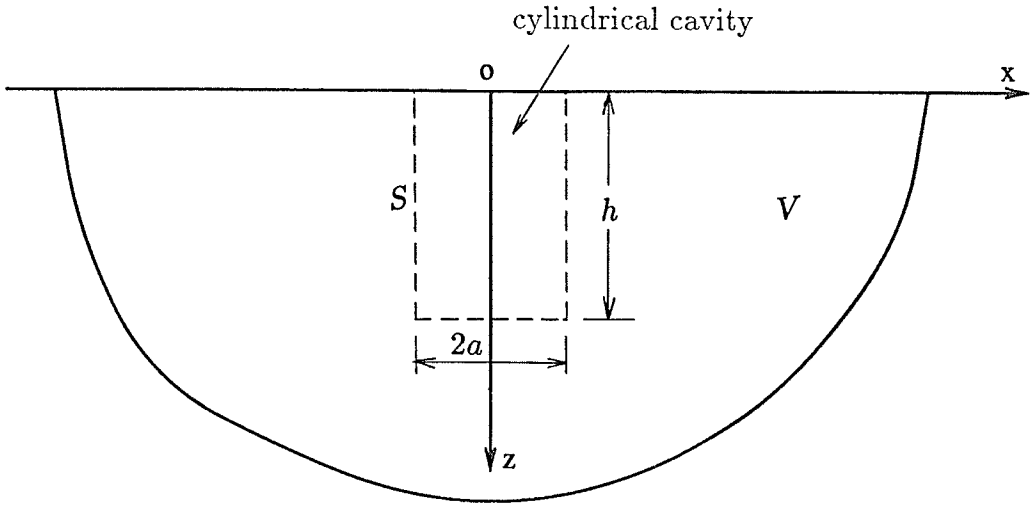

Figure 6.8 Elastic half space with a cylindrical cavity

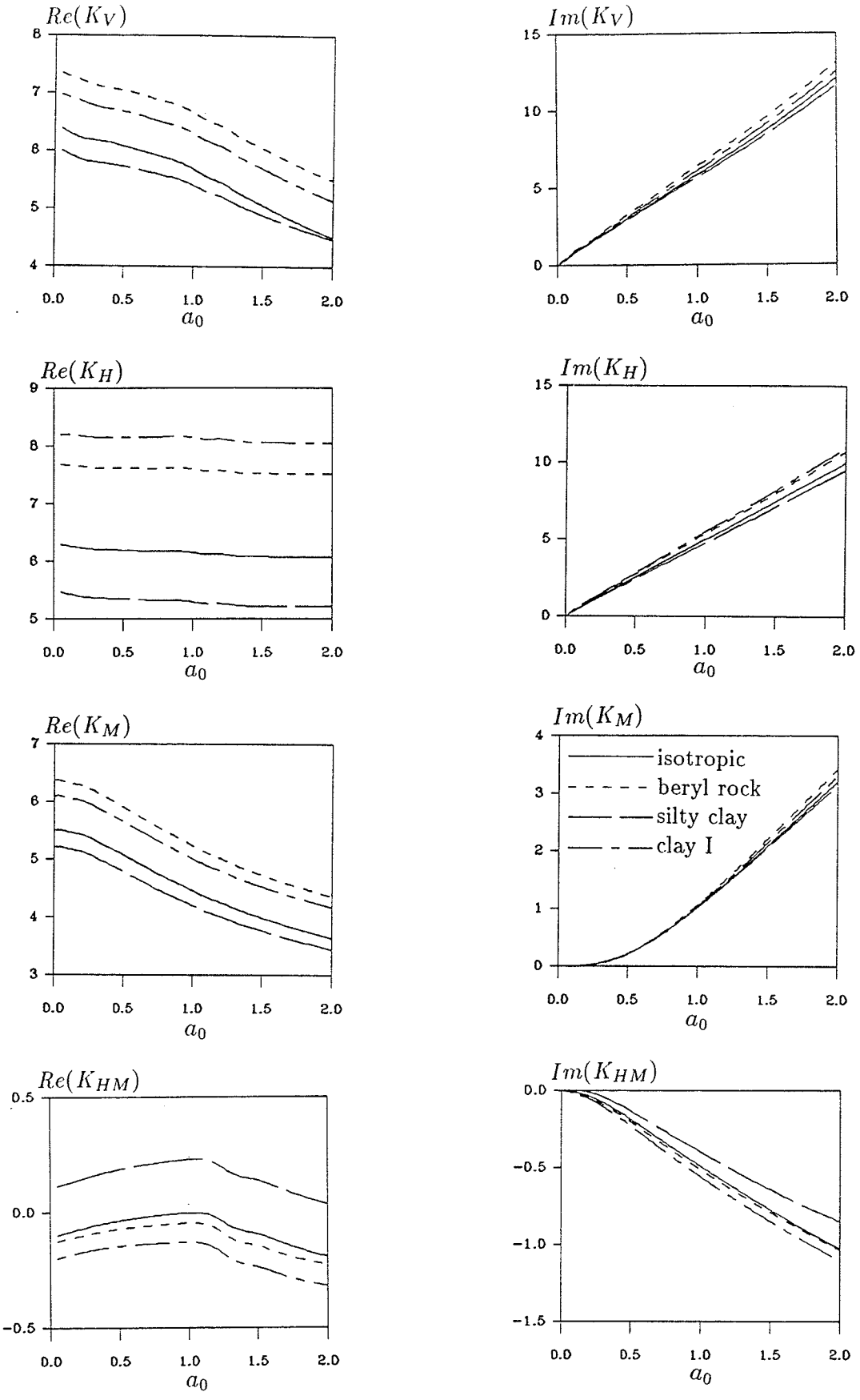

Figure 6.9 Impedances of a rigid cylindrical foundation ($h/a = 0.25, M = 10$)

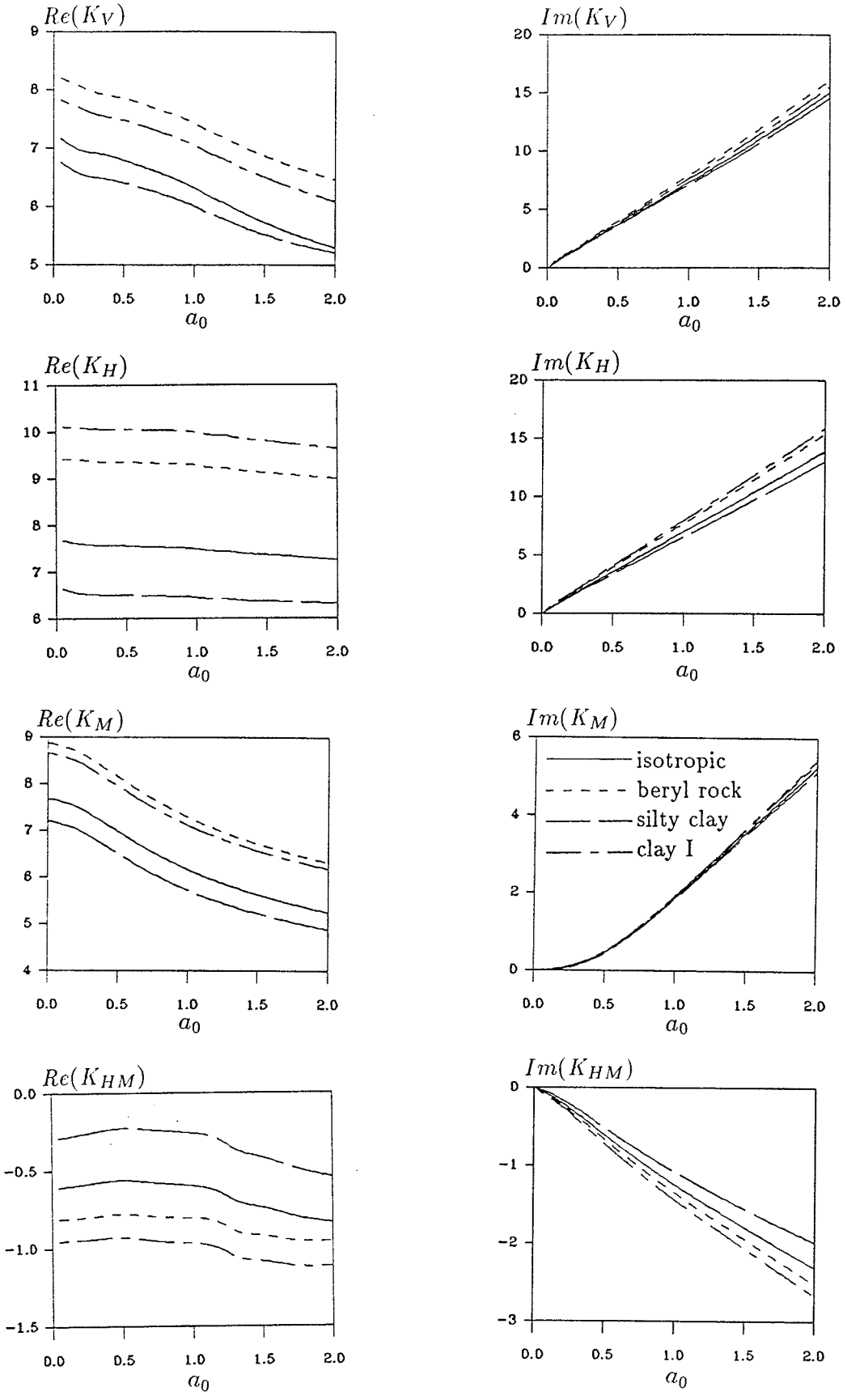

Figure 6.10 Impedances of a rigid cylindrical foundation ($h/a = 0.50, M = 12$)

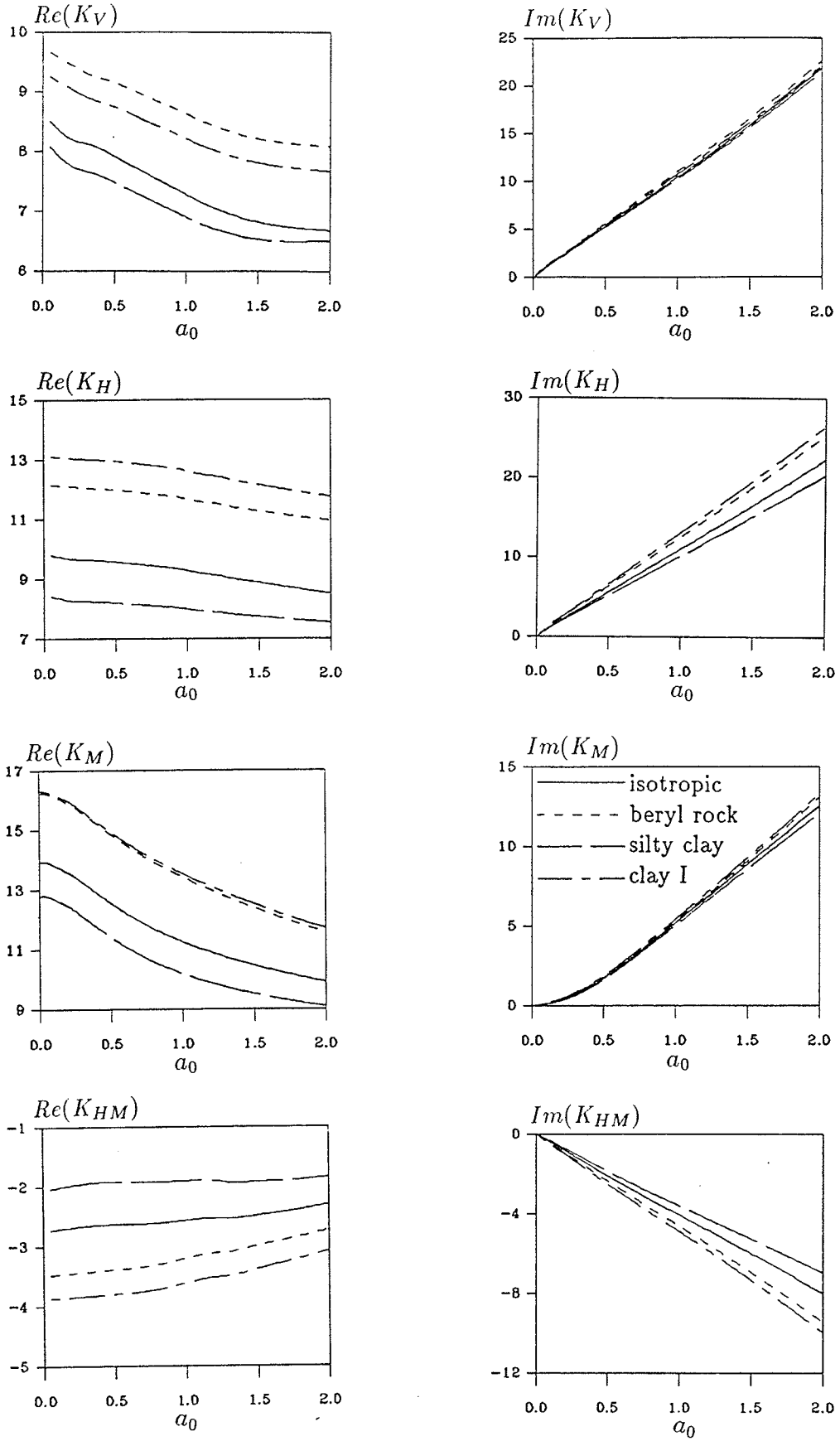

Figure 6.11 Impedances of a rigid cylindrical foundation ($h/a = 1.0, M = 15$)

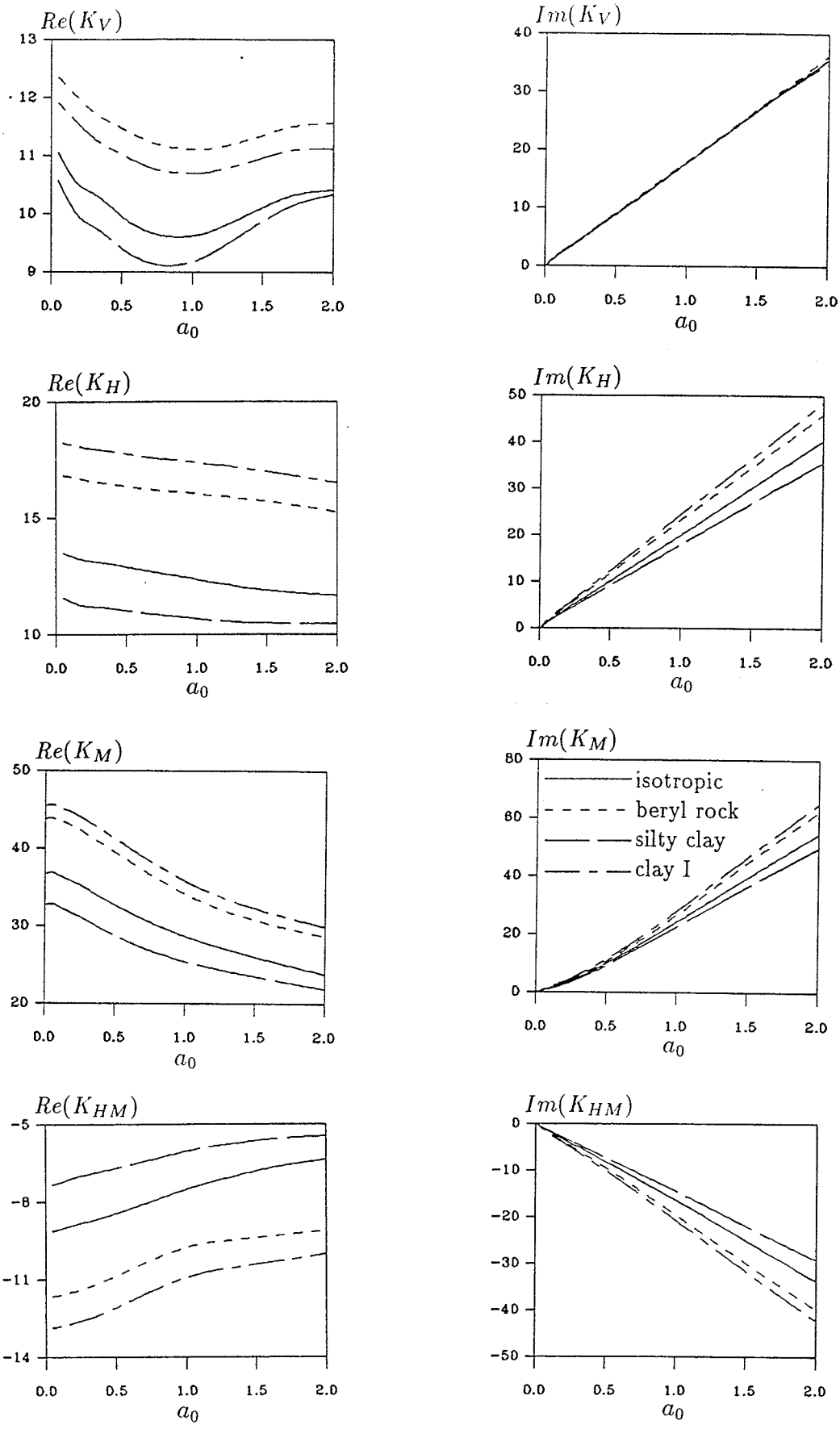

Figure 6.12 Impedances of a rigid cylindrical foundation ($h/a = 2.0, M = 17$)

Chapter 7

AN EXACT STIFFNESS MATRIX METHOD FOR MULTI-LAYERED MEDIA

7.1 GENERAL

An exact stiffness matrix method is presented in this Chapter to compute displacements and stresses of a multi-layered transversely isotropic elastic medium. It is noted that once the displacements and stresses corresponding to a buried point load are computed then different types of boundary-value problems related to layered domain can be solved by using the boundary integral equation method as illustrated in Chapters 3 and 6. The analytical general solutions derived in Chapter 2 for 3-D static problems and in Chapters 4 and 5 for elastodynamic problems can be used to construct exact stiffness matrices for a layer and an underlying half space.

In the classical matrix approach used to compute the response of layered systems the general solutions derived in Chapters 2, 4 and 5 are used for each layer and a set of linear simultaneous equations based on the boundary conditions at the top surface and continuity conditions at layer interfaces are established to determine arbitrary coefficients corresponding to each layer in the layered system shown in Fig 7.1. It is noted that for a 2-D problem, the general solution involves four coefficients for a layer and two coefficients for the underlying half plane resulting in a total of $4N + 2$ arbitrary coefficients. Similarly for a 3-D problem six coefficients are encountered for each layer and three coefficients for the underlying half space resulting in a total of $6N + 3$ arbitrary coefficients. If the multi-layered domain has two or more different materials and the loading is applied internally then the algebraic equation system can not be solved analytically. However, the simultaneous equation system can be solved numerically for discrete values

of Fourier transform parameter for 2-D problems or Hankel transform parameter for 3-D problems. Thereafter the general solutions can be used to compute displacements and stresses by using numerical integration procedures. Thomson (1950) presented a matrix decomposition of the simultaneous equation system by taking into consideration the block diagonal form of the system. A systematic numerical implementation of Thomson's procedure for layered media was given by Haskell (1953, 1960). The Thomson-Haskell algorithm becomes numerically unstable due to the presence of certain exponential terms.

As an alternative to the classical approaches based on the determination of layer arbitrary coefficients, a numerically stable exact stiffness matrix approach is presented in the ensuing sections to evaluate the static and dynamic response of a multi-layered transversely isotropic elastic half plane/space. In the present method the exact general solutions of a homogeneous transversely isotropic elastic medium are used to explicitly construct layer and half space stiffness matrices which describe the relationship between the integral transforms of displacements and stresses at the surfaces.

Without loss of generality, the ensuing sections concentrate on the development of the exact stiffness matrix method for time-harmonic response of a multi-layered orthotropic half plane and a multi-layered transversely isotropic half space subjected to axisymmetric excitations. Selected numerical results for displacements and stresses of multi-layered half planes as well as half spaces are presented in this study to portray the influence of layering, degree of material anisotropy and the frequency of excitation on the response. The stiffness matrix formulations can be readily extended to study three-dimensional static, time-harmonic and transient responses of layered media by using the general solution presented in Chapters 2 and 5.

7.2 2-D TIME-HARMONIC STIFFNESS MATRICES

Consider a multi-layered transversely isotropic elastic half space with a total of N layers of finite thickness. The layers and interfaces of the multi-layered region are labelled as shown in Fig 7.1. The material constants, mass density and thickness of the nth layer are denoted by $c_{ij}^{(n)}, \rho^{(n)}$ and h_n, respectively. Let $\tilde{u}_i^{(n)}$ denotes the Fourier transform of displacements of the nth interface and $\tilde{\sigma}_{ij1}^{(n)}$ and $\tilde{\sigma}_{ij2}^{(n)}$ denote the Fourier transform of stress components σ_{ij} at the top and bottom surface of the nth layer, respectively. Then, the following relationships can be established for the nth layer of the system shown in Fig 7.1 by using the general solution presented in Section 4.3.

$$\tilde{\mathbf{u}}^{(n)} = \mathbf{G}^{(n)}\mathbf{a}^{(n)} \tag{7.1}$$

$$\tilde{\boldsymbol{\sigma}}^{(n)} = \mathbf{F}^{(n)}\mathbf{a}^{(n)} \tag{7.2}$$

where

$$\tilde{\mathbf{u}}^{(n)} =< \tilde{u}_x^{(n)} \quad \tilde{u}_z^{(n)} \quad \tilde{u}_x^{(n+1)} \quad \tilde{u}_z^{(n+1)} >^T \tag{7.3}$$

$$\tilde{\boldsymbol{\sigma}}^{(n)} =< \tilde{\sigma}_{xz1}^{(n)} \quad \tilde{\sigma}_{zz1}^{(n)} \quad \tilde{\sigma}_{xz2}^{(n)} \quad \tilde{\sigma}_{zz2}^{(n)} >^T \tag{7.4}$$

$$\mathbf{a}^{(n)} =< A^{(n)} \quad B^{(n)} \quad C^{(n)} \quad D^{(n)} >^T \tag{7.5}$$

$$\mathbf{G}^{(n)} = \begin{pmatrix} \varpi_1 e_{1,n}^{-1} & -\varpi_1 e_{1,n} & \varpi_2 e_{2,n}^{-1} & -\varpi_2 e_{2,n} \\ e_{1,n}^{-1} & e_{1,n} & e_{2,n}^{-1} & e_{2,n} \\ \varpi_1 e_{1,n+1}^{-1} & -\varpi_1 e_{1,n+1} & \varpi_2 e_{2,n+1}^{-1} & -\varpi_2 e_{2,n+1} \\ e_{1,n+1}^{-1} & e_{1,n+1} & e_{2,n+1}^{-1} & e_{2,n+1} \end{pmatrix} \tag{7.6}$$

$$\mathbf{F}^{(n)} = c_{44} \begin{pmatrix} \eta_3 e_{1,n}^{-1} & -\eta_3 e_{1,n} & \eta_4 e_{2,n}^{-1} & -\eta_4 e_{2,n} \\ \eta_5 e_{1,n}^{-1} & \eta_5 e_{1,n} & \eta_6 e_{2,n}^{-1} & \eta_6 e_{2,n} \\ -\eta_3 e_{1,n+1}^{-1} & \eta_3 e_{1,n+1} & -\eta_4 e_{2,n+1}^{-1} & \eta_4 e_{2,n+1} \\ -\eta_5 e_{1,n+1}^{-1} & -\eta e_{1,n+1} & -\eta_6 e_{2,n+1}^{-1} & -\eta_6 e_{2,n+1} \end{pmatrix} \tag{7.7}$$

where

$$e_{i,j} = e^{\delta \xi_i z_j}, \qquad i = 1,2; \quad j = 1,2,...,N+1 \tag{7.8}$$

In eqn (7.5), $A^{(n)}, B^{(n)}, C^{(n)}$ and $D^{(n)}$ denote the arbitrary coefficients corresponding to the nth layer where $z_{n-1} \leq z \leq z_n$. In addition coefficients $\varpi_i, \xi_i (i = 1, 2)$ and $\eta_i (i = 1, 2, ..., 6)$ appearing in eqns (7.6), (7.7) and (7.8) are defined by eqns (4.24), (4.26) and (4.23), respectively.

In view of eqns (7.1), (7.2), (7.6) and (7.7), the layer stiffness matrix $\mathbf{K}^{(n)}$ which describes the relationship between the $\tilde{\mathbf{u}}^{(n)}$ and $\tilde{\boldsymbol{\sigma}}^{(n)}$ corresponding to the nth layer can be expressed as

$$\tilde{\boldsymbol{\sigma}}^{(n)} = \mathbf{K}^{(n)} \tilde{\mathbf{u}}^{(n)} \tag{7.9}$$

where

$$\mathbf{K}^{(n)} = symm.[k_{ij}], \quad i, j = 1, 2, 3, 4 \tag{7.10}$$

$$k_{1j} = \ell_j [\eta_3 (p_j + q_j \lambda_{1n}) + \eta_4 (g_j + d_j \lambda_{2n})], \quad j = 1, 2, 3, 4 \tag{7.11a}$$

$$k_{2j} = \ell_j [\eta_5 (p_j - q_j \lambda_{1n}) + \eta_6 (g_j - d_j \lambda_{2n})], \quad j = 2, 3, 4 \tag{7.11b}$$

$$k_{33} = k_{11}, \quad k_{34} = -k_{12} \tag{7.11c}$$

$$k_{44} = k_{22} \tag{7.11d}$$

$$\lambda_{in} = e^{-\delta \xi_i h_n}, \quad i = 1, 2 \tag{7.12a}$$

$$\ell_j = 1, \quad j = 2, 4; \qquad \ell_j = -1, \quad j = 1, 3 \tag{7.12b}$$

and the parameters $p_i, q_i, g_i, d_i (i = 1, 2, 3, 4)$ are defined as

$$p_1 = \frac{-\delta c_{44}}{F} [(\varpi_1 + \varpi_2)(\lambda_{2n}^2 - 1) - 2\varpi_2 (\lambda_{1n} \lambda_{2n} - 1)] \tag{7.13a}$$

$$p_2 = \frac{\delta c_{44}}{F} [(\varpi_1 + \varpi_2)\varpi_2 (\lambda_{2n}^2 - 1) - 2\varpi_2 \varpi_1 (\lambda_{1n} \lambda_{2n} - 1)] \tag{7.13b}$$

$$p_3 = \frac{\delta c_{44}}{F} [(\varpi_1 + \varpi_2)\lambda_{1n} (\lambda_{2n}^2 - 1) - 2\varpi_2 \lambda_{2n} (\lambda_{1n} \lambda_{2n} - 1)] \tag{7.13c}$$

$$p_4 = \frac{-\delta c_{44}}{F} [(\varpi_1 + \varpi_2)\varpi_2 \lambda_{1n} (\lambda_{2n}^2 - 1) - 2\varpi_1 \varpi_2 \lambda_{2n} (\lambda_{1n} \lambda_{2n} - 1)] \tag{7.13d}$$

$$g_1 = \frac{-\delta c_{44}}{F} [(\varpi_1 + \varpi_2)(\lambda_{1n}^2 - 1) - 2\varpi_1 (\lambda_{1n} \lambda_{2n} - 1)] \tag{7.14a}$$

$$g_2 = \frac{\delta c_{44}}{F}[(\varpi_1 + \varpi_2)\varpi_1(\lambda_{1n}^2 - 1) - 2\varpi_2\varpi_1(\lambda_{1n}\lambda_{2n} - 1)] \tag{7.14b}$$

$$g_3 = \frac{\delta c_{44}}{F}[(\varpi_1 + \varpi_2)\lambda_{2n}(\lambda_{1n}^2 - 1) - 2\varpi_1\lambda_{1n}(\lambda_{1n}\lambda_{2n} - 1)] \tag{7.14c}$$

$$g_4 = \frac{-\delta c_{44}}{F}[(\varpi_1 + \varpi_2)\varpi_1\lambda_{2n}(\lambda_{1n}^2 - 1) - 2\varpi_1\varpi_2\lambda_{1n}(\lambda_{1n}\lambda_{2n} - 1)] \tag{7.14d}$$

$$q_1 = \frac{-\delta c_{44}}{\varpi_1 - \varpi_2}[(\varpi_1 + \varpi_2)\lambda_{1n}p_1 + 2\varpi_2\lambda_{2n}c_1 - 1] \tag{7.15a}$$

$$q_2 = \frac{\delta c_{44}}{\varpi_1 - \varpi_2}[(\varpi_1 + \varpi_2)\lambda_{1n}p_2 + 2\varpi_2\lambda_{2n}c_2 - \varpi_2] \tag{7.15b}$$

$$q_3 = \frac{-\delta c_{44}}{\varpi_1 - \varpi_2}[(\varpi_1 + \varpi_2)\lambda_{1n}p_3 + 2\varpi_2\lambda_{2n}c_3] \tag{7.15c}$$

$$q_4 = \frac{\delta c_{44}}{\varpi_1 - \varpi_2}[(\varpi_1 + \varpi_2)\lambda_{1n}p_4 + 2\varpi_2\lambda_{2n}c_4] \tag{7.15d}$$

$$d_1 = \frac{\delta c_{44}}{\varpi_1 - \varpi_2}[2\varpi_1\lambda_{1n}p_1 + (\varpi_1 + \varpi_2)\lambda_{2n}c_1 - 1] \tag{7.16a}$$

$$d_2 = \frac{-\delta c_{44}}{\varpi_1 - \varpi_2}[2\varpi_1\lambda_{1n}p_2 + (\varpi_1 + \varpi_2)\lambda_{2n}c_2 - \varpi_1] \tag{7.16b}$$

$$d_3 = \frac{\delta c_{44}}{\varpi_1 - \varpi_2}[2\varpi_1\lambda_{1n}p_3 + (\varpi_1 + \varpi_2)\lambda_{2n}c_3] \tag{7.16c}$$

$$d_4 = \frac{\delta c_{44}}{\varpi_1 - \varpi_2}[2\varpi_1\lambda_{1n}p_4 + (\varpi_1 + \varpi_2)\lambda_{2n}c_4] \tag{7.16d}$$

in which

$$F = 4\varpi_1\varpi_2(\lambda_{1n}\lambda_{2n} - 1)^2 - (\varpi_1 + \varpi_2)^2(\lambda_{1n}^2 - 1)(\lambda_{2n}^2 - 1) \tag{7.17}$$

At this stage it is important to note that the layer stiffness matrix $\mathbf{K}^{(n)}$ is a function of only the layer thickness, layer material properties, frequency of excitation and the Fourier transform parameter ζ. The elements k_{ij} are functions of $\varpi_1, \varpi_2, \eta_i (i = 1, 2, ..., 6)$ and $\lambda_{in} (i = 1, 2)$. All these functions are numerically very stable and $\mathbf{K}^{(n)}$ is found to be a well-conditioned matrix for all values of ζ and h_n. Unlike Thomson-Haskell technique there are no squared large exponential terms that must vanish identically in the numerical evaluation. Only negative exponentials that decrease rapidly with increasing ζ or h_n are involved in k_{ij}.

For the underlying half plane, the general solutions involve only two coefficients $A^{(N+1)}$ and $C^{(N+1)}$ due to the regularity condition for displacements and

stresses at $z \to \infty$ (physically it is equivalent to the condition that rigid body displacements are removed). The stiffness matrix of the bottom half plane can be expressed as

$$\tilde{\boldsymbol{\sigma}}^{(N+1)} = \mathbf{K}^{(N+1)} \tilde{\mathbf{u}}^{(N+1)} \tag{7.18}$$

where

$$\tilde{\boldsymbol{\sigma}}^{(N+1)} = < \tilde{\sigma}_{xz1}^{(N+1)} \quad \tilde{\sigma}_{zz1}^{(N+1)} >^T \tag{7.19}$$

$$\tilde{\mathbf{u}}^{(N+1)} = < \tilde{u}_{x}^{(N+1)} \quad \tilde{u}_{z}^{(N+1)} >^T \tag{7.20}$$

$$\mathbf{K}^{(N+1)} = \bar{g}_1 \begin{pmatrix} (\eta_3 - \eta_4) & \bar{g}_2[(\kappa - 1)(1 - \zeta^2) + \alpha\xi_1\xi_2] \\ symm. & (\varpi_1\eta_6 - \varpi_2\eta_5) \end{pmatrix} \tag{7.21}$$

and

$$\bar{g}_1 = \frac{\delta c_{44}}{(\varpi_1 - \varpi_2)}, \quad \bar{g}_2 = \frac{\xi_2 - \xi_1}{\kappa\xi_1\xi_2} \tag{7.22}$$

It is noted that exponential terms are not involved in the expression of $\mathbf{K}^{(N+1)}$ and its elements depend on the material properties, frequency of excitation and the parameter ζ.

7.3 GLOBAL STIFFNESS MATRIX

The global stiffness matrix of the multi-layered half plane is assembled by using the layer stiffness matrices and continuity condition of stresses σ_{xz} and σ_{zz} at layer interfaces. For example, the stress continuity conditions at the nth interface can be expressed as,

$$< [\tilde{\sigma}_{xz2}^{(n-1)} + \tilde{\sigma}_{xz1}^{(n)}] \quad [\tilde{\sigma}_{zz2}^{(n-1)} + \tilde{\sigma}_{zz1}^{(n)}] >^T = < \tilde{p}_{x}^{(n)} \quad \tilde{p}_{z}^{(n)} >^T \tag{7.23}$$

where $\tilde{p}_i^{(n)}$ is the Fourier transform of the externally applied traction in the i-direction ($i = x, z$) at the nth interface.

The consideration of eqn (7.23) at each layer interface together with eqns (7.10) and (7.21) results in the following global equation system.

$$\begin{pmatrix} \mathbf{K}^{(1)} & & & \\ & \mathbf{K}^{(2)} & & \\ & & \ddots & \\ & & & \mathbf{K}^{(N)} \\ & & & & \mathbf{K}^{(N+1)} \end{pmatrix} \begin{pmatrix} \tilde{u}_x^{(1)} \\ \tilde{u}_z^{(1)} \\ \\ \\ \\ \tilde{u}_x^{(N+1)} \\ \tilde{u}_z^{(N+1)} \end{pmatrix} = \begin{pmatrix} \tilde{p}_x^{(1)} \\ \tilde{p}_z^{(1)} \\ \\ \\ \\ \tilde{p}_x^{(N+1)} \\ \tilde{p}_z^{(N+1)} \end{pmatrix} \tag{7.24}$$

The global stiffness matrix of eqn (7.24) is a well-conditioned symmetric matrix and has a fixed band width equal to 4. It is naturally constrained against rigid body displacements due to the presence of $\mathbf{K}^{(N+1)}$. If a half plane is not present at the bottom then the bottom plane at $z = z_N$ has to be restrained to eliminate the rigid body displacements. In the numerical evaluation of the response of a multi-layered half plane the eqn (7.24) is solved repetitively for discrete values of Fourier transform parameter ζ and the response is calculated by numerically evaluating Fourier integrals given by eqn (4.6b). Stresses at the top and bottom interfaces of a layer can be obtained by using eqns (7.9) and the corresponding general solutions. If displacements within points in a layer is required then it is convenient to define a set of fictitious planes through these points and to consider these as additional layers. Alternatively eqn (7.1) can be used to compute $\mathbf{a}^{(n)}$ for a layer and thereafter compute displacements using the corresponding general solutions. This, however, may involve numerically ill-conditioned matrices such as $\mathbf{G}^{(n)}$ for large values of ζ. If loads are applied within a layer then fictitious interfaces are considered at the loading levels. It is also noted that the eigenvalues of the stiffness matrix in eqn (7.24) correspond directly to the wave numbers (or velocities) of the surface waves of the layered system and the eigenvectors are the corresponding displacements at layer interfaces. In addition the size of the final equation system [*ie.* eqn (7.24)] is equal to $2(N+1)$

which is nearly one-half of that corresponding to the classical approach based on the solution of layer arbitrary coefficients $A^{(n)}, B^{(n)}, C^{(n)}$ and $E^{(n)}$. This reduction of the size of final equation system together with the symmetry of the system and the fact that the displacements are directly determined as the basic unknowns further add to the computational efficiency of the formulation.

7.4 AXISYMMETRIC TIME-HARMONIC STIFFNESS MATRICES

This Section presents the derivation of stiffness matrices of a multi-layered transversely isotropic half space (Fig 7.1) subjected to axisymmetric time-harmonic excitations. The general solution for axisymmetric displacements and stresses of a homogeneous transversely isotropic medium can be obtained from the general solutions given in eqns (5.13)-(5.17) for a 3-D time-harmonic problem. It is noted that in the axisymmetric case m=0 and $E = F \equiv 0$ in the solutions given by eqns (5.13)-(5.17). Let $\breve{u}_i^{(n)}(i = r, z)$ denote the Hankel transform of displacement components $u_i^{(n)}$ and $\breve{\sigma}_{ij1}^{(n)}$ and $\breve{\sigma}_{ij2}^{(n)}(i, j = r, z)$ denote the Hankel transform of stress components σ_{ij} at the top and bottom surface of the nth layer, respectively. A set of equations similar to eqns (7.1) and (7.2) can be established for the axisymmetric problem by introducing the following equations of $\breve{\mathbf{u}}^{(n)}, \breve{\boldsymbol{\sigma}}^{(n)}, \mathbf{G}^{(n)}$ and $\mathbf{F}^{(n)}$.

$$\breve{\mathbf{u}}^{(n)} = < \breve{u}_r^{(n)} \quad \breve{u}_z^{(n)} \quad \breve{u}_r^{(n+1)} \quad \breve{u}_z^{(n+1)} >^T \tag{7.25}$$

$$\breve{\boldsymbol{\sigma}}^{(n)} = < \breve{\sigma}_{rz1}^{(n)} \quad \breve{\sigma}_{zz1}^{(n)} \quad \breve{\sigma}_{rz2}^{(n)} \quad \breve{\sigma}_{zz2}^{(n)} >^T \tag{7.26}$$

$$\mathbf{G}^{(n)} = \begin{pmatrix} a_1 e_{1,n}^{-1} & a_1 e_{1,n} & a_2 e_{2,n}^{-1} & a_2 e_{2,n} \\ -a_7 e_{1,n}^{-1} & a_7 e_{1,n} & -a_8 e_{2,n}^{-1} & a_8 e_{2,n} \\ a_1 e_{1,n+1}^{-1} & a_1 e_{1,n+1} & a_2 e_{2,n+1}^{-1} & a_2 e_{2,n+1} \\ -a_7 e_{1,n+1}^{-1} & a_7 e_{1,n+1} & -a_8 e_{2,n+1}^{-1} & a_8 e_{2,n+1} \end{pmatrix} \tag{7.27}$$

$$\mathbf{F}^{(n)} = c_{44} \begin{pmatrix} -b_{51} e_{1,n}^{-1} & b_{51} e_{1,n} & -b_{52} e_{2,n}^{-1} & b_{52} e_{2,n} \\ b_{21} e_{1,n}^{-1} & b_{21} e_{1,n} & b_{22} e_{2,n}^{-1} & b_{22} e_{2,n} \\ b_{51} e_{1,n+1}^{-1} & -b_{51} e_{1,n+1} & b_{52} e_{2,n+1}^{-1} & -b_{52} e_{2,n+1} \\ -b_{21} e_{1,n+1}^{-1} & -b_{21} e_{1,n+1} & -b_{22} e_{2,n+1}^{-1} & -b_{22} e_{2,n+1} \end{pmatrix} \tag{7.28}$$

The coefficients $a_1, a_2, a_7, a_8, b_{21}, b_{22}, b_{51}$and b_{52} appearing in above equations are defined in eqn (5.17); e_{1n} and e_{2n} are defined eqn (7.8), respectively.

The relationship between $\breve{\mathbf{u}}^{(n)}$ and $\breve{\boldsymbol{\sigma}}^{(n)}$ corresponding to the nth layer can be expressed by eqn (7.9). The elements k_{ij} of the layer stiffness matrix for the axisymmetric time-harmonic problems are given by

$$k_{1j} = [b_{51}(q_j\lambda_{1n} - p_j) + b_{52}(d_j\lambda_{2n} - g_j)], \quad j = 1,2,3,4 \tag{7.29a}$$

$$k_{2j} = [b_{21}(p_j + q_j\lambda_{1n}) + b_{22}(g_j + d_j\lambda_{2n})], \quad j = 2,3,4 \tag{7.29b}$$

$$k_{3j} = [b_{51}(p_j\lambda_{1n} - q_j) + b_{52}(g_j\lambda_{2n} - d_j)], \quad j = 3,4 \tag{7.29c}$$

$$k_{44} = -[b_{21}(p_4\lambda_{1n} + q_4) + b_{22}(g_4\lambda_{2n} + d_4)] \tag{7.29d}$$

where λ_{1n} and λ_{2n} are as defined in eqn (7.12a) and the parameters p_i, q_i, d_i, g_i (i=1,2,3,4) are defined as

$$p_1 = \frac{\delta c_{44}}{F}[(a_2a_7 + a_1a_8)(\lambda_{1n}\lambda_{2n} - 1)a_8 - 2a_2a_8(\lambda_{2n}^2 - 1)a_7] \tag{7.30a}$$

$$p_2 = \frac{\delta c_{44}}{F}[(a_2a_7 + a_1a_8)(\lambda_{1n}\lambda_{2n} - 1)a_2 - 2a_2a_8(\lambda_{2n}^2 - 1)a_1] \tag{7.30b}$$

$$p_3 = \frac{\delta c_{44}}{F}[(a_2a_7 + a_1a_8)(\lambda_{1n}\lambda_{2n} - 1)a_8\lambda_{2n} - 2a_2a_8(\lambda_{2n}^2 - 1)a_7\lambda_{1n}] \tag{7.30c}$$

$$p_4 = \frac{\delta c_{44}}{F}[(a_2a_7 + a_1a_8)(\lambda_{1n}\lambda_{2n} - 1)a_2\lambda_{2n} - 2a_2a_8(\lambda_{2n}^2 - 1)a_1\lambda_{1n}] \tag{7.30d}$$

$$g_1 = \frac{\delta c_{44}}{F}[(a_2a_7 + a_1a_8)(\lambda_{1n}\lambda_{2n} - 1)a_7 - 2a_1a_7(\lambda_{1n}^2 - 1)a_8] \tag{7.31a}$$

$$g_2 = \frac{\delta c_{44}}{F}[(a_2a_7 + a_1a_8)(\lambda_{1n}\lambda_{2n} - 1)a_1 - 2a_1a_7(\lambda_{1n}^2 - 1)a_2] \tag{7.31b}$$

$$g_3 = \frac{\delta c_{44}}{F}[(a_2a_7 + a_1a_8)(\lambda_{1n}\lambda_{2n} - 1)a_7\lambda_{1n} - 2a_1a_7(\lambda_{1n}^2 - 1)a_8\lambda_{2n}] \tag{7.31c}$$

$$g_4 = \frac{\delta c_{44}}{F}[(a_2a_7 + a_1a_8)(\lambda_{1n}\lambda_{2n} - 1)a_1\lambda_{1n} - 2a_1a_7(\lambda_{1n}^2 - 1)a_2\lambda_{2n}] \tag{7.31d}$$

$$q_1 = \frac{1}{a_1a_8 - a_2a_7}[-(a_7a_2 + a_8a_1)\lambda_{1n}p_1 - 2a_8a_2\lambda_{2n}g_1] \tag{7.32a}$$

$$q_2 = \frac{1}{a_1a_8 - a_2a_7}[-(a_7a_2 + a_8a_1)\lambda_{1n}p_2 - 2a_8a_2\lambda_{2n}g_2] \tag{7.32b}$$

$$q_3 = \frac{1}{a_1a_8 - a_2a_7}[a_8 - (a_7a_2 + a_8a_1)\lambda_{1n}p_3 - 2a_8a_2\lambda_{2n}g_3] \tag{7.32c}$$

$$q_4 = \frac{1}{a_1 a_8 - a_2 a_7}[a_2 - (a_7 a_2 + a_8 a_1)\lambda_{1n} p_4 - 2a_8 a_2 \lambda_{2n} g_4] \tag{7.32d}$$

$$d_1 = \frac{1}{a_1 a_8 - a_2 a_7}[2a_7 a_1 \lambda_{1n} p_1 + (a_7 a_2 + a_8 a_1)\lambda_{2n} g_1] \tag{7.33a}$$

$$d_2 = \frac{1}{a_1 a_8 - a_2 a_7}[2a_7 a_1 \lambda_{1n} p_2 + (a_7 a_2 + a_8 a_1)\lambda_{2n} g_2] \tag{7.33b}$$

$$d_3 = \frac{1}{a_1 a_8 - a_2 a_7}[2a_7 a_1 \lambda_{1n} p_3 + (a_7 a_2 + a_8 a_1)\lambda_{2n} g_3 - a_7] \tag{7.33c}$$

$$d_4 = \frac{1}{a_1 a_8 - a_2 a_7}[2a_7 a_1 \lambda_{1n} p_4 + (a_7 a_2 + a_8 a_1)\lambda_{2n} g_4 - a_1] \tag{7.33d}$$

in which

$$F = [(a_2 a_7 + a_1 a_8)(\lambda_{1n}\lambda_{2n} - 1)]^2 - 4a_1 a_2 a_7 a_8 (\lambda_{1n}^2 - 1)(\lambda_{2n}^2 - 1) \tag{7.34}$$

For the underlying half space, the relationship between displacements and stresses at the interface can be expressed by eqn (7.18). The relevant displacement and stress vectors and the stiffness matrix are given by

$$\breve{\boldsymbol{\sigma}}^{(N+1)} =< \breve{\sigma}_{rz1}^{(N+1)} \quad \breve{\sigma}_{zz1}^{(N+1)} >^T \tag{7.35}$$

$$\breve{\mathbf{u}}^{(N+1)} =< \breve{u}_{r}^{(N+1)} \quad \breve{u}_{z}^{(N+1)} >^T \tag{7.36}$$

$$\mathbf{K}^{(N+1)} = \bar{g}_1 \begin{pmatrix} (b_{31} - b_{32}) & \bar{g}_2[(\kappa - 1)(1 - \zeta^2) + \alpha\xi_1\xi_2] \\ symm. & (a_1 b_{22} - a_2 b_{21}) \end{pmatrix} \tag{7.37}$$

where

$$\bar{g}_1 = \frac{\delta}{(a_1 - a_2)}, \quad \bar{g}_2 = \frac{\xi_2 - \xi_1}{\kappa\xi_1\xi_2} \tag{7.38}$$

The global stiffness matrix of the multi-layered axisymmetric problem can be obtained by considering the boundary and continuity conditions of σ_{rz} and σ_{zz} at layer interfaces and following the same solution procedure as that presented in section 7.3 for a layered plane system. The global solution equation system for this axisymmetric problem can be expressed in eqn (7.24) with the displacement vector and the external load vector being defined as

$$< \breve{u}_{r}^{(1)} \quad \breve{u}_{z}^{(1)} \quad \ldots \quad \breve{u}_{r}^{(N+1)} \quad \breve{u}_{z}^{(N+1)} >^T \tag{7.39}$$

and

$$< \breve{p}_r^{(1)} \quad \breve{p}_z^{(1)} \quad \ldots \quad \breve{p}_r^{(N+1)} \quad \breve{p}_z^{(N+1)} >^T \tag{7.40}$$

respectively. $\breve{p}_i^{(n)}$ is the Hankel transform of the externally applied traction in the i-direction ($i = r, z$) at the nth interface. Once again the axisymmetric global stiffness matrix, as that for a 2-D problem, is a well-conditioned symmetric matrix with a band width equal to 4.

The layer stiffness matrix of a layer and an underlying half space can be derived under three-dimensional excitations. The relevant three-dimensional general solutions for displacement and stress for a transversely isotropic medium subjected to static and dynamic loads are given in Chapters 2 and 5, respectively. Explicit derivation of stiffness matrices for 3-D problems are not attempted here since the concepts are identical to those encountered in 2-D problems. However, in 3-D problems the layer and half space stiffness matrices are of the size 6×6 and 3×3 respectively and consequently the elements of matrices become algebraically more complicated. However, all algebraic manipulations can be effectively handled by a suitable computer algebra code.

7.5 NUMERICAL SOLUTIONS

7.5.1 **Numerical Scheme**

Computer codes based on the preceeding analysis have been developed to evaluate the dynamic response of multi-layered transversely isotropic elastic half planes and half spaces. The tasks performed by the computer codes can be described as *a*) the computation and assembly of stiffness matrices corresponding to each layer and the underlying half plane/space of the multi-layered system to establish eqn (7.24) for a specified value of the integral transform parameter ζ; *b*) the solution of eqn (7.24) to obtain the interlayer displacement vector in the integral transform domain and *c*) the evaluation of the Fourier and Hankel

integral transforms integrals by using an adaptive version of Filon's numerical integration scheme (Tranter 1956). Note that once the values of $\tilde{u}_i$ (or $\breve{u}_i$) and $\tilde{\sigma}_{ij}$ (or $\breve{\sigma}_{ij}$) corresponding to a certain elevation (*ie.* z-coordinate) are computed, thereafter the displacements and stresses at any arbitrary epicentral distance (*ie.* x-coordinate for a 2-D problem and r-coordinate for a axisymmetric problem) at that elevation can be computed simply by using the relevant inverse integral transform formulae.

In accordance with reality, materials are assumed to be attenuating [*ie.* complex c_{ij} or α, β and κ which may be frequency dependent] as in Chapters 4 and 5. This also results in the path of integration (*ie.* real ζ-axis) free of any singularities. This technique with one percent complex part has been used in the present study to evaluate all integrals.

The numerical stability and the accuracy of the present stiffness matrix technique have been verified through the comparison with the explicit analytical solutions for a homogeneous orthotropic half plane and a transversely isotropic half space presented in Sections 4.8 and 5.8. A homogeneous half plane consisting of beryl rock under a uniformly distributed load of intensity q_0 and width '$2a$' applied at a depth 'a' below the free surface and a homogeneous beryl rock half space under a patch load of radius a applied vertically with a depth a below the free surface are considered for this purpose. The half plane/space are discretized by using two models; the first model has 10 layers (uniform thickness h/a=0.5) with an underlying half plane and the second model has 25 layers (h/a=0.2) with a bottom half plane/space. Comparison of numerical results corresponding to the two multi-layered models with those explicit solution presented in Sections 4.8 and 5.8 shows less than one percent difference.

7.5.2 Numerical solutions for multi-layered plane problems

In this study, selected numerical results corresponding to five layered systems are presented. The properties of different materials considered in the nu-

merical study are given in Table 1.1. The thickness distribution of the first set of layered systems considered in the numerical study is given in Table 7.1. The three layered systems defined in Table 7.1 are subjected to vertical and horizontal uniform strip loads of intensity q_0 and width '$2a$'. This problem can be considered as an approximation of the response of a flexible strip footing on layered anisotropic soils and pavement systems subjected to dynamic loadings. The numerical results are presented in terms of nondimensional displacements (compliances) $u^*_{ij}(x,z) = u_{ij}(x,z)c^{(1)}_{44}/(aq_0)$, where u_{ij} denotes the displacement in the i-direction $(i = x, z)$ due to an applied load acting in the j-direction $(j = x, z)$ and $c^{(1)}_{44}$ is the moduli c_{44} of the top layer (Fig 7.1). A nondimensional frequency a_0 defined as $a_0 = a\omega[\rho^{(1)}/c^{(1)}_{44}]^{1/2}$ where $\rho^{(1)}$ is the mass density of the top layer is also used.

Figures 7.2 and 7.3 show the influence of frequency of excitation over the range $0.5 < a_0 < 3.0$ on displacements u^*_{xx} and u^*_{zz} at the centre point of a uniform strip loading applied at the surface $(z = 0)$ and at a depth $0.5a$ below the surface, respectively. The frequency range $0.5 < a_0 < 3.0$ is selected since most machine foundation vibrations are in this range (Gazetas 1983). The strong influence of layering on the response is clearly noted in Figures 7.2 and 7.3. Comparison of displacements corresponding to the three soil systems indicates that it is very difficult to relate the influence of degree of anisotropy of materials in a layered system to the features of the response. System 1 is a homogeneous orthotropic medium and the real and imaginary parts of displacements u^*_{xx} and u^*_{zz} vary smoothly with the frequency. In the case of the two layered systems the variation of displacements with the frequency shows considerable oscillations especially for the imaginary parts. The real parts of the displacements generally decrease with the frequency for all three systems under both vertical and horizontal loadings. Imaginary parts of the displacements increase with the frequency for the homogeneous soil (system 1) but do not follow a definite trend for the other

two systems due to oscillatory variations. Comparison of Figures 7.2 and 7.3 indicates that the real parts of displacements for all three systems are higher for surface loading when compared to buried loading. On the other hand, imaginary parts of displacements are higher for the buried loading case when compared to the surface loading indicating more geometric dissipation under buried loading. However, the general features of compliance profiles shown in Figs 7.2 and 7.3 are quite similar.

The next set of solutions corresponds to two layered systems encountered in computing and electronic devices. The response of a SiC substrate with a Al_2O_3 layer and an aluminum substrate with a nylon layer under a time-harmonic vertical concentrated load applied at coordinate origin (Fig 7.1) is studied. Figure 7.4 shows the variation of nondimensional displacement $u^*_{zz}(= \frac{u_{zz}c^{(1)}_{44}h_1}{P_0}$, where P_0 is the magnitude of the concentrated load and $h_1$is the thickness of the layer) with the horizontal distance at the surface (z=0) and at the material interface. Solutions are presented for three values of nondimensional frequency a_0 $[= h_1\omega(\rho^{(1)}/c^{(1)}_{44})^{1/2}]$. As can be seen from Fig 7.4(a) $Re[u^*_{zz}(0,0)]$ is singular near the origin of the coordinate system for all frequencies due to the fact that loading is applied at the coordinate origin. Surface and interface displacements show relatively smooth variation with the horizontal distance for both layered systems. In the case of Al_2O_3/SiC system normalised displacements are higher than that corresponding to nylon/aluminum system. Comparison of material properties given in Table 1.1 indicates that the nylon/aluminum system can be considered as a flexible film on a rigid substrate due to the large difference between material moduli of the two materials. In fact, it can be seen from Fig 7.4b that the interface displacements of nylon/aluminum system is very close to zero for all three values of frequency. In addition, the surface displacements of nylon/aluminum system is significant only near the loading region $|x/h| < 1.0$ indicating the presence of more or less a conically deformed region which is characteristic to a point loaded

very flexible layer on a rigid substrate. On the other hand, Al_2O_3/SiC system shows more gradual distribution of the displacements with the horizontal distance and the presence of significant interface displacements.

Figure 7.5 shows the shear and normal stresses along the material interface of Al_2O_3/SiC and nylon/aluminum system under a vertical concentrated load of magnitude P_0 applied at the origin. It is noted from Fig 7.5 that the shear stress along the interface is negligible for nylon/aluminum system for all three frequencies. Significant shear stresses are noted along the interface of Al_2O_3/SiC system. The real part of normal stress along the interface of nylon/aluminum system is generally larger than that of Al_2O_3/SiC. It is also noted that imaginary part of the normal stress is nearly zero for nylon/aluminum system indicating that the loading and the normal stress along the interface are nearly in-phase. A significant imaginary component is noted for normal stress along the interface of Al_2O_3/SiC system. In general the amplitude of interface vertical stress is higher for the nylon/aluminum system when compared to Al_2O_3/SiC system since the former behaves as a flexible layer on a rigid substrate. On the other hand, more shear stress are generated in the Al_2O_3/SiC system due to the higher vertical displacement gradients (in x-direction) that exist along the material interface. The variation of interface stress with the frequency is quite smoother in the case of nylon/aluminum system but shows complicated oscillatory behaviour for Al_2O_3/SiC system. Generally the magnitudes of both real and imaginary parts of stress increase with increasing frequency in the case of nylon/aluminum system. The solution presented in Figs 7.4 and 7.5 are useful in the study of flaws and characteristics of material interfaces by using non-destructive testing methods.

7.5.3 Numerical solutions for multi-layered axisymmetric problems

Next, a homogeneous and two multi-layered transversely isotropic half spaces defined in Table 7.1 are considered under time-harmonic axisymmetric loadings.

The applied loading is assumed to act vertically and uniformly distributed over a circular area of radius of a with intensity q_0. In practice, this problem can be considered as the simulation of a flexible footing on a layered elastic soil. A nondimensional displacement $u^*_{zz}(r,z)$ and a nondimensional frequency a_0 as defined in Section 7.5.2 are used.

Figure 7.6 shows the influence of frequency of excitation over the range $0.5 < a_0 < 3.0$ on displacement u^*_{zz} at the centre point $(r = 0)$ of an uniform patch loading applied at the surface $(z = 0)$ and at a depth $0.5a$ below the surface, respectively. The strong influence of layering on the response is clearly noted in Figure 7.6. Comparison of displacements corresponding to the three soil systems indicates that it is very difficult to relate the influence of degree of anisotropy of materials in a layered system to the features of the response. System 1 is a homogeneous transversely isotropic medium and the real and imaginary parts of displacements u^*_{zz} vary smoothly with the frequency. In the case of the two layered systems the variation of displacements with the frequency show oscillations especially for the imaginary parts. The real parts of the displacements generally decrease with the frequency for all three systems. Comparison of the present results indicates that the real part of displacements for all three systems are slightly higher for surface loading when compared to the buried loading.

7.6 CONCLUSIONS

A stiffness matrix method based on exact analytical general solutions for elastodynamics of layered transversely isotropic system is presented to compute displacements and stresses of a multi-layered orthotropic elastic half plane subjected to arbitrary time-harmonic loadings and a multi-layered transversely isotropic half space subjected to axisymmetric time-harmonic loadings. The Fourier and Hankel transform of displacements at layer interfaces are considered as the basic

unknowns in the analysis for plane and axisymmetric problems respectively. Explicit solutions for stiffness matrices of a layer with a finite thickness and a half plane/space are presented. An adaptive version of Filon's numerical integration is used to numerically integrate the Fourier and Hankel integrals encountered in the analysis. The present method has the advantage that the stiffness matrices involve only negative exponentials and other numerically stable terms. In addition the size of the final equation system is nearly one-half of that corresponding to the conventional matrix approach based on layer arbitrary coefficients and has a band width equal to four. Selected numerical results presented in this study for five different layered systems indicate that the response of a layered anisotropic medium depend significantly on the frequency of excitation, degree of anisotropy of materials, thickness of layers and the configuration of layering. The response is governed by a complex combination of above parameters and it is difficult to filter the influence of each parameter on the response. The present method can be effectively used to compute the kernel functions (Green's functions) required in the application of boundary integral equation method for layered anisotropic media. It can be also used to verify the accuracy of approximate stiffness methods such as those proposed by Waas (1980), Kausel and Peek (1982) and other numerical techniques. With the aid of computer algebra codes the present methodology can be extended to develop a highly stable and computationally efficient stiffness matrix approach for evaluation of static, time-harmonic and transient responses of layered isotropic and anisotropic half-spaces under three-dimensional loadings.

Table 7.1: Thickness distributions of multi-layered systems

	Layer thickness		
system No	h_1	h_2	h_3
1	∞		
(h/a)	(layered soil)	–	–
2	0.3	0.7	∞
(h/a)	(layered soil)	(beryl rock)	(isotropic)
3	1.0	1.0	∞
(h/a)	(layered soil)	(beryl rock)	(isotropic)

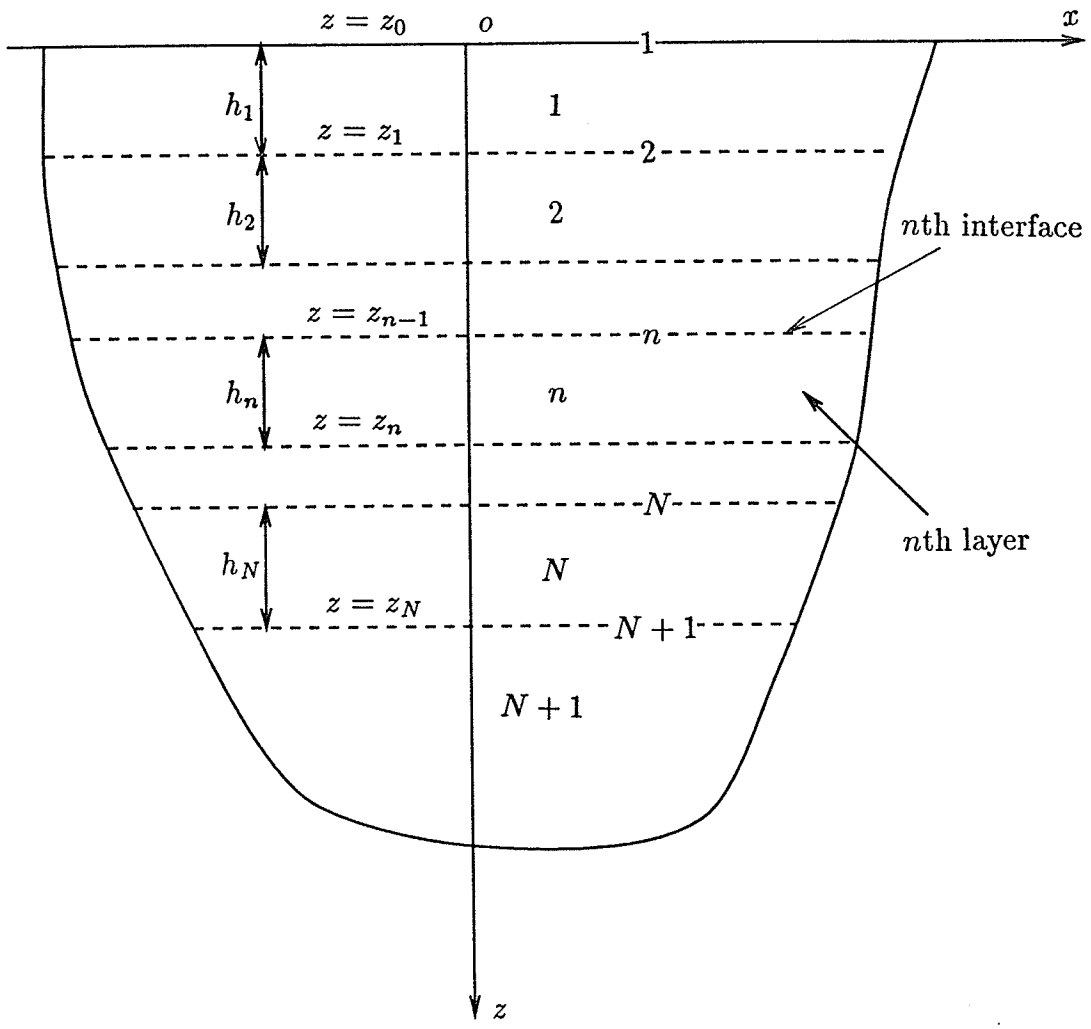

Figure 7.1 Geometry of multi-layered system

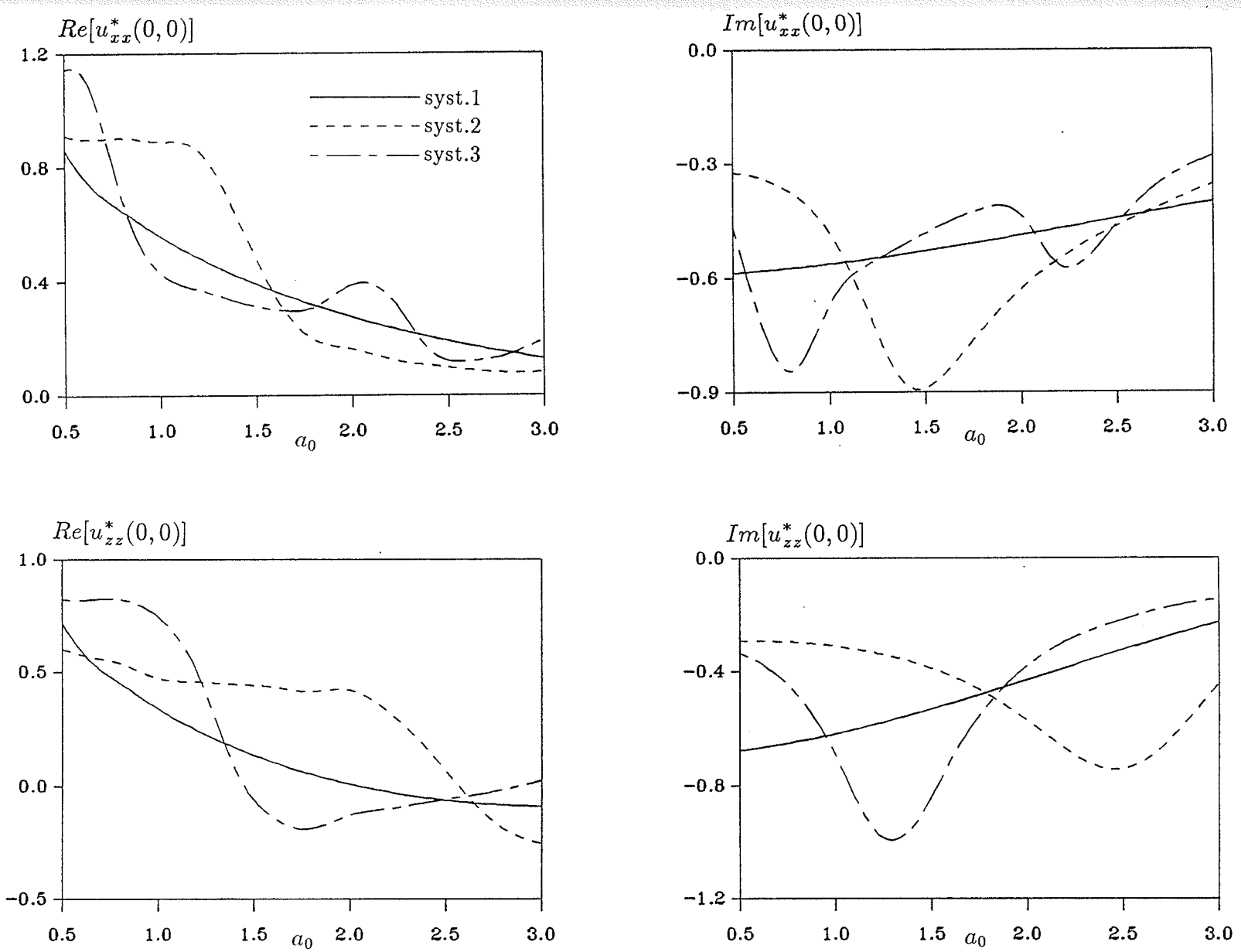

Figure 7.2 Normalized displacements u^*_{xx} and u^*_{zz} due to strip loads at $z/a = 0$.

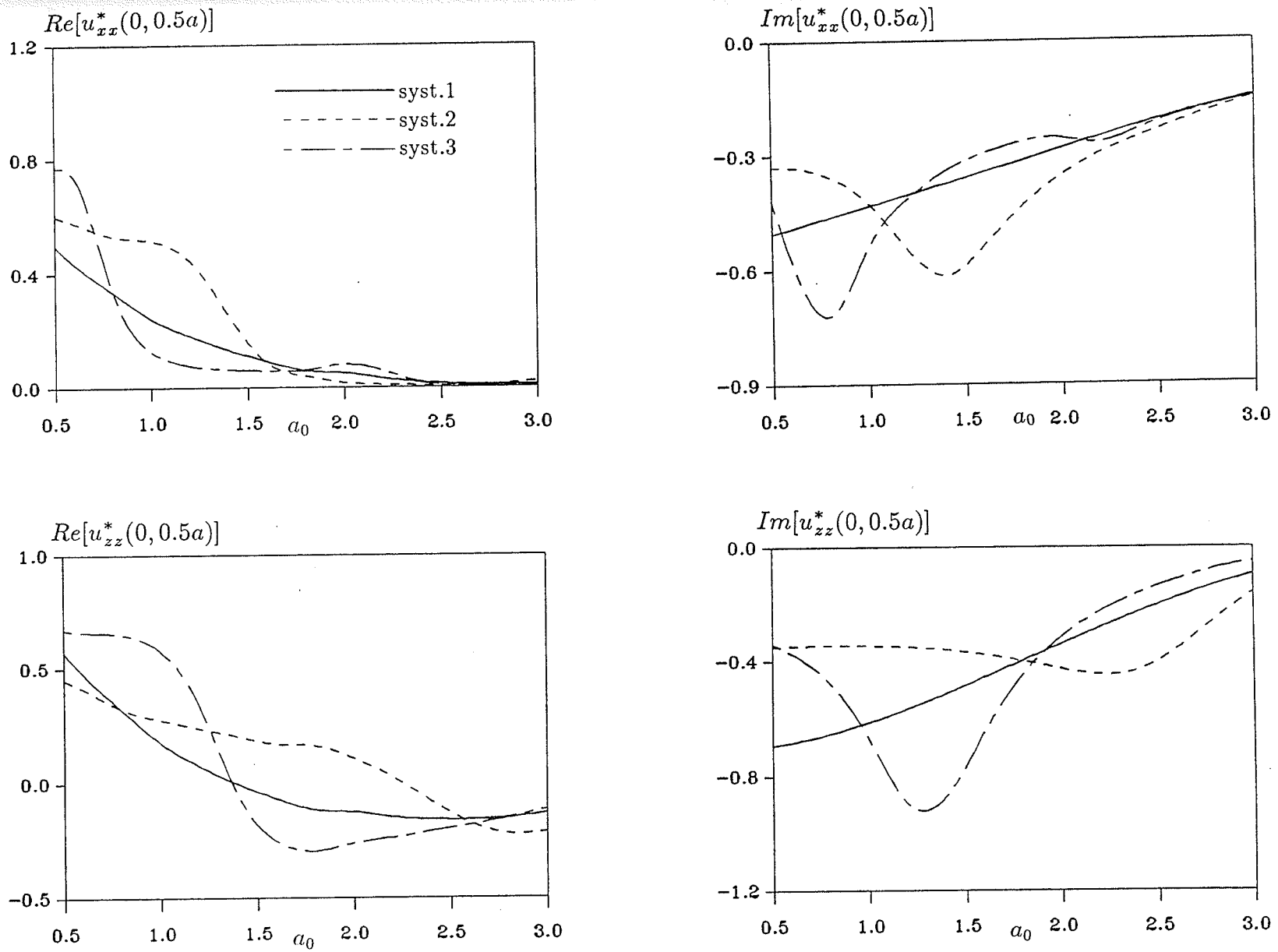

Figure 7.3 Normalized displacements u^*_{xx} and u^*_{zz} due to strip loads at $z/a = 0.5$

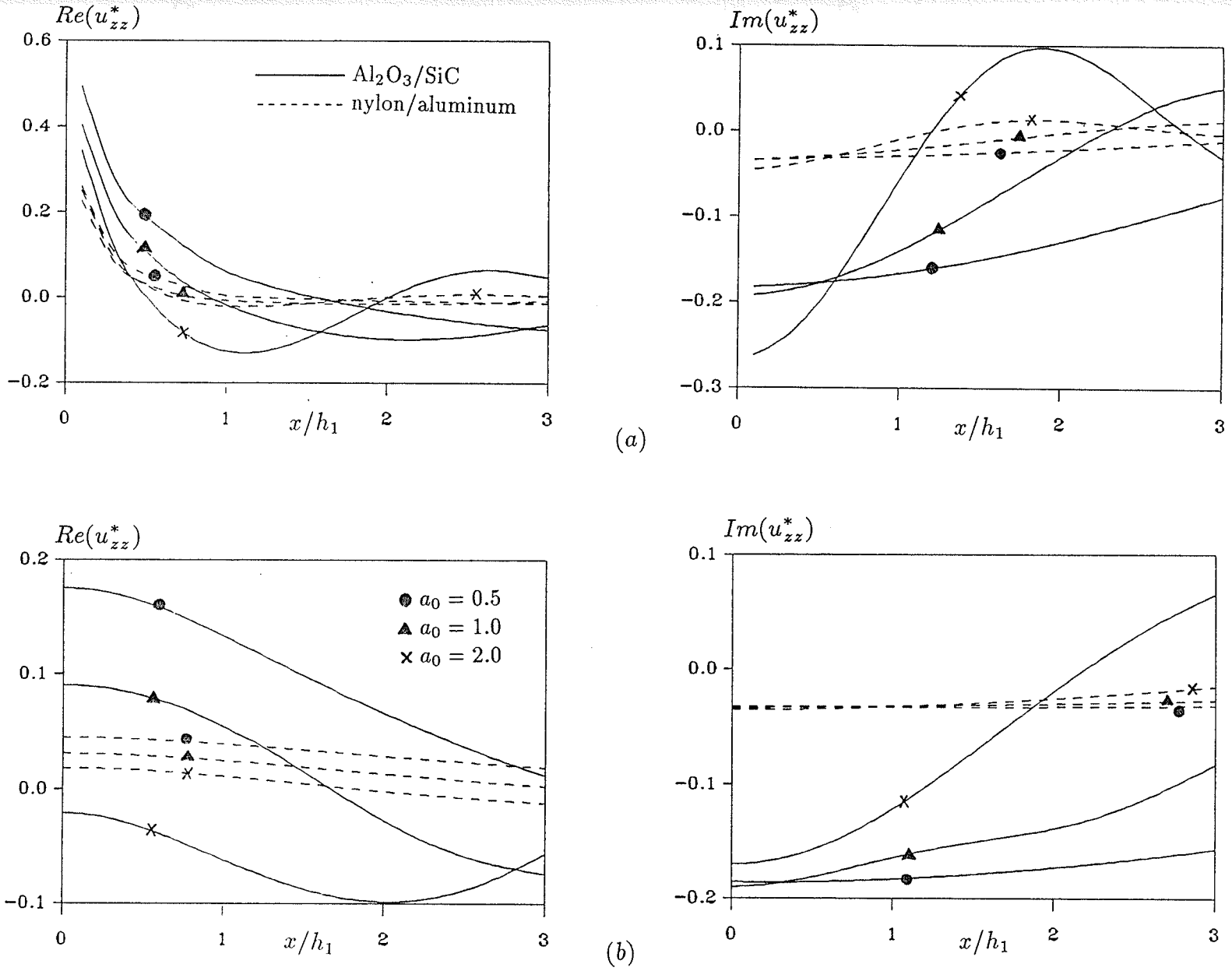

Figure 7.4 . Normalized displacement u^*_{zz} of Al_2O_3/SiC and nylon/aluminum systems due to a vertical point load applied at coordinate origin. *a*): u^*_{zz} along the surface ($z/h_1 = 0$); *b*): u^*_{zz} along the interface ($z/h_1 = 1.0$).

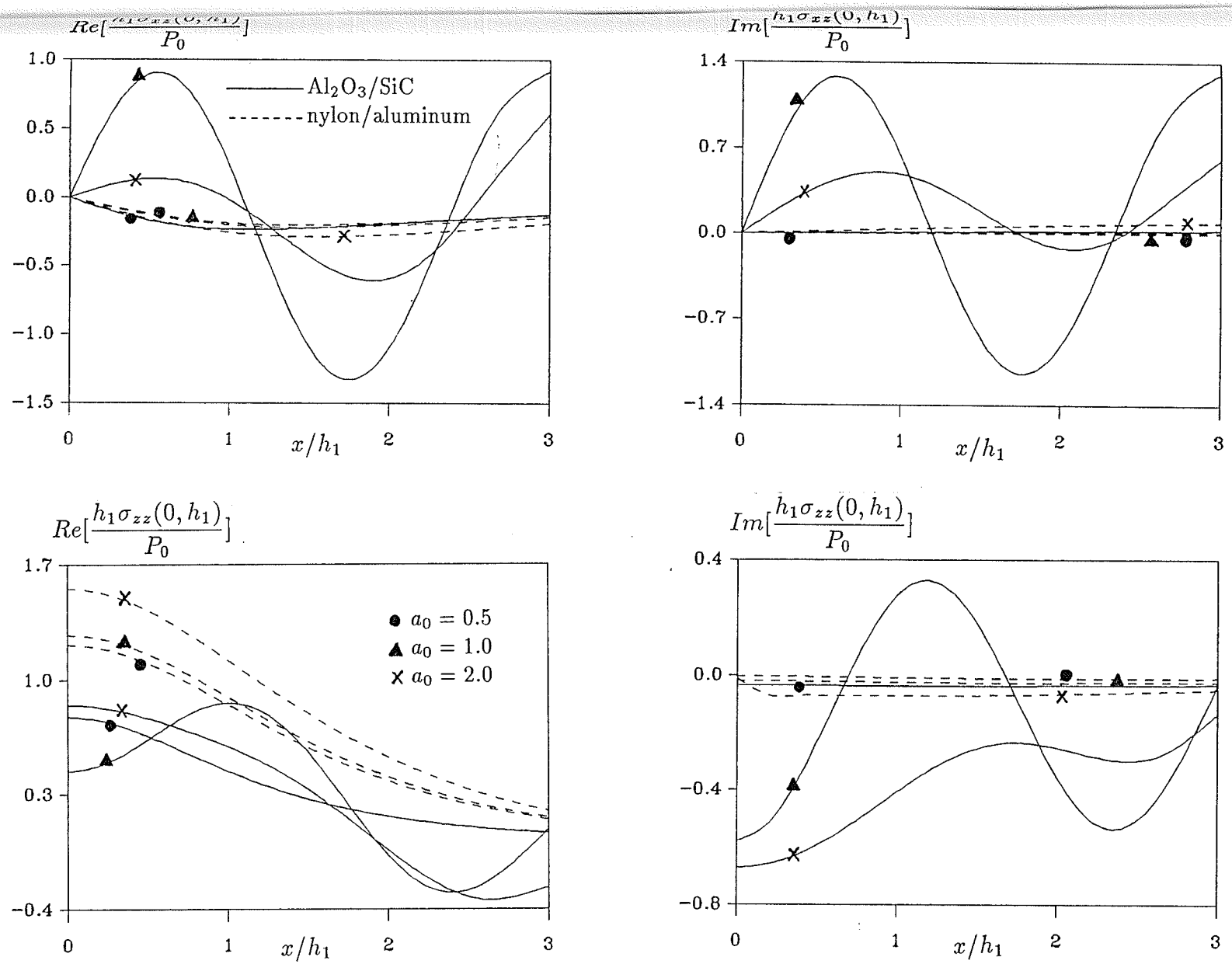

Figure 7.5 Normalized stresses σ^*_{xz} and σ^*_{zz} along the material interface of Al_2O_3/SiC and nylon/aluminum systems due to a vertical point load applied at coordinate origin.

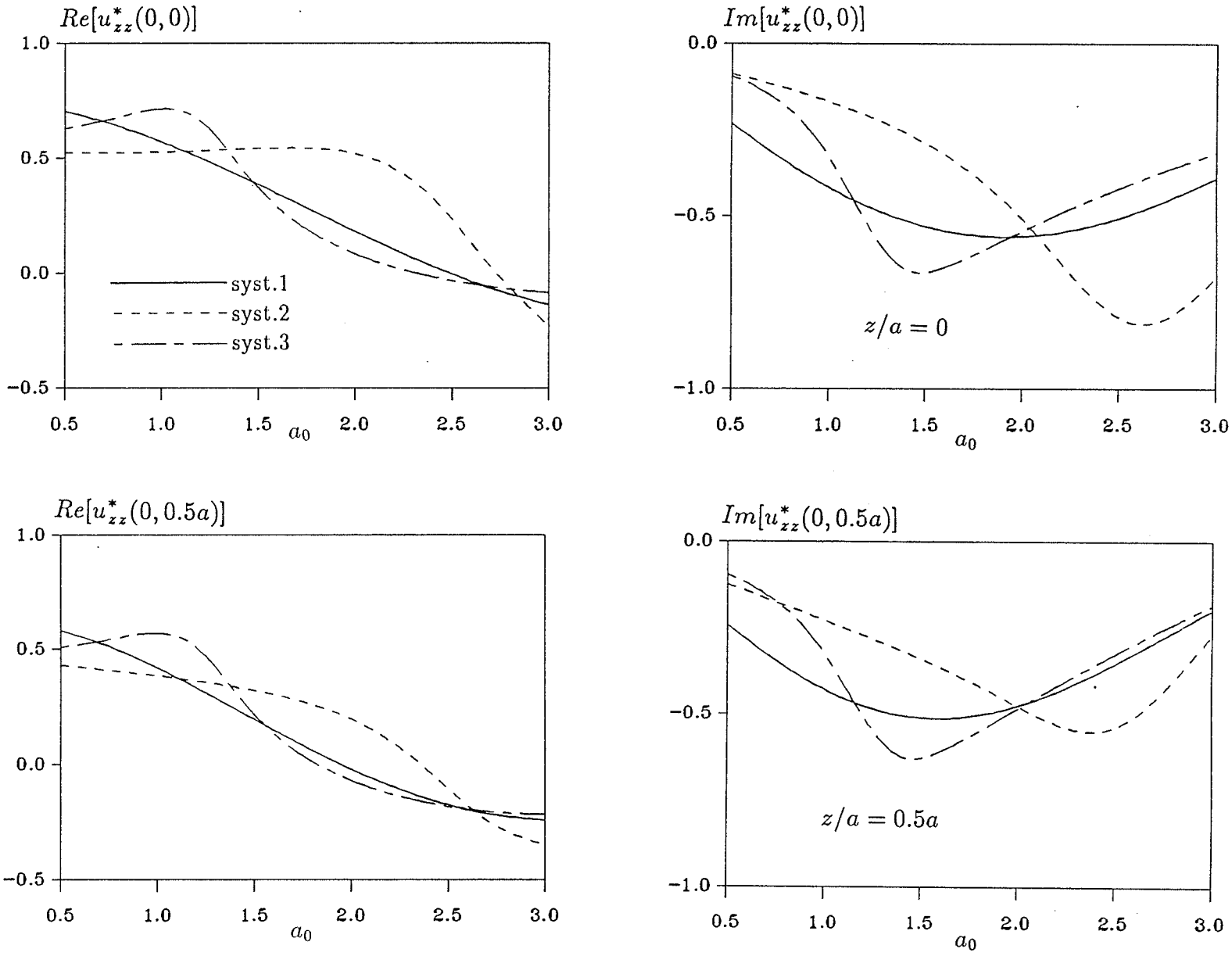

Figure 7.6 Normalized displacement u^*_{zz} due to a patch load.

Chapter 8

CONCLUDING REMARKS

8.1 CONCLUSIONS

In this final Chapter, the major conclusions of the present study are summarised. It should be mentioned here that separate conclusions are presented at the end of Chapters 3-7 based on the analysis and numerical solutions presented in those Chapters. The following are the major findings and conclusions of the present study.

1) Equations governing static and dynamic (time-harmonic and transient) deformations of a homogeneous transversely isotropic medium can be solved by using appropriate integral transform techniques. Fundamental solutions corresponding to buried loadings and displacement jumps can be derived explicitly for a homogeneous transversely isotropic elastic half space. These solutions are expressed in terms of semi-infinite integrals with oscillatory integrands which are singular at certain points within the range of integration.
2) It is found that the integrands of the semi-infinite integrals encountered in the fundamental solutions corresponding to internal loadings are very complicated and these integrals cannot be evaluated by analytical means in most cases. It is also found that the semi-infinite integrals encountered in 2-D and 3-D problems can be evaluated accurately by using Filon's integration scheme and the extended trapezoidal rule respectively. Negligible material attenuation is used in all numerical calulation to facilitate numerical integration along the real axis of the integral transform parameter. The numerical inversion scheme proposed by Hosono is found to yield accurate solutions for transient problems.
3) The exact stiffness matrix method developed in this study results in an accurate and numerically stable algorithm to compute fundamental solutions for

multi-layered media. Unlike the conventional algorithm based on the determination of layer arbitrary coefficients, the present method involves matrices which contain only negative exponential of the transform parameter and requires lesser computational effort due to the presence of a banded symmetric matrix which is nearly half the size of that encountered in the conventional algorithms.

4) Numerical solutions presented in this study for homogeneous transversely isotropic media indicates that in the case of static and low frequency dynamic loadings ($a_0 < 2.0$) the influence of material anisotropy on vertical and horizontal displacements (or stiffnesses) are governed mainly by nondimensional material constants $\bar{c}_{33}$ and $\bar{c}_{11}$. Numerical solutions corresponding to dynamic problems indicates that at high frequencies the response is governed by a complex combination of the degree of anisotropy and the frequency of excitation. Material anisotropy has a relatively lesser influence on stresses when compared to displacements. In the case of layered transversely isotropic media the influence of material anisotropy on the response cannot be related to a single material coefficient.

8.2 SUGGESTIONS FOR FUTURE WORK

The comprehensive set of Green's functions together with the boundary element code presented in this thesis can be applied to analyse a variety of interesting problems. However, only a few such problems were considered here due to obvious reasons. It is suggested that problems related to a single pile, pile groups, transient response of rigid footings, wave scattering by cavities and cracks in anisotropic media, interface fracture problems *etc.* be analysed by using the tools developed in this thesis. In addition, transient fundamental solutions presented in Chapters 4 and 5 for homogeneous media should be further investigated by using analytical techniques to obtain time-domain solutions. Such solutions are

very useful in the interpretation of seismic data and signal profiles in NDE methods. Finally, the exact stiffness matrix method presented in Chapter 7 should be extended to compute 3-D fundamental solutions for multi-layered transversely isotropic half spaces.

REFERENCES

Apsel, R.J. and Luco, J.E. (1983), 'On the Green's functions for a layered half space Part II', *Bulletin of the Seismological Society of America*, **73**(4), 931-951.

Apsel, R.J. and Luco, J.E. (1987), 'Impedance functions for foundations embedded in a layered medium: An integral equation approach', *Earthquake Enggrg. Struct. Dyn.*, **15**(2), 213-221.

Banerjee, P. and Butterfield, R. (1981), *Boundary Element Methods in Engineering Science*, McGraw-Hill, New York, N.Y.

Barnett, D.M. and Lothe, J. (1974), 'Consideration of the existence of surface wave (Rayleigh wave) solution in anisotropic elastic crystals', *J. Physics*, **F4**(5), 671-686.

Beskos, D.E. (1987), 'Boundary element methods in dynamic analysis', *Applied Mech. Reviews*, **40**(1), 1-23.

Boussinesq, I. (1895), *Applications des Potentiels*, Paris.

Brebbia, C.A., Telles, J.C.F. and Wrobel, L.C. (1984), *Boundary Element Techniques*, Springer-Verlag, Berlin and New York.

Buchwald, V.T. (1961), 'Rayleigh waves in transversely isotropic meia', *Quarterly J. Mech. and Appl. Mathematics*, **14**(4), 293-317.

Cagniard, L. (1962), *Reflection and Refraction of Progressive Seismic Waves*, McGraw-Hill, New York.

Chadwick, P. and Smith, G.D. (1977), 'Foundations of the theory of surface waves in anisotropic elastic materials', *Advances in Appl. Mech.*, **17**, 303-376, Academic Press, New York.

Chan, K.S., Karasudhi, P. and Lee, S.L. (1974), 'Force at a point in the interior of a layered elastic half space', *Int. J. Solids Struct.*, **10**(11), 1179-1199.

Chen, W.T. (1966), 'On some problems in transversely isotropic elastic materials', *J. Appl. Mech.*, ASME, **33**(6), 347-355.

Crouch, S.L. and Starfield, A.M. (1983), *Boundary Element Methods in Solid Mechanics*, George Allen and Unwin, London.

Davies, B. and Martin, B (1979), 'Numerical inversion of Laplace transform: a survey and comparison of methods', *J. Comp. Phys.*, **33**, 1-32.

Desai, C.S. and Christian, J.T. (Eds.), (1977), *Numerical Methods in Geotechnical Engineering*, McGraw-Hill, New York.

Dunkin, J.W. (1965), 'Computation of modal solutions in layered elastic media at high frequency', *Bull. Seism. Soc. Am.*, **55**, 335-348.

Eason, G., Noble, B. and Sneddon, I.N. (1955), 'On certain integrals of Lipschitz-Hankel type involving products of Bessel functions', *Philos. Trans. R. Soc. London Ser. A*, **247**, 529-551.

Eason, G. (1966), 'The displacements produced in an elastic half-space by a suddenly applied surface force', *J. Inst. Maths. Appl.*, **2**, 299-326.

Elliott, H.A. (1948), 'Three-dimensional stress distributions in hexagonal aeolotropic crystals', *Proc. Cambridge Philosophical Soc.*, **44**, 522-533.

Eringen, A.C. and Suhubi, E.S. (1975), *Elastodynamics*, Vol.2, Academic Press, New York.

Eubanks, R.A. and Sternberg, E. (1954), 'On the axisymmetric problem of elasticity theory for a medium with transverse isotropy', *J. Rational Mech. Analysis*, **3**, 89-101.

Freedman, J.M. and Keer, L.M. (1972), 'Vibratory motion of a body on an orthotropic half plane', *J. Applied Mechanics*, ASME, **39**, 1033-1040.

Gazetas, G. (1981), 'Strip foundations on cross-anisotropic soil layer subjected to static and dynamic loading', *Geotechnique*, **31**, 161-179.

Gazetas, G. (1983), 'Analysis of machine foundation vibrations: state of the art', *Soil Dyna. Earthquake Eng.*, **2**, 2-42.

Gerrard, C.M. and Harrison, W.J. (1971), 'The analysis of a loaded half-space comprised of anisotropic layers', C.S.I.R.O., *Aust. Div. App. Geomech.*

Tech. Pap., No.10.

Gilbert, F. and Backus, G.E. (1966), 'Propagator matrices in elastic wave and vibration problems', *Geophysics*, XXXI, 326-332.

Gould, P.L. (1983), *Introduction to Linear Elasticity*, Springer-Verlag, New York.

Green, A.E. and Zerna, W. (1968), *Theoretical Elasticity*, Clarendon Press, Oxford, U.K.

Haskell, N.A. (1953), 'The dispersion of surface waves on multilayered media', *Bull. Seism. Soc. Am.*, **43** 17-34.

Haskell, N.A. (1960), 'Crustral reflection of plane SH waves', *J. Geophys. Res.*, **65**, 4147-4150.

Haskell, N.A. (1962), 'Crustral reflection of plane P and SV waves' *J. Geophys. Res.*, **67**, 4751-4767.

Heinrich, S.M. (1991), 'Torsional stress interference in transversely isotropy', *J. Engng. Mechanics*, ASCE, **117**, 478-487.

Hosono, T. (1979), *Trans. Inst. Elect. Engrs Jpn*, **54**, 44-.

Hu, H.C. (1954), 'On the equilibrium of a transversely isotropic elastic half-space', *Scientia Sinica*, **3**, 463-479.

Karasudhi, P., Keer, L.M. and Lee, S.L. (1968), 'Vibratory motion of a body on an elastic half space', *J. Appl. Mechanics*, ASME, **35**, 697-705.

Kausel, E. and Peek, R. (1982), 'Dynamic loads in the interior of a layered stratum: an explicit solution', *Bull. Seism. Soc. Am.*, **72** 1459-1481.

Knopoff, L. (1964), 'A matrix method for elastic wave problems', *Bull. Seism. Soc. Am.*, **54** 431-438.

Kobayashi, S. (1984), 'Fundamentals of boundary integral equation methods in elastodynamics', *Topics in Boundary Element Research*, (Ed. C.A. Brebbia), 1-45, Springer, Berlin.

Kobayashi, S., Nishimura, N. and Kishima, T. (1986), 'A BIE analysis of wave propagation in anisotropic media', *Boundary Elements VIII*, Springer-

Verlag, Berlin, Germany, 425-434.

Kraut, E.A. (1962), 'Propagation of a pulse from a surface line source on a transversely isotropic elastic half-space', *Ph. D. thesis*, University of California, Los Angeles.

Lamb, H. (1904), 'On the propagation of tremors over the surface of an elastic solid', *Philosophical Transactions of the Royal Society of London*, Series A, **203**, 1-42.

Laturelle, F.G. (1990), 'The stresses produced in an elastic half-space by a normal step loading over a circular area: an analytical and numerical results', *Wave Motion*, **12**, 107-127.

Lekhnitskii, S.G. (1963), *Theory of anisotropic elastic bodies*, Holden-Day Publishing Co., San Francisco, Calif.

Luco, J.E. (1982), 'Linear soil-structure interaction: a review', *Earthquake Ground Motion and Its Effects on Structures*, AMD-Vol.53 (Ed. S.K.Datta), ASME, New York, 41-57.

Luco, J.E. and Apsel, R.J. (1983), 'On the Green's functions for a layered half-space: Part I', *Bull. Seism. Soc. Am.*, **73**, 909-929.

Mansur, W.J. (1983), 'A time-stepping technique to solve wave propagation problems using the boundary element method', *Ph.D. Thesis*, Univ. of Southampton.

Mindlin, R.D. (1936), 'Note on the Galerkin and Papkovich stress functions', *Bull. Amer. Meth. Soc.*, **42**, 373-376.

Mitra, M. (1963), 'Note on the transient disturbance due to finite sources in an elastic half-space', *Indian J. Mech. Math.*, **1**, 22-26.

Ohsaki, Y. (1973), 'On movement of a rigid body in semi-infinite elastic medium', *Proc. of Japan Earthquake Engrg. Symp.*, Japan, 245-252.

Pan, Y.C. and Chou, T.W. (1976), 'Point force solution for an infinite transversely isotropic solid', *J. Appl. Mech.*, ASME, **43**, 1-5.

Pan, Y.C. and Chou, T.W. (1979), 'Green's function solutions for semi-infinite transversely isotropic materials', *Int. J. Engng. Sci.*, **17**, 545-551.

Payton, R.G. (1983), *Elastic Wave Propagation in Transversely Isotropic Media*, Martinus, Nijhoff, The Netherlands.

Pestel, E.C. and Leckie, F.A. (1963), *Matrix Methods in Elastomechanics*, McGraw-Hill, New York, N.Y.

Piessens, R. (1975), 'Bibliography on numerical inversion of the Laplace transform and applications', *J. Comp. Appl. Math.*, **1**, 115-126.

Rajapakse, R.K.N.D. (1988), 'A torsion load transfer problem for a class of non-homogeneous elastic solids', *Int. J. Solids Structures*, **24**, 139-151.

Rajapakse, R.K.N.D. and Shah, A.H. (1988), 'Impedances of Embedded rigid strip foundations', *Earthquake Engineering and Structural Dynamics*, **16**, 255-273.

Rizzo, R.J. (1967), 'An integral equation approach to boundary value problems in classical elastostatics', *Q. Appl. Math.*, **25**, 83-95.

Saada, A.S. (1974), *Elasticity: Theory and Applications*, Pergamon Press, Oxford, U.K.

Saxena, H.S. and Dhaliwal, R.S. (1990), 'A penny-shaped crack at the interface of two bonded dissimilar transversely isotropic elastic half spaces', *Engng. Fracture Mechanics*, **37**, 891-899.

Schwab, F. (1970), 'Surfaces-wave dispersion computations: Knopoff's method', *Bull. Seism. Soc. Am.*, **60**, 1491-1520.

Seal, S.H. and Kausel, E. (1989), 'Point loads in cross-anisotropic layered half spaces', *J. Engrg. Mech.* ASCE, **115**, 509-524.

Selvadurai, A.P.S. (1979), 'On the displacement of a penny-shaped rigid inclusion embedded in a transversely isotropic elastic medium', *Solid Mechanics Archives*, **4**, 163-172.

Selvadurai, A.P.S. (1980), 'Asymmetric displacements of a rigid disc inclusion

embedded in a transversely isotropic elastic medium of infinite extent', *Int. J. Engng. Science*, **18**, 979-986.

Selvadurai, A.P.S. (1982), 'The static Reissner-Sagoci problem from an internally loaded transversely isotropic half space', *Int. J. Engng. Science*, **20**, 1365-1372.

Selvadurai, A.P.S. (1984), 'Stress intensity factors for internally indented cracks in transversely isotropic elastic soils', *Winter Annual Meeting*, ASME, Dec. 9-14, New Orleans, LA.

Selvadurai, A.P.S. and Rajapakse, R.K.N.D. (1985), 'On the load transfer from a rigid cylinder inclusion into an elastic half space', *Int. J. Solids Structures*, **21**, 1213-1229.

Selvadurai, A.P.S. and Rajapakse, R.K.N.D. (1987), 'Variational scheme for analysis of torsion of embedded nonuniform elastic bars', *J. Engrg. Mechanics*, ASCE, **113**, 1534-1550.

Sneddon, I.N. (1951), *Fourier Transforms*, McGraw-Hill, New York.

Stoneley, R. (1949), 'The seismological implications of aelotropy in continental structures', *MNRAS, Geophysical Supplement*, **5**, 343-353.

Synge, J.L. (1956), 'Elastic waves in anisotropic media', *Proc. Roy. Irish Acad.*, A **58**, 323-334.

Thomson, W.T. (1950), 'Transmission of elastic waves through a stratified solid medium', *J. Appl. Phys.*, **21**, 89-93.

Tranter, C.J. (1956), *Integral Transforms in Mathematical Physics*, 2nd Ed., Wiley, New York.

Tsai, Y.M. (1984), 'Indentation of a penny-shaped crack by an oblate spheroidal rigid inclusion in a transversely isotropic medium', *J. Applied Mechanics*, ASME, **51**, 811-815.

Vable, M. and Sikarskie, D.L. (1988), 'Stress analysis in plane orthotropic material by the boundary element method', *Int. J. Solids Structures*, **24**, 1-11.

Wass, G. (1972), 'Linear two-dimensional analysis of soil dynamics problems in semi-infinite layered media', Ph.D *thesis*, University of California, Berkeley, California.

Wass, G. (1980), 'Dynamics Belastete Fundamente auf Geschichtetemn Baugrund', VDI *Berichte*, **381**, 185-189 (in German).

Wang, Y., Rajapakse, R.K.N.D. and Shah, A.H. (1991), 'Dynamic interation between flexible strip foundations', *Earth. Engrg. Stru. Dynamics*, **20**, 441-454.

Warburton, G.B., Richardson, J.D. and Webster, J.J. (1971), 'Forced vibrations of two masses on an elastic half space', *J. Appl. Mech.*, ASME, **38**, 148-156.

Washizu, K. (1982), *Variational methods in elasticity and plasticity*, 2d Ed., Pregamon Press, New York, N.Y.

Watson, T.H. (1970), 'A note on fast computation of Rayleigh wave dispersion in the multilayered elastic half space', *Bull. Seism. Soc. Am.*, **60**, 161-166.

Wong, H.L. and Luco, J.E. (1986), 'Dynamic interaction between rigid foundations in a layered half-space', *Soil Dynamics and Earthquake Engineering*, **5**, 149-158.

Zienkiewicz, O.C., Kelly, D.W. and Bettes, P. (1977), 'The coupling of the finite element and boundary solution procedures', *Int. J. Numer. Meth. Engng.*, **11**, 355-375.

Zureick, A.H. and Eubanks, R.A. (1988), 'Spheroidal cavity with prescribed asymmetric traction in three-dimensional transverse isotropy', *J. Engrg. Mech.*, ASCE, **114**, 24-48.

Zureick, A.H. (1989), 'Spheroidal cavity with prescribed asymmetric displacements in three-dimensional transverse isotropy', *J. Engrg. Mech.*, ASCE, **115**, 2427-2439.